Muscle Modeling and Parameterization for Use in Control via Electrical Stimulation

by

Heather L. Beck Abushanab

Submitted to the Department of Mechanical Engineering
in partial fulfillment of the requirements for the degree of

Doctor of Philosophy in Mechanical Engineering

at the

MASSACHUSETTS INSTITUTE OF TECHNOLOGY

January 1995

Author .....
Department of Mechanical Engineering
January 9, 1995

Certified by .....
Professor William K. Durfee
Associate Professor, University of Minnesota
Thesis Supervisor

Accepted by .....
Ain A. Sonin
Chairman, Departmental Committee on Graduate Students

Muscle Modeling and Parameterization for Use in Control via Electrical Stimulation

by

Heather L. Beck Abushanab

Submitted to the Department of Mechanical Engineering
on January 9, 1995, in partial fulfillment of the
requirements for the degree of
Doctor of Philosophy in Mechanical Engineering

Abstract

Functional electrical stimulation (FES) is a promising technology for restoring function to individuals paralyzed by spinal cord injury. Control with FES is difficult because the actuator (stimulated muscle) is a complex, non-linear, time-varying system. Without adequate knowledge of the muscle properties, robust control is difficult to achieve. To address this problem a non-linear, lumped-parameter model of the input/output relationship between stimulation amplitude and joint angle was developed. Rapid parameterization techniques, needed to customize the models to individuals, were developed. The parameterization procedures depended only on external measurements of joint kinematics and net joint torque. The rapid identification procedures compared favorably to traditional identification methods for prediction of isometric joint torque and joint angle. The model was used to predict joint angle response to a variety of stimulation inputs including step, ramp, swept-sine and random binary amplitude pulse trains. Simulations showed that prediction with this model is better than prediction with other models previously published in the literature.

Committee Members: Professor William Durfee
Professor Neville Hogan
Professor Anuradha Annaswamy
Professor Marc Raibert

Thesis Supervisor: Professor William K. Durfee
Title: Associate Professor, University of Minnesota

Acknowledgments

This thesis is the culmination of several years of work. The assistance and support of many individuals was immensely helpful during that time. My advisor, Will Durfee gave me the opportunity to work on a very interesting topic, and provided terrific guidance and encouragement. His unending confidence in my abilities helped me to trust myself. My committee members, Neville Hogan, Marc Raibert, and Anu Annaswamy, deserve thanks for their time, support, and constructive criticism.

The Newman Lab was a terrific place to work and the FES group, Michael, Elaine, Jeff, and Zoher were great colleagues. I missed their company and their cooking the last six months. Luckily, Karon and Zebo provided friendly support and companionship since the FES group disbanded. Thanks to Karen, Naomi, Peter, Benji, Krishna and Michel for putting up with my experiments. Special thanks to Joe for his computer expertise and Justin for endless help with lots of random questions.

Woodie Flowers, Derek Rowell, Bob Mann, and Bora Mikic are just a few of the many MIT professors who watched out for me during both my undergraduate and graduate years.

Special thanks to MEGAwomen, some of the most unique and talented women anywhere. I will be watching your careers and cheering your accomplishments like they were my own.

The staff in the ME Department also deserve thanks. By the time I arrived at MIT, Leslie Regan, was like an old friend. In the years that followed "Ask Leslie" became the tried-and-true answer to all my toughest questions.

I built much of my experimental hardware with Norm Berube's help. Without him, I would still be in the machine shop looking for an edge finder.

In the past, I acknowledged my parents. Now, I feel lucky to acknowledge two sets of parents, who have loved me and cheered for me through this endeavor. Final thanks go to my husband Dan. His patience and help, especially during the final months, often went unacknowledged. I noticed and appreciated it all. I look forward to the extra time we can spend together, now that this thesis is complete.

Contents

Chapter 1

Introduction

Functional electrical stimulation (FES) is a technology to activate motoneurons in the peripheral nervous system to produce muscle contractions. A controlled electrical pulse applied to a nerve depolarizes the cell membrane. This action potential propagates down the length of the axon, causing a contraction in the enervated muscle. Several applications for electrical stimulation are already in common use. One of the most successful of these applications is the cardiac pacemaker. Other applications include high frequency stimulation to reduce chronic back pain and selective stimulation to control muscle exercise following injury or reconstructive surgery.

FES has the potential to restore some mobility to people paralyzed by spinal cord injury. Spinal cord injury (SCI) or trauma to the vertebrae of the spinal column which severs or damages the spinal nerves, results in a communication block between the nerves above and below the site of injury. The location of the damage generally determines the severity of the resultant disability. The motoneurons and muscles below the injury site, which are often intact and healthy, cannot communicate with the central nervous system, so the individual looses voluntary control of these muscles. In most cases, the peripheral motor system can be activated with electrical stimulation. If the paralyzed muscle are activated in an appropriate sequence, a paraplegic can stand with FES. Limited forms of gait have also been achieved.

In the US there are 250,000 spinal cord injured individuals with 8,000 new cases reported each year [54, 69]. Diving accidents, car accidents, and gun shot wounds

cause most spinal cord injuries, so it is not surprising that the vast majority of victims are injured between the ages of 15 and 29.

In recent years, the survival rate after SCI has been dramatically improved. Prior to World War II, 90% of SCI victims died within 3 years of injury, so rehabilitation was not a concern. During World War II, advances in the treatment of shock and infection reduced the mortality rate to 20%. Today, the 6-10% mortality rate is accompanied by a near normal life expectancy after injury.

The typical SCI individual is young and active with many years of life left to enjoy and the rehabilitation challenge for this population segment has increased importance as survival rates improve. The Americans with Disabilities Act mandates improved efforts to rehabilitate all disabled persons, including the spinal cord injured, and highlights the need for improvement even more. To date, the most common rehabilitative aid for paraplegics is the wheel chair. This effective, energy efficient means of restoring mobility is not sufficient. Many buildings are still inaccessible to wheel chairs, despite recent improvements. Secondary and tertiary complications of SCI, like pressure sores, osteoperosis and cardiopulmonary disease result from sitting all day. Although FES may never replace the wheel chair as the primary mobility aid, it can provide a beneficial alternative in restricted environments. In addition, the psychological benefits of standing and walking, even for limited periods of time, should not be underestimated.

Researchers at many sites around the world have developed systems which allow SCI subjects to stand or walk for limited periods of time in the controlled environment of the research lab [4, 13, 48, 56]. Despite the number of centers with FES gait programs, it remains primarily a research tool. The first commercial FES system for gait received FDA approval in 1994, but it only attempts a very crude form of gait. None of the clinical systems restore mobility even close to the pre-injury level.

Several problems must be addressed before full gait restoration can be achieved. Robust control of the muscle with FES is needed to guarantee predictable, reliable gait. The best control to date is achieved by individually tuning each stimulation channel in the clinic with trial and error techniques. A more systematic approach

must be developed if more than a handful of subjects are to benefit from the technology. The muscle behavior in response to stimulation is non-linear and unknown. Procedures to characterize the individual muscle response to stimulation are required. Muscle fatigues rapidly under FES, so strategies to prevent or detect fatigue are critical. Product safety and ease of use also must be addressed before any system gains wide spread use in the population it proposes to serve.

To move beyond some of these problems, additional basic research on the relationship between electrical stimulation and muscle force is needed. Many experiments have resulted in a preliminary understanding of this relationship [11, 62, 64, 67, 73] in isolated animal muscles, however, little research has been done to extend this understanding to intact human muscle.

1.1 Specific Aims

This thesis approaches the problems of FES control from a systems engineering perspective and attempts to lay the ground work for model based control. A systems engineer requires a working model of the plant, to design a controller, so this work investigates appropriate models of the muscle-tendon-joint system of intact humans. For model based controllers to be successful, they must be designed for individual users, so the individual system must be characterized or parameterized.

The first goal of this work was to choose an appropriate lumped parameter model to characterize the muscle-tendon-joint system. The model must capture the essential behavior of the system, but it must also be simple enough for use in control. The second goal was to develop methods to parameterize the model for individual systems. The parameterization methods must be easy to perform, since the system may need to be recalibrated frequently. The methods must be accurate, fast, and require limited equipment beyond what is already needed for FES control. The final goal was to gain insight into the behavior of the intact muscle and the complexity of joint control with FES, so that specific future goals can be stated. This work did not attempt to implement model based control, but focused instead on developing an

appropriate model which can be customized to describe individual joints and predict the performance of controllers yet to be developed.

1.2 Thesis Contents

Chapter 2 of this thesis reviews the literature on muscle models, FES controllers and limb dynamics needed to place this work in its proper context. Chapter 3 describes selection of an appropriate muscle-tendon-joint model which compromises between accuracy, ease of identification and simplicity for controller implementation. Chapter 4 explains the theoretical basis for various identification algorithms which were examined in the experiments. Chapter 5 details the physical set up, laboratory equipment and experimental protocols. The experiments identify parameters for the muscle-tendon-joint model of the knee under stimulation of the quadriceps muscle with both traditional and non-traditional methods. Simulations of the model are used to provide insight into the accuracy of the identification routines and the models they parameterize.

The results of both experiments and simulations are presented in Chapter 6 and discussed in Chapter 7. The identification methods are compared for ease of implementation and accuracy. The ability of the model to predict joint angle output is quantified and compared to other models which have appeared in the literature. The significance of the research and the need for additional studies are examined. Chapter 8 summarizes the main conclusions and contributions of this work and itemizes additional questions which need to be addressed.

Chapter 2

Literature Review: Muscle Modeling and FES Control

This literature review will focus on muscle control with functional electrical stimulation. FES has been used in many different muscles to elicit contractions for a variety of purposes. Although this thesis is principally interested in applications to paraplegic standing and gait, insight can be gained from experiments targeted towards other applications. Two prior theses from this research group contain literature reviews which are relevant to this work. Karu [52] provides an excellent overview of muscle physiology and the non-linear phenomenon observed in response to muscle stimulation. Chiou [20] presents a thorough account of the development of Hill-type muscle models. Neither of these topics will be repeated in this review.

Two general approaches have been used in the development of control strategies for FES. The first clinically based approach focuses on achieving and improving results through trial and error. In this way, clinicians have realized FES gait in the laboratory environment although the standard four channel gait protocol which is now in use at many sites is still far from optimal. Feedback control has been investigated with PID and compensator controllers in a similar iterative manner.

With the second approach, model-based controller design, an investigator develops a model of the muscle system and uses the model to design an appropriate controller. A multitude of models have been proposed. Most researchers have focused on linear

muscle models or linearized muscle models. Linear models work well for isometric force regulation, where a wide range of both open- and closed-loop controllers have been tested on isometric muscle. Less research nas gone into non-isometric control where linear models seem to be less successful for these positioning tasks. Some work has been reported on non-linear Hill-type lumped parameter models for use in control. Although the literature is limited, this approach shows potential.

There is significant literature concerning the control of muscle with FES. The following review is organized by research group.

2.1 Case Western Reserve University

Case Western Reserve University is the home of the largest FES research center in the world. They have made many advances in the control of muscle. Early laboratory work focused on the control of isometric force in isolated cat muscle with a variety of control schemes. At the same time, clinical work was performed with trial and error methods to achieve some improvement with feedback control.

1980 - Crago, Mortimer, and Peckham [25] designed a closed-loop force feedback system for control of isometric force in cat soleus muscle. The controller combined recruitment and temporal modulation to achieve a linear relationship between modulator input and force output. The controller used a PI structure with a proportional gain of 1 and an integral gain of 10.

1980 - Crago, Peckham, Thrope [26] studied isometric force modulation in cat soleus muscle and human finger and thumb muscles. No control was applied. They achieved force modulation by both pulse width modulation and pulse amplitude modulation.

1985 - Wilhere, Crago, and Chizeck [82] modeled the muscle and stimulator as a linear discrete-time process with a single zero and two poles. They designed a digital, closed-loop controller to cancel part of the plant dynamics. The remaining controller parameters were chosen analytically to accommodate a 10:1 change in recruitment gain, instead of attempting to cancel the nonlinear static gain. The controller, tested

on cat soleus and plantaris muscle held isometrically, achieved stable and repeatable responses to a variety of inputs, however, the step response did not always meet design specifications.

1985 - Streeter, Chizeck, Kobetic [74] investigated the characteristics of quadriceps muscle of paraplegics. The relationship between input stimulus pulse width and knee joint angle characterized the dynamic response of the system. They found that the system can be modeled as a second-order linear dynamic block cascaded with a static nonlinearity. The model was not used for control.

1985 - Chizeck, Lalonde, Chang, Rosenthal, Marsolais [21] used a feedback controller to regulate electrically stimulated stance in paraplegics. A modified digital PID controlled each human joint (2 knees, 2 ankles). No assumptions were made about the plant. The controller effected good standing quality and disturbance rejection, but allowed only a short standing duration.

1986 - Bernotas, Crago, and Chizeck [14] developed a discrete time model of electrically stimulated isometric muscle. The model consisted of a static non-linear block and a linear dynamic element. Three discrete-time deterministic autoregressive moving average (DARMA) models were investigated for the dynamic element. Parameters were estimated with a recursive least squares algorithm. A second order DARMA model with a zero at the origin gave a substantially better fit than a lower order model and less improvement was seen with a more complex model. Experiments with cat soleus muscle and a single-pole, single-zero controller determined that a second order model was adequate. This method allowed for real-time parameter estimation and the possibility of adaptive control.

1987 - Bernotas, Crago, and Chizeck [15] used an adaptive control system based on the second-order DARMA model investigated in [14] to control isometric force in a cat tibialis anterior muscle. This was compared to a fixed parameter single-pole, single-zero controller. The two controllers showed minor differences.

1988 - Chizeck, Crago, and Kofman [22] designed a digital controller with one pole and one zero to modulate isometric force in fast and slow twitch (soleus and plantaris) cat muscle. The most complex model described in [14] was used as the

system model. The controller was robust to slow changes in muscle characteristics and changes of gain of over 10 times. They concluded that this controller performed better than the one reported in [82], however no direct comparison was made with [15] and the reported results are comparable.

1989 - Chow and Chizeck [24] used recursive constrained least squares to identify isometric quadriceps muscle in paraplegics. The non-linear, time-varying IRC was identified jointly with the dynamics. The dynamics were modeled as in [22], and the IRC was fit to a third order polynomial with a dead zone and a region of saturation. By applying constraints based on prior knowledge of the recruitment curve shape, they were able to get a better estimation of the IRC. No control was described.

1991 - Lan and Crago [57] investigated a model reference control strategy for arm movements with an antagonistic muscle model. Results were given for simulation only.

1991 - Crago, Nakai, and Chizeck [27] described a fixed parameter digital controller which combined position and force feedback to control hand grasp. The controller gain and pole were tuned for performance and were not designed based on a model.

1991 - Chizeck, Lan, Palmieri, and Crago [23] used stimulus period modulation with pulse width modulation to improve position control of agonist/antagonist muscle pairs in a cat. Stimulation of the tibialis anterior and either medial gastrocnemius or lateral gastrocnemius controlled the ankle joint. No model was used although a costimulation mapping was developed based on the threshold of the muscle response and the maximum pulse width of the stimulator. The controller was quite complex and will not be described in detail here. Both reciprocal muscle activation and coactivation were examined. For single muscle activation, combined modulation produced better control of the transient responses, but increased the total number of stimulation pulses. For coactivation, the controller modulated the stimulation frequency of the two muscles reciprocally, increasing one while decreasing the other. This resulted in better control with fewer stimulation pulses than coactivation with only pulse width modulated stimulation. A companion paper [58] compared the performance of this controller with the fixed parameter controller from [22] and the adaptive controller

described in [15]. The three controllers were tested for isometric torque tracking, unloaded position tracking, and control of transitions between isometric and unloaded conditions. Adaptive control was not significantly better than fixed parameter control, but stimulus period modulation helped improve control during isometric and transition tasks. The researchers concluded that muscle length-tension and force-velocity nonlinearities affected all three controllers similarly.

1992 - Shue, Crago, and Chizeck [70] examined three Hill type models for their ability to fit input/output data measured during simultaneous modulation of recruitment and joint angle in the cat ankle with stimulation of the soleus. The models predicted joint torque output based on the inputs recruitment (output of the IRC) and joint kinematics. The first model calculated muscle output as the product of three independent factors: activation dynamics, torque-angle, and torque-velocity properties, and assumed linear torque-angle and torque-velocity relationships. A first order difference equation modeled the activation dynamics. Only four parameters were needed to fully specify the model. to identify. A second model with 6 independent parameters was also tested. The 6 parameter model had a second-order difference equation for activation and an asymmetric torque-velocity factor (slope discontinuity at zero velocity). A third model was studied which coupled activation with velocity. In this coupled model the muscle output was the product of two independent factors: activation/attachment dynamics and torque-angle relation. Activation was a first order difference equation coupled to an asymmetric torque-velocity factor, with the assumption that this reflects the physiological process of attachment and detachment of cross bridges and the decreased number of attached bonds during movement. The torque-angle relation was linear. A batch, non-linear least-squares identification algorithm was implemented. All three models gave good fits to the data. With the uncoupled models, parameter values depended strongly on the experimental conditions, but the coupled model parameters showed significantly less dependence. The models were also tested for their use in on-line adaptation. Adaptation was possible for both coupled and uncoupled models, but the excitation requirements for the coupled model were much more stringent. Prediction without adaptation in the uncoupled models

produced large errors.

2.2 University of Twente, Netherlands

This research group is headed by Peter Veltink. In 1989 he spent time at Case Western as a visiting scientist where he began his work in non-linear control of muscle contraction. Since that time he has continued to pursue a non-linear, model based approach to muscle control.

1989 - Veltink, Bialy, Chizeck,and Crago [77] proposed a non-linear strategy for controlling joint angle when attached to a known second-order load. They modeled the joint system with a non-linear discrete version of the Hill model with second-order, critically damped activation dynamics and a non-linear recruitment curve. The active torque-angle and torque-velocity functions were assumed to be piece-wise linear with an unspecified number of line segments. They modeled the passive muscle characteristics with a single joint compliance parameter. Identification was performed on cat soleus muscle in steps. Results showed the feasibility of open-loop, non-linear control, although the operating range was limited.

1991 - Veltink et al [78] presented computer simulations of an optimal algorithm to control FES-induced cyclical leg movements.

1991 - Veltink [79] used the control algorithm developed in [78] to optimize the stimulation sequence for controlling a freely swinging lower leg with quadriceps stimulation. He approximated the lower leg as a second-order linear system with subcritically damped dynamics. The muscle was modeled as an ideal torque generator at the knee producing a rectangular torque pulse per cycle in response to a stimulation burst at a constant recruitment level and stimulation frequency. A digital PID controller tuned through root locus system analysis, adjusted the burst time. Veltink concluded that this approach produces good cycle-to-cycle control of the knee joint and may be an important alternative to explicit trajectory tracking.

1992 - Veltink, Chizeck and Crago [80] expanded on the work presented in [77] using the same model structure. They found the passive joint compliance from si-

nusoidal perturbations of the joint. Isometric stimulation at six angles produced the active torque-angle curve For shortening muscle,isokinetic experiments at constant stimulation determined the torque-velocity function. A second experiment identified these properties with a second-order dynamic load attached. The muscle was stimulated at five recruitment levels. Subtracting the known load and passive torque components from the steady-state response and dividing the result by the recruitment level produced the active torque-angle relationship . The active torque-velocity component was found by stimulating at maximal recruitment. During each stimulation period. the active torque component was computed, based on knowledge of the load, passive joint compliance, active torque-angle curve and the activation. The activation was determined during this procedure by adjusting the pole location to minimized hysteresis in this curve. For lengthening muscle, the torque-velocity curve was assumed to be 1. A modified torque-velocity component incorporating a first-order time process, was also examined. Veltink found the compliance model of the passive joint was not adequate, since there was significant non-linearity, hysteresis and dependence on prior stimulation and movement history. The active torque-angle and torque-velocity properties were both dependent on measurement method. They tested three controllers in this study: 1) non-linear open-loop compensator, 2) PID controller, and 3) combined non-linear compensator and PID controller. The model was inverted to produce the non-linear open-loop compensator. Since there was a two step time delay in the model, the reference signal was needed two time steps ahead. The PID zeros of the controller were chosen to cancel the poles of the approximate linear activation dynamics and load model. The gain was adjusted to produce between 15 and 25 % overshoot in response to a 5 deg step input. For the final controller, a PID was added to the non-linear compensator to compensate for modeling errors and external disturbances. The model and controllers were tested on a single input consisting of a moderate ramp followed by a steady-state region followed by a descending ramping over a range of 25 deg of joint angle. The non-linear compensator responded faster than the PID to changes in command. The combined non-linear compensator/PID controller improved tracking performance. The modified torque-

velocity curve produced significant model improvement.

1994 - Franken, Veltink, et al [38] presented a model of the freely swing lower leg along with methods for identifying the model parameters in paraplegics. Their passive model contained single linear parameters for joint damping and limb inertia. The torque-angle dependence was divided into two components, gravity and compliance. A quick release experiment estimated the limb inertia. To find the other parameters, the limb was excited by stimulating the quadriceps muscle with a pseudo-random binary stimulation sequence. A two step procedure estimated the parameters. First, a linear least-squares algorithm estimated the linear parameters, while the non-linear compliance parameter was held constant at a nominal value. Second, a non-linear Levenberg-Marqardt algorithm estimated the torque-angle parameters. They found that the non-linear compliance term contributed significantly to the lower leg dynamics.

1994 - Franken, Veltink, et al [39] explored three models of the lower limb of paraplegics under quadriceps stimulation. Franken compared two torque generator models, one including only recruitment and the other incorporating second-order contraction dynamics, to a non-linear Hill type model with single segments for the active torque-angle and torque-velocity curves. He used the passive model from [38] as a parallel structure in all three models. The muscle was stimulated with a five minute pseudo-random binary stimulation sequence. Franken then extracted epochs from the data beginning with a single stimulation pulse preceded and succeeded by 250 ms with stimulation (essentially an isolated twitch). These sets of epochs were processed to estimate the model parameters. For the linear models, a generalized least squares algorithm estimated the parameters. Levenberge-Marquadt non-linear estimation parameterized the non-linear model. The parameterized models were used to predict the response of the limb with varying prediction intervals. At the beginning of each prediction interval, the kinematic trajectory was initialized with actual data values. A Runge-Kutta integration routine was used integrate the model over the prediction interval, and the error was computed. For prediction over short time intervals, the simplest model was sufficient.

1994 - Franken, Veltink, Baardman, Redmeyer, and Boom [37] used experimentally optimized stimulation patterns to control cyclic swing of the leg in two paraplegic subjects. They used surface stimulation of the hip flexors, hamstrings, and quadriceps to produce a desired hip angle range, foot clearance, and knee extension. Time varying mechanical output was most noticeable in the hip flexors, with quadriceps and hamstrings performance remaining relatively constant over time. After initial optimization, they used a discrete time PID controller similar to [79] to compensate for the varying performance of the hip flexors on a cycle-to-cycle basis. The controller did not account for errors during a given cycle, but adapted to errors from the previous cycle. Stimulation pulse width and pulse amplitude were set to achieve maximal recruitment. Burst duration was the control parameter. Franken found that cycle-to cycle control can compensate for slowly changing muscle properties due to fatigue or potentiation. The controller cannot compensate for external disturbances encountered during a cycle.

2.3 Ljubljana, Yugoslavia

This was the first group to develop four channel gait and to achieve walking for spinal cord injured paraplegics [55]. Much of the work of this group is clinically based.

1967 - Vodovnik, working with Crochetiere and Reswick from Case [81, 28] used a linear model and antagonist muscle pairs in a feedback loop to control the postion of the arm. They achieved some success in positioning the arm, but concluded that more basic study of the dynamic properties of muscle were necessary in order to refine the system.

1974 - Trnkoczy [75] investigated the variability of isometric muscle moment about the ankle due to electrode position and time. He found enough variability to make feedback control nearly impossible for times longer than a few minutes and attributed much of the variability to unpredictable displacement of tissue between the electrodes and the stimulated nerve.

1974 - Stanic and Trnkoczy [72] used FES to position the ankle joint of hemiplegic

and able-bodied subjects using position feedback and an analog controller. Results showed that the static and dynamic properties of regulated movements were adequate, but the main deficiency of the system was poor long-term repeatability.

1990 - Bajd, Kralj, Turk, and Benko [5] examined the symmetry of the lower leg response to FES in paraplegics. They found an 80 % symmetry between the characteristic properties (stimulation threshold, recruitment curve slope, dynamic twitch response, and maximal isometric torque) of the right and left legs. Symmetry between the responses may simplify voluntary FES control.

1991 - Zefran, Bajd, and Kralj [90] presented a kinematic model of FES gait assisted by crutches. They concluded that computer simulations can provide information about adequate choices for step length, muscle activation, and positioning of the crutches which may be especially important during training for FES assisted walking.

2.4 Technion-Israel Institute of Technology

There are several papers from the group led by Inbar in the area of FES control. In general they model human, non-isometric muscle with a non-linear static gain followed by a linear dynamic system. They use stimulation pulse width as the input to the models with joint angle output. The static non-linearity is generally treated as a threshold followed by a linear gain. They argue that additional non-linearities in the system are small and can be neglected. The order of the linear dynamic block is chosen for its best fit to the data.

1986 - Allin and Inbar published companion papers [2, 3] which described modelling, identification, and control of the human elbow flexion/extension and wrist pronation/supination systems. They used a least squares identification technique with a pseudo-random binary input sequence to fit a third-order, linear digital model for the dynamic block. Two controllers were tested, a third-order feedforward controller and a model reference adaptive controller. The performance of the two controllers was similar, but the adaptive controller did not require a lengthy identification procedure

before each control session to achieve adequate performance. Control of individual joints was successful for short periods of time, but multiple joint control was less successful.

1989 - Sacher, Hatwell and Inbar [68] described a discrete model of the paraplegic knee. This model combined agonist and antagonist muscle groups into a single bidirectional system such that negative inputs were equated with stimulation of the antagonist muscle. The non-linear gain was modeled as a single gain with negative and positive thresholds. This block was identified first and removed from the data which was subsequently fit to a linear system with a delay. They concluded that a fourth order denominator and a first order numerator was optimal for modeling this data. The model was not used for control. They do not specify which muscles were stimulated during this experiment.

2.5 Stanford University

Felix Zajac and his group at Stanford University produced scaling guidelines for Hill-based muscle models which make it possible to simulate systems with multiple muscles without estimating the properties of each muscle experimentally. This work has application well beyond FES and has contributed significantly to understanding the complexity of a complete FES control system.

1986 - Zajac, Topp and Stevenson [88] proposed a dimensionless second-order, non-linear dynamic model of the musculotendon actuator. The model required only four actuator specific parameters to characterize a specific muscle.

1987 - Kang and Zajac [51] used a planar computer model to look at paraplegic posture induced by FES. First-order activation dynamics were matched to experimental observation of human twitches. Contraction dynamics were modeled as in [88] and then simulated for individual muscles. The contraction dynamics were then further approximated by a first-order linear differential equation to avoid problems of non-linearity. The skeleton model consisted of five rigid links: head, trunk, thigh, shank, and foot, connected with pivot joints. The modeled arm motion as an exter-

nal disturbance, and linearized the equations of motion about the upright posture. A feedback control strategy was used to minimize the energy expenditure of muscle. Simulation results showed that strong muscles should be activated first to reduce energy liberation, and that considerable interaction between the segments of the model occurrs.

1989 - Zajac [89] presented a thorough discussion of muscle and tendon properties and his justification for scaling models of the musculotendon actuator. This work expanded on [88] by incorporating an additional actuator specific parameter, maximum shortening velocity, but did not discuss experimental verification of the model.

1990 - Yamaguchi and Zajac [87] presented a simulation study which explored the feasibility of FES-assisted gait. A three dimensional, eight degree of freedom skeletal model was used for the study. Seven rigid-body segments (feet, shanks, thighs and trunk) were used. The stance leg was confined to move in the sagittal plane, but the swing leg and trunk were allowed to move in the frontal plane as well. Joint damping and ligament constraints limited the joints' ranges of motion. Moments about the hip and knee were computed with standard vector subtraction, but the model of the knee took into account the mechanical influence of the patella. Muscles were modeled as described in [89]. A dynamic programming algorithm determined a minimal set of muscle actuators and a base line of activation to produce the desired gait. Each muscle controller was then tuned to produce the activation sequence determined by the dynamic programming. The optimization process pointed out some critical phases for control in the gait cycle. These included knee and ankle stability during single leg support, frontal plane stability of the hip, toe and heel clearance during swing, and control of step length and duration. Ten muscle groups were needed to produce a step. These included soleus, gastrocnemius, vasti, gluteus med/minimus, and iliopsoas of the stance leg along with iliopsoas, vasti, hamstrings and dorsiflexors of the swing leg. The simulated activation sequence was similar to EMG data of able-bodied humans assimilated from the literature, with some variations. Information was generated about the power expended and absorbed by each muscle and tendon during a gait cycle. The study showed that normal gait is theoretically possible with FES.

2.6 Rancho Los Amigos Rehabilitation Engineering Center

This group's work has focused on clinical applications of FES.

1989 - Tu, McNeal and Baker [76] described a computer system to generate isometric recruitment data from the twitch response of human muscle.

1989 - McNeal, Nakai, Meadows, and Tu [63] used trial and error tactics to develop a stimulation pattern for trajectory tracking of knee position in paraplegics. They optimized the command input by hand for each successive part of the trajectory. They found progressive degradation of the response with repeated trials. They also found that desired trajectories could be achieved on subsequent days with simple scaling of the stimulation pattern.

2.7 Massachusetts Institute of Technology and the University of Minnesota

This group is led by William Durfee who began his work at MIT and is continuing at the University of Minnesota. He has attempted to approach the FES control problem from multiple directions. Muscle and skeletal models are being used for identification and control. Hybrid FES systems are also being tested to circumvent the muscle modelling problem.

1989 - Durfee [30, 32] evaluated simple open- and closed-loop controllers which used antagonist cat muscles to position a single joint. He also looked at the effect of cocontraction verses reciprocal activation and found that an open-loop control algorithm which allows cocontraction works as well as P-D closed-loop reciprocal control.

1989 - Durfee and MacLean [34, 61] tested several methods for quick estimation of the isometric recruitment curve (IRC) in isolated cat tibialis anterior and medial gastrocnemius muscle. Second-order, critically-damped linear system dynamics were

assumed and were estimated by computing 1/tpeak of the response to an impulse. This system estimate was used in a ramp deconvolution method to produce adequate IRC estimates with much shorter testing times than the traditional step response method requires. Open loop isometric tracking was successful with these IRC estimates; however, performance degraded with time and fatigue, emphasizing the need for frequent recalibration of the IRC.

1991 - Hausdorff and Durfee [46, 45] characterized the isometric torque variability of quadriceps and hamstrings muscle groups and found that smaller amounts of variation occurred than was reported in the literature for other muscle groups. Larger variations were seen for more stimulation activity indicating that the torque is dependent on stimulation history. They modeled the muscle as a series of position dependent static non-linearities followed by constant muscle dynamics (second-order, critically-damped). For isometric torque, open-loop feedforward control worked well for short periods of time. Open-loop position control was not as accurate, indicating that the muscle model was not adequate for non-isometric conditions. They found that the use of four recruitment curves at four angles improved the accuracy of open-loop feedforward position regulation indicating that the position dependence of the static non-linearity was important, but does not out weigh the importance of the position dependence of the muscle dynamics.

1991 - Durfee and Palmer [35, 64] used a non-linear, non-isometric muscle model based on a Hill type structure to describe isolated cat tibialis anterior and medial gastrocnemius muscle. They assumed an infinitely stiff series elastic element, second-order activation dynamics and piece-wise linear curves to describe both the passive and active relationships. They identified the passive parameters by applying pseudo-random kinematic inputs to the muscle and measuring the resulting passive force. A linear least-squares estimation alogrithm fitted this data to produce the passive length-tension and force-velocity curves. The active properties were found by stimulating the muscle at a constant force level, applying a pseudo-random kinematic input, and measuring the resulting force. Manipulation of the model equations transformed the multiplicative structure of the active muscle properties to a linear form, which

allowed for linear estimation techniques. The model predicted force output for large variations in both kinematic and stimulation inputs. The model was not used in a control algorithm.

2.8 Louisiana State University

This group performs their research mainly in isolated cat muscle. Most of the work focuses on understanding and characterizing the behavior of muscle.

1985 - Solomonow [71] described a method for muscle recruitment which accesses the small, slow, non-fatiguing fibers first, as is the case with CNS recruitment, by blocking excitation of the faster, bigger fibers. He was able to produce fine, linear gradations of muscle force across the available force range.

1987 - Zhou, Baratta, and Solomonow [91] described isometric force control of cat medial gastrocnemius muscle.

1989 - Baratta, Zhou, and Solomonow [10] explored the frequency response of the cat soleus muscle when subjected to several motor drive strategies. They found that the frequency response of the muscle was constant over a wide range of strategies.

1990 - Baratta and Solomonow [7] measured the frequency response of nine cat muscles under isometric conditions. They concluded that all nine muscles could be characterized as second-order, critically-damped linear systems.

1991 - Baratta and Solomonow [9] examined the effect of the viscoelastic tendon stiffness on the dynamic response of the cat tibilais anterior muscle under isometric conditions. Their results suggest that, under isometric conditions, the tendon acts like a very stiff force transmission linkage and does not significantly alter the dynamic performance of the muscle in the mid-force range (20-80 % of maximal).

1991 - Baratta and Solomonow [8] examined the dynamic response of the cat tibialis anterior muscle during sinusoidally varying orderly stimulation of motor units and varying isotonic loads. The muscle's dynamic performance consisted of three components: displacement gain, displacement attenuation, and a time delay. Only the displacement gain was sensitive to the load mass. The displacement gain could be

understood by examination of the the active and passive length-tension relationships so that larger loads yielded smaller displacements. At very low loads, the combined effect of low stiffness in the tendon and the length-tension relationship resulted in slightly lower displacements.

1992 - Gareis, Solomonow, Baratta, Best, and D'Ambrosia [41] measured the length-force relations of nine skeletal muscles in the cat. The active-, passive- and total-force patterns varied widely among the muscles. For seven of the muscles, a simple model incorporating muscle architecture were successfully fit to the data. A new model which adds spatially and temporally the individual muscle compartments was needed to describe the tibialis anterior and the medial gastrocnemius.

2.9 Observations

It is clear from this review that significant progress has been made in the ability to control muscle force. It is also clear that significant control problems still exist. No one has yet demonstrated control of muscle force for long periods of time (more than 30 seconds). The changing properties of muscle make this a significant control issue. Adaptive control shows some promise for overcoming this obstacle. Linear models have been successful at describing the behavior of isometric muscle; however, they are inadequate for describing behavior under non-isometric conditions, and non-linear models have been explored in a very limited way. Computer simulation studies have shown that non-linear models are a better description of muscle behavior. Limited experimental work in animals shows that non-linear models can model force output in the presence of random stimulation and kinematic inputs. The overwhelming amount of research to data has been performed in the isolated muscles of animal model, which may or may not translate directly to intact human muscle. Additional research is needed to refine and test non-linear models for application to human muscle systems. The preliminary work shows controller design based on non-linear models holds promise for improving open- and closed-loop control, but more research is needed.

It is in the context of this body of work that the goals for this thesis were defined. An appropriate model structure and specific procedures to parameterize the model for an individual muscle-joint system in an intact human are needed to lay the foundation for the model-based, non-linear control which seems to hold so much promise.

Chapter 3

Development of the Model

Many mathematical models have been proposed for muscle, including non-linear springs, simple torque generators, variations of the Hill-type lumped parameter model, and the Huxley sliding filament models. Winters and Woo [85] review these models while Chiou [20] provides a comprehensive account of the development of Hill-type models. The previous chapter looked at muscle models which have been used in the context of muscle control through FES. The simple linear models discussed do not sufficiently describe complex muscle-joint mechanics operating over the full joint range. The limited work with non-linear models shows promise. Clearly, the literature shows that a non-linear model is needed to capture the essential behavior of muscle under FES control.

This thesis develops a model which can predict the position of a human limb in response to a stimulation sequence applied to muscle. As the model is presented, each modeling term will be defined. A glossary of terms is presented in Table 3.1 at the end of the chapter.

It was important to consider up front how to estimate and verify the model parameters and how to implement the model in a controller. The model was to be used with human muscles stimulated through surface electrodes. Although it is interesting and perhaps useful to know the force that an individual muscle produces due to stimulation, this is difficult to determine for surface stimulation of intact muscle. Under these conditions it is at present imp ble to know precisely which muscle or portion

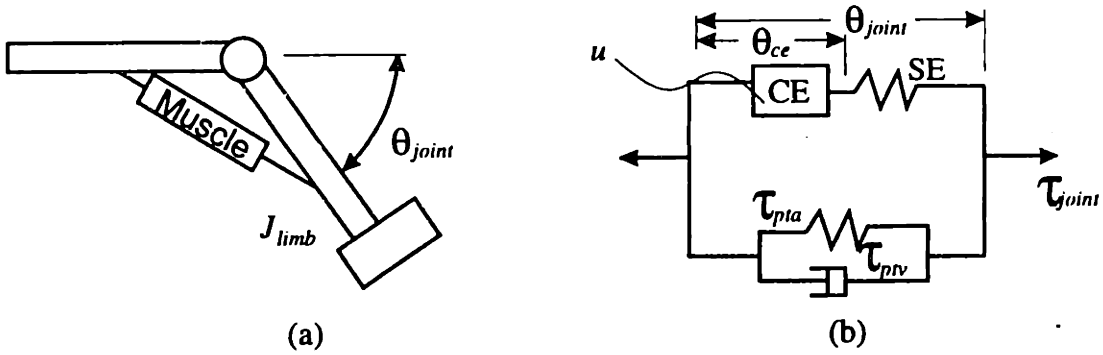

Figure 3-1: Basic joint-based, lumped parameter muscle model. (a) Body segments are modeled as rigid bodies connected by an ideal pin joint. The muscle actuates the joint. (b) A schematic of the muscle model. The parallel structure of the lumped parameter model includes the passive stiffness and damping properties of the joint/muscle, τ_{pta} and τ_{ptv}. The stimulation input, u, excites the contractile element, CE, which is placed in series with a series elastic element, SE. This active branch combines in parallel with the passive joint properties to produce a torque.

of the muscle is activated, where the muscle insertion points are located, and how the relationship between electrode placement and motor point changes with limb configuration. With these issues in mind, a joint-based, lumped-parameter model was selected. Each stimulation channel activates a separate torque producing element, acting in parallel with other torque producers as well as the passive joint elements. Figure 3-1 (b) shows a schematic representation of the parallel structure of the muscle properties. In this example a single stimulation channel is used to activate a single muscle group. For applications where more than one stimulation channel controls the muscle, additional groups may be added to the model in parallel. Rigid bodies connected by ideal pin joints model the body segment or limbs.

The passive model properties, which include non-linear stiffness and damping terms, result from the passive characteristics of all tissue associated with the joint. This includes the passive properties of the agonist and antagonist muscles, any inactive muscle groups, ligaments, tendons and other passive tissue that lie across the joint. All of these lumped passive characteristics combine together into the passive torque-angle τ_{pta} and torque-velocity τ_{ptv} elements of the model.

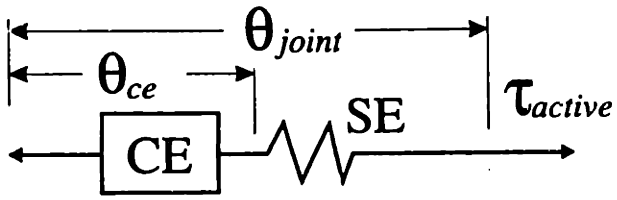

Figure 3-2: Active Muscle Properties. The contractile element, CE, is the force generating element of the muscle. For FES applications it is activated by the stimulation input. The series elastic element, SE, displays the quick-stretch response of actual muscle. For multiple simtulation channels, each active channel has its own CE and SE. The active muscle acts in only one direction, as either an agonist or antagonist.

3.1 Active Muscle Properties

The torque producing element or active muscle can be modeled in a variety of ways. For Hill-type models, a contractile element (CE) placed in series with a non-linear, series elastic element (SE), as shown in Figure 3-2, model each stimulation channel. The quick-stretch response observed in actual muscle is described by this series compliance. The contractile element torque depends on four terms: a normalized torque due to stimulation level and time $f_{stim}(u,t)$, a normalized active torque-angle property $f_{ata}(\theta_{ce})$, a normalized active torque-velocity property $f_{atv}(\dot{\theta}_{ce})$, and a scaling factor τ_{scale} which recovers absolute muscle torque. The stimulation dependent term consists of a static non-linear gain and a linear dynamic system block, which is further described in Section 3.2. The factors combine multiplicatively to produce the contractile element torque.

$$\tau_{active} = \tau_{ce} = f_{stim}(u,t) \times f_{ata}(\theta_{ce}) \times f_{atv}(\dot{\theta}_{ce}) \times \tau_{scale} \tag{3.1}$$

The portion of the joint angle associated with the contractile element, θ_{ce}, is related to the joint angle through the SE so that,

$$\theta_{ce} = \theta_{joint} - \theta_{se} \tag{3.2}$$

This formulation of the muscle model causes some problems. Identification of the

active torque-angle and torque-velocity properties requires direct measurement of θ_{ce}. Since θ_{ce} is a conceptual variable and does not relate directly to any given angle or length it is impossible to measure. Even if θ_{ce} could be physically separated from the joint angle, carrying out the measurement would require access to the interior of the muscle. An isolated muscle experiment can access the muscle interior, but experiments with intact human subjects prohibit this.

Additional problems arise from this model structure during numerical simulation. Equations (3.3) - (3.6) show state equations for this model where the mechanical states are joint angle, θ_{joint}, joint velocity, $\dot{\theta}_{joint}$, and the contractile element angle, θ_{ce}.

$$\frac{d}{dt}\theta_{joint} = \dot{\theta}_{joint} \tag{3.3}$$

$$\frac{d}{dt}\dot{\theta}_{joint} = \frac{1}{J_{limb}}[\tau_{ce} + \tau_{pta}(\theta_{joint}) + \tau_{ptv}(\dot{\theta}_{joint})\ ] \tag{3.4}$$

$$\tau_{ce} = \tau_{se} = K_{se}(\theta_{ce} - \theta_{joint}) \tag{3.5}$$

$$\frac{d}{dt}\theta_{ce} = f_{atv}{}^{-1}\ (\frac{\tau_{ce}}{f_{stim}(u,t) \times f_{ata}(\theta_{ce}) \times \tau_{scale}}) \tag{3.6}$$

Equation (3.4) represents the sum of torque about the joint, and Equation (3.6) arises from Equation (3.1). The parallel arrangement of the contractile element and the series elastic element means they experience the same torque.

This formulation requires an invertible active torque-velocity relationship and causes a divide-by-zero problem when the denominator of the $f_{atv}{}^{-1}$ argument approaches zero. The denominator approaches zero when f_{stim} approaches zero. Zero output from f_{stim} indicates inactivity of the active portion of the model. In simpler terms, the active muscle branch does not produce torque when the f_{stim} output is zero, so in effect, the model becomes a purely passive system. This physical fact leads to the practical implementation shown in Equations (3.7) - (3.10) to replace Equation (3.6). When the denominator of Equation (3.4) approaches zero, the simulation switches from the full model equations to a purely passive system model.

$$if \qquad f_{stim}(u,t) \times f_{ata}(\theta_{ce}) \times \tau_{scale} < tol \tag{3.7}$$

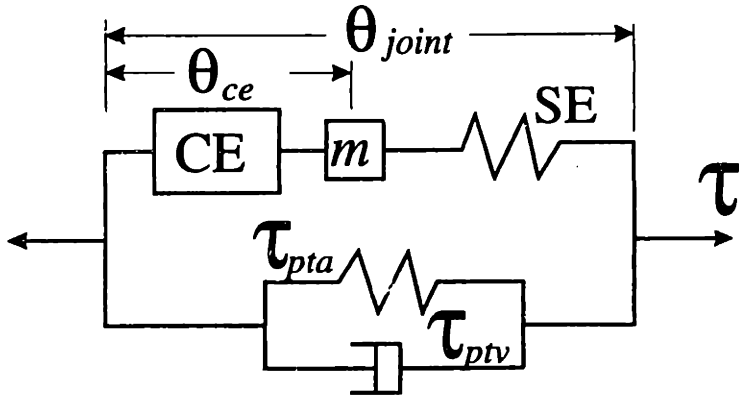

Figure 3-3: A small mass, m, can be added to the active muscle.

$$then \quad \tau_{ce} = 0 \tag{3.8}$$

$$and \quad \frac{d}{dt}\dot{\theta}_{joint} = \frac{1}{J_{limb}}[\ \tau_{pta} + \tau_{ptv}\ ] \tag{3.9}$$

$$else \quad \frac{d}{dt}\theta_{ce} = f_{atv}{}^{-1}\left(\frac{\tau_{ce}}{f_{stim}(u,t) \times f_{ata}(\theta_{ce}) \times \tau_{scale}}\right) \tag{3.10}$$

Modifying the model structure also solves the inversion problem. A small mass inserted between the CE and the SE (Figure 3-3) results in the following state equations:

$$\frac{d}{dt}\theta_{ce} = \dot{\theta}_{ce} \tag{3.11}$$

$$\frac{d}{dt}\dot{\theta}_{ce} = \frac{1}{m}[\ K_{se}(\theta_{joint} - \theta_{ce}) - f_{stim} \times f_{ata}(\theta_{ce}) \times f_{atv}(\dot{\theta}_{ce}) \times \tau_{scale}\ ] \tag{3.12}$$

$$\frac{d}{dt}\theta_{joint} = \dot{\theta}_{joint} \tag{3.13}$$

$$\frac{d}{dt}\dot{\theta}_{joint} = \frac{1}{J_{limb}}[\ -K_{se}\ (\theta_{joint} - \theta_{ce}) + \tau_{pta}(\theta_{joint}) + \tau_{ptv}(\dot{\theta}_{joint})\ ] \tag{3.14}$$

Adding the mass solves the numerical divide-by-zero problem, but increases the system order and adds an additional parameter for identification. This model structure retains the ability to predict the quick stretch response, but it does not solve the identification dilemma which exists due to the inaccessibility of θ_{ce} measurements.

Assuming an infinitely stiff SE makes identification of the active parameters feasi-

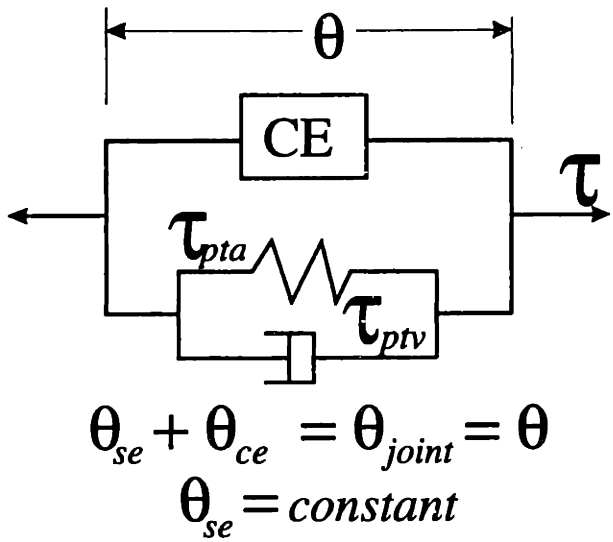

Figure 3-4: Active muscle model assuming an infinitely stiff SE. This assumption makes it possible to measure θ_{ce}.

ble and eliminates the divide-by-zero problem (Figure 3-4). This assumption simplifies the relationship between θ_{ce} and θ_{joint}, reducing it to a simple coordinate transformation, such that

$$\theta_{ce} = \theta_{joint} - \theta_{se}. \tag{3.15}$$

where θ_{se} is the fixed angle of the infinitely stiff SE. Now the contractile torque depends on joint angle and joint velocity

$$\tau_{active} = f_{stim}(u,t) \times f_{ata}(\theta) \times f_{atv}(\dot{\theta}) \times \tau_{scale} \tag{3.16}$$

$$where\ \theta = \theta_{joint}. \tag{3.17}$$

This model structure (Figure 3-4), with an infinitely stiff SE, was selected for the purposes of this thesis. By neglecting the series elastic element in this manner, the model cannot predict the quick stretch response of isolated muscle responding to a sudden application of force. This loss is not critical, since a quick-stretch is unlikely in the context of FES gait. Remember that the dynamics and force development characteristics associated with the SE are *not* lost, but lumped into the dynamics of the CE. Section 6.4 further explores this idea as it relates to identification of the CE

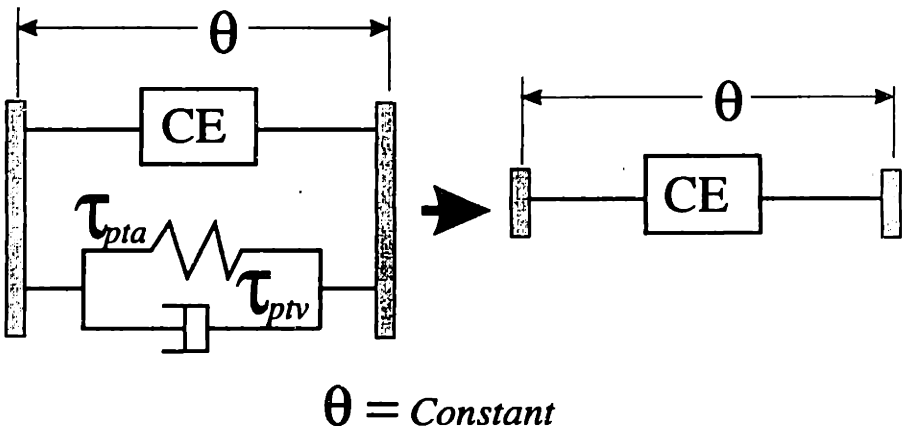

Figure 3-5: Isometric Model. The joint angle is fixed, so the joint velocity and acceleration are zero. The passive terms contribute a fixed torque to the isometric torque. The active f_{ata} and f_{atv} terms are also constant.

dynamics.

3.2 Isometric Muscle Properties

When the joint is held at a fixed joint angle, constant passive and active angle dependent and angular velocity dependent terms are produced and the complex joint-muscle model is reduced to a much simpler model (Figure 3-5). The following equations specify the output torque.

$$\tau_{joint} = \tau_{ce} + \tau_{passive} = C_0 \; f_{stim}(u,t) + C_1 \tag{3.18}$$

$$where, \quad C_0 = f_{ata}(\theta) \times f_{atv}(0) \times \tau_{scale} \tag{3.19}$$

$$and \quad C_1 = \tau_{pta}(\theta) \tag{3.20}$$

In this case, θ is the fixed joint angle and τ_{ptv} equals zero when there is no velocity. The *isometric* muscle model describes the muscle behavior under constant length conditions. In the joint-space representation, the term isometric refers to constant joint angle conditions. Hence, the stimulation dependent muscle property, $f_{stim}(u,t)$, represents the isometric joint-muscle model. A Hammerstein structure [47], which

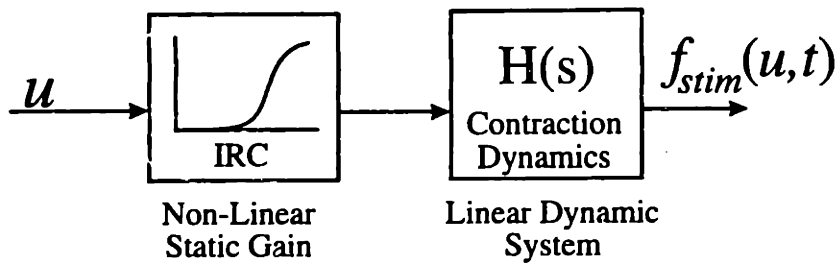

Figure 3-6: The Hammerstein structure is a non-linear static gain followed by a linear dynamic system. By separating the linear and non-linear blocks in this way, identification becomes easier.

consists of a non-linear static gain followed by a linear dynamic system models the isometric system (Figure 3-6). The non-linear static gain, termed the Isometric Recruitment Curve (IRC), measures the total isometric torque generated at a given stimulation level. The linear dynamic block represents the twitch response of the muscle. A second-order, critically-damped system with an impulse response of

$$h(t) = te^{-ta}, \tag{3.21}$$

is an acceptable model of isolated muscle [7, 34]. The parameter, a, completely defines the system. Such a simple model makes rapid parameterization easy. Higher-order, repeated-poles models are also identified by a single parameter. Of the higher-order, repeated-poles systems a third-order, repeated-poles model provides the best fit to the isometric impulse response of the intact muscle. Section 4.1 describes identification of this linear dynamic block and Section 6.2 describes the difference in fit between 2nd- and 3rd-order models.

3.3 Model Assumptions

Several critical assumptions should be kept in mind when evaluating the model's usefulness. These assumptions make the model suitably easy to parameterize while maintaining sufficient complexity to capture the essential features of the system. The most basic assumption made is that the multiplicative structure of the parallel con-

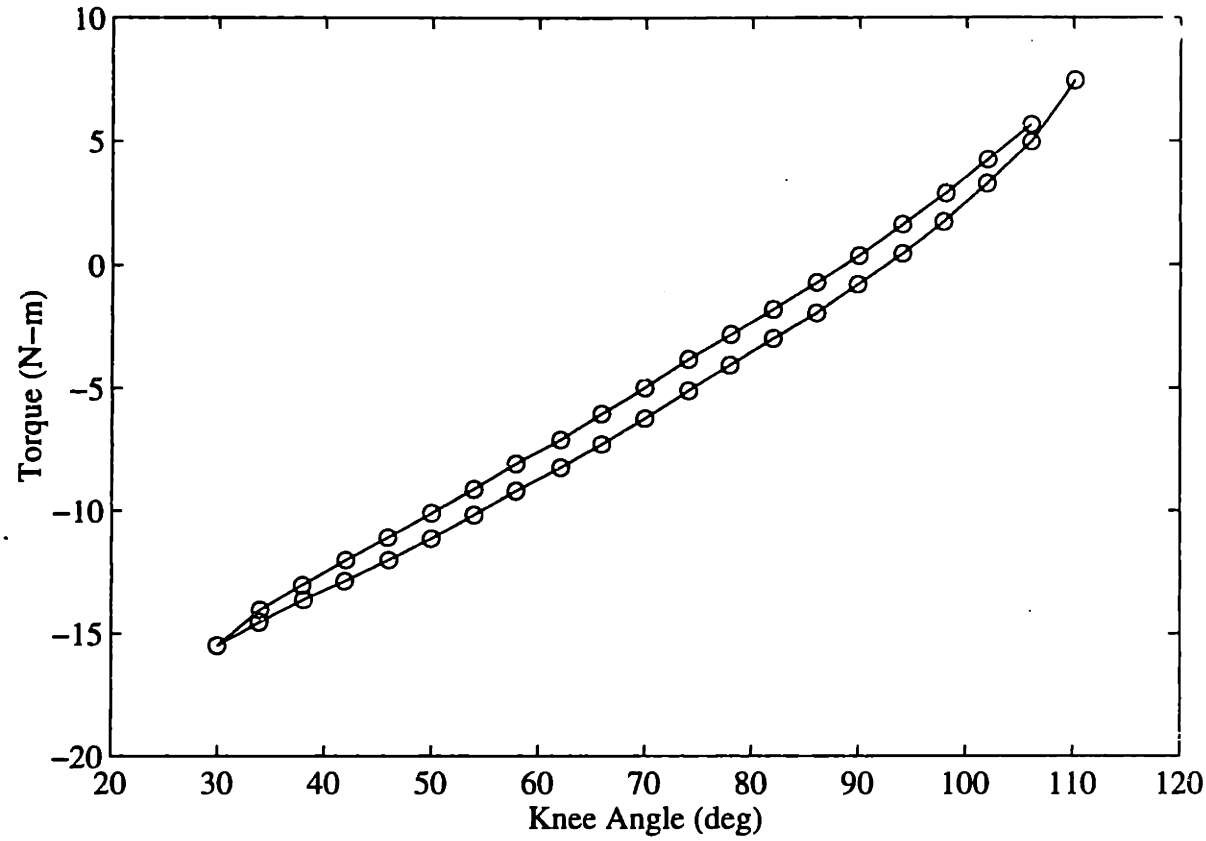

Figure 3-7: Hysteresis is observed in the passive torque-angle property. This curve was obtained from the knee joint of an able-bodied human.

tractile element is an appropriate description of the intact muscle-tendon-joint system. Although it appears similar to a Hill-type model, the model structure is not equivalent to a Hill-type lumped muscle model translated into joint space (see Appendix G). Previous work which justified use of a Hill-type model for isolated muscle [35] cannot confirm that this structure describes intact joints.

The model also assumes the independent passive relationships can be represented by functions of angle and angular velocity. This neglects hysteresis in the torque-angle relationship of passive muscle which has been observed in this study (Figure 3-7). Most bioelastic solids exhibit some form of hysteresis. Collagen, found in tendons and ligaments, displays considerable hysteresis at very low strain rates and may be the major source of hysteresis seen in the joint stiffness [40]. The effect of hysteresis on identification of the model is further explored in Section 6.6.

In this model, the shapes of the independent CE curves, torque-angle, f_{ata} and torque-velocity, f_{atv} do not change over the full range of joint angles, joint velocities, and stimulation level. Even in isolated muscle, it has been shown that these terms are somewhat coupled [67]; however the coupling is small and many researchers have used separated functions to describe this relationship. Identification is simplified by assuming a separable structure, and a wider range of control structures are possible with separable models.

The muscle contraction dynamics are independent of stimulation level. Many individual motor units make up a muscle. Each motor unit has its own contraction speed, dependent on fiber size, and activation threshold, which is largely dependent on the fiber location relative to the stimulation site. Depending on the level of stimulation, the number and type of active motor units varies. A conglomeration of the contraction of all these individual units produces the global contraction dynamics which may vary with stimulation level. In prior studies of isolated cat muscle, the variation in twitch dynamics with stimulation level was small [34]. Figure 3-8 shows the variation in twitch response measured for different impulse levels applied to the quadriceps muscle of an able-bodied human subject. This variation is also small.

The previous section discussed the infinitely stiff SE assumption. This assumption will receive additional attention in Section 6.4 of the results.

The proposed muscle model assumes stationary muscle properties. This assumption neglects fatigue [17, 49], tetanic potentiation [16, 18], and the physiologically changing properties of muscle. Over long periods of time, the muscle force properties change due to physiological changes in the muscle caused by exercise and other factors as well as repositioning of the electrodes [75]. Reparameterization of the system on a regular basis accounts for these day-to-day changes. Over short periods of time, the muscle properties also change due to fatigue [30]. External stimulation of the muscle produces a decay in force at a much higher rate than stimulation via the central nervous system (CNS). Rapid fatigue is a problem for FES applications, but the effect can be lessened by a more controlled use of stimulation.

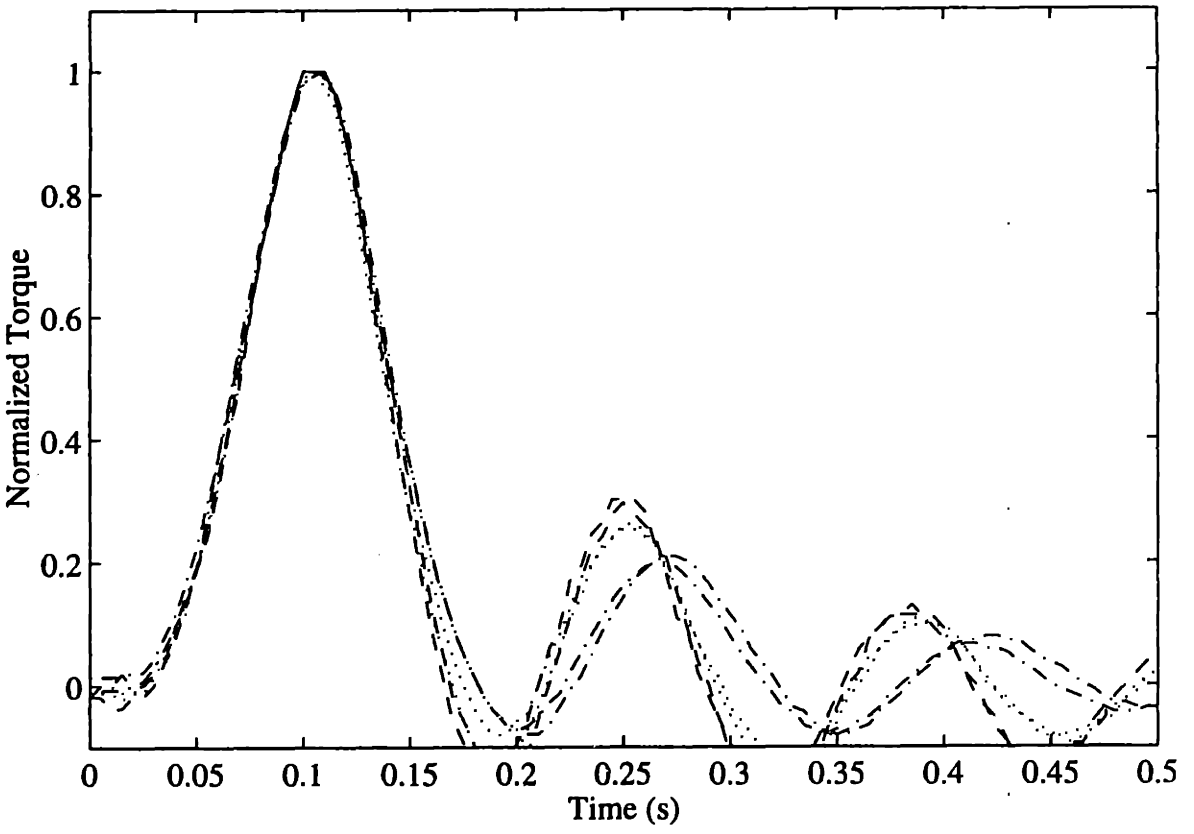

Figure 3-8: Variation in twitch response of able-bodied quadriceps muscle for stimulation levels of (−−) 30, (···) 35, and (− · −) 40 mA. Although the shapes change some, the peaks are the same and the shape variations are small.

3.4 Summary

Figure 3-9 shows the full muscle-tendon-joint model used in this thesis. In subsequent chapters it will be referred to as "the model" or the "full model" to distinguish it from other lumped parameter models which could be used to describe the muscle-joint mechanics. As described in Section 3.2 the full model reduces to the isometric

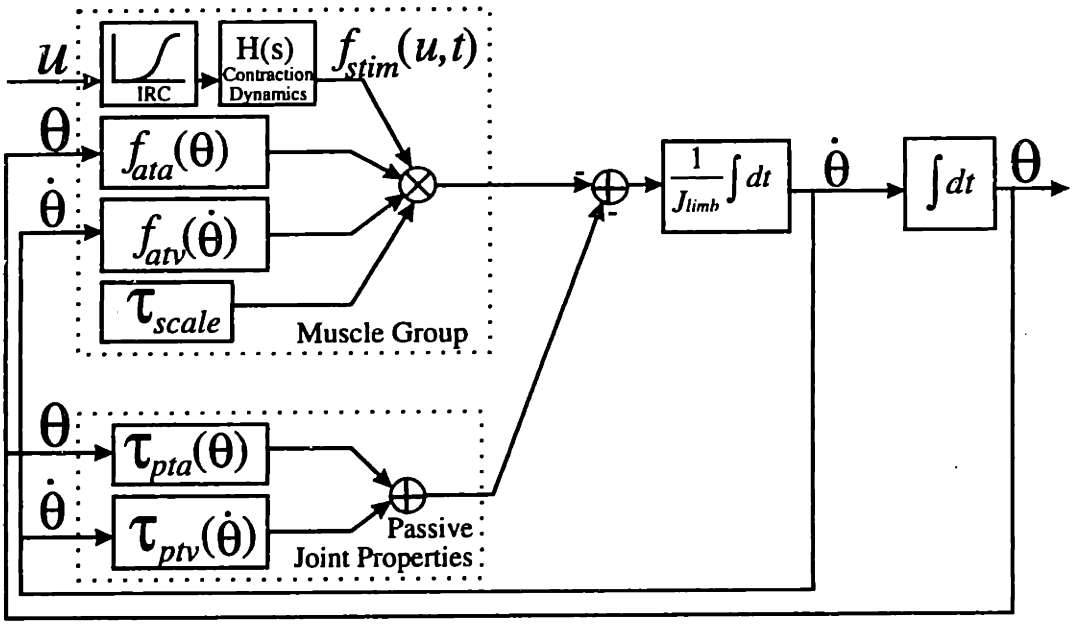

Figure 3-9: This block diagram of the full muscle-tendon-joint model shows the multiplicative structure of the active portion of the model and the parallel summation of the active and passive properties.

model (Figure 3-6) when the joint angle is held fixed. Piece-wise linear curves model all the functions $\tau_{pta}(\theta)$, $\tau_{ptv}(\dot{\theta})$, $f_{ata}(\theta)$, and $f_{atv}(\dot{\theta})$. Piece-wise linear curves are a good choice for modeling non-linear relationships of unknown shape, because, small line segments can approximate any curve without prior knowledge of the curve shape.

Table 3.1: Glossary of Symbols

Symbol	Definition	Refer To
θ or θ_{joint}	Joint angle. In this case, joint angle is measured in degrees of flexion with full extension equaling 0 degrees.	Fig. 3-1
θ_{ce}	Contractile element angle. The portion of the joint angle which is subscribed to the contractile element. This is a conceptual variable which does not have a true physical meaning.	Pg. 31
θ_{se}	Series elastic element angle. The portion of the joint angle which is subscribed to the series elastic element. In the full model, this angle is a constant.	Pg. 31
$\dot{\theta}$	Angular velocity. Without a subscript, this symbol refers to the angular velocity of the joint. Subscripts indicate other velocities.	Pg. 31
$\ddot{\theta}$	Joint angular acceleration	
τ_{pta}	Passive Torque-angle Relationship: non-linear passive stiffness in joint coordinates	Pg. 30 & 37
τ_{ptv}	Passive Torque-velocity Relationship: non-linear passive damping in joint coordiantes	Pg. 30
J_{limb}	Limb Inertia.	Fig. 3-1
$\tau_{passive}$	Passive Torque. One of two parallel branches of the model. Sum of passive torques (τ_{pta}, τ_{ptv} and the inertial torques).	Pg. 54
$\tau_{net\ joint}$	The net torque, or applied torque, about the joint. This can be measured by a torque sensor. The net torque is non-zero if the limb is moved by external forces, like a motor.	Pg. 47
IRC	Isometric Recruitment Curve: Non-linear static gain. Dependent on stimulation amplitude input. Traditionally, it is a measure of the isometric torque output in response to stimulation level.	Pg. 35
Contractile Element (CE)	The torque generating element of the active branch of the model. Physically, it relates to the actin/myosin filaments of muscle which produce muscle force, but in this model the underlying mechanics are not considered.	Pg. 31

Table 3.1 (continued)

Symbol	Definition	Refer To
Series Elastic Element (SE)	Non-linear stiffness placed in series with the contractile element. It can be thought of as a model of the tendon, but there is some series compliance in actual muscle also. This element was assumed infinitely stiff for purposes of this modeling project.	Pg. 31
K_{se}	Non-linear series elasticity of the series elastic element.	Pg. 32
$f_{stim}(u,t)$	Non-linear stimulation dependent muscle dynamics. This term is produce by cascading the output of the IRC with the linear contraction dynamics.	Pg. 35
f_{ata}	Active Torque-angle Relationship: non-linear active muscle stiffness in joint coordinates. Part of the multiplicative structure of the contractile element.	Pg. 106
f_{atv}	Active Torque-velocity Relationship: non-linear damping active muscle, measured in joint coordiantes. Part of the multiplicative structure of the contractile element.	Pg. 107
τ_{scale}	Active Torque scaling factor or static gain: Part of the mutiplicative structure of the contractile element.	Pg. 31
τ_{active} or τ_{ce}	Active Torque or Contractile Element Torque. Model branch parallel to the passive torque. It is produced by the contractile element and is a multiplicative combination of f_{stim}, f_{ata}, f_{atv}, and τ_{scale}.	Eq. (3.1)

Chapter 4

Identification Algorithms

This chapter describes the theoretical basis for and implementation of the parameter identification algorithms. By controlling the stimulation input and/or kinematic trajectory (θ,$\dot{\theta}$, and $\ddot{\theta}$) various portions of the model can be isolated for identification.

4.1 Isometric Muscle Identification

At a constant fixed joint angle, the model reduces to a stimulation dependent term which can be modeled by a Hammerstein structure (Figure 3-6). The linear dynamic block represents the contraction dynamics or twitch response of the muscle. All the dynamic information in this block appears in the impulse response of the system. This research explored both a second-order, critically-damped model and a third-order repeated poles model. For a second-order, critically-damped model, the response to an impulse is

$$h_2(t) = t\ e^{-a_2 t} \tag{4.1}$$

The system poles, a_2 are easily found from the peak of the response.

$$a_2 = \frac{1}{t_{peak}}. \tag{4.2}$$

A second-order model of contraction dynamics is common in the literature [11, 12, 14, 62]. Initial results showed that the second-order, critically-damped model was

not a particularly good fit to the impulse response of human quadriceps muscle, so third-order dynamics were also explored. The impulse response for the third-order, repeated-poles model is

$$h_3(t) = t^2\, e^{-a_3 t} \tag{4.3}$$

with the poles located at

$$a_3 = \frac{2}{t_{peak}}. \tag{4.4}$$

Cross plotting the output of the static nonlinear gain with the input produces the isometric recruitment curve (IRC). The Hammerstein structure allows several methods for estimating the output of the IRC block by taking advantage of the linear property of the dynamic block. Step, impulse, and ramped inputs are all potential methods to estimate the shape of the IRC.

4.1.1 Step Response Method

The step response method is the generally accepted means of identifying the IRC [6, 25, 26, 32, 34]. With this method, a step in stimulation amplitude activates the muscle for a period of time long enough to allow the linear dynamic block to reach steady-state. The steady-state torque is related to the IRC output by a simple gain. Cross plotting the steady-state torque with the stimulation amplitude produces the shape of the IRC. This simple method tends to fatigue the muscle. To prevent fatigue, the step response method requires considerable rest between stimulation bursts.

4.1.2 Impulse Response Method

The impulse response method is also a point by-point method for generating an IRC [34, 76]. A single stimulation pulse applied to the system produces a twitch. Plotting the resulting peak torque against the input amplitude produces the IRC shape. This non-fatiguing method does not require long rest periods, so multiple data points can be generated in a short period of time. For linear contraction dynamics, the normalized IRC generated by the impulse response method will be identical to that

generated by the step response method. For the muscle system, which has some non-linearity, the accuracy of the method will depend on the severity of the response non-linearity.

4.1.3 Ramped Inputs

A ramped amplitude stimulation pattern applied to the system generates a continuous response to a range of stimulation amplitudes [3, 91, 39]. Direct plotting of the response signal against the input signal does not produce the IRC because the contraction dynamics contaminates the response. A long slow ramp should result in a near perfect IRC without post-processing, since the muscle dynamics would not be excited; however, fatigue exists with long ramp times. To produce an IRC with acceptable accuracy requires a fast ramp time and post-processing to remove the effects of the dynamic block. The following sections discuss three possible post-processing methods: correlation, deconvolution with an ideal impulse response, and deconvolution with an averaged impulse response.

Correlation

The first post-processing method involves computation of the correlation between input and response. The dynamics are modeled as a pure signal delay equal to the time at which the correlation between input, $u(t)$, and output, $r(t)$, is a maximum. The correlation is defined as:

$$Corr(u,r) = \int_{-\infty}^{\infty} u(\tau + t)\ r(\tau) d\tau, \tag{4.5}$$

where $r(t)$ and $u(t)$ represent the system response and input respectively. This function is often called the *lag*. The time of maximum correlation represents the delay between the input and response. Shifting the response by the delay time and cross plotting against the input produces the IRC. This is essentially equivalent to lining up the peaks of the input and output and cross-plotting the data, but the correlation method can shift the data even when the response curve has an indistinct peak.

Deconvolution

For known linear system dynamics, $h(t)$, deconvolution of the response $r(t)$ removes the dynamics from the system response and recovers the output of the IRC, $s(t)$ [34]. The convolution integral is defined as:

$$r(t) = s * h \equiv \int_{-\infty}^{\infty} s(\tau)h(t-\tau)d\tau. \tag{4.6}$$

In the frequency domain, the convolution integral is equivalent to multiplication.

$$s * h \Longleftrightarrow S(f)H(f) = R(f). \tag{4.7}$$

To perform deconvolution, an FFT transforms the time response into the frequency domain. The frequency representation of the system estimate divides the transformed response and produces a frequency representation of the dynamic system input

$$S(f) = \frac{R(f)}{H(f)}. \tag{4.8}$$

The inverse FFT of $S(f)$ cross-plotted against the stimulation input estimates the IRC. This process is sensitive to measurement noise and to the accuracy of the system estimate. In addition, numerical divide by zero errors can occur during the frequency domain division. Two different system estimates are used for the deconvolution.

The first deconvolution method uses an ideal second-order, critically-damped estimate of the system. The peak time of the impulse response defines the system poles as described in the beginning of this section. Because the ideal impulse does not exactly match the experimental impulse response, some error is expected from this method.

The second deconvolution method uses the averaged impulse responses as an estimate of the system dynamics. This improves the system estimate to include all the dynamics. Linear system theory shows that the impulse response contains all of the dynamic information about a linear system. Deconvolution is a linear process which works properly only on linear systems. If significant non-linearities exist in the

dynamics, this method will produce erroneous results.

4.2 Passive Identification Algorithms

The passive model properties include passive torque-angle, $\tau_{pta}(\theta)$, passive torque-velocity, $\tau_{ptv}(\dot{\theta})$, and the limb inertia, J_{limb}. For zero stimulation input, only the passive properties contribute to the overall joint torque. The following equation describes the dynamics of the motion when the limb is forced to move through a fixed kinematic trajectory.

$$\tau_{netjoint} = J_{limb}\,\ddot{\theta} + \tau_{ptv}(\dot{\theta}) + \tau_{pta}(\theta). \tag{4.9}$$

Sections 4.2.1 through 4.2.3 describe three methods for identifying passive properties: sequential identification, simultaneous linear estimation, and free swing identification.

4.2.1 Sequential Identification

The position, velocity and acceleration dependent terms can be identified sequentially beginning with the torque-angle properties. If the limb is moved to a fixed position and held there long enough for the transient dynamics to die away, the velocity and acceleration terms become zero and Equation (4.9) reduces to

$$\tau_{netjoint} = \tau_{pta}(\theta). \tag{4.10}$$

The static net joint torque measured at several positions over the full range of joint angles creates the torque-angle curve. The limb is then moved with a constant angular velocity. Under this zero acceleration condition Equation (4.9) becomes

$$\tau_{net\ joint} = \tau_{ptv}(\dot{\theta}) + \tau_{pta}(\theta). \tag{4.11}$$

Rearranging the terms gives

$$\tau_{ptv}(\dot{\theta}) = \tau_{net\ joint} - \tau_{pta}(\theta). \tag{4.12}$$

Finally, the inertia was estimated from measurements of the subject weight, w in kilograms and limb length, l in meters [84].

$$J_{limb} = (0.061w)(0.735l)^2 \tag{4.13}$$

This equation calculates the limb mass as a fixed percentage of the total body mass. Likewise, the radius of gyration is designated as a fixed percentage of the distance between body landmarks. For the shank and foot, the landmarks are the femoral condyles and the medial malleolus.

4.2.2 Simultaneous Linear Estimation

The position-, velocity- and acceleration-dependent passive torque components can be fit simultaneously using a single data set, through least squares fitting. This process determines a good fit by minimizing the square of the error between the measured and fit data. Implementing the least squares fitting solution in matrix format uses singular value decomposition. The following sections describe the general process and specific formulation of the problem for simultaneous fitting to the piece-wise linear curves, $\tau_{pta}(\theta)$ and $\tau_{ptv}(\dot{\theta})$, and the inertia.

Description of general linear least squares

The general linear least squares algorithm fits a set of measured data points, $(x_i, y_i), i = 1, \ldots, N$ to any number of functions of x. Equation (4.14) expresses this model:

$$\hat{y}(x) = \sum_{k=1}^{M} c_k X_k(x) \tag{4.14}$$

where $X_1(x), \ldots, X_M(x)$ are arbitrary fixed functions of x. These basis functions can be non-linear. The process finds a set of parameters, $c_1, \ldots, c_M$, to minimize the error between the measured data y and the predicted data $\hat{y}$. The merit function is defined as:

$$\chi^2 = \sum_{i=1}^{N} \left[\frac{y_i - \sum_{k=1}^{M} c_k X_k(x)}{\sigma_i} \right]^2 \tag{4.15}$$

where, σ_i is the measurement error of the ith data point. In this case all of the points have the same measurement error, so σ can be set to 1. For a given set of basis functions, the set of linear parameters which minimizes χ^2 produces the best fit to the model based on least squares error.

This minimization problem can be solved by matrix techniques. The M basis functions evaluated at each of the N independent data points, $x_1 - x_N$, make up an $N \times M$ design matrix A with

$$A_{ij} = X_j(x_i) \qquad 1 \leq i \leq N, \quad 1 \leq j \leq M. \tag{4.16}$$

The N dependent data points, $y_1 - y_N$, define a vector b

$$b_i = y_i. \tag{4.17}$$

The vector $\bar{c}$ contains the M parameters, $c_1, \ldots, c_M$. In matrix form, the minimization equation becomes

$$\chi^2 = |A \cdot \bar{c} - b|^2 . \tag{4.18}$$

General least squares fitting is appropriate for identification where a limited set of data is to be processed and on-line identification is not needed. For extremely large data sets or real-time identification, recursive least squares fitting is also appropriate.

Solution by singular value decomposition

Even in the presence of matrix singularities or near singularities, singular value decomposition can solve matrix equations, like the one in Equation (4.18) and is the method of choice for solving most linear least squares problems [66].

The following linear algebra theorem explains the basis for singular value decomposition: Any $N \times M$ matrix A can be written as a product of an $N \times M$ column-orthogonal matrix U, an $M \times M$ diagonal matrix W with positive or zero elements (the singular values), and the transpose of an $M \times M$ orthogonal matrix V.

$$A = U \cdot W \cdot V^T \tag{4.19}$$

Matrices U and V are othogonal in the sense that

$$\begin{aligned} U^T \cdot U &= I_N \\ \text{and} & \\ V^T \cdot V &= I_M \end{aligned} \tag{4.20}$$

Systematic application of a series of Householder Transformations and Givens Rotations quickly finds the matrix W and appropriate matrices U and V. These matrix manipulations produce equivalent matrices with zero elements at selected matrix positions. Most linear algebra texts describe these procedures in detail [36, 43, 59, 83].

With the matrix W known, the original problem

$$A \cdot \bar{c} \doteq b \tag{4.21}$$

can be replaced by the equivalent problem

$$\begin{bmatrix} W \\ 0 \end{bmatrix} p \doteq g \tag{4.22}$$

where

$$g = U^T \cdot b \tag{4.23}$$

and

$$\bar{c} = V \cdot p. \tag{4.24}$$

Since W is a diagonal matrix, Equation (4.22) breaks up into three types of equations

which depend on the dimensions N and M and the number of non-zero singular values:

$$\begin{aligned} w_j p_j &= g_j, \quad \text{if } j \leq n \text{ and } w_j \neq 0, \\ 0 \cdot p_j &= g_j, \quad \text{if } j \leq n \text{ and } w_j = 0, \\ 0 &= g_j, \quad \text{if } j > M. \end{aligned} \tag{4.25}$$

An exact solution exists only if $g_i = 0$ whenever $w_i = 0$ or $j > M$. If an exact solution does not exist, then the best solution minimizes the error. If some of the singular values are zero, then the minimization is not unique. In this case, the solution which produces the shortest length p vector is often desirable. So

$$p_i = 0, \quad \text{if } w_i = 0 \text{ or if } j > M. \tag{4.26}$$

In practice, singular values which are not exactly zero also cause problems finding the p vector. If the singular value w_i is small (less than N times the precision of the machine) p_i should be set to zero [66]. Once the vector p has been found, the parameter vector $\bar{c}$ is recovered by Equation (4.24).

Specific formulation for piece-wise linear curves and the muscle-tendon-joint model

To formulate the linear least squares fitting problem specifically for the identification application required here, the basis functions must be defined. Piece-wise linear curves are used to model both the passive torque-angle and torque-velocity curves. To understand this implementation, consider the full range of a given independent variable, x, divided into $M - 1$ smaller ranges. A set of values, $\tilde{x}_j : j = 1, \cdots, M$, define the end points of the smaller ranges. For each range, the corresponding c_j's define a linear segment. The selected c_j's produce the best fit of $y_i(x_i)$ for all x_i in the range $(\tilde{x}_j, \tilde{x}_{j+1}]$.

$$\hat{y}_i(x_i) = \sum_{j=1}^{M-1} \left(\frac{c_{j+1} - c_j}{\tilde{x}_{j+1} - \tilde{x}_j} \cdot [x_i - \tilde{x}_j] + c_j \right) \cdot \delta_j(x_i) \tag{4.27}$$

where:

$$\delta_j(x) = \begin{cases} 1 & \text{if } \tilde{x}_j < x \leq \tilde{x}_{j+1} \\ 0 & \text{else.} \end{cases} \tag{4.28}$$

Rearranging Equation (4.27) gives an equation form linear in c_j

$$\hat{y}_i(x_i) = \sum_{j=1}^{M-1} c_{j+1} \cdot \frac{x_i - \tilde{x}_j}{\tilde{x}_{j+1} - x_j} \cdot \delta_j(x_i) + \sum_{j=1}^{M-1} c_j \cdot \left[1 - \frac{x_i - \tilde{x}_j}{\tilde{x}_{j+1} - x_j}\right] \cdot \delta_j(x_i), \tag{4.29}$$

which reveals the basis functions to be:

$$X_j(x_i) = \begin{cases} 1 - \frac{x_i - \tilde{x}_j}{\tilde{x}_{j+1} - x_j} & \text{if } \tilde{x}_j < x_i \leq \tilde{x}_{j+1} \\ \frac{x_i - \tilde{x}_j}{\tilde{x}_{j+1} - x_j} & \text{if } \tilde{x}_{j-1} < x_i \leq \tilde{x}_j \\ 0 & \text{else.} \end{cases} \tag{4.30}$$

For the muscle-tendon-joint model application, the passive model equation depends on three variables: angular position, velocity and acceleration. For this specific multivariable application, the model equation becomes:

$$\hat{\tau}_{net\ joint_i}(\theta_i, \dot{\theta}_i, \ddot{\theta}_i) = \sum_{j=1}^{M_\theta} c_j X_j(\theta_i) \ + \sum_{j=M_\theta+1}^{M_\theta+M_{\dot{\theta}}} c_j X_j(\dot{\theta}_i) \ + \ J_{limb}\ddot{\theta}_i. \tag{4.31}$$

Equation (4.30) defines each basis function, X_j. $M_\theta - 1$ segments describe $\tau_{pta}(\theta)$ and $M_{\dot{\theta}} - 1$ segments describe $\tau_{ptv}(\dot{\theta})$. A single constant parameter J_{limb} models the inertia, so the total number of passive parameters is $M_\theta + M_{\dot{\theta}} + 1$.

Generating/choosing appropriate inputs

To accurately identify all of the terms described in the previous section, the algorithm requires a kinematic input which spans the position-velocity space. A truly random trajectory is not necessary, but the trajectory must cover the full position and velocity ranges. A sum of six sine waves with random (although limited) frequency and phase was used to generate pseudo-random, bandwidth limited kinematic trajectories. Filtered white noise signals also produce acceptable trajectories; however, the sum of sines formulation allows analytic computation of the velocity and acceleration

resulting from a given position trajectory. This makes it easier to ensure coverage of the position-velocity space.

4.2.3 Free Swing Identification

For a freely swinging limb released from some non-zero initial condition, the net torque about the joint is zero. The following equation describes the dynamics of free swing:

$$0 = J_{limb}\,\ddot{\theta} + \tau_{ptv}(\dot{\theta}) + \tau_{pta}(\theta). \tag{4.32}$$

The linear estimation techniques described for the simultaneous estimation method can estimate the passive properties under these free swing conditions as well. In this case, Equation (4.32) is underconstrained because of the zero net joint torque. The estimation algorithm cannot distinguish between Equation (4.32) and a scaled version of the equation such as:

$$0 = \ddot{\theta} + \frac{1}{J_{limb}}\tau_{ptv}(\dot{\theta}) + \frac{1}{J_{limb}}\tau_{pta}(\theta). \tag{4.33}$$

To produce the proper scale for the parameters, at least one parameter must be known. τ_{pta}, found from the sequential identification, was assumed to be known and the remaining parameters were fit to the equation

$$-\tau_{pta}(\theta) = J_{limb}\,\ddot{\theta} + \tau_{ptv}(\dot{\theta}). \tag{4.34}$$

The model equation for the free swing condition is

$$-\hat{\tau}_{pta_i}(\theta_i) = \sum_{j=1}^{M_{\dot{\theta}}} c_j X_j(\dot{\theta}_i) + J_{limb}\ddot{\theta}_i \tag{4.35}$$

and the number of parameters to fit is $M_{\dot{\theta}} + 1$.

4.3 Active Identification

The active model properties include active torque-angle, $f_{ata}(\theta)$, and active torque velocity, $f_{atv}(\dot{\theta})$. These properties combine multiplicatively with the stimulation dependence to form the active torque contribution from a given stimulation channel. To identify these properties, the limb must move through a kinematic trajectory which covers the angle-angular velocity phase plane while stimulating the muscle.

Under these conditions, the passive torque are computed based on the kinematic data.

$$\tau_{passive} = J_{limb}\ddot{\theta} + \tau_{ptv}(\dot{\theta}) + \tau_{pta}(\theta). \tag{4.36}$$

The stimulation input, modulated by the active properties, produces the active torque

$$\tau_{active} = f_{stim}(u,t) \times f_{ata}(\theta) \times f_{atv}(\dot{\theta}) \times \tau_{scale}, \tag{4.37}$$

so that the full dynamic description of the moving limb is:

$$J_{limb}\ddot{\theta} + \tau_{ptv}(\dot{\theta}) + \tau_{pta}(\theta) = - f_{stim}(u,t) \times f_{ata}(\theta) \times f_{atv}(\dot{\theta}) \times \tau_{scale}. \tag{4.38}$$

Dividing the passive term by the contraction dynamics and taking the log of the result reformulates the problem so the active terms combine in summation.

$$log(\frac{-\tau_{passive}}{f_{stim}(u,t)}) = log(f_{ata}(\theta)) + log(f_{atv}(\dot{\theta})) + log(\tau_{scale}). \tag{4.39}$$

The same linear estimation techniques described in section 4.2.2 can identify f_{ata} and f_{atv} with this model formulation if we assume that the functions are made up of piece-wise linear curves in the log domain. The model equation in this case is:

$$log(\frac{-\hat{\tau}_{passive}}{f_{stim}(u,t)}) = \sum_{j=1}^{M_\theta} c_j X_j(\theta_i) + \sum_{j=M_\theta+1}^{M_\theta+M_{\dot{\theta}}} c_j X_j(\dot{\theta}_i) + log(\tau_{scale}). \tag{4.40}$$

and the number of active parameters is $M_\theta + M_{\dot{\theta}} + 1$. The basis functions are defined as piece-wise linear curves in the log domain, and they have the same form as the

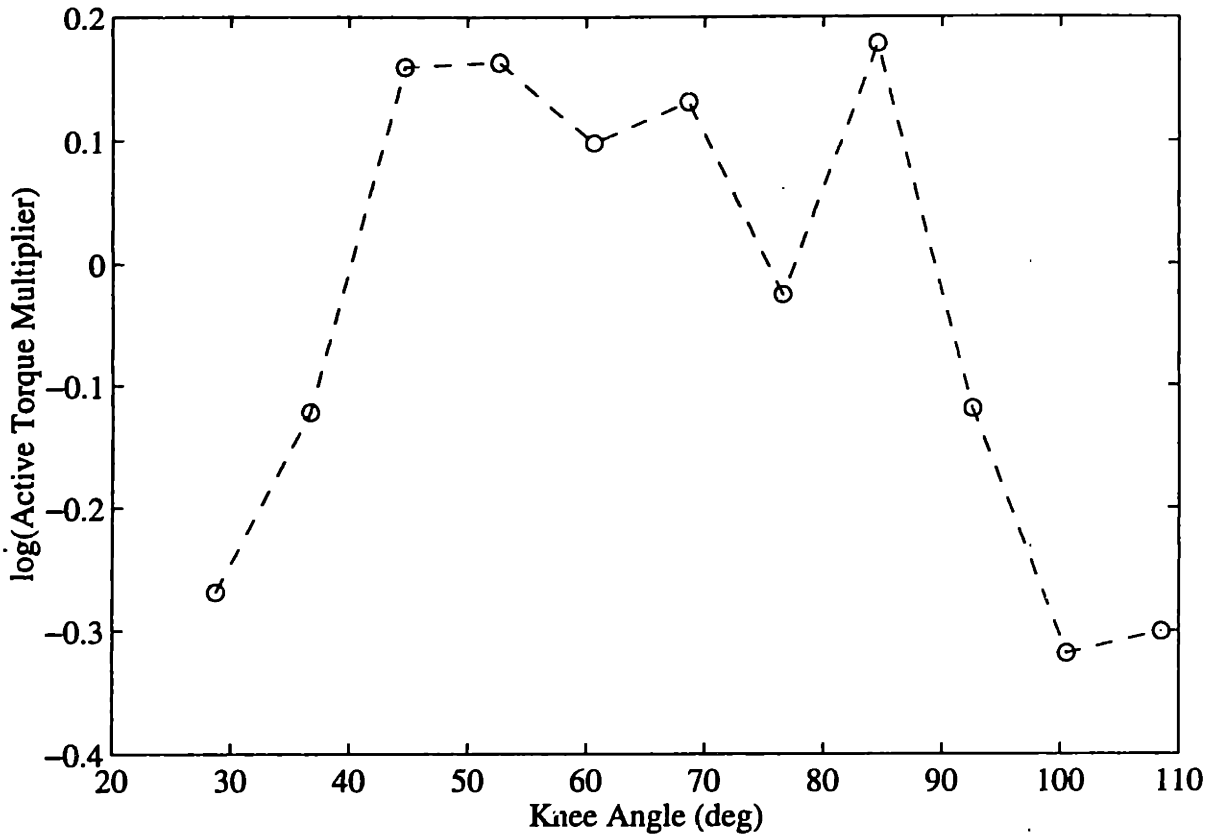

Figure 4-1: (o) Active torque-angle parameters identified in the log domain. (−−) Piece-wise linear curves used as basis function in the log domain.

basis functions described in Equation (4.30). Once the parameter vector c has been found in the log domain, the parameters can be returned to the real number domain by taking the inverse log of each parameter. It should be kept in mind that fitting to line segments in the log domain is not the same as fitting to line segments in the real domain. Instead, it is akin to fitting to exponential segments in the real domain. If the estimating segments are short, the difference between a true line segment and an exponential is quite small. Figures 4-1 and 4-2 give a clearer picture of what is happening. Figure 4-1 shows the active torque-angle parameters identified in the log domain for a single individual. The piece-wise linear segments connecting these points define the functions which minimized the fitting error in the log domain. Figure 4-2 shows the active torque-parameters after they have been returned to the real domain. The dashed lines connecting the parameters represent the actual functions which were

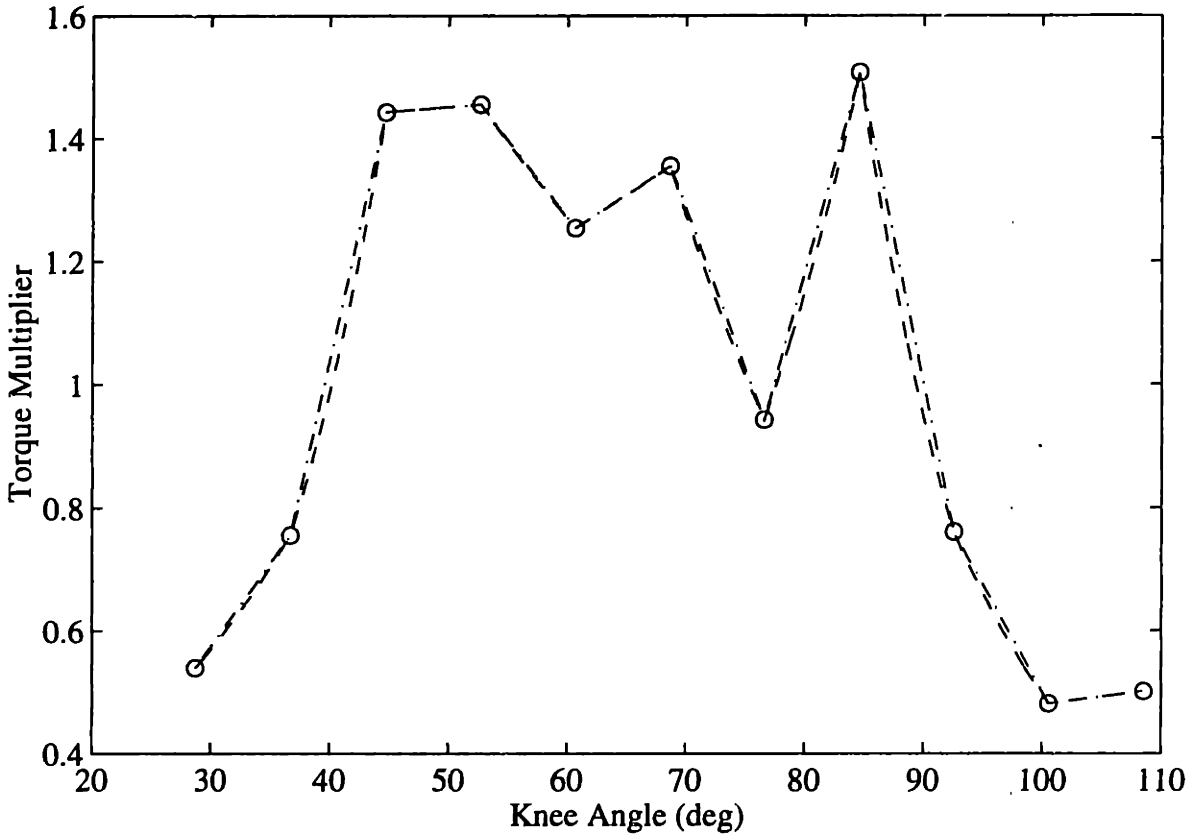

Figure 4-2: (o) Active torque-angle parameters transformed into the real domain by taking the inverse log of the identified parameter vector. (−−) Basis functions transformed into the real domain. (− · −) Piece-wise linear approximation to the fitted basis functions. A small amount of error is introduced by this approximation.

used to fit the data in the log domain. The dash-dot lines are piece-wise linear curves connecting the parameters in the real domain. The difference between the actual minimizing basis functions and the piece-wise linear curves is quite small. For ease of computation, these piece-wise linear approximations of the basis functions were actually used to interpolate between the parameters for simulation purposes. A very small amount of error is introduced by this approximation, and it is especially small when compared to errors due to data compression and signal noise.

Chapter 5

Experimental Methods

The experiments described in this chapter parameterize the muscle-tendon-joint model, presented in Chapter 3, for the quadriceps muscle-knee joint system. The previous chapter presented the theoretical basis for these experiments. The knee joint and quadriceps muscle of able-bodied human subjects served as the test bed for the parameterization techniques and the model structure.

Several factors made the knee joint a better system choice for these experiments than other joints in the body. The research goal is to restore function to the lower limbs, so the leg joints were of primary interest. The three joints in the lower limb, the hip, knee and ankle are all used in gait. The ankle contributes little to the swing phase of gait other than insuring that the foot does not scrape the floor during swing phase. Without muscular control of the ankle, foot drop can be easily prevented with an ankle-foot orthosis. Both the hip and the knee are important during the dynamic, swing-phase of gait. The principle hip flexors, the iliopsoas group, are deep muscles which are inaccessible with surface stimulation. The principle knee flexors, the quadriceps group, and extensors, the hamstrings, are both accessible with surface stimulation. Because the hip is a multidegree of freedom joint while the knee is primarily single degree of freedom, the knee is a simpler system. In addition, it is much easier to fix the hip and move the knee than vice-versa. These practical considerations determined the choice of the knee joint for experimental study.

Three experimental protocols were used to explore parameterization techniques.

The first two experiments examined the isometric muscle properties and methods to parameterize the contraction dynamics and the isometric recruitment curve. The first of these isometric experiments compared IRC estimation by five different techniques: step response, impulse response, and 3 ramp response methods. Based on results from this experiment, a second isometric experiment compared the IRCs estimated from the step response method and the ramp correlation method for isometric torque prediction. This experiment also examined 2nd- verses 3rd-order estimates of the contraction dynamics. The final experiment estimated parameters for the full non-isometric muscle-tendon-joint model (Figure 3-9), using ramp correlation to estimate the IRC and a 3rd-order, repeated-poles model of the contraction dynamics.

5.1 Equipment

Figure 5-1 shows the experimental set-up common to all the experiments described in this chapter.

The set-up consists of a custom made instrumented knee bench, a computer, an electrical stimulator, and a motor electronics box.

An IBM compatible 33MHz 386 computer performed control and data acquisition for the experiments through an Analog Devices 12 bit RTI-815A I/O card. The A/D channels accepted inputs ranging from +/-10V over a digital range of -2048 to +2047. The two D/A channels set the stimulator amplitude and triggered the stimulation pulses.

Park [65] and Hausdorff [45] originally built the knee bench as a tool for testing strategies to control knee position. During the present experiments, the subject sat or reclined on the bench platform. Two rigid plates and velcro straps secured the subject's shank to a brace. The knee rotation center was aligned with a large gear which served as the rotation center of the brace (Figure 5-2). To minimize unwanted movement, velcro straps secured the thigh to the bench. Hard limit stops on the gear prevented the limb from hyperextending or flexing to an extreme. The range of motion extended from 10 degrees to 110 degrees of knee flexion.

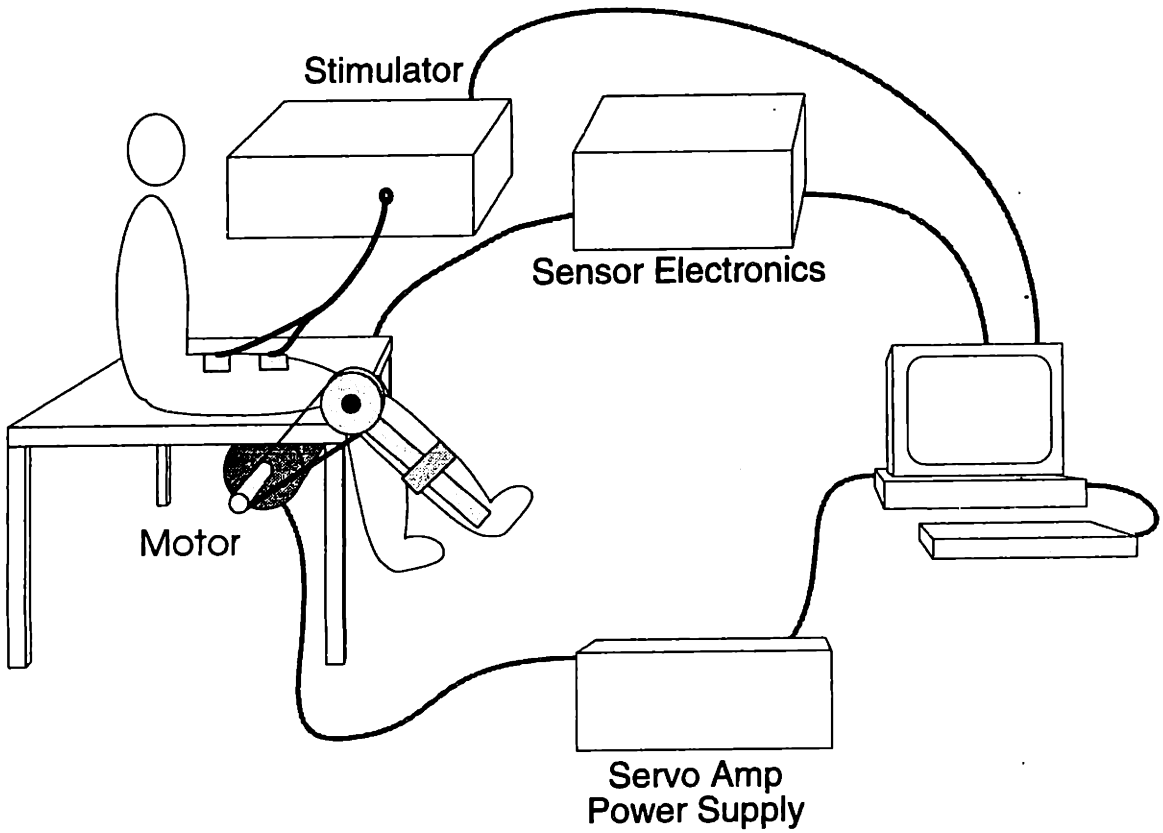

Figure 5-1: The Experimental set-up consists of a bench; position, velocity and torque transducers at the knee joint; a computer; an electrical stimulator; a motor; and electronics to drive the motor.

An Omnitech Robotics model MC3628 motor controller card and an Electro-Craft 0643-03-003 DC brush motor controlled the motion of the knee. The motor was fitted with a Bayside NEMA 42 planetary gear head with 20:1 gear reduction and low backlash. An Oldham style coupler connected the output shaft of the gear head to a second shaft. This coupler made it easy to disconnect the motor from the rest of the system and allow the leg to swing freely. A timing belt (Stock Drive steel reinforced cable designed for low backlash) transmission coupled this second shaft to the brace gear with a 4:1 reduction. The maximum output torque of the motor, 0.625 N-m, provided 50 N-m of torque at the knee. An Omnitech Robotics 6-80 pwm servo amp connected to an Omnitech Robotics PS 300W-72V DC power supply, activated

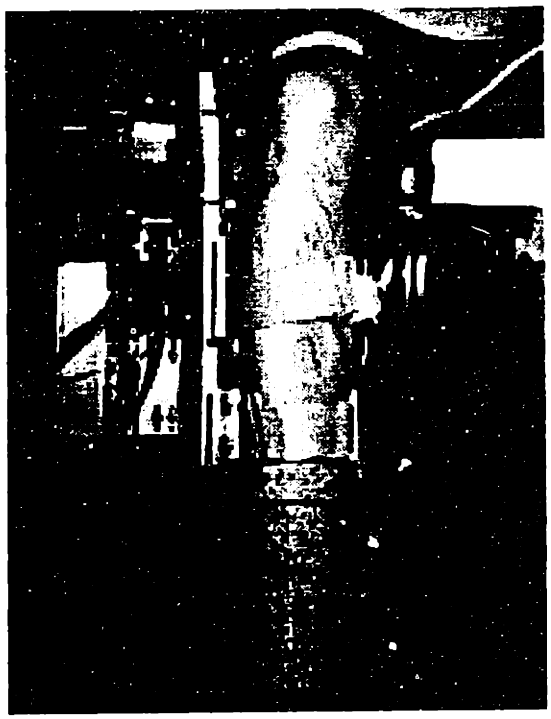

Figure 5-2: The knee joint is aligned with the brace joint and secured to rigid plates by velcro straps.

the motor. Appendix A shows a schematic of the relevant circuitry. Limit switches prevented the motor from forcing the limb against the mechanical limit stops. A large red Emergency stop button was placed next to the subject to cut power to both the motor and the stimulator with a single action.

The bench was equipped with torque, position, velocity, and acceleration sensing capabilities. The strut of the brace was instrumented with Micromeasurement WA series 1/2 bridge strain gauges with each arm at 120 ohms. An Analog Devices 2B31K chip filtered and amplified the output of the strain gauges such that 1 digital unit equaled 0.0381 N-m. The A/D could measure a maximum of 78 N-m without saturation. To calibrate the strain gauges, the strut was locked in the horizontal position and weights of known mass were hung on the end of the strut, 0.33m from the joint center.

A potentiometer (Venitron 8190 5K, 1 % linearity, continuous turn), coupled to the motor shaft through a small timing belt, measured the angular position of the

joint. One potentiometer rotation equaled 120 degrees of knee rotation. Calibration of the position sensor was done with a plumb line hung at the center of the brace joint and a protractor to measure the angle of the strut. Appendix C shows the potentiometer calibration curve.

A timing belt connected the motor shaft to a Harowe 1211-003 P.M. DC tach generator with an output of 20.8 V/krpm. This tachometer had significant phase delay at low velocities, so it was not used in these experiments. Instead, post-processing of the position signal with a generalized cross-validation method for spline fitting smoothed the potentiometer signal and simple difference differentiation produced the velocity [29, 86].

A Sensotec Model JTF (AG111; +/- 10 g) accelerometer placed on the subject's calf approximately 11 inches from the rotation center of the joint measured acceleration. The sensor was not mounted on the brace, because vibration of the beam corrupted the acceleration signal. The active direction of the sensor corresponded to the direction tangential to rotation. The actual distance from the joint to the sensor was measured with a ruler, recorded on the data sheet (see Appendix E) and used to scale the linear acceleration signal to the appropriate angular acceleration measurement. An Analog Devices IB31 Wide Bandwidth Strain Gage Signal Conditioner conditioned and amplified the accelerometer signal. Because the accelerometer was not mounted in the horizontal plane, the signal had to be compensated for the effects of gravity. The accelerometer response to gravity was determined before each experimental session by using the motor to servo the limb to a fixed angular position and recording the position and acceleration signals (see Appendix C for a typical calibration curve). This calibration table was used to remove the effect of gravity from the signal during the experiments.

Chesler [19] designed and built the electrical stimulator used for these experiments. Appendix A documents a few minor changes made to the stimulator for the purposes of these experiments. The stimulator produced controlled current pulses, ranging between 0-100 mA. The pulse width was fixed at 300 μs with a 33 Hz stimulation frequency.

Programs, written in C and compiled with Microsoft C v 6.0, controlled the experiments and processed the data. Many of the numerical processing routines made use of functions from Numerical Recipes [66]. Plotting routines and some utility functions were derived from the Graph Distribution package [31]. The smoothing and differentiation routines were originally implemented in FORTRAN by Trujillo [29]. The C version used here was produced by an f2c translator and was later modified by Durfee.

5.2 Experimental Set-Up

The knee bench, computer, motor control box and stimulator were arranged to accommodate subjects in the lab (Figure 5-3).

Figure 5-3: The experimental equipment was arranged to easily accommodate the subjects. The motor control box is on the far left, the sensor electronics are mounted below the bench platform, and the stimulator/EMG processor is on the right. The subject is holding the Emergency stop button.

5.2.1 Subjects and Pre-Experiment Preparation

Able-bodied human subjects were chosen for this experiment because they were readily available, easy to schedule, and easy to accommodate in the laboratory. Although the muscle characteristics of spinal cord injured individuals may differ from those of able-bodied subjects, identification methods that are successful with able-bodied

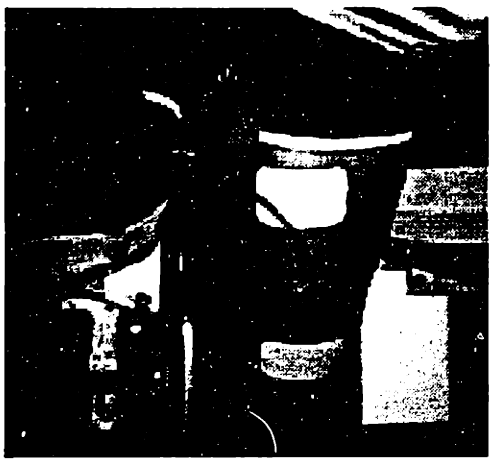

Figure 5-4: This picture shows the approximate location of the stimulation and EMG electrodes. The small EMG electrode is placed between the two large white stimulating electrodes.

subjects should translate to SCI individuals. Relaxed muscles of able-bodied subjects have been shown to be a good model for conditioned muscle in a spinal cord injured individual [81] and many other researchers have used able-bodied subjects in FES control studies [2, 28, 46].

All subjects were informed of the benefits and risks of the experiments and signed a consent form (see Appendix D). The subject's name, initials and the experiment session number were recorded, along with age, height, weight, and leg length. The subjects ranged in age from 18 to 31. Height ranged between 5'2" to 6'3" and leg length ranged between 13" to 18.5".

Surface electrodes, placed just above the knee and below the hip (slightly towards the groin) stimulated the quadriceps muscle (see Figure 5-4). These easy-to-apply electrodes (Tens 5000 series, #86905240 2in x 3.5in) do not require surgery or needles for insertion and easily activate large, bulky muscles like the quadriceps. In most cases the active electrode was placed closest to the knee, unless the subject felt more comfortable reversing the electrodes. The sticky electrodes stayed in place on the skin without additional restraint.

The subjects determined their individual maximum stimulation amplitude by manually increasing the amplitude with the knee held fixed at 90 degrees of flexion.

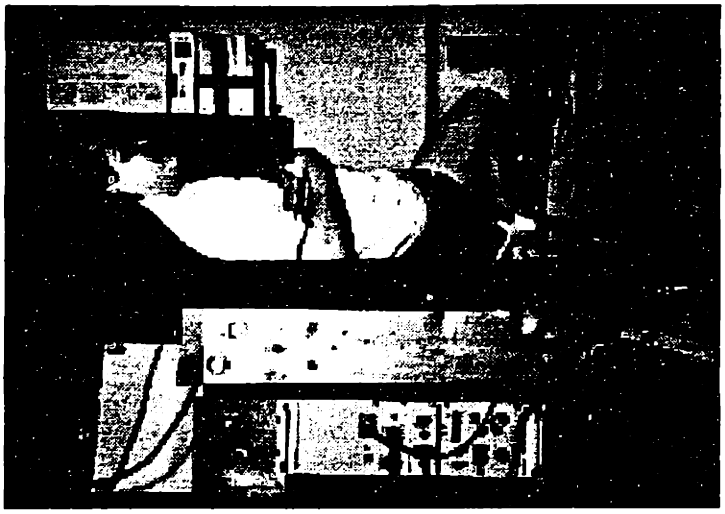

Figure 5-5: The subjects reclined on the bench in order to increase relaxation and prevent hip motion.

The computer screen displayed the torque measurements and stimulation amplitude. Very low levels of stimulation did not produce any torque. When the stimulation reached a threshold for torque development, the threshold amplitude was recorded on the experimental data sheet (see Appendix E). The subject increased the stimulation amplitude to the highest level tolerable. When the subject reached this level, stimulation was shut off and this amplitude was recorded as the maximum stimulation level. Maximum stimulation amplitude ranged between 30-60 mA and produced a maximum isometric torque from 10-60 N-m.

Because the quadriceps muscle is multi-articular, motion of the hip joint results in changes of the muscle state which are not reflected in the knee joint angle or velocity, and cannot be predicted by the present single-joint model formulation. The subject reclined on the knee bench as shown in Figure 5-5 in an effort to restrict the hip motion during the experiments. In this position, the subject could easily maintain the same posture for an entire experiment.

Able-bodied subjects must maintain relaxed muscles during the experiments, since voluntary contractions can introduce error in the measurements. Preventing cocontraction is difficult, but several things were done to help relax the subjects and minimize cocontraction. The subjects were engaged in relaxation exercises in which they

were asked to actively concentrate on relaxing each part of the body beginning with the toes, then the foot, ankle, shin, and continuing until the entire body was relaxed. Most of the subjects had participated in previous FES experiments, and these subjects were better able to relax.

A muscle contracts by propagation of an action potential through the muscle. This action potential or electrical pulse, commonly known as an electromyogram (EMG) can be detected by a sensor electrode. Voluntary muscle activity cannot be measured during electrical stimulation because the contractions produced by the stimulation cannot be distinguished from voluntary contractions. This limits the usefulness of EMG as a monitor for voluntary activity, but it can still be helpful. For these experiments, surface EMG electrodes were placed over the quadriceps muscle, as shown in Figure 5-4. The optimum electrode position was found by maximizing the difference in the EMG signal between the contracted and relaxed state. The computer sampled the EMG signal at 1kHz immediately before and after each portion of the experiment. At the conclusion of each section a computer graph displayed the pre- and post-experiment EMG. A noticeable difference between the two signals indicated voluntary contraction, and that portion of the experiment was repeated. Figure 5-6 shows a typical EMG recording before and after a portion of the experiment. There is no noticeable difference between the pre- and post-experiment EMG signal.

As described in Section 3.3, electrically stimulated muscle fatigues rapidly during constant stimulation. To prevent fatigue, the experiment protocol minimized the amount of stimulation and allowed ample rest between stimulation bursts.

5.3 Isometric Muscle Parameterization Experiment

This set of experiments explored the various methods for identification of the isometric recruitment curve (IRC) and the contraction dynamics. Section 4.1 describes the theoretical basis for these experiments. A preliminary experiment on five sub-

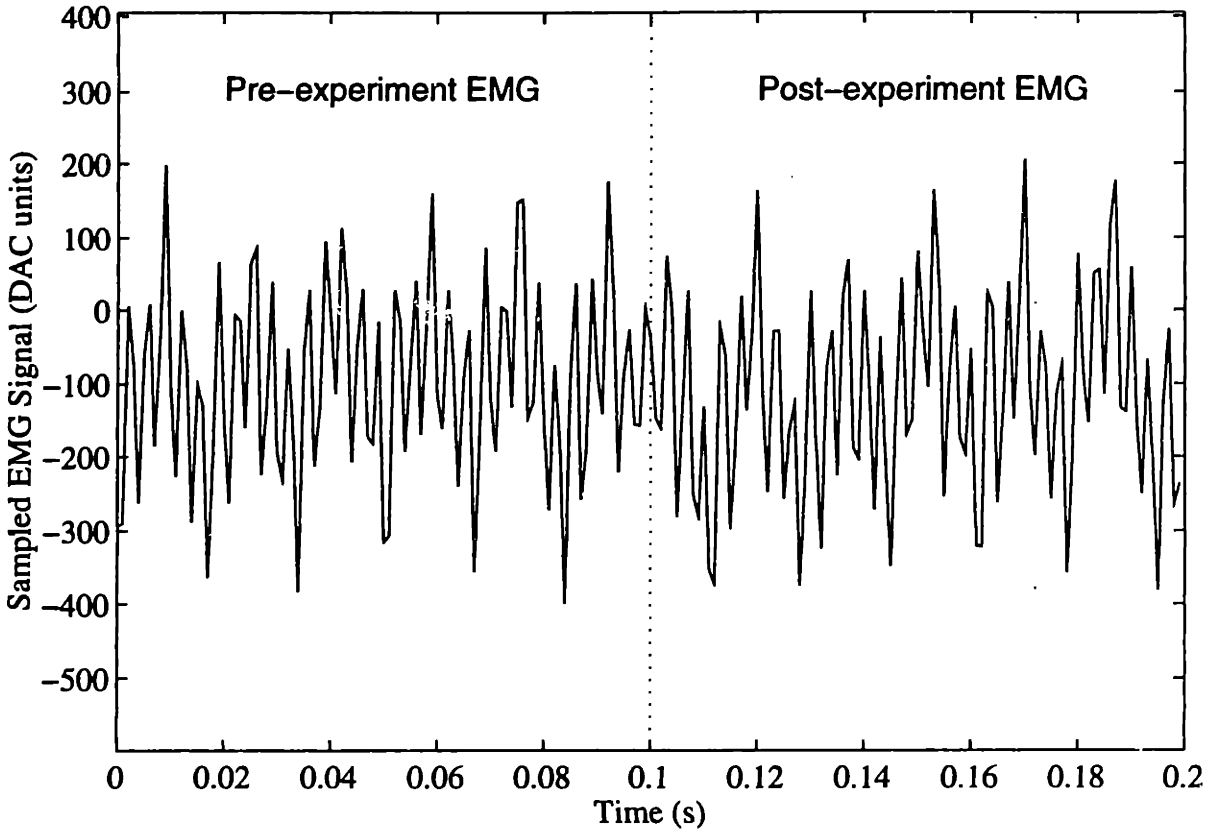

Figure 5-6: A typical EMG signal pre- and post-experiment. There is no noticeable difference between the EMG level during the first tenth second of data (pre-experiment) and the last tenth second of data (post-experiment). This indicates that the subject remained relaxed throughout the experiment.

jects measured the IRC with five experimental paradigms: step response, impulse response, ramp correlation, ramp deconvolution with an ideal impulse response, and ramp deconvolution with an averaged impulse response.

A more focused experiment which included 24 subjects was based on the results of this preliminary experiment. This experiment compared IRCs from the step response and ramp correlation protocols for ability to predict isometric torque output. This second study also explored second- versus third-order system dynamic estimates.

The protocol for both the preliminary experiment and the focused experiment appears in Appendix F. For all the methods described in this section, the knee was held flexed at 90 degrees. Immediately before each stimulation burst, the torque

was sampled 50 times in rapid succession, averaged and recorded as an offset. This offset torque was subtracted from subsequent torque measurements. Just prior to each experiment, the muscle received a 3 s conditioning pulse [16, 18, 44] at 75 % of maximum stimulation range. The IRCs produced with each method were normalized for comparison across methods.

5.3.1 Step Response Method

For the step response method, a 3 s stimulation burst activated the muscle. During the burst, the stimulator ramped up to the test level during the first 0.5 s and held constant at that level for the remaining 2.5 s. The torque was sampled at 200 Hz and averaged during the last 0.5 s of stimulation. Ten stimulation amplitudes ranged from subject threshold to maximum stimulation. 30 seconds of relaxation followed each stimulation burst. This method resulted in a 9 segment piece-wise linear IRC.

5.3.2 Impulse Response Method

The impulse method activated the muscle with 30 single stimulation pulses ranging in stimulation level from below threshold to the subject's maximum. The stimulator delivered the pulses once every second and the computer recorded the peak torque following each pulse. This method resulted in a 29 segment piece-wise linear IRC.

5.3.3 Ramped Inputs

The ramp response methods stimulated the muscle with two impulse and two cosine ramps and measured the torque with a 200 Hz sampling rate through the whole experiment. The cosine amplitude stimulation profile was used instead of a true ramp input to minimize dynamic excitation which occurs at discontinuities of the input. Figure 5-7 shows the stimulation timing diagram for this experiment. Maximum stimulation was used for the impulses. The cosine ramps began at 5 mA below threshold and went up to the maximum stimulation level. The cosine stimulation lasted for 2, 4, and 10 s during the initial experiment with 1 s of zero stimulation between ramps. A 4 s ramp

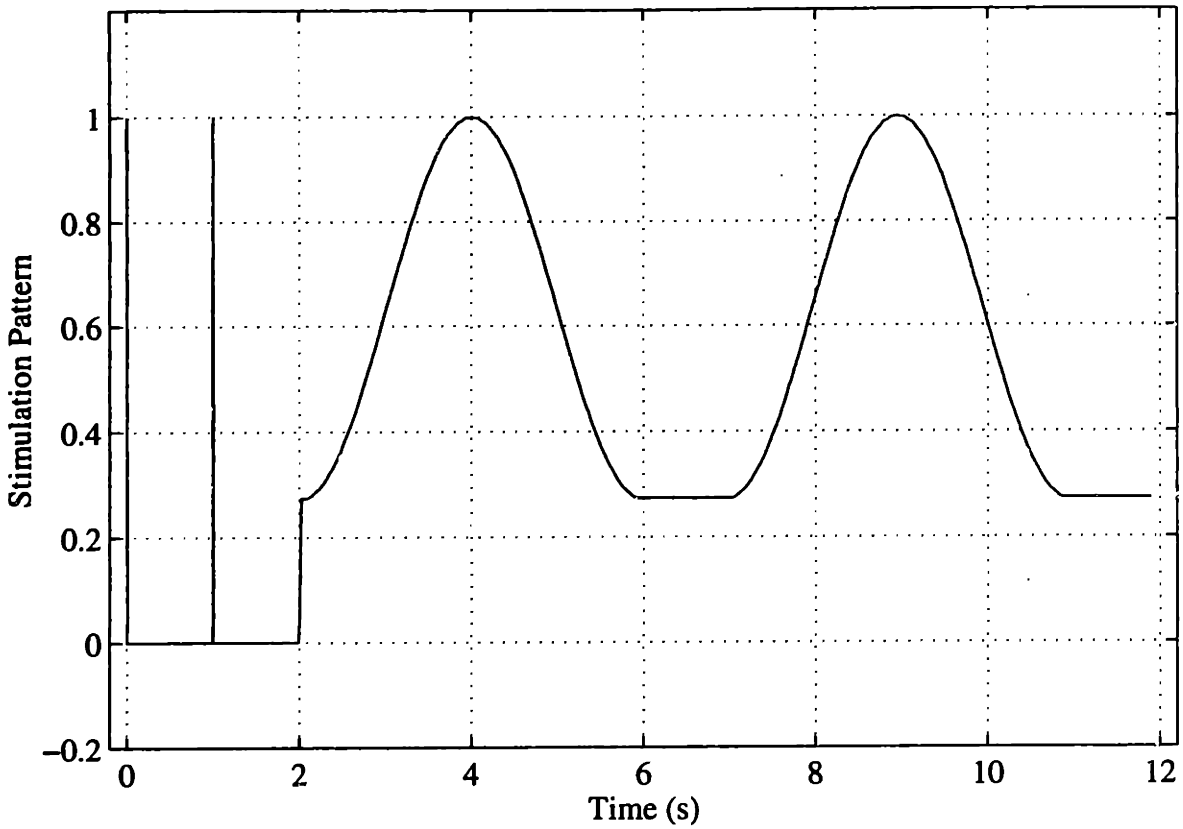

Figure 5-7: Timing diagram for ramped stimulation experiments. This diagram shows ramps of 4 s. Ramp durations of 2 and 10 s were also tested. Subject comfort level determined the magnitude of stimulation. The ramp stimulation started at 5 mA below the subject's measured stimulation threshold.

time was used during subsequent experiments. Averaging the two impulse responses smoothed the data. Post-processing was performed on each ramp response with the three methods: correlation, ramp deconvolution with an ideal impulse response and ramp deconvolution with an actual impulse response. The two IRCs produced from the two ramps were averaged to produce a single IRC. The Numerical Recipes routines **correl** and **convlv** were used to compute the correlation and deconvolution respectively. The number of piece-wise linear IRC segments resulting from the ramp methods depended on the stimulation frequency and the ramp duration. A 4 s ramp produced a 65 segment IRC.

5.3.4 Isometric Torque Prediction

As part of the second isometric identification experiment, the estimated IRCs were used to predict the isometric torque response of the muscle system to a predetermined stimulation sequence. The muscle was stimulated with the prescribed stimulation pattern, shown in Figure 5-8, while the torque was sampled at 200 Hz. The pattern was scaled for each of the 24 subject, 46 muscles, so that maximum stimulation corresponded to the subject's maximum. The mid-level plateaus occurred at 5 mA above threshold and 25%, 50%, and 75% of the IRC response range. A C program

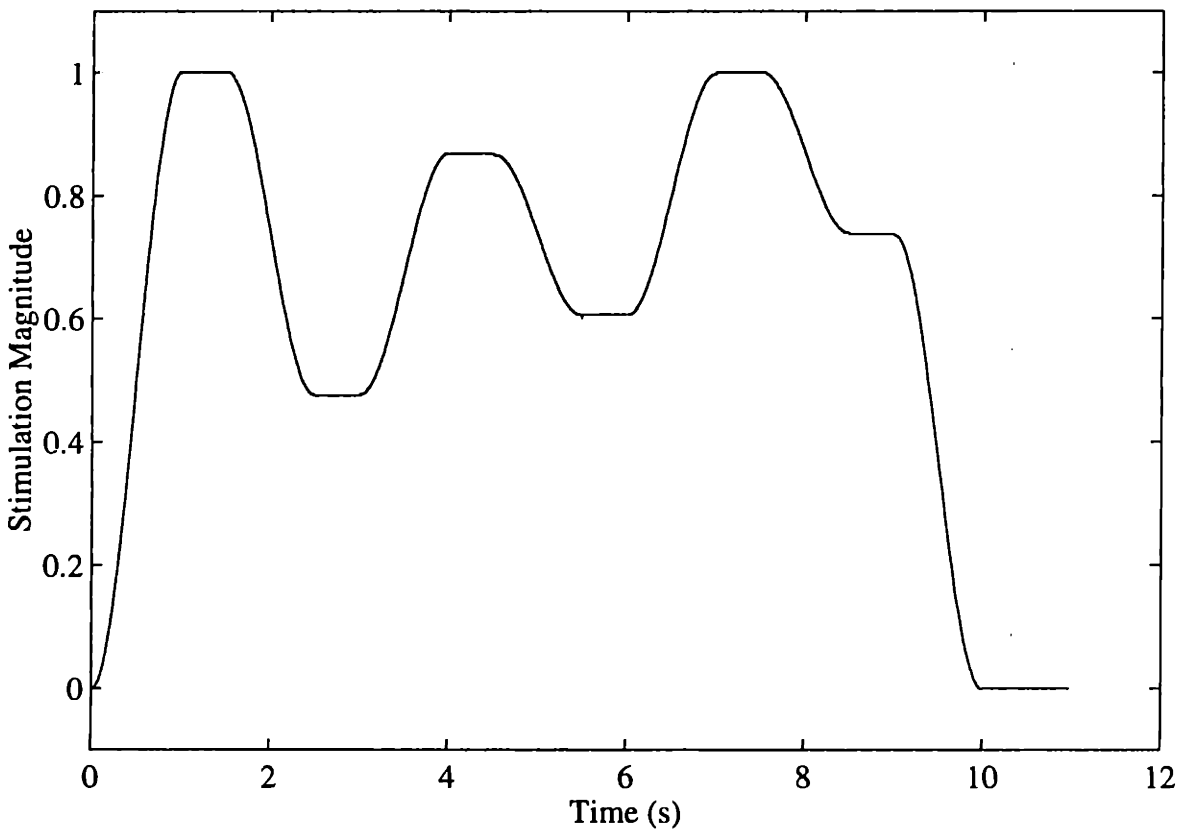

Figure 5-8: This stimulation profile was used to compare the predictive ability of the isometric model identified with various methods. Maximum Stimulation was determined by subject comfort level. Mid-level plateaus occur at 5 mA above threshold, 25 %, 50 %, and 75 % of the stimulation range between the minimum and maximum stimulation.

simulated the isometric torque response to this stimulation pattern for each parameter

set. The predicted and measured responses were compared for step response versus ramp correlation IRCs and 2nd- versus 3rd-order system estimates.

5.4 Non-isometric Model Identification Experiment

This set of experiments identified all of the model properties needed to predict the joint angle response to a prescribed stimulation input. Ten subjects were used. For six subjects, the experiment was repeated on their other leg, so a total of 16 data sets were collected. The protocol for this experiment also appears in Appendix F. The isometric recruitment curve was estimated using the ramp correlation protocol. The contraction dynamics were estimated as a 3rd-order, repeated-poles system based on the impulse response.

The passive properties, passive torque-angle, $f_{pta}(\theta)$, passive torque-velocity, $f_{ptv}(\dot{\theta})$, and the limb inertia, J_{limb} were estimated using three different methods. Sequential identification measured each passive property independently. Simultaneous estimation determined all the passive functional relationships from a single data set through linear estimation and least squares fitting (see Section 4.2.2). The third method, termed the free swing method, was patterned after the experiments of Franken and Veltink [38]. For the first two methods, the motor moved according to a prescribed kinematic trajectory. The actual trajectory was recorded along with the torque generated during the motion. In the final method, the leg swung freely while the muscle was activated with a prescribed binary stimulation input. This caused the leg to move through an unspecified trajectory. All three of these methods produce piecewise linear curves of the position and velocity dependent passive relationships. For the purposes of these experiments, no distinction was made between the position dependent torques caused by gravity and those caused by joint stiffness. Section 7.4.4 discusses this point further.

An experimental paradigm similar to the free swing identified the active properties.

5.4.1 Sequential Passive Identification

The experiments described in this section identified each of the passive joint properties separately, beginning with $\tau_{pta}(\theta)$.

Step-wise position measurements

This experiment began with the leg flexed at 90 degrees. The torque reading at this position served as an offset which was subtracted from the torque readings at each subsequent position. The motor moved the limb to the first, and largest flexion angle, 110 deg and held the joint angle constant for 10 s. The joint angle, static torque, and accelerometer reading were sampled 50 times in rapid succession and the average readings were recorded. The motor moved the limb through a series of 20 fixed angular positions, evenly spaced and decreasing from the 110 deg of flexion to full extension. For most subjects, full extension occurred at about 30 degrees because of the thigh orientation on the bench. After the 20th data point, the motor reversed directions and the measurements were repeated going from extension to flexion. The two independent measurements were averaged to produce the passive torque-angle relationship $\tau_{pta}(\theta)$ and an accelerometer calibration curve.

Constant velocity measurements

$\tau_{ptv}(\dot{\theta})$ was found by moving the leg with a constant velocity and measuring the torque. For each velocity tested, the motor moved the limb to the reference position (90 degrees of flexion) and the offset torque was measured. Then the motor moved the limb with constant velocity for two seconds in the negative (extension) direction. 200 Hz position and torque sampling occurred during the constant velocity move. After a 10 s pause, the motor reversed direction to move the limb at the same speed, in the positive (flexion) direction for an additional two seconds. A total of eight speeds (16 velocities) were tested. Post-processing removed the position dependent torque, determined by the previous experiment, and averaged the remaining torque during the last one second of each constant velocity trial. The motor accelerated

the limb during the first one second of the trial, so this data was not used in the post-processing.

The inertia was estimated from body segment and mass information (Equation (4.13)).

5.4.2 Simultaneous Passive Identification

The protocol for simultaneous identification began by moving the limb to 90 degrees of flexion and measuring the reference torque. The motor then moved the limb to the initial position of a predetermined pseudo-random trajectory. The desired trajectory was read from a stored data file and scaled to cover the angular range of the individual subject. When the subject was ready, the motor moved the limb through the prescribed trajectory. Trajectory updates to the motor controller board were sent at a rate of 1kHz. The position, acceleration and torque were sampled at a frequency of 200 Hz. The experiment was repeated for a second trajectory. Each kinematic trajectory lasted 10 s.

Figure 5-9 shows one of the trajectories. Linear least-squares fitting and singular value decomposition estimated the passive relationships, τ_{pta}, τ_{ptv}, and J_{limb} from one data set (Section 4.2.2). The numeric algorithms for singular value decomposition were taken from the Numerical Recipes routine **svdfit** [66].

5.4.3 Free Swing Passive Identification

For this final passive identification method, the motor was decoupled from the transmission, so the leg swung freely. A random binary (RB) stimulation train lasting 10 s, stimulated the muscle. The stimulation amplitude was adjusted for each subject to just produce full knee extension at steady state. Figure 5-10 shows one of the stimulation trains. The leg moved in response to the stimulation. The position and acceleration were sampled at a frequency of 200 Hz. Post-processing of the data required simulation of the contraction dynamic response to the stimulation pattern and removal of the data corresponding to non-zero activation, so that only the pas-

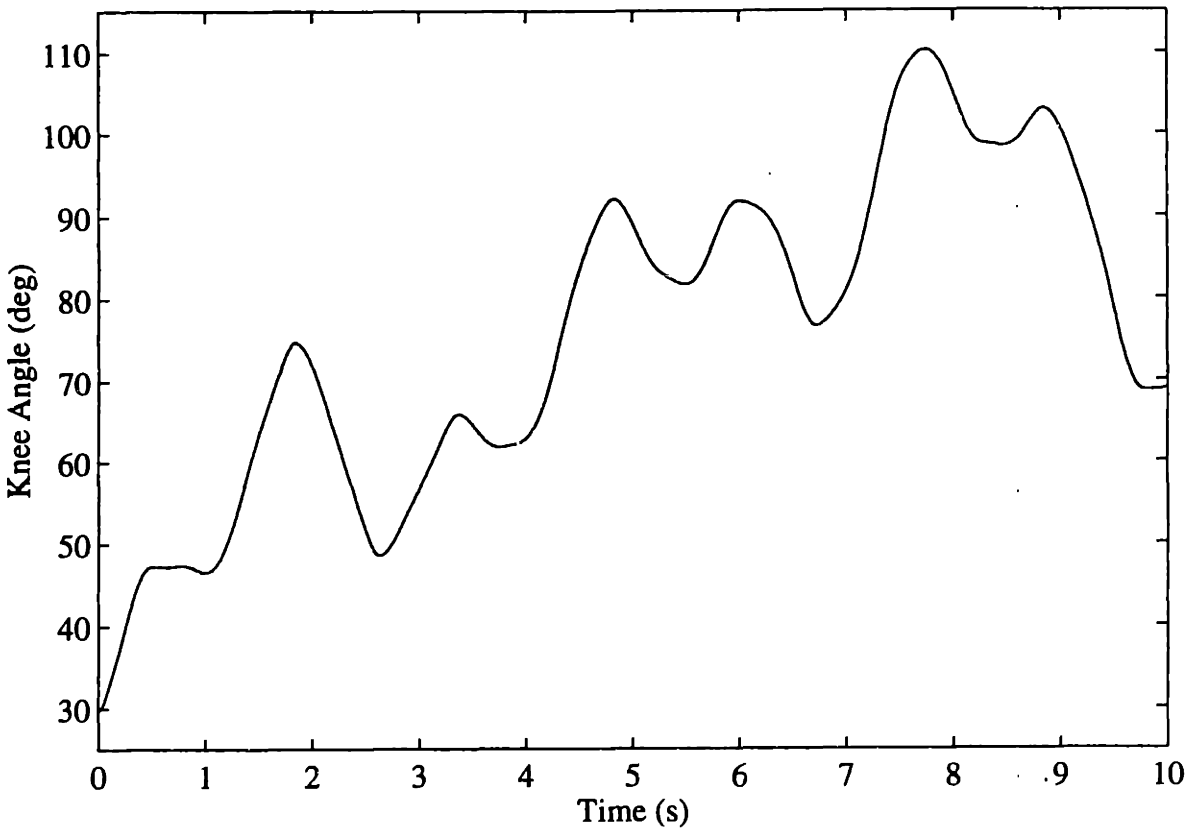

Figure 5-9: One of the pseudo-random kinematic trajectories used for Simultaneous identification of the passive system dynamics. The range was adjusted for each subject to prevent hyperextension of the knee.

sive response remained. The position-dependent torque was computed based on the relationship identified in the sequential identification protocol. J_{limb} and τ_{ptv} were fit to this computed torque using the least squares algorithms described in section 4.2.2.

5.4.4 Active Identification

The free swing procedures described in the previous section were also used to identify the active properties. A denser random binary stimulation train activated the muscle for this set of experiments. Figure 5-11 shows one of the stimulation patterns used in this procedure. During post-processing, the contraction dynamics response, $f_{stim}(u,t)$ to the given input was computed. Data points corresponding to pure passive dynamics, indicated by an activation of less than 0.01, were removed from the

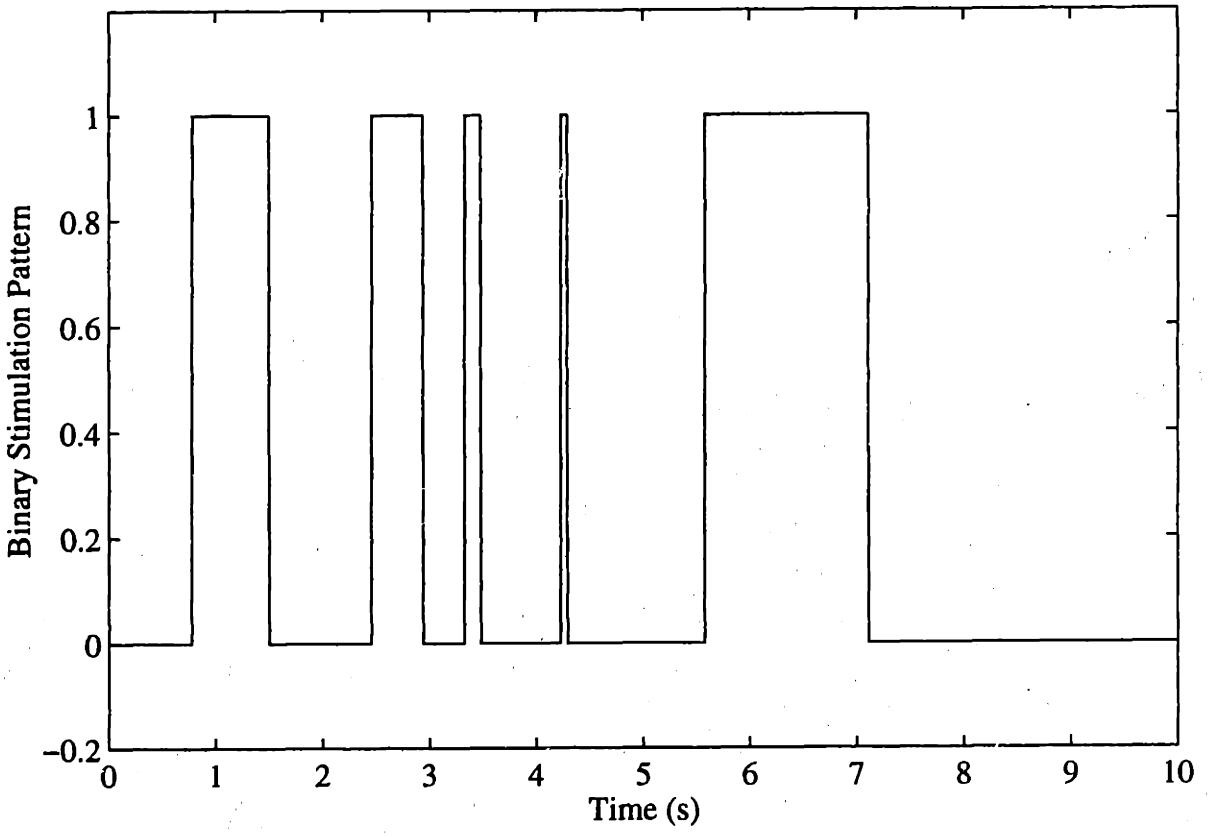

Figure 5-10: One of the random binary stimulation trains used for the Free Swing Passive Identification Method. The maximum stimulation was chosen for each subject, as the lowest level to produce full extension of the joint.

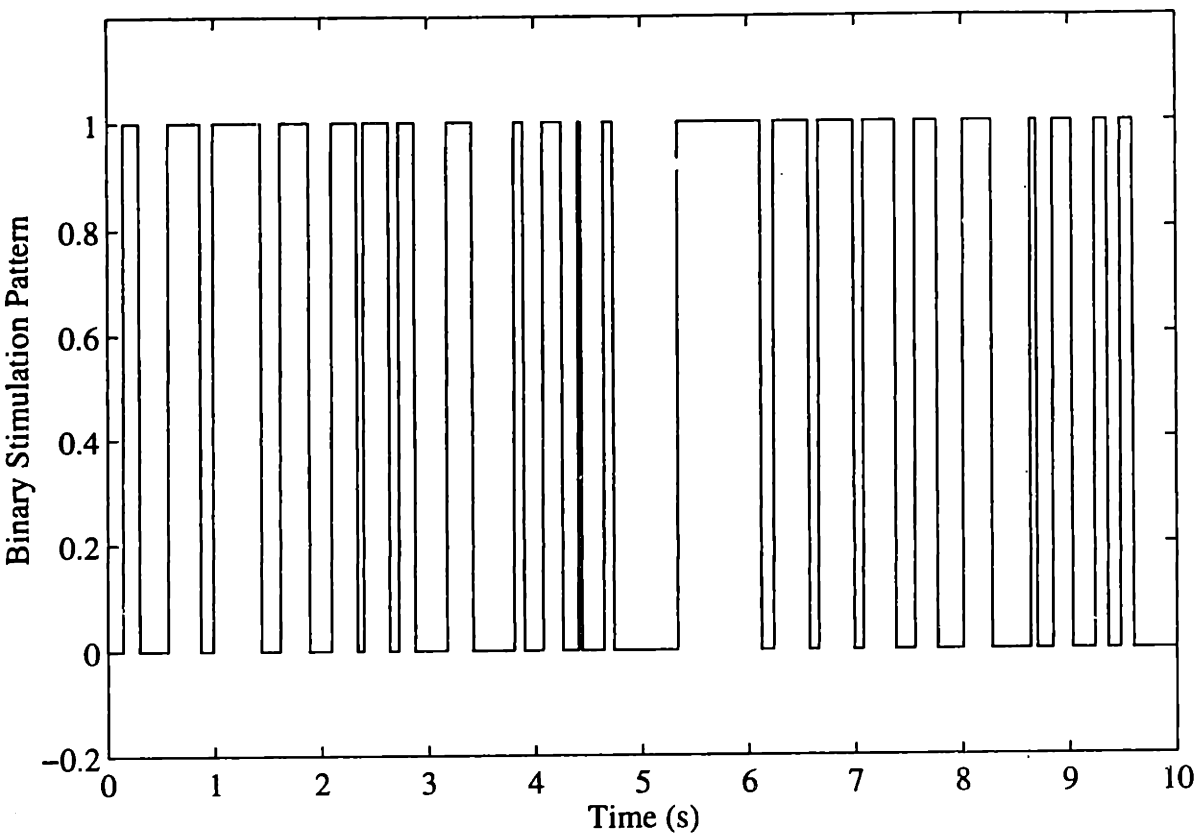

Figure 5-11: One of the random binary stimulation trains used for the Active Identification. The maximum stimulation was chosen as the lowest level to produce full extension of the joint.

data set. For each of the three passive parameter sets, obtained from the three passive identification methods, the passive joint torques were computed from the kinematic trajectory and passive model parameters. Linear estimation and singular value decomposition estimated the active properties as described in Section 4.3. Because the active identification was dependent on the previously identified passive properties, each active data set produced three different active torque-angle and torque-velocity curves, each corresponding to the method used to identify the passive properties.

5.4.5 Knee Angle Prediction

In order to test the predictive ability of the model, several test stimulation patterns were applied to the muscle. With the motor disconnected and the leg swinging freely,

various predetermined stimulation patterns activated the muscle. Sampling of the position and acceleration occurred at 200 Hz. Figure 5-12 shows the step, ramp and swept sinewave patterns used as inputs. It was important to test several different inputs to insure that the model could predict knee angle response for inputs different from those used to identify the model. For each subject, the step amplitude corresponded to 75% of the range between threshold and maximum. Stimulation began at 0.5 s and continued at a constant amplitude for 3 s, followed by 1.5 s of data sampling with no stimulation. For the ramp input, the stimulation amplitude increased linearly from zero to maximum stimulation over 5 s and then decreased linearly back to zero in the following 5 s. The swept frequency sinewave input amplitude cycled between 5 mA above subject threshold to the maximum stimulation. The first cycle period lasted 5 s, the second 2 s and the third 1 s. An additional 1 s of data collection with no stimulation followed the swept sinewave input. The random binary stimulation patterns from the active identification protocols were also used as inputs for prediction.

A C program simulated the knee angle response to each input for each parameter set. There were three parameter sets for each subject, which corresponded to the three passive identification protocols. The predicted and measured responses were compared.

5.5 Simulations

Numerical simulations served two purposes in this study. As discussed in Sections 5.3.4 and 5.4.5, simulations tested the ability of the model to predict isometric torque and knee angle output. In addition, simulations produced data for testing the identification algorithms. The simulations were implemented in C using the Numerical Recipes routine **rk4** [66], a 4th order variable-step runge-kutta integration algorithm.

Simulations of the isometric identification experiments used the ramped input, defined in section 5.3.3, to produce simulated responses from Hammerstein structures with both ideal second- and third-order, repeated-poles dynamics. The simulated data

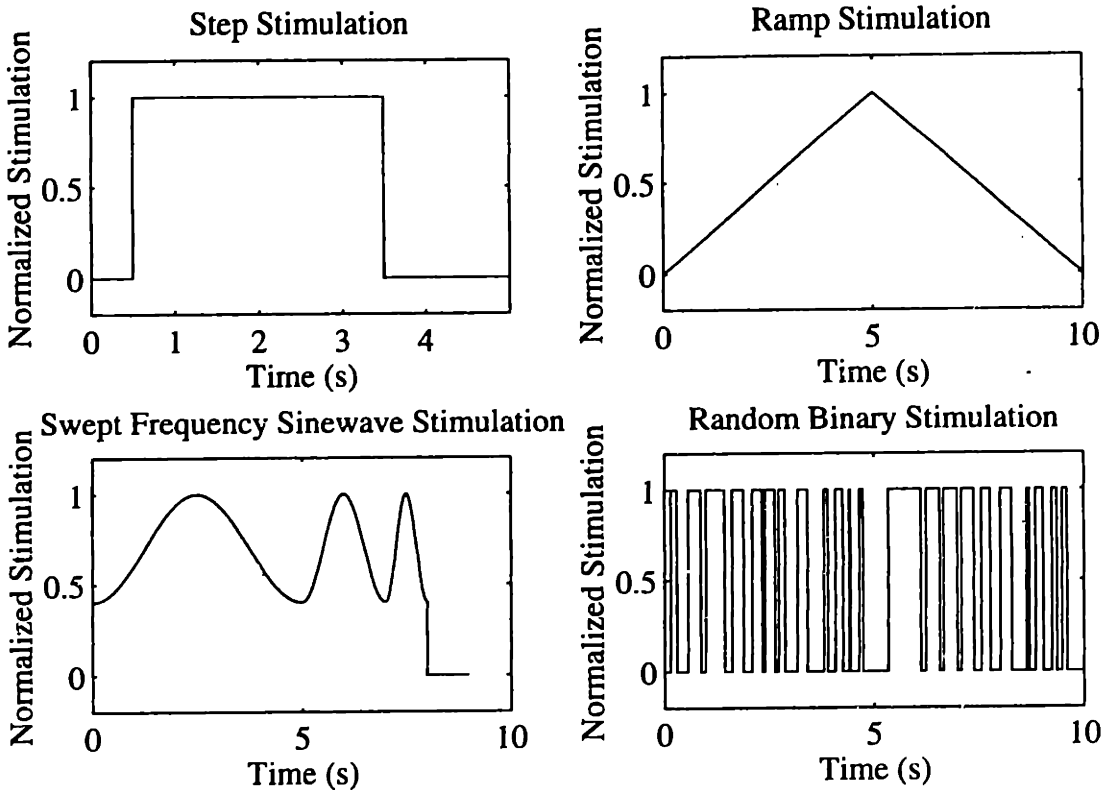

Figure 5-12: These stimulation profiles were used to compare the model parameters and their ability to predict knee angle.

was processed with the correlation and deconvolution algorithms, to insure that the original IRC could be recovered. Non-linear isometric systems, which included a series elastic element (see Section 3.1) were simulated for various levels of stiffness. These simulations explored the effect of the series elastic element on the impulse response and the accuracy of the IRC identification procedures.

Simulations of the passive dynamics explored the effect of hysteresis, static friction and noise on the identification algorithms. The same programs which identified the experimental system, estimated the simulated system. Separate simulations included passive torque-angle curves with hysteresis and passive torque-velocity curves with static friction. Filtered white noise as well as noise correlated tc the acceleration were added to the simulated data records.

Simulations of the active system were used to explore the effects of logarithmic data compression and noise on the active identification algorithm.

5.5.1 Simplified Models

Two simplified versions of the muscle-tendon-joint model were simulated and compared to the full model. Several researchers have published papers which use these simplified models. The first simplification assumes no active dependence on angle or angular velocity. This produces a simple torque generator model, equivalent to the full model if $f_{ata}(\theta) = 1$ and $f_{atv}(\dot{\theta}) = 1$. Franken and Veltink [39] as well as many other researchers, describe this torque generator model. The second simplification models both the active torque-angle and torque-velocity properties by single line segments. Equations 5.1 and 5.2 describe the single segment model.

$$f_{ata}(\theta) = A\theta + B \tag{5.1}$$

$$f_{atv}(\dot{\theta}) = C\dot{\theta} + D \tag{5.2}$$

Shue and Chizeck [70] used these single-segment properties to model the dynamics of cat muscle while Franken and Veltink [39] used them to model a human knee joint. Both the torque generator and single-segment models were parameterized with the free swing data from each subject and simulated for the step, ramp, swept sinewave and pseudo-random binary test inputs described in Figure 5-12. The predictive ability of these simplified models was compared to the predictive ability of the full model.

Chapter 6

Results

This chapter describes the results of the identification experiments detailed in Chapter 5.

6.1 Estimation of Isometric Recruitment Curves

Section 4.1 described the estimation methods used in this experiment. Each IRC was normalized for comparison between estimation methods, since the methods do not give the same peak torque response. The preliminary IRC study determined qualitative differences between the estimation methods. The focused study produced statistical measures of the differences between the ramp correlation method and the traditional step response method.

6.1.1 Step Response versus Other Methods

For most subjects, the impulse response method predicted a lower gain than the step response method for all stimulation levels lower than the maximum (see Figure 6-1). Notice the difference in slopes and the significant difference in threshold location. This mismatch at threshold makes the impulse method an especially bad method to estimate the isometric recruitment curve.

Figure 6-2 shows a typical response to a 2s ramp, shifted by the correlation and

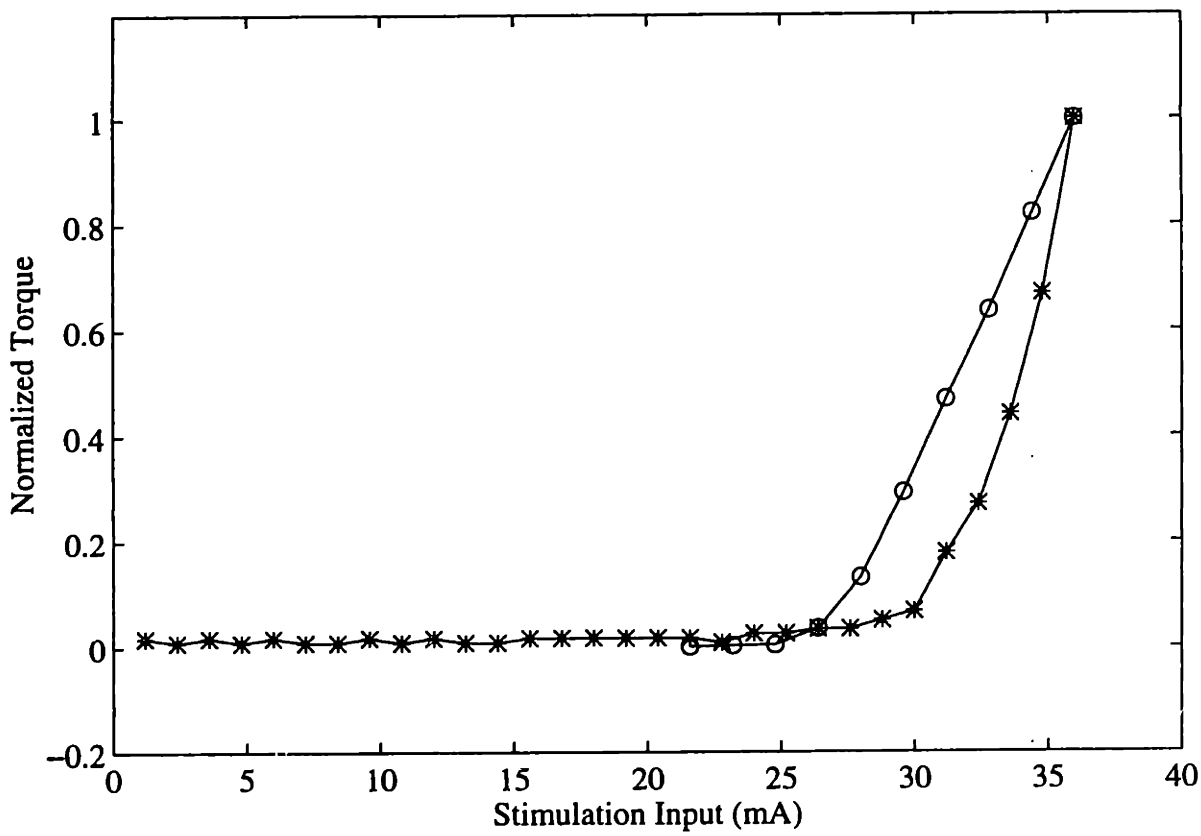

Figure 6-1: The impulse response method (∗) produced an IRC with a lower gain than the step response method (o). The mismatch at threshold makes the impulse method an especially bad method to estimate the IRC.

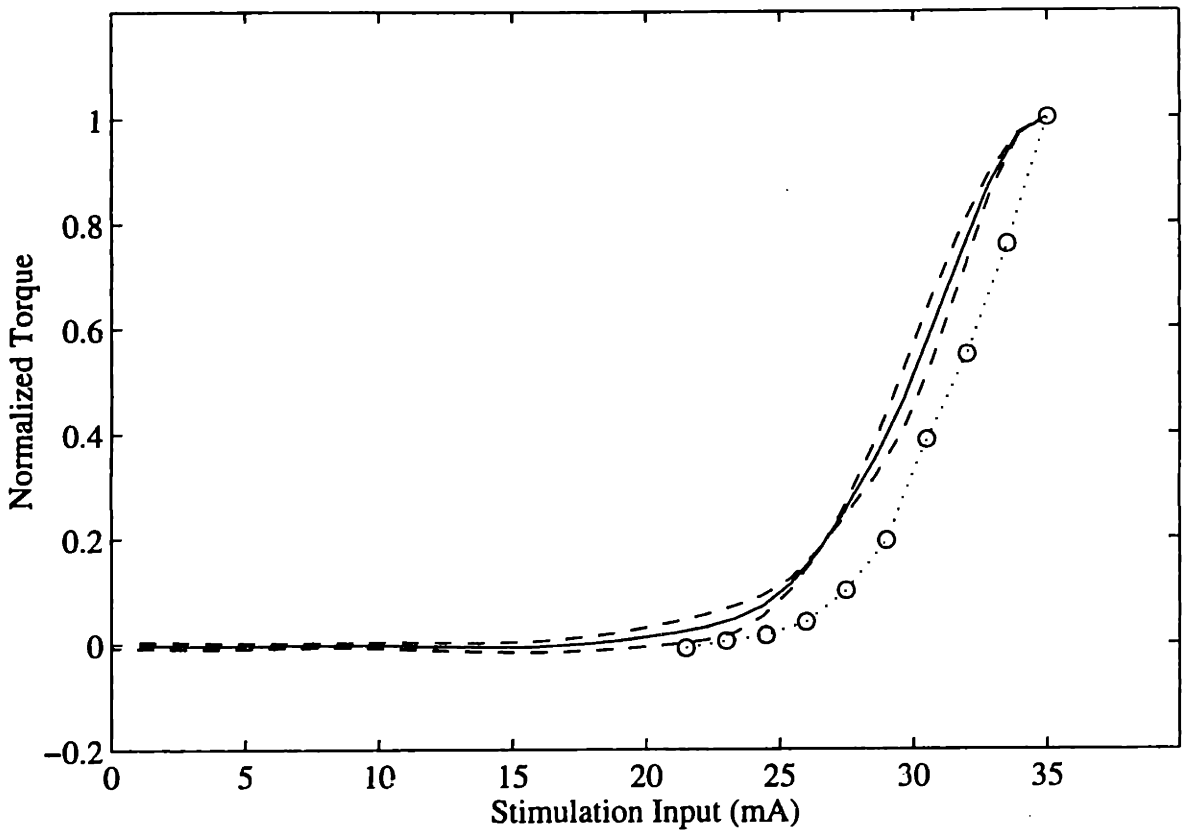

Figure 6-2: (−−) ramp response (2s ramp time) shifted by correlation method and cross plotted against the input. (−) IRC produced by averaging the ascending and descending legs of the shifted ramp. (o) IRC produced by the step response method. Small amounts of hysteresis appeared with the correlation method. Threshold prediction at this short ramp time did not agree well with the step response method.

plotted against the input. Averaging the ascending and descending legs produced the IRC. For all subjects, ramp correlation with a 2s ramp time produced smooth curves with small amounts of hysteresis. The same graph displays the step response IRC from the same subject. In many cases, as with this subject, the short ramp time produced error in the threshold estimate. For longer ramp times, (see Figure 6-3) ramp correlation IRCs showed good agreement with the step response IRCs, with smaller errors near threshold and some minor discrepancies in slope.

Figure 6-4 shows a ramp response deconvolved by an ideal second-order, critically-damped impulse and the IRC produced by averaging the ascending and descending legs of the response. The ramp time for this data set was 2 s. The graph also displays

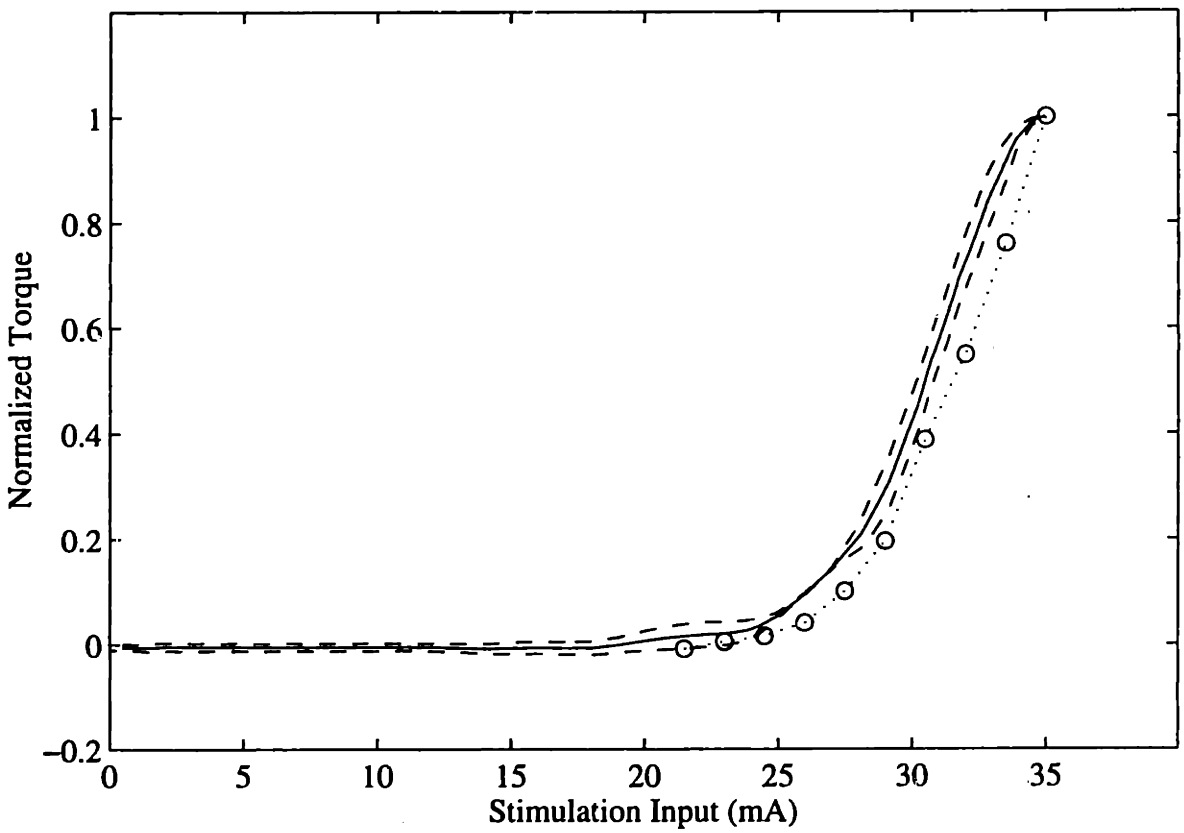

Figure 6-3: (−−) ramp response (4s ramp time) shifted by correlation method and cross plotted against the input. (−) IRC produced by averaging the ascending and descending legs of the shifted ramp. (o) IRC produced by the step response method. Small amounts of hysteresis still appear at longer ramp times,but threshold prediction improved.

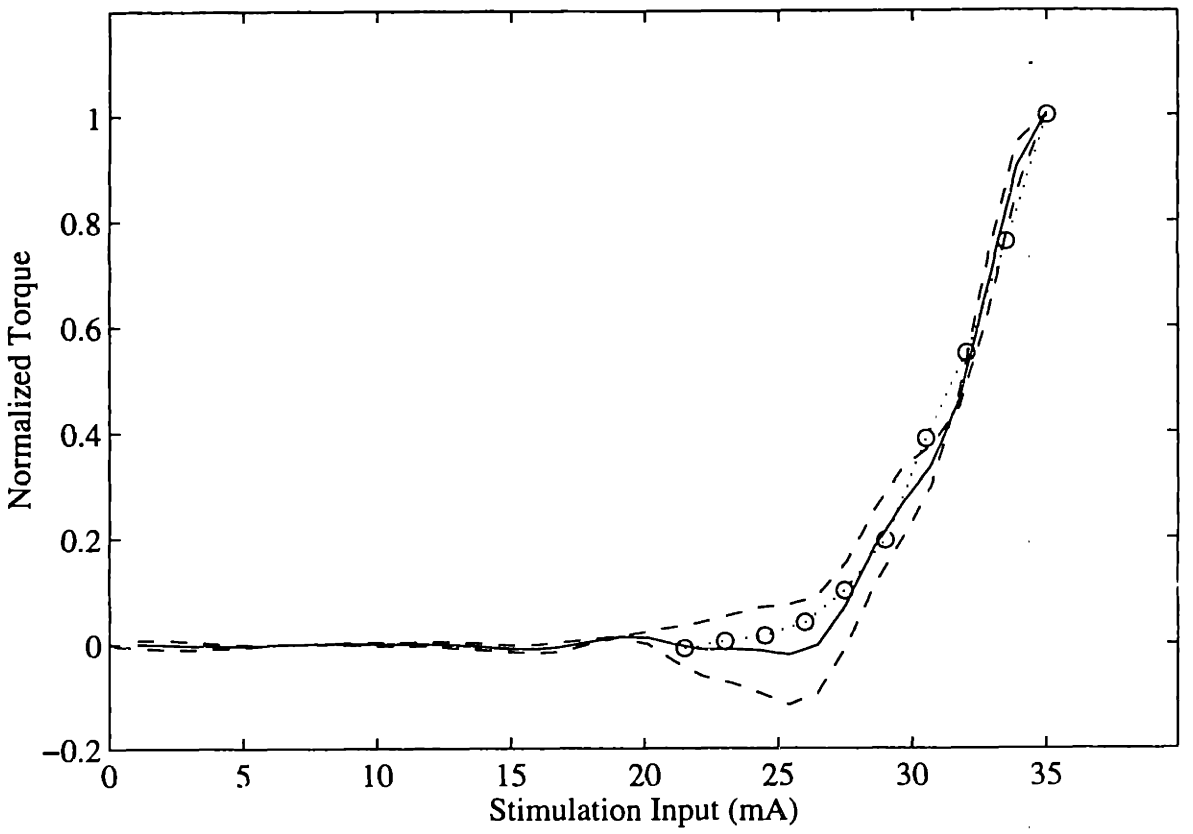

Figure 6-4: (−−) ramp response (2s ramp time) deconvolved with an ideal impulse response and plotted against the stimulation input. (−) IRC produced by averaging the two legs of the deconvolved ramp response. (o) IRC produced by the step response method. deconvolution with an ideal impulse produced hysteresis and oscillations in the descending leg of the deconvolved ramp. Notice the negative gain the threshold region, which is a characteristic error of this deconvolution method.

the step response IRC from the same subject. This typical data set displayed some common features seen for all subjects which resulted directly from this processing method. The short ramp time caused considerable hysteresis and significant oscillations in the descending leg of the deconvolved ramp. These oscillations dipped below zero for many subjects. For this particular subject, averaging resulted in a negative gain near the threshold region of the IRC. Mismatch between the idealized impulse response and the actual system response caused this error. A good match existed between the ascending portion of a the second-order, critically-damped impulse response and the actual impulse response, but the descending portion of the system response had a much steeper slope and shorter tail. The negative IRC values make accurate prediction of threshold difficult with this processing method. Longer ramp times diminish the inaccuracies of this method, since the contraction dynamics play less of a role for slower inputs.

The IRCs produced by deconvolution through the recorded impulse response also displayed specific traits. Figure 6-5 shows a ramp response from this method and the IRC produced by averaging the ascending and descending legs of the response. The graph also displays the step response IRC for the same subject. This deconvolution method produced more hysteresis than the previous two ramp processing methods, but less oscillation and the descending leg of the response never dipped below zero. The region of the IRC near threshold displayed some oscillations, which made the threshold somewhat indistinct. Again, with longer ramp times the inadequacies of this method diminish.

Each of the three ramped methods produced nearly identical IRCs for the longest ramp time (10s) (see Figure 6-6). A slow input did not excite the dynamics, so post-processing to remove the dynamics made little difference. In fact cross plotting the response and input directly also produced a reasonable IRC at this ramp time. The shortest ramp time (2s) resulted in considerable differences between the methods and some error in prediction of threshold with all methods when compared to the step response method. Deconvolution with an ideal critically-damped, second-order impulse response produced the worst threshold prediction. A moderately timed ramp

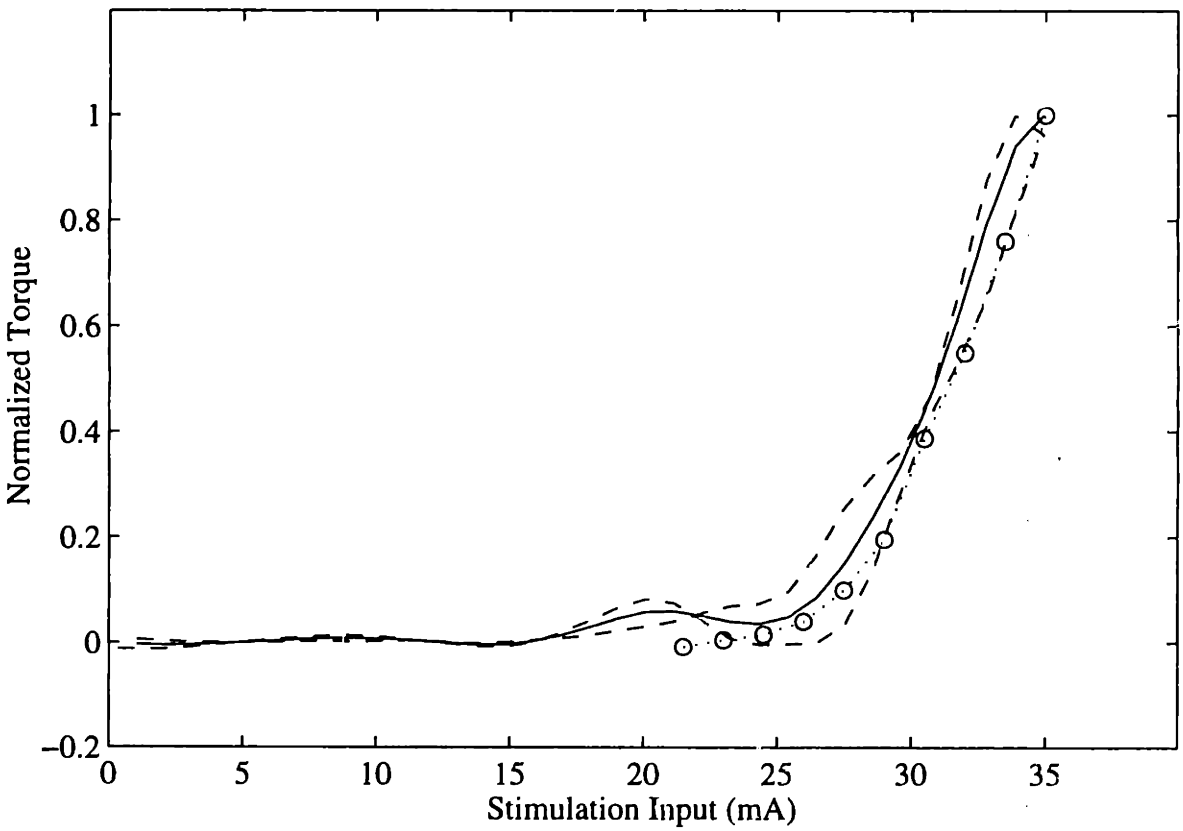

Figure 6-5: (−−) ramp response (2s ramp time) deconvolved with a measured impulse response and plotted against the stimulation input. (−) IRC produced by averaging the two legs of the deconvolved ramp response. (o) IRC produced by the step response method. deconvolution with the measured impulse response produces large hysteresis, but fewer oscillations than the ideal impulse deconvolution.

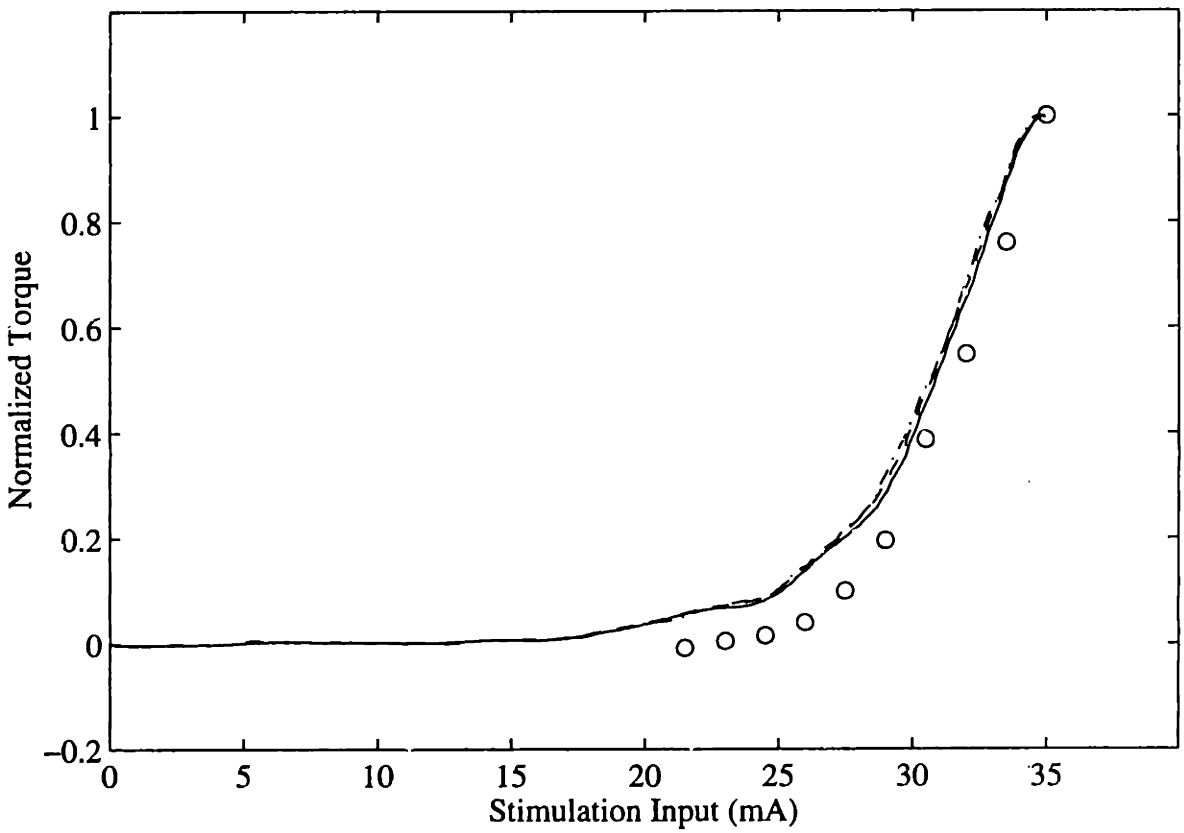

Figure 6-6: IRC estimates from 10s ramp responses processed by (−) deconvolution with an ideal impulse,(− −) deconvolution with a measured impulse response, (− · −) the correlation method. (o) step response IRC from the same subject. All three ramp methods produce similar IRC estimates at long ramp times.

of 4s produced a good match to the step response IRC with all three processing methods.

Because it was impossible to know the true isometric recruitment curve precisely, it was impossible to conclusively determine if any of the five methods gave an accurate estimate of the IRC. The traditionally accepted method of estimation, the step response method fatigues the muscle. The impulse response method predicted a different threshold than the step response method. All three of the ramp methods produced considerable differences for short ramp times (2s), but all of these methods were acceptable for ramp times of 4s and more. The correlation method involved simple processing and avoided numerical division problems which can occur with the deconvolution methods. The added complexity of the deconvolution methods did not produce significantly different results. Based on these results, the ramp correlation method with a 4s ramp time was chosen for more quantitative comparison to the step response method.

6.1.2 Step Response versus Ramp Correlation - Isometric Torque Prediction

This experiment focused on the difference between the ramp correlation method with a 4s ramp and the step response method in their ability to predict isometric torque. Of the 24 subjects in this experiment, 22 were tested on both legs to produce a total of 46 complete data sets. Isometric simulations with third-order contraction dynamics and each IRC estimate predicted the torque response of the muscle system to the stimulation pattern presented in Figure 5-8. The maximum isometric torque output was determined by scaling the simulation result by a constant to get a best fit. Figure 6-7 compares typical predictions against the experimental result. Equations 6.1 and 6.2 computed the normalized RMS error and averaged RMS error, respectively, for each prediction.

$$E_{RMS} = \sqrt{\frac{\sum_1^N \left(\frac{prediction-data}{data}\right)^2}{N}}. \tag{6.1}$$

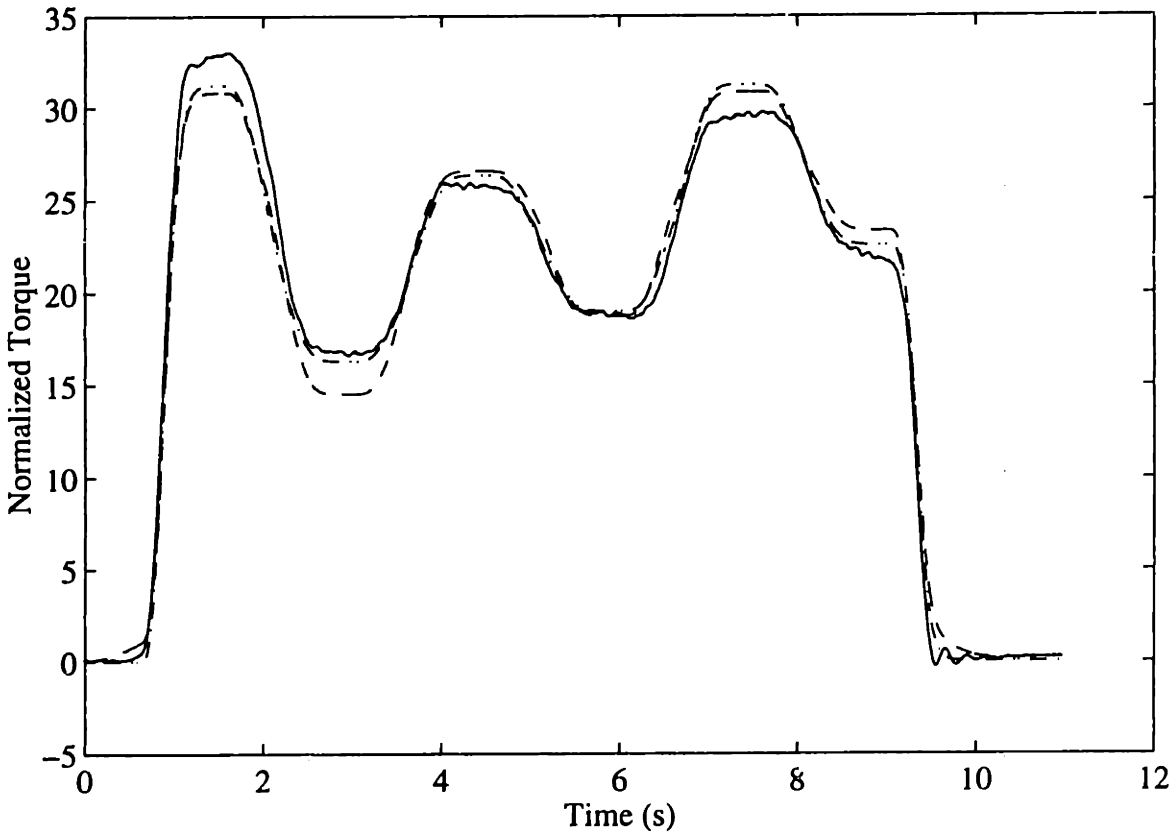

Figure 6-7: (−) Experimental system response and predicted responses with third-order contraction dynamics and IRCs estimated from (− −) correlation method and (− · −) step response method.

$$E_{AVE} = \frac{\sqrt{\sum_1^N (prediction - data)^2}}{\sum_1^N data}. \tag{6.2}$$

A Student's t-test compared the relative predictive ability of the two IRC estimates across subjects by determining the significance of the difference between the error pairs. The following equation shows the mathematics of the comparative t-test.

$$t = \frac{\bar{d}}{\frac{S_d}{\sqrt{n}}} \tag{6.3}$$

where $\bar{d}$ is the average error difference between the step response and correlation estimates. A positive value for $\bar{d}$ indicates the step response method produced more error on average. S_d is an estimate of the standard deviation of the differences based on the 46 data sets, n is the number of points, in this case 46, and t is the test statistic. For a sample size of 46, at a 95 % confidence level, the critical t value equals 2.02. Significant difference existed between the methods if $t > 2.02$ or $t < -2.02$. Table 6.1 shows the values of t for comparisons between the step and ramp methods. For all cases, t lies between the critical values, so even though the correlation method produced less error, the difference was insignificant. The ramp correlation method produced an IRC estimate which could predict isometric torque as well as the step response IRC.

6.2 Identification of Contraction Dynamics from an Impulse Response

Figure 6-8 shows a typical impulse response normalized and compared to both a second-order, critically-damped linear system and a repeated-poles, third-order system. The RMS error between the actual impulse response and the predicted impulse response from second- and third-order models were computed with the following equa-

	E_{RMS}		E_{AVE}	
	2nd order system	3rd order system	2nd order system	3rd order system
Average Difference $\overline{d}$	0.2246	0.2394	0.9505	0.8095
Standard Deviation S_d	1.6601	1.638	0.000175	0.0013
Test statistic t	0.9177	.9907	0.9505	0.8095

Table 6.1: Statistics obtained from a t-test comparing isometric torque prediction errors for step response and ramp correlation IRCs. The critical t value for this test at 95 % confidence level is 2.02. No statistical difference exists between prediction using IRCs produced with the step response or ramp correlation methods.

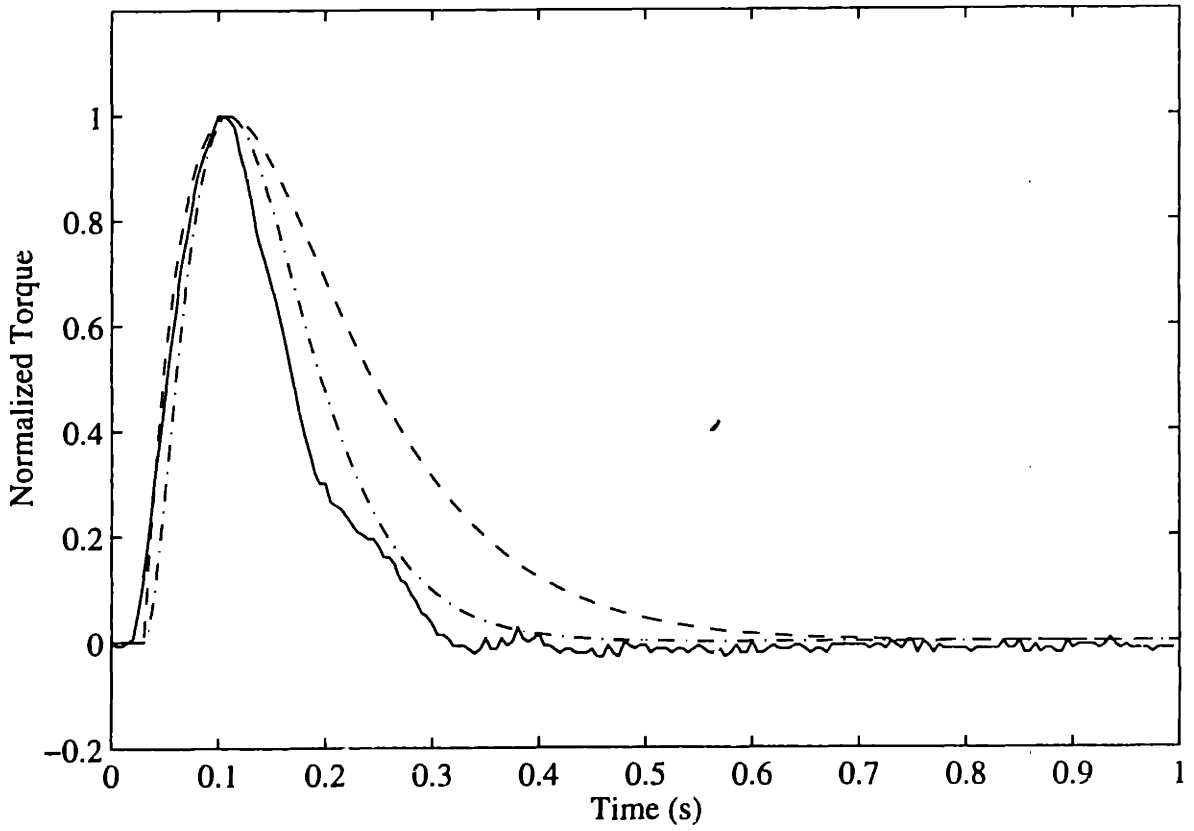

Figure 6-8: Impulse responses: (−) Experimental, (−−) second-order, critically-damped system w/ poles at 12.5 s^{-1}, and (−·−) third-order, repeated-poles system w/poles at 25 s^{-1}. The third-order system response fit the experimental response better.

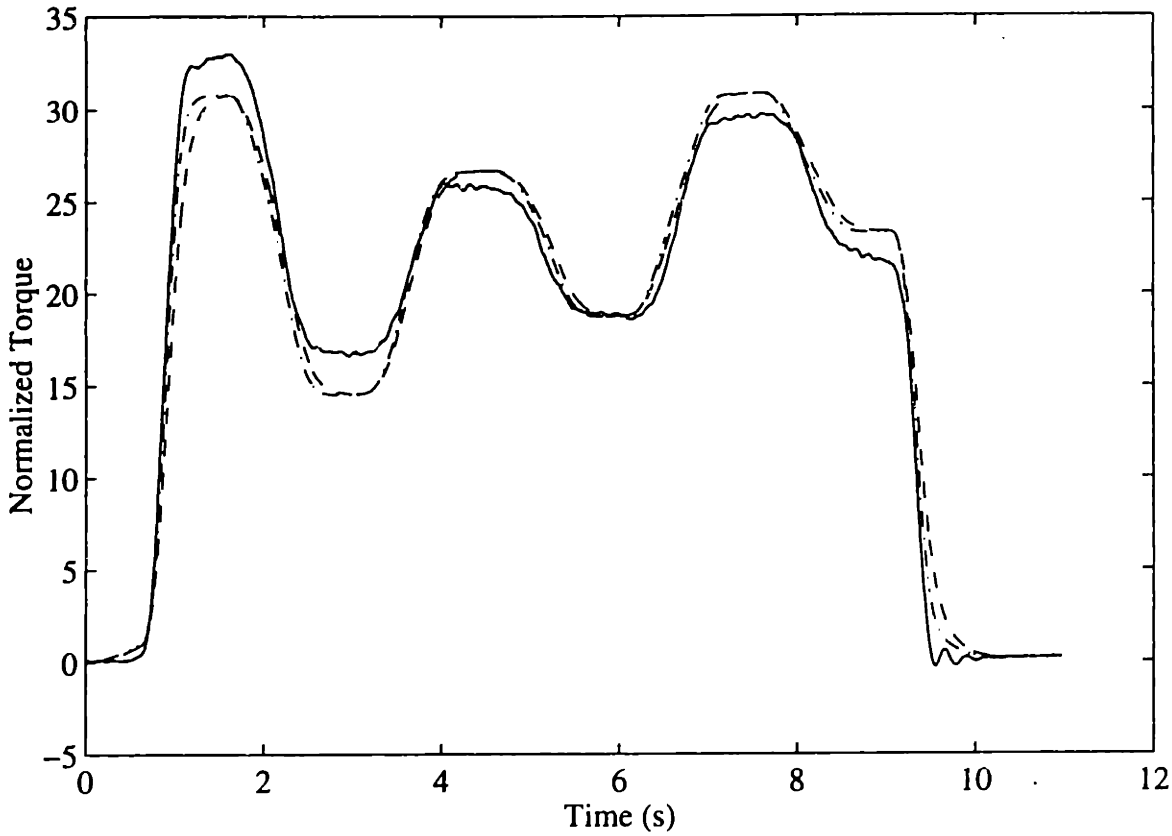

Figure 6-9: Isometric torque response to a prescribed input: (−) Experimental, (−−) second-order, critically damped system w/ poles at 12.5 s^{-1}, and (− · −) third-order, repeated poles system w/poles at 25 s^{-1}.

tion:

$$E = \sqrt{\frac{\sum_1^N (prediction - data)^2}{N}} \tag{6.4}$$

The comparative t-test (Equation (6.3)) determined the significance of the error differences predicted by each dynamic estimate. The t value for the difference between the errors, 204.56, was overwhelmingly significant at all confidence levels given in the t-tables. A positive error difference indicated the third-order model produced a significantly better fit than the second-order model.

Simulations using the second- and third-order system estimates predicted the isometric torque response of each subject to the prescribed input shown in Figure 5-8. Figure 6-9 shows a typical result. The prediction errors, normalized RMS error and averaged RMS error, were computed and compared with the t-test. Table 6.2 shows

the results of the t-test. On average, the third-order system estimate produced less error; however, the difference was significant for the normalized RMS error statistic only. This particular stimulation pattern contained large flat sections where the

	E_{RMS}	E_{AVE}
Average Difference $\overline{d}$	0.2707	0.000175
Standard Deviation S_d	0.454	0.000683
Test statistic t	4.0436	1.2204

Table 6.2: Statistics obtained from a t-test comparing isometric torque prediction errors for second- and third- order system estimates. The critical t value for this at 95 % confidence level is 2.02. The normalized RMS error E_{RMS} showed significant difference between second- and third-order system estimates, but the averaged RMS error E_{AVE} showed no statistical difference.

transient dynamics have died out. The major source of error in these predictions is a mismatch in the IRC rather than a mismatch in contraction dynamics. Because the IRC was the same for each simulation, the difference in error produced by the second-order system estimate versus the third-order system estimate was not significant in the average RMS error. A more dynamic input may have shown a more significant difference.

6.3 Isometric Simulations

Simulations explored the theoretical accuracy of the correlation method for identification of the IRC. Simulations with second-order, critically-damped systems as well as non-linear system contraction dynamics lent some insight into the reliability of this estimation method under various conditions.

To test the accuracy of the ramp correlation method under ideal conditions, an ideal isometric system, with the IRC shown as the solid line in Figure 6-10, was simulated with linear second-order, critically-damped contraction dynamics. The simulated system response to the identification input (see Figure 5-7) was processed

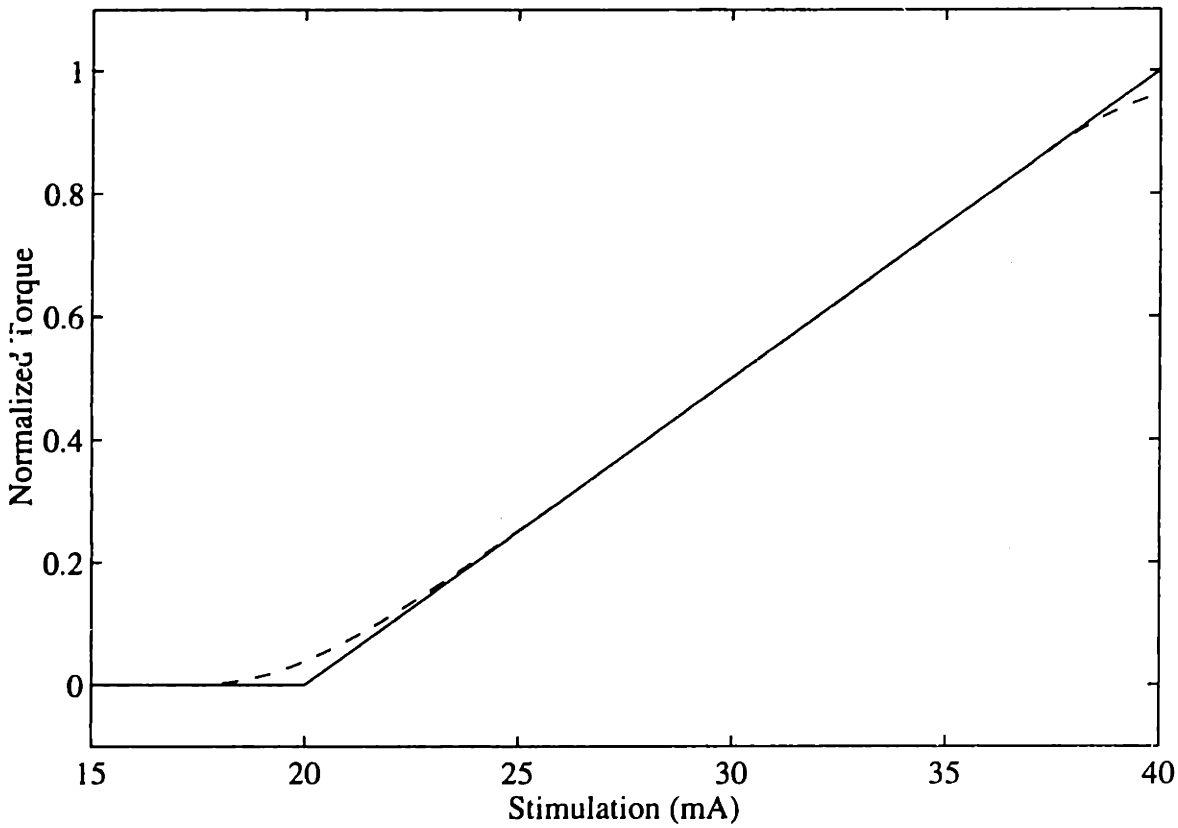

Figure 6-10: This IRC (−) was used to simulate the isometric identification experiment. The simulated system response was processed with the ramp correlation method and the estimated IRC (− −) was produced. Notice some error occurred near threshold.

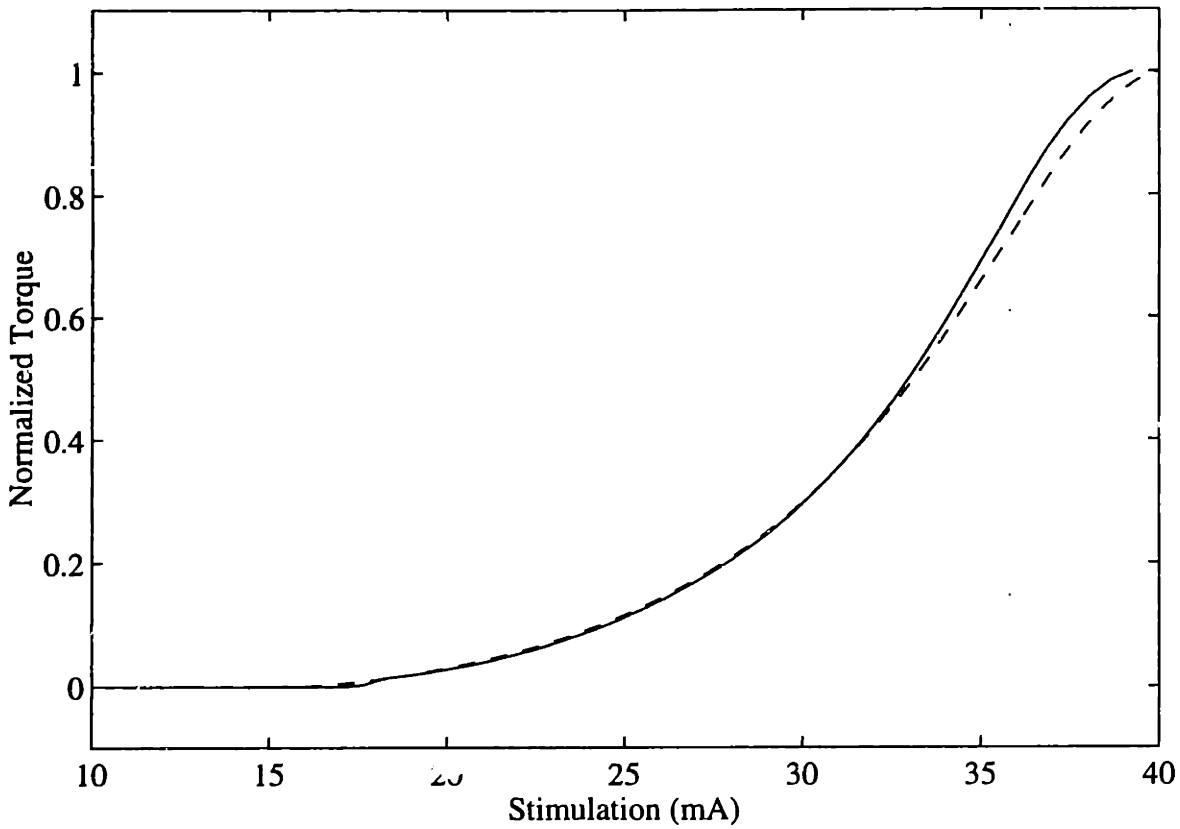

Figure 6-11: In this case, the original IRC (−) did not have a slope discontinuity. The estimated IRC (−−) matches quite well to the original IRC.

with the correlation method to produce an estimate of the isometric recruitment curve. The dashed line in Figure 6-10 represents the estimated IRC. This simulation showed that the correlation method did not accurately predict threshold. The correlation estimation method predicted threshold at a slightly lower stimulation level, and concurrently slightly over estimated the IRC magnitude at stimulation levels near threshold. The worst estimates occurred for simulated IRCs with a sharp discontinuity at threshold (as in Figure 6-10). When a smooth IRC was simulated the correlation method estimated the IRC almost exactly (Figure 6-11). An IRC with a sharp discontinuity probably does not reflect the physical situation. Instead, the real IRC lies between the prediction obtained by the correlation method and a curve consisting of a straight line with a deadzone and a region of saturation. In any case, the IRC would be bounded in the low amplitude range between these two estimates.

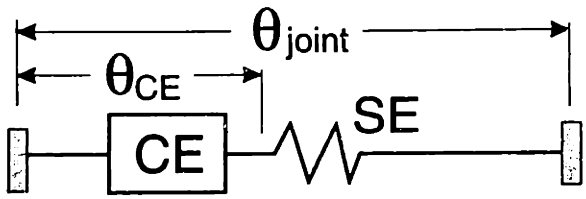

Figure 6-12: The isometric system if the series elastic element is not neglected. Interaction between the SE and the active torque-velocity relationship modify the dynamics of the isometeric torque response.

6.4 The Effect of the Series Elastic Element

The model structure chosen for this thesis assumed that series elasticity in the active branch of the muscle model could be neglected (see Section 3.1). This assumption effectively lumped the series elasticity of the musculo-tendon unit into the dynamics of the contractile element. Baratta and Solomonow found that during mid-range isometric contractions (20-80 % of maximum isometric torque) the dynamic response of the tendon in cat tibialis anterior was minimal [9], but the effect was greater at very low and very high force levels. Other researchers, Zajac [89] in particular, make the point that to achieve accurate modeling of many muscles, the significant series elasticity of the tendon cannot be neglected, and that the muscle itself displays significant series elasticity. If the series elastic element is not neglected, Figure 6-12 shows the non-linear isometric model that resuits. In this non-linear model, the contractile element develops a torque, which causes the series elastic element to stretch and the contractile element to contract until equilibrium occurs. The interaction between the torque-velocity property of the contractile element and the series elastic element produces the non-linear torque characteristics of the system.

6.4.1 Effect of Series Elastic Element on Twitch Response

Figure 6-13 shows the impulse response of an isometric muscle system with and without the series elastic element. The peak of the twitch response of the system with series elasticity was significantly delayed from the linear system response. The added

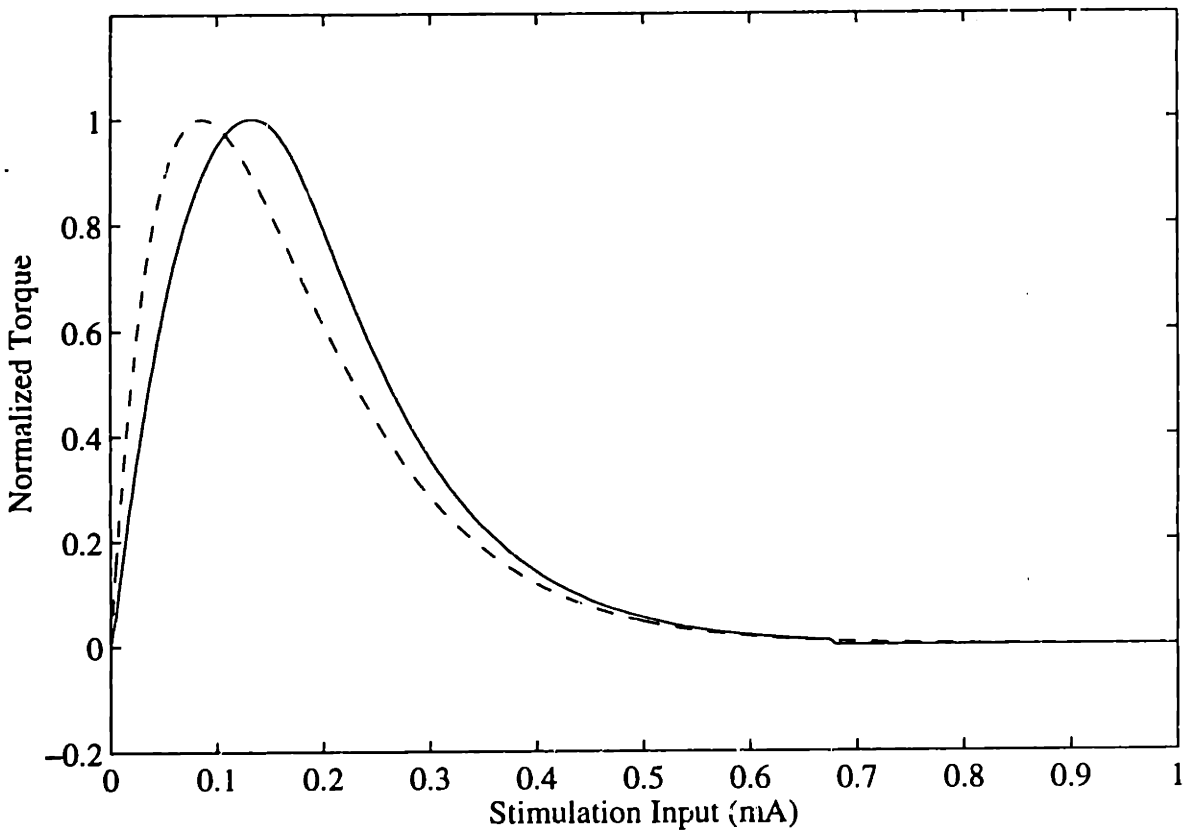

Figure 6-13: Impulse response simulated with a (−−) second-order, critically-damped linear system (poles = 11.7 s^{-1}) and a (−) non-linear system with second-order linear contraction dynamics (poles = 11.7 s^{-1}) coupled to an SE ($K_{se} = 35\ \frac{N \cdot m}{deg}$).

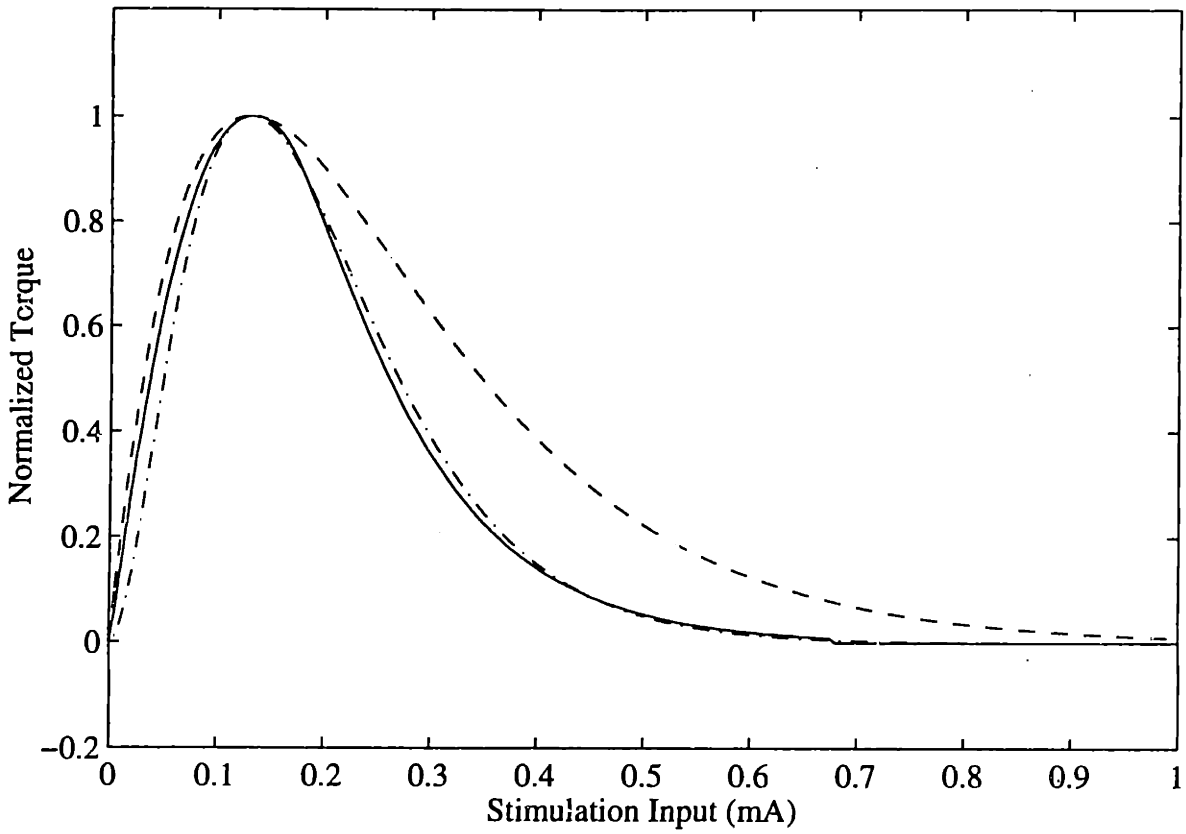

Figure 6-14: Simulated impulse response of a (−) non-linear system with second-order linear contraction dynamics (poles = 11.7 s^{-1}) coupled to an SE ($K_{se} = 35\ \frac{N \cdot m}{deg}$). Fits to linear repeated poles systems: (−−) second-order (poles = 7.69 s^{-1}) and (-.) third-order (poles = 15.38 s^{-1}).

damping from the active torque-velocity term slowed things down causing this shift in the response peak. The torque-velocity term is active because the series elastic element allows motion of the contractile element. Figure 6-14 shows this non-linear impulse response matched to second- and third-order, repeated-poles linear dynamics based on the peak of the response. The shifted peak and decreased tail of the non-linear system's response was better matched to a third-order linear response than a second-order response. The combination of the series elastic spring and the torque-velocity relationship added an independent energy storage element and effectively increased the order of the system. Addition of the SE alone, without the torque-velocity relationship would not have increased the system order. If the contractile element in Figure 6-12 produces a torque without an active torque-velocity factor,

the torque is described by:

$$\tau_{ce} = \tau_{scale} \times f_{stim}(u,t) \times f_{ata}(\theta_{ce}). \tag{6.5}$$

Since

$$\tau_{ce} = \tau_{se} = K_{se}\theta_{se} \tag{6.6}$$

and

$$\theta_{se} = \theta_{joint} - \theta_{ce}, \tag{6.7}$$

$$K_{se}(\theta_{joint} - \theta_{ce}) = \tau_{scale} \times f_{stim}(u,t) \times f_{ata}(\theta_{ce}). \tag{6.8}$$

If the function $f_{ata}(\theta_{ce})$ is linear, Equation (6.8) can be solved explicitly. If not, it can be solved iteratively. In either case, the number of state variables in these equations is determined by the order of the activation, $f_{stim}(u,t)$. The series elastic element does not introduce an additional state to the model equations. Although the series elastic element represents an energy storage element, in this construction, it is not an independent energy storage element. In contrast, when the torque-velocity relationship is included, the order of the model equations does increase (Equations (3.5)-(3.6)) and the SE becomes an independent energy storage element. This may explain why the analysis of experimental twitches in Section 6.2 showed that third-order fits were significantly better than second-order fits, despite the prevalence in the literature to use second-order models for isolated muscles.

6.4.2 Effect of Series Elastic Element on IRC Estimation

Simulations of the identification experiment on systems including the series elastic element explored the effect of K_{se} on estimation of the IRC. Linear spring constants of 4.0, 35 and 1000 $\frac{N \cdot m}{deg}$ were simulated. Figure 6-15 shows the IRC used in the simulations and the IRC estimates produced by the correlation method. The IRCs estimated for all of these tests were similar and agreed with each other more closely than they agreed with the original IRC. This suggests that discrepancies in the IRC estimate were caused by the identification and processing methods, not the magni-

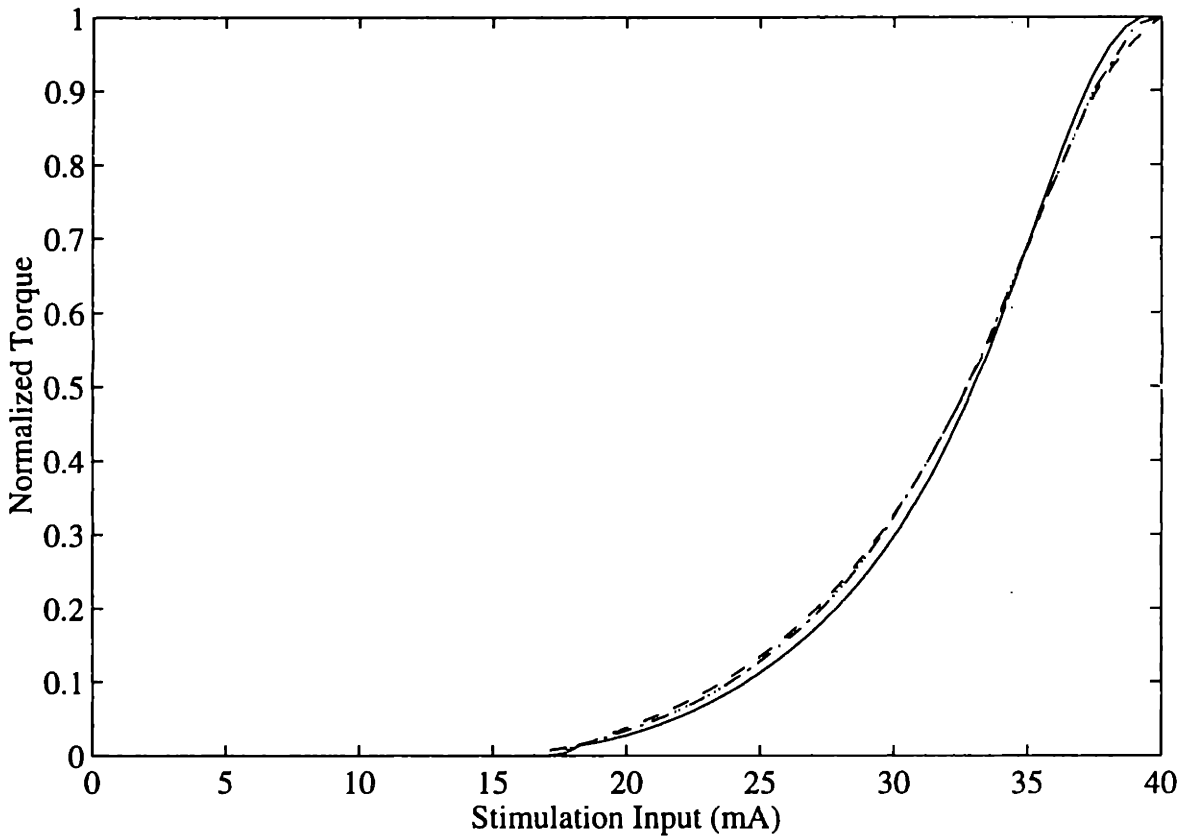

Figure 6-15: $(-)$ IRC simulated in non-linear systems. IRCs estimated with the correlation method using simulated identification data with various series elastic elements: $(--)$ $K_{se} = 4\ \frac{N \cdot m}{deg}$, $(- \cdot -)$ $K_{se} = 35\ \frac{N \cdot m}{deg}$, and $(\cdots)$ $K_{se} = 1000\ \frac{N \cdot m}{deg}$.

tude of the series elastic element. This conclusion is of course dependent on the force-length property of the contractile element. A typical force-length curve with modest slopes (similar to those of Joyce, Rack and Westbury [50]), produced these results. A steeper force-length curve in combination with a soft series elastic spring could cause more distortion to the IRC. These simulations used reasonable parameter estimates, according to the literature, and the results corresponded well to the observed experimental results.

6.4.3 Effect of the Series Elastic Element on Isometric Torque Tracking Predictions

As was stated in Section 6.4.1 the non-linear system delays the peak of the twitch response. The simulated non-linear impulse responses, with K_{se} equal to 4, 35, and 1000 $\frac{N \cdot m}{deg}$, were fit to second- and third-order models by determining the peak of the impulse responses. Figures 6-16 to 6-18 show the isometric torque response of the three non-linear systems and their corresponding linear estimates to a test input. The simplified systems predicted the behavior of the more complex system in a gross way. For all three spring stiffnesses, the linear models accurately predicted the steady state torque levels; although, slight variations occurred at low stimulation amplitudes due to errors in IRC estimation. This confirmed the accuracy of the IRC estimation and again highlighted the slight discrepancy that can occur at low stimulation amplitudes. As expected, a second-order linear estimate best approximated the stiffest system where K_{se}=1000 $\frac{N \cdot m}{deg}$. This system was effectively infinitely stiff, since the system response was nearly identical to a linear system response. For the 4.0 and 35 $\frac{N \cdot m}{deg}$ stiffnesses, the third-order system estimate matched the non-linear dynamic response better than the second-order estimate. This confirmed the experimental results which showed that a third-order linear system estimate was a good approximation of the real non-linear musculo-tendon system.

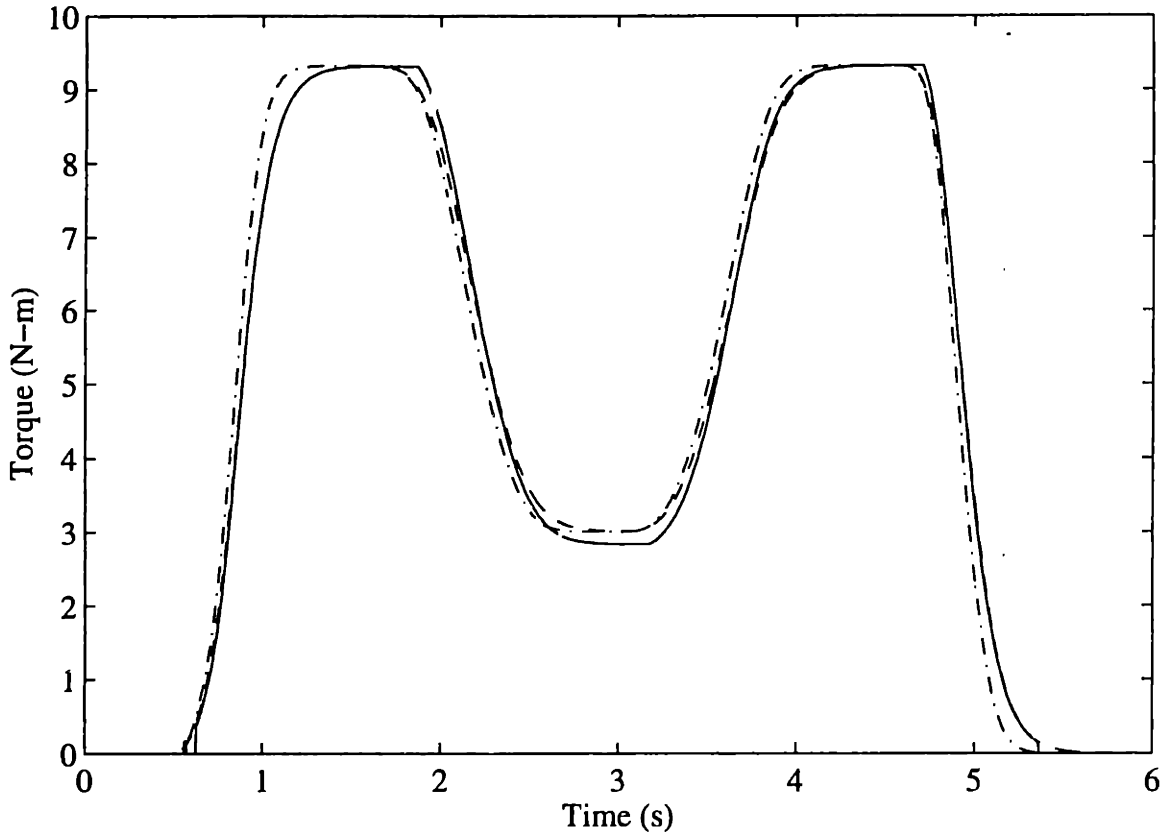

Figure 6-16: $(-)$ Simulated non-linear system response $K_{se} = 1000\ \frac{N \cdot m}{deg}$, poles=11.7 s^{-1}. Repeated-poles linear systems estimated from simulated identification of the non-linear system: $(--)$ Second-order, poles=11.76 s^{-1} and $(- \cdot -)$ Third-order, poles=23.52 s^{-1}. This spring constant is very stiff and can be approximated as infinitely stiff.

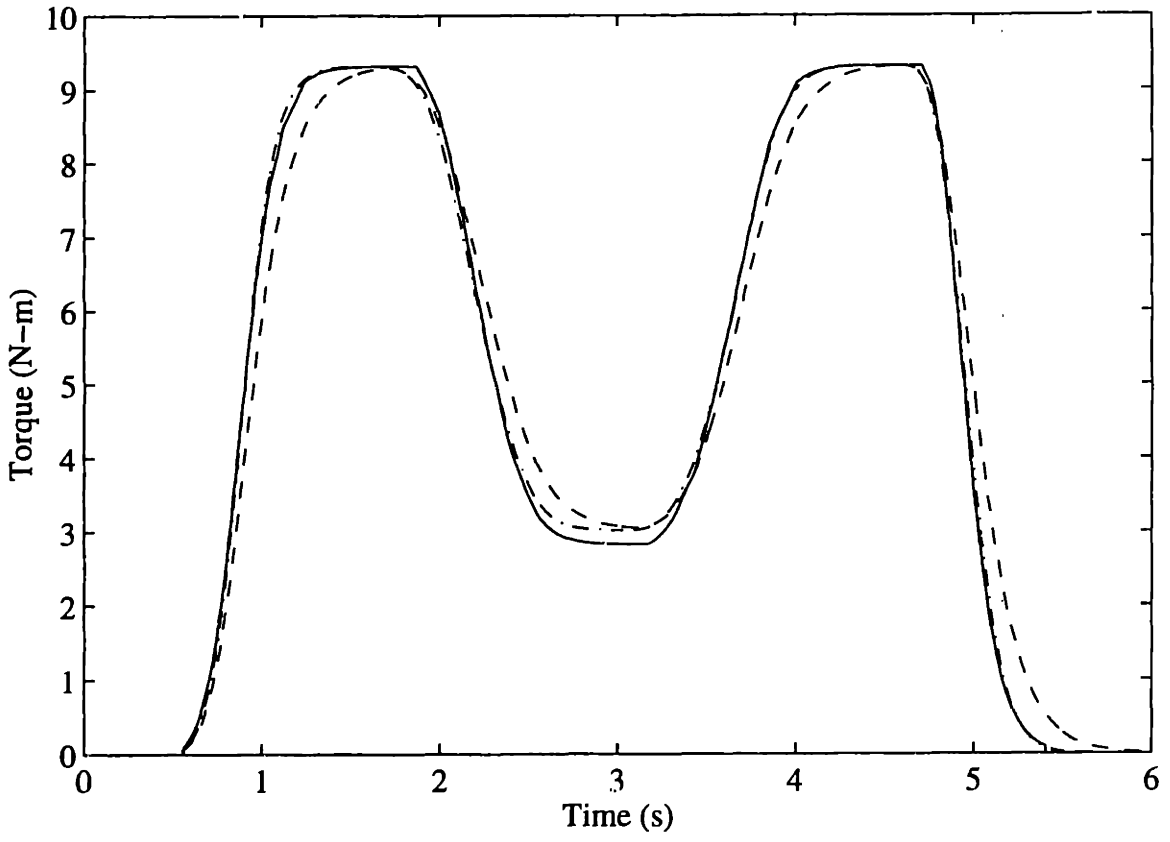

Figure 6-17: (−) Simulated non-linear system response $K_{se} = 35\ \frac{N \cdot m}{deg}$, poles=11.7 s^{-1}. Repeated-poles linear systems estimated from simulated identification of the non-linear system: (− −) Second-order, poles=8.33 s^{-1} and (− · −) Third-order, poles=16.66 s^{-1}. This spring constant is moderately stiff. Both linear estimates show some error in low plateau region due to IRC estimation errors. The third-order linear estimate matches the non-linear system in the dynamic portions of the response.

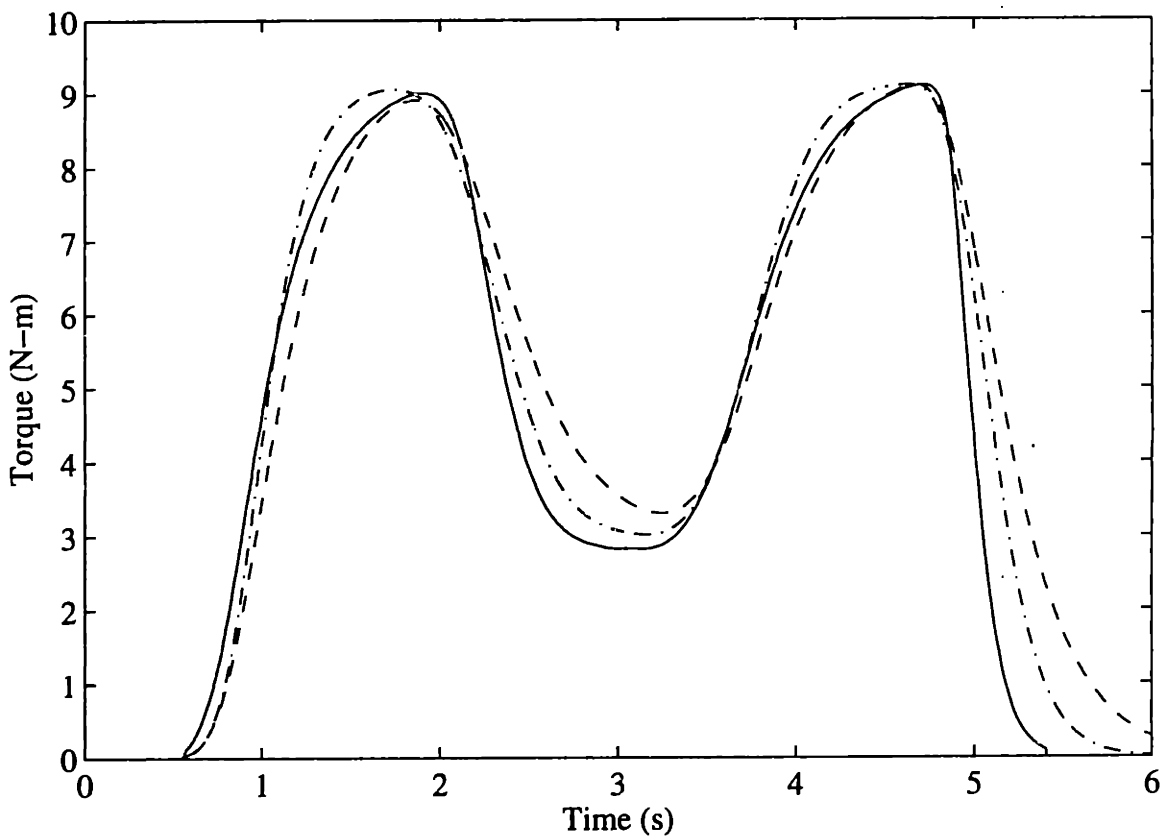

Figure 6-18: (−) Simulated non-linear system response $K_{se} = 4\ \frac{N \cdot m}{deg}$, poles=11.7 s^{-1}. Repeated-poles linear systems estimated from simulated identification of the non-linear system: (−−) Second-order, poles=4.88 s^{-1} and (−·−) Third-order, poles=9.76 s^{-1}.

6.5 Passive Identification

Three identification methods parameterized the passive dynamic properties of the full model. Section 5.4 described sequential identification, simultaneous linear estimation and free swing identification. This section describes the results of the passive identification.

The passive torque-angle and torque-velocity curves must be referenced to a specific angle and angular velocity. For the sequential identification experiments, an offset measured by the torque transducer at a constant 90 deg of flexion was removed from the data during measurement. This forced the sequential passive curves to pass through 0.0 N-m at 90 deg of flexion and 0.0 $\frac{deg}{s}$ angular velocity. 90 deg and 0.0 $\frac{deg}{s}$ were used as reference values for the other estimation methods. Curves identified by linear estimation do not naturally pass through these points because the estimation algorithm is underconstrained. A constant torque added to the position curve and subtracted from the velocity curve produces the same residual fitting error, and represents an equally valid solution. The curves produced by linear estimation were shifted by a constant torque to force the curves to pass through the reference values. This shifting allowed comparison between curves derived from different methods, without effecting prediction or simulation of the passive output.

Figures 6-19 and 6-20 compare the torque-angle and torque-velocity curves obtained with the three methods for a single subject. All three methods found nearly identical torque-angle curves for all 16 data sets (see Figure I-1 for the torque-angle curves from the other subjects). In contrast, the torque-velocity curves found with the three techniques differed consistently across methods for all 16 subjects. The free swing method identified the lowest level of damping between the three methods. For most subjects, this method found similar damping in the positive and negative velocity regions. Simultaneous linear estimation also identified similar damping in the positive and negative velocity regions, but this method produced a larger overall damping relationship. Sequential identification estimated the largest velocity dependent torques. The characteristic torque-velocity curve produced by this method

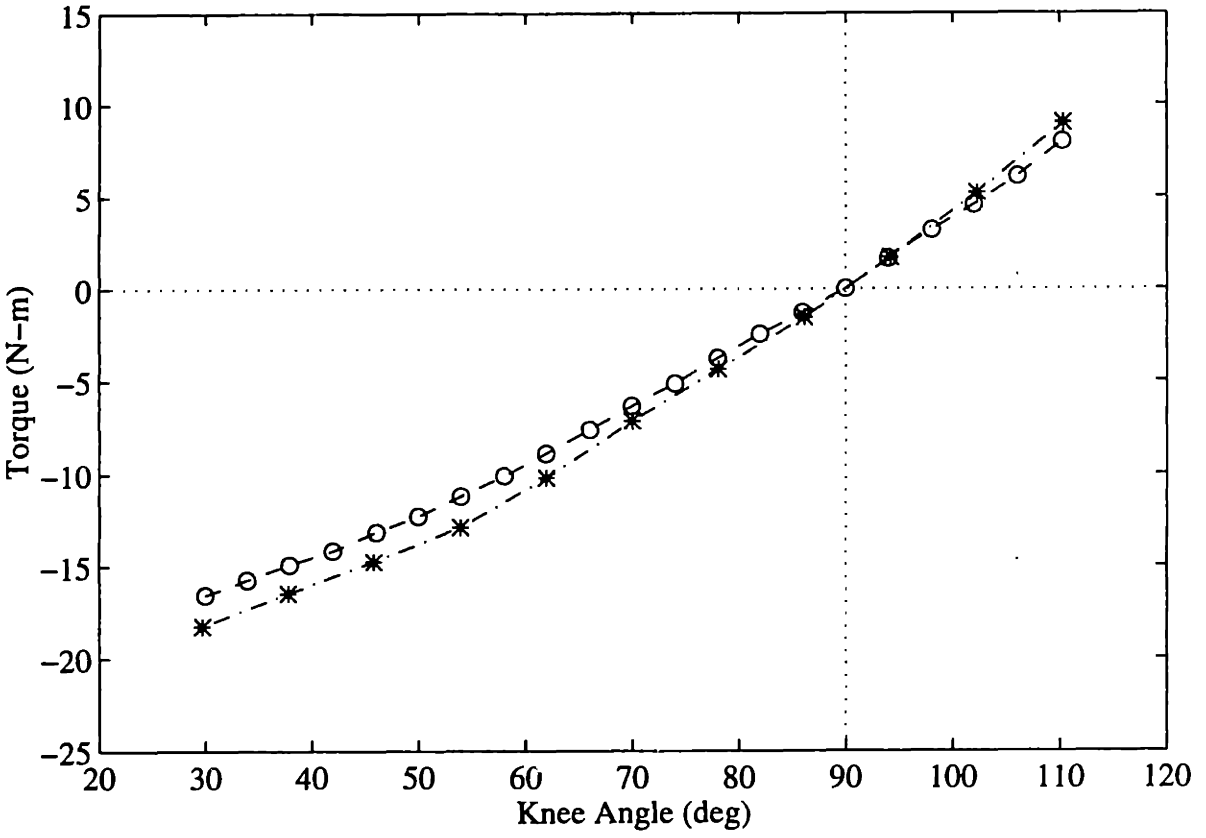

Figure 6-19: Passive torque-angle curves identified by $(-\circ-)$ sequential identification and $(-\cdot*\cdot-)$ simultaneous estimation. The free swing identification used the torque-angle curve from the sequential method. The curves are nearly identical.

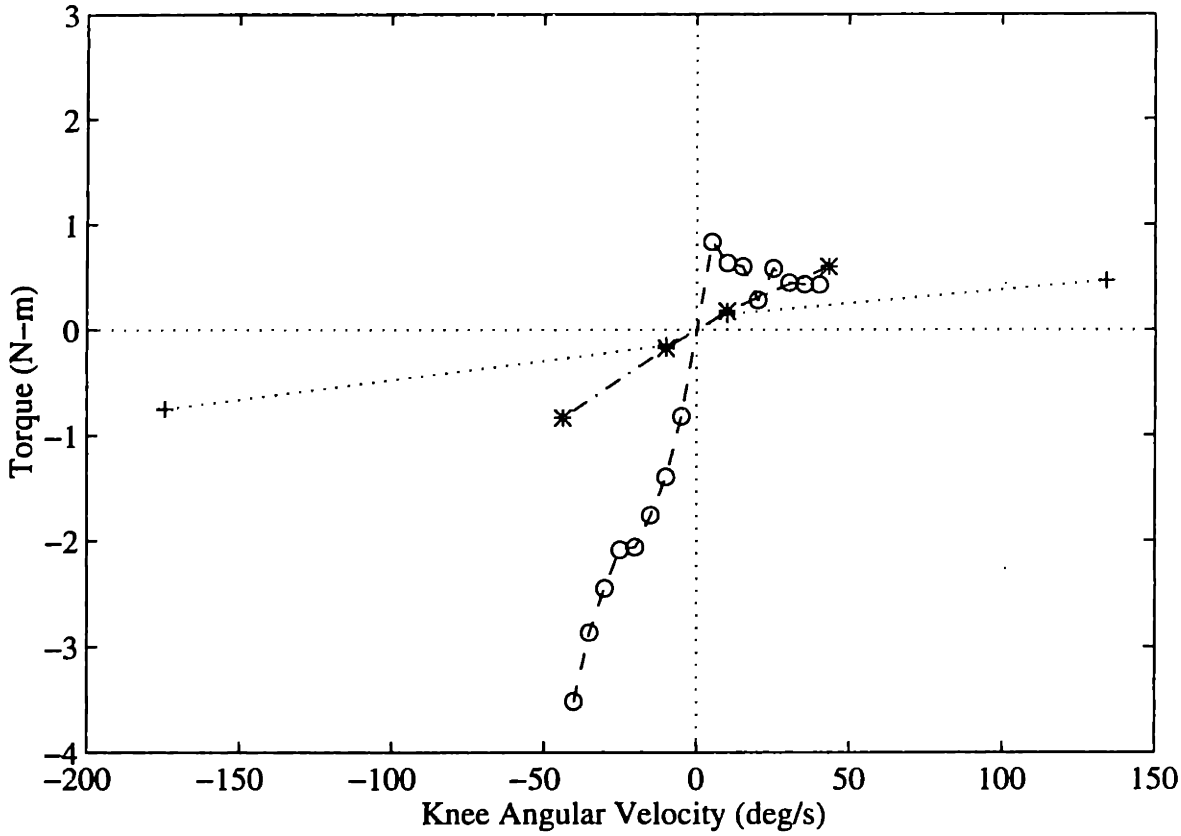

Figure 6-20: Passive torque-velocity curves identified by $(-\circ-)$ sequential identification, $(-\cdot*\cdot-)$ simultaneous estimation and $(\cdots+\cdots)$ free swing identification. Large differences are seen between the different methods, although the overall magnitudes are small for all methods when compared to the torque-angle curves.

consisted of comparatively high damping in the negative velocity region, with a shallow slope in the positive velocity region. In some cases, (as with the curve in Figure 6-20), this method produced a flat or negative slope in the positive velocity region.

The velocity ranges tested by each method differed. The sequential method limited the velocity range to +/- 40 $\frac{deg}{s}$. It was difficult to accelerate the limb and maintain constant velocity over the limited angle range for velocities higher than 40 $\frac{deg}{s}$. Likewise, the simultaneous estimation protocol used kinematic trajectories with velocity ranges of approximately the same magnitude. It may be possible to test higher velocity trajectories with this method, but subject comfort and safety concerns become issues at higher velocity levels. Free swing identification tested a much higher range of velocities, typically +/-150 $\frac{deg}{s}$. The velocity range for this method differed for each subject, depending on the dynamic response of the limb. Because the free swing method relied on the subject's own muscles to initiate movement, there was no need (and no possible way) to limit the velocity magnitude. All the subjects' limbs had larger dynamic velocity ranges than were tested by either the sequential or simultaneous methods (see Figure I-2 for data from the other subjects). Despite their differences all three methods measure small torque contributions compared to torque contributions from the torque-angle property.

The inertia identified with the two linear estimation methods differed from each other and from the inertia calculated from subject leg length and weight information. Table 6.3 shows the inertia estimated or calculated by each identification method for the 16 joint-limb systems tested. The table includes average inertia and standard deviations for each method. For all subjects, the free swing method produced consistently lower inertia estimates than the simultaneous method. The computed inertia values ranged from 0.217 - 0.596 $N \cdot m \cdot s^2$, while the free swing estimated inertias ranged from 0.168 - 0.487 $N \cdot m \cdot s^2$, and the simultaneous estimated inertias ranged from 0.230 - 0.704 $N \cdot m \cdot s^2$.

Some of the inertia difference can be explained by systematic error in the measurement procedures. The computed inertia contained both measurement error and estimation error. This simple estimation method, which calculated inertia from leg

Subject	Computed Inertia	Free Swing	Simultaneous
bksl1	0.252102	0.232621	0.304241
nccl1	0.303668	0.277312	0.370131
nccr1	0.303668	0.28476	0.386747
eycr1	0.229183	0.205119	0.261842
eycl1	0.217151	0.226891	0.33117
malr1	0.595877	0.322003	0.533424
kipl1	0.343202	0.194806	0.295646
kipr1	0.343202	0.210849	0.276166
pskr1	0.444043	0.390758	0.526549
jtcr1	0.425708	0.286479	0.410811
jtcl1	0.425708	0.313408	0.401644
jadr1	0.419978	0.226891	0.517381
jadl1	0.419978	0.419978	0.560353
jxwr1	0.303668	0.167877	0.229756
jxwl1	0.303668	0.21887	0.235486
pgmr1	0.446334	0.487015	0.704739
Average	0.361071	0.279102	0.39663
Std	0.09946	0.089255	0.137222

Table 6.3: Inertia ($N \cdot m \cdot s^2$) values estimated from the two linear estimation methods and calculated from leg length and weight information.

length and subject weight measurements, does not account for variation in body type or distribution of weight within the body. The error in this calculation technique is +/- 10 %. In addition, the leg length measurements were only accurate to 0.5 in. This led to +/- 10 % error in the inertia calculations due to measurement error. The free swing and simultaneous inertia estimations have up to +/- 5 % absolute error due to variation in the placement of the accelerometer, however this error should not effect the relative error between the two methods. Most of the computed values agree with the estimated inertias within these large measurement error bounds; however, the errors do not account for differences between the free swing and simultaneous methods. The acceleration of the simultaneous trajectories was smaller than the acceleration of the free swing trajectories, making the simultaneous inertia estimation more susceptible to signal noise. This decrease in signal to noise ratio may account for some of the difference between these two estimates.

6.6 Simulations of Passive Identification

Simulated data tested the linear estimation algorithms used for the simultaneous and free swing identification methods. Figure 6-21 shows the passive torque-angle and torque-velocity curves used to simulate a system with hysteresis. The same graphs also show the curves produced by processing the simulated data with the linear estimation algorithm. The algorithm produced an estimated torque-angle curve which was an average of the curve containing hysteresis. To compensate for the hysteresis, the algorithm produced a torque-velocity curve with a discontinuity across zero. Figure 6-22 shows a similar result for a system without hysteresis, but including a simple discontinuous torque-velocity curve as a model of static friction.

Varying levels of white noise were simulated to see how noise affected the accuracy of the identification algorithm. For low noise levels (less than +/- 0.5 N-m) and moderate damping ratios (b=.02 $\frac{N \cdot m \cdot s}{deg}$), the algorithm had no trouble identifying the appropriate torque-angle and torque-velocity curves (see Figure 6-23). Figure 6-24 shows identification of a system in the presence of comparatively large levels of white

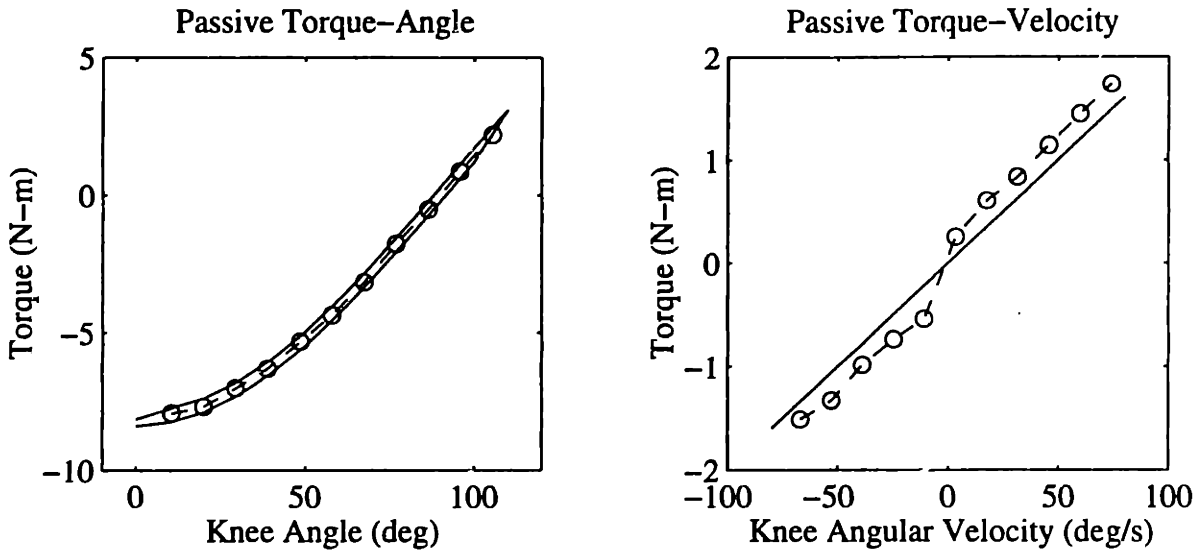

Figure 6-21: The solid curves (–) were used to simulate the behavior of a passive system during the simultaneous identification experiment. Linear estimation on this simulated data set produced the estimated (– o –) curves. Hysteresis in the torque-angle curve was interpreted by the algorithm as a discontinuity across zero in the torque-velocity curve.

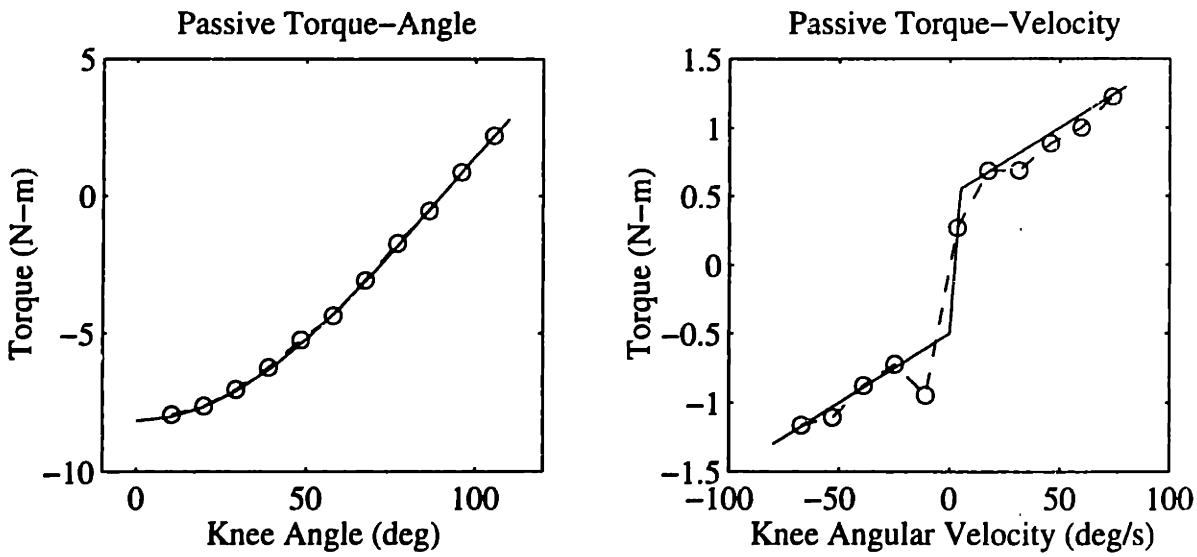

Figure 6-22: (–) Simulated passive system with static friction in the torque-velocity curve, (– o –) Estimated with simultaneous identification algorithm. The algorithm can identify static friction.

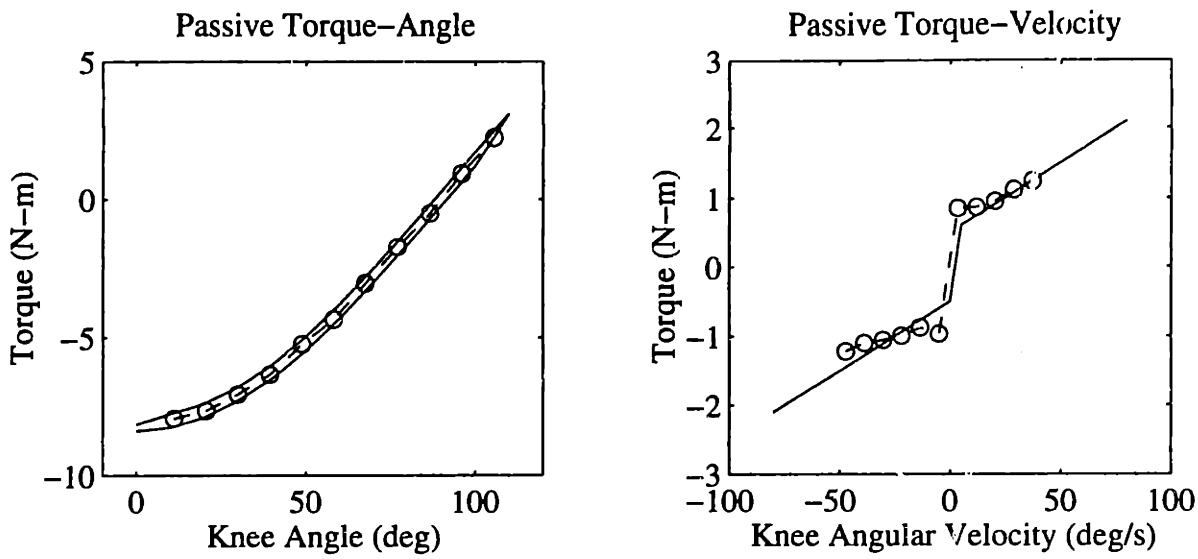

Figure 6-23: (−) Simulated passive joint-limb system. White noise (+/-0.5 $N \cdot m$) was added to the torque simulated by this model. (− o −) Estimated with simultaneous identification algorithm. Low levels of white noise did not compromise identification of the passive properties.

noise (+/-2.5 $N \cdot m$). This system included 0.5 $N \cdot m$ of hysteresis in the torque-angle curve and 1 $N \cdot m$ of static friction in the torque-velocity relationship with a small damping ration of 0.002 $\frac{N \cdot m \cdot s}{deg}$. In this case the noise level was more than twice the magnitude of the torque contribution from the torque-velocity relationship, a much higher noise level than would be expected experimentally. This large noise level caused some error in the identified parameters. Most of the error appeared in the torque-velocity curve, with some small error in the torque-angle curve. The overall shape of the torque-velocity curve was still apparent, but the end points of the piece-wise linear segments were noisy.

Figure 6-25 shows an identified system in which the noise was correlated to the first one second of the simulation run. Overall the estimate was good; however there was some error in the low angle region of the torque-angle curve. The simulated trajectory traversed this low angle region during the initial 1s of the trial, when the most noise occurred. For this particular input, the low angle region was not revisited in the later part of the trajectory, so the algorithm produced a distorted estimate of the torque-

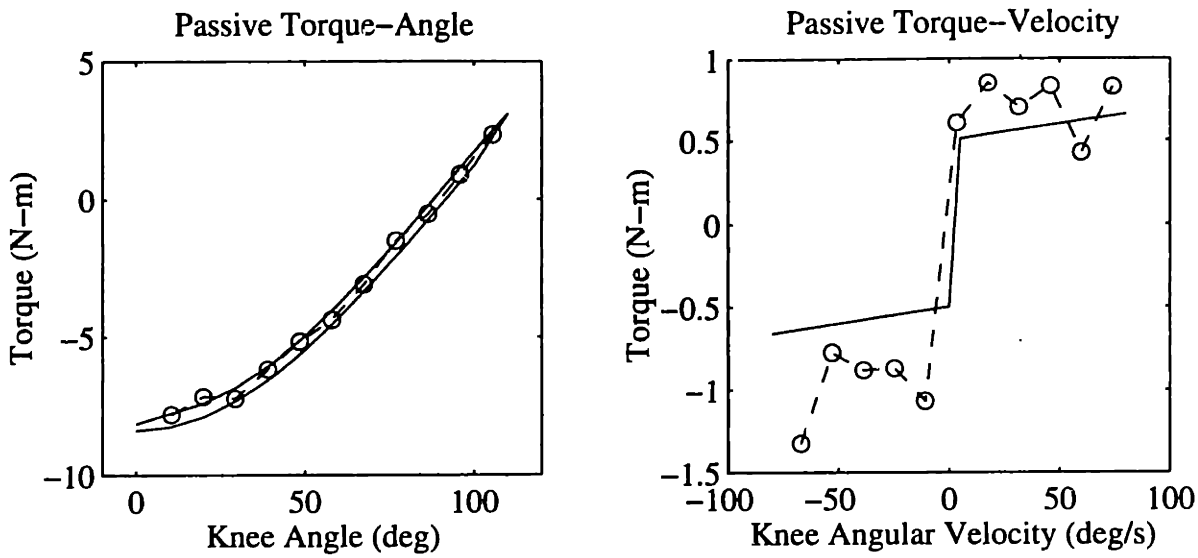

Figure 6-24: (–) Simulated passive system. A large amount of white noise (+/-2.5 $N \cdot m$) was added to the simulated torque. (-· o –) Estimated from simultaneous identification algorithm. The estimation algorithm had some trouble identifying the torque-velocity curve when the noise torque was larger than the velocity dependent torque. The basic shape and magnitude of the estimated torque-velocity curve was correct, but considerable noise was seen in the individual end points of the piece-wise linear segments. This noise level was higher than would be expected experimentally.

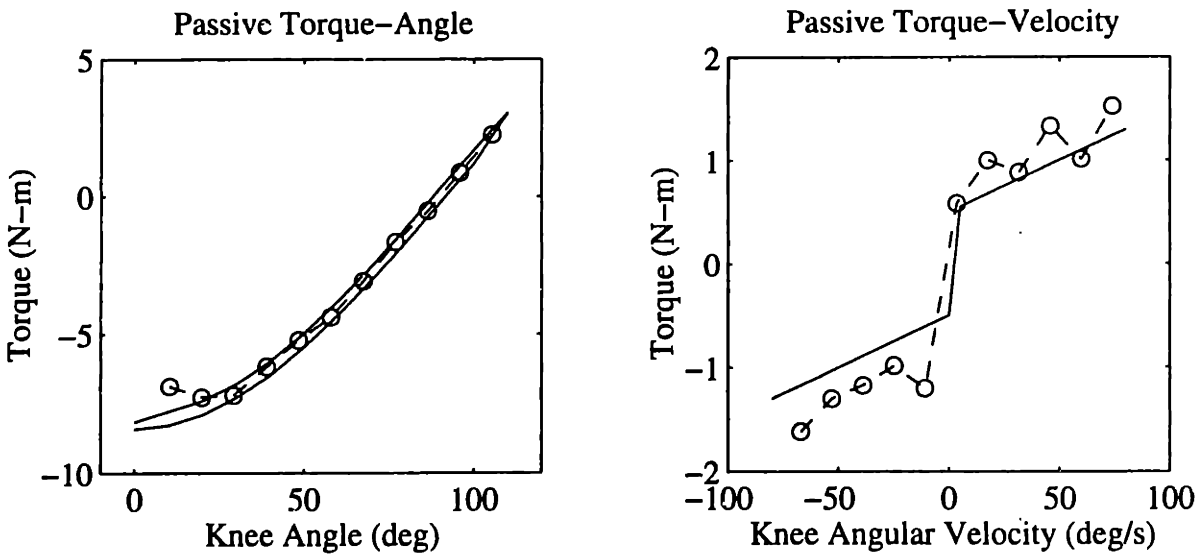

Figure 6-25: (–) Simulated Passive System, (– o –) Estimated from simultaneous identification algorithm. Noise, correlated to the initial 1s of the trajectory, produced some error in the torque-angle curve, but did not interfere with identification of the torque-velocity curve.

angle curve in this region. For other trajectories, where the initial angle region was traversed at a later time in the curve, the torque-angle curve was identified correctly. A similar result was observed experimentally where motion of the limb produced high frequency vibrations in the brace strut. The largest vibrations, and corresponding torque noise, occurred at the beginning of a trajectory. Kinematic trajectories which traversed the low angle region only during this noisy phase produced torque-angle curves like the one in Figure 6-25.

In summary, simulations showed that the linear estimation algorithms used to process data from the simultaneous and free swing protocols could identify passive systems with varying characteristics. The algorithm translated hysteresis in the torque-angle curve into static friction in the torque-velocity curve, while it correctly identified static friction. Torque-angle hysteresis does exist in the muscle-joint-limb system. The identification algorithm can identify properties which will predict this behavior, even though hysteresis was neglected. The algorithm can handle noise magnitudes less than the torque contribution of the torque-velocity property. Noise magnitudes larger than the torque-velocity contribution resulted in noisy identification of the piece-wise linear torque-velocity curve, but the overall shape of the original curve can still be discerned. This result highlights the importance of low level noise signals for identification. Correlated noise also caused some identification error. To prevent noise correlation, the kinematic trajectory must cover the angle-angular velocity plane and each angle should be encountered at different times during the trajectory. This simulation only looked at noise correlated to the beginning of the trajectory, but other correlations may exist in an experimental system. The simulations indicated that care should be taken to eliminated correlated noise from experimental measurements.

6.7 Active Identification

A single experimental method was used to identify the active torque-angle and torque-velocity properties; however, the identification depended on the passive system estimate. Each passive parameter set produced a different set of active parameters. If the

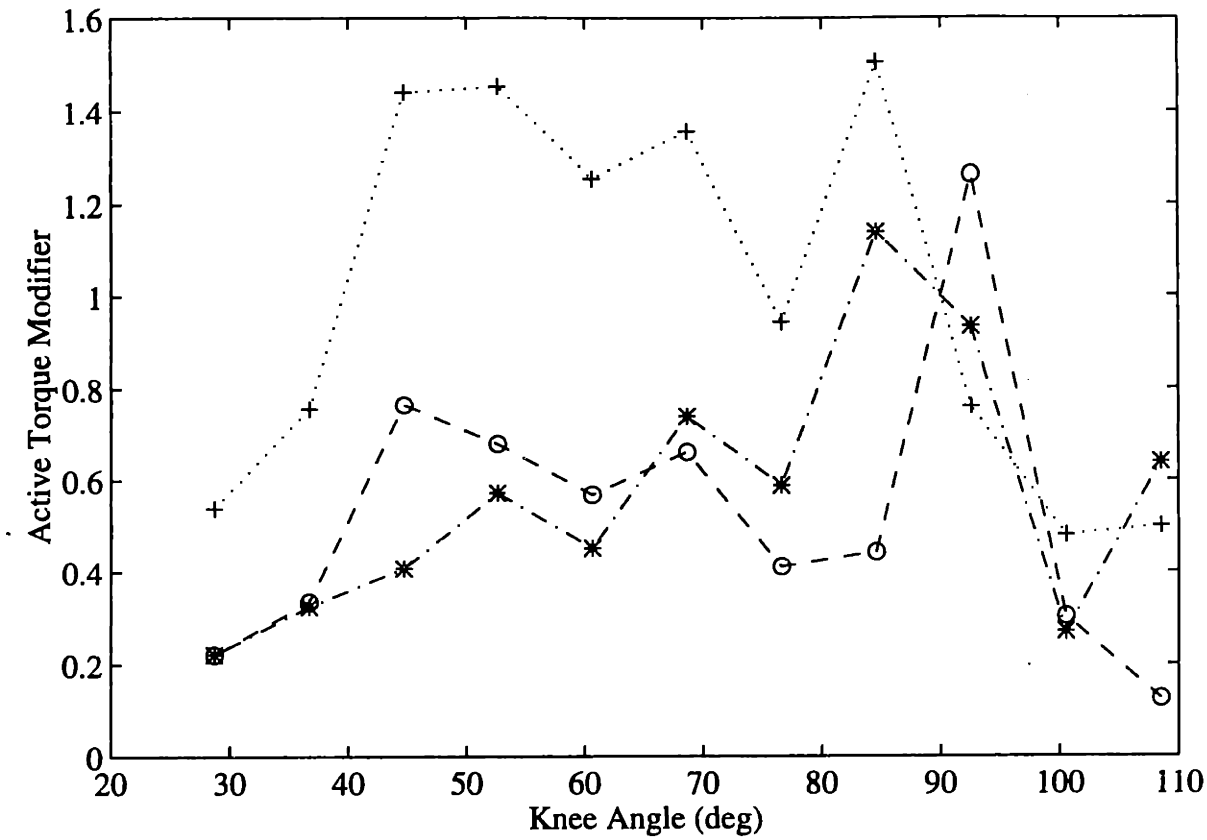

Figure 6-26: Active torque-angle curves identified from the same experimental data. The identification is dependent on the passive dynamic properties. The passive dynamic estimates in each case came from $(-\,o\,-)$ sequential identification, $(-\cdot *\cdot -)$ simultaneous estimation and $(\cdots+\cdots)$ free swing identification. The free swing passive parameters produced a bell shaped active torque-angle curve for nearly every subject.

passive functions contained significant errors, the error would propagate to the active parameters. The active torque-angle and torque-velocity curves were arbitrarily normalized to one at 90 deg for the torque-angle curve and 0 $\frac{deg}{s}$ for the torque-velocity curve. The normalization factors were lumped into the scaling factor τ_{scale} to retain the overall response magnitude. In the same way that the passive curves were shifted to compensate for an underconstrained identification problem, normalizing the active curves compensated for the underconstrained identification of the active properties.

Figures 6-26 and 6-27 show the active torque-angle and torque-velocity properties identified from the same active data set, with different passive dynamic estimates. The

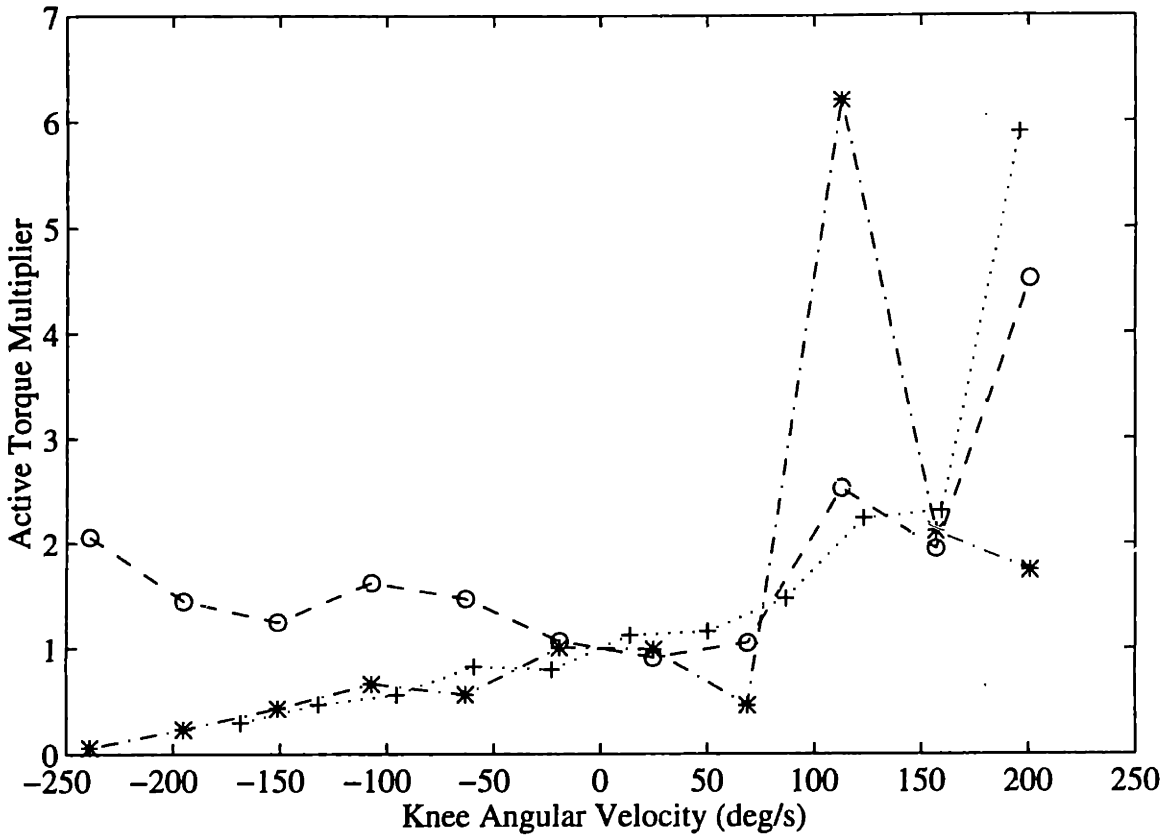

Figure 6-27: Active torque-velocity curves identified from the same experimental data. The identification is dependent on the passive dynamic properties. The passive dynamic properties in each case were from (− o −) sequential identification, (− · ∗ · −) simultaneous estimation, and (· · · + · · ·) free swing identification. In all cases, the active curve produced by the free swing passive properties shows a small magnitude in the negative velocity region and slopes upward towards the positive velocity region.

torque-angle curves produced from the free swing passive properties always appeared qualitatively as bell shaped curves with low magnitudes at both extremes of the angle range and some noise interspersed with the data. The peak of the torque-angle curve occurred somewhere in the middle of the angle range, but the location was not consistent from subject to subject. The torque-velocity curves identified from the free swing passive properties have low magnitudes in the negative velocity region and slope upward towards a maximum at the extreme of the positive velocity region. Curve shapes produced from the other two passive parameter sets were not consistent. See Figures I-3 and I-4 for the active curves identified for the other subjects.

6.8 Simulation of Active Identification

Simulated active torque-angle and torque-velocity curves were used to explore the effects of logarithmic data compressions on the active parameters. Figure 6-28 shows a set of active curves used to simulate a set of active data. On the same graph is displayed the active curve identified by the algorithm from the simulated data set. The top and bottom row of graphs displays the same information, but the bottom graphs are plotted on a log scale. For purposes of these simulations, the scaling factor τ_{scale} was lumped into the active torque-angle curve and the curves were not normalized. In the log domain, the simulated and estimated curve are almost indistinguishable. In the real domain, small errors in the torque-angle curve are observed.

The same identification was repeated with simulated white noise added to the identification signal. The noise was added in the real domain, so it gets compressed unequally in the log domain prior to linear estimation. Figure 6-29 shows the effect of noise on parameter estimation. The noise level shown here is about 10 % of the signal level. This very large noise level produced large errors in the extreme negative velocity region of the torque-velocity curve as viewed in in the log domain (lower plot). This large error becomes insignificant in the real domain. The torque-angle curve shows error in the log domain near 90 deg of flexion which is magnified in the real domain. The relationship between errors in the torque-angle and torque-velocity curves is better understood by looking at a phase plane picture of the kinematic trajectory. The kinematic data used in these simulations is displayed on a phase plane plot in Figure 6-30. Many of the data points which fall between 80 and 100 degrees of flexion, also fall in the extreme negative velocity region (below -160 $\frac{deg}{s}$). This indicates that the estimation errors in the two curves are coupled. Because of the distortion that occurs in moving between the log and real domains, negative errors in the torque-velocity curve were compressed while positive errors in the torque-angle curve were magnified. Even though the noise resulted in a noisy torque-angle curve, the overall shape of the curve is still apparent. The noise level simulated in this example is large, however, it is not unrealistic since errors in estimation of the

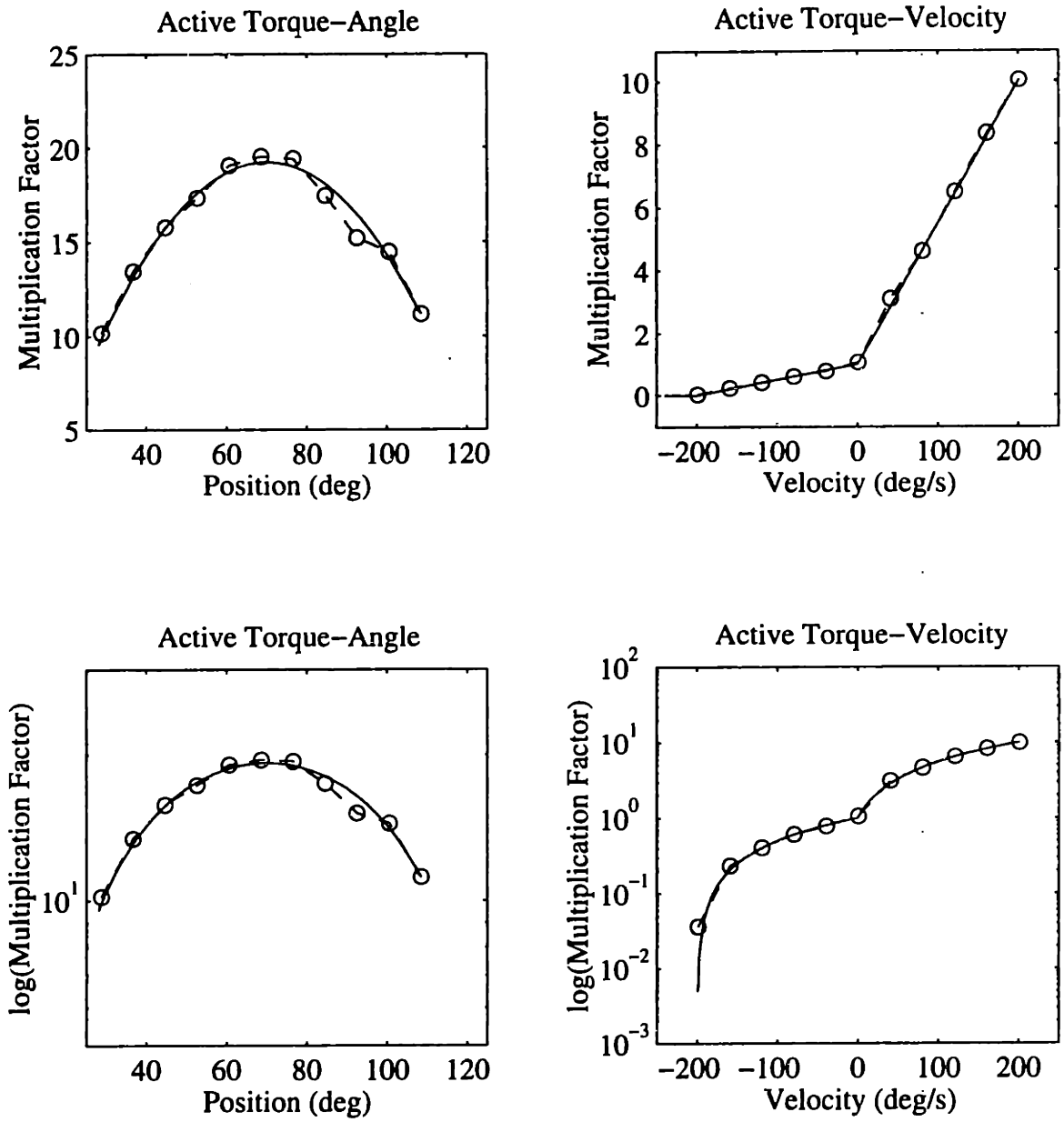

Figure 6-28: Active properties (−) Simulated and (−o−) estimated with active linear estimation procedure. The top and bottom rows show the same curve in the real and log domains. Small estimation errors are barely visible in the log domain, but are magnified in the real domain.

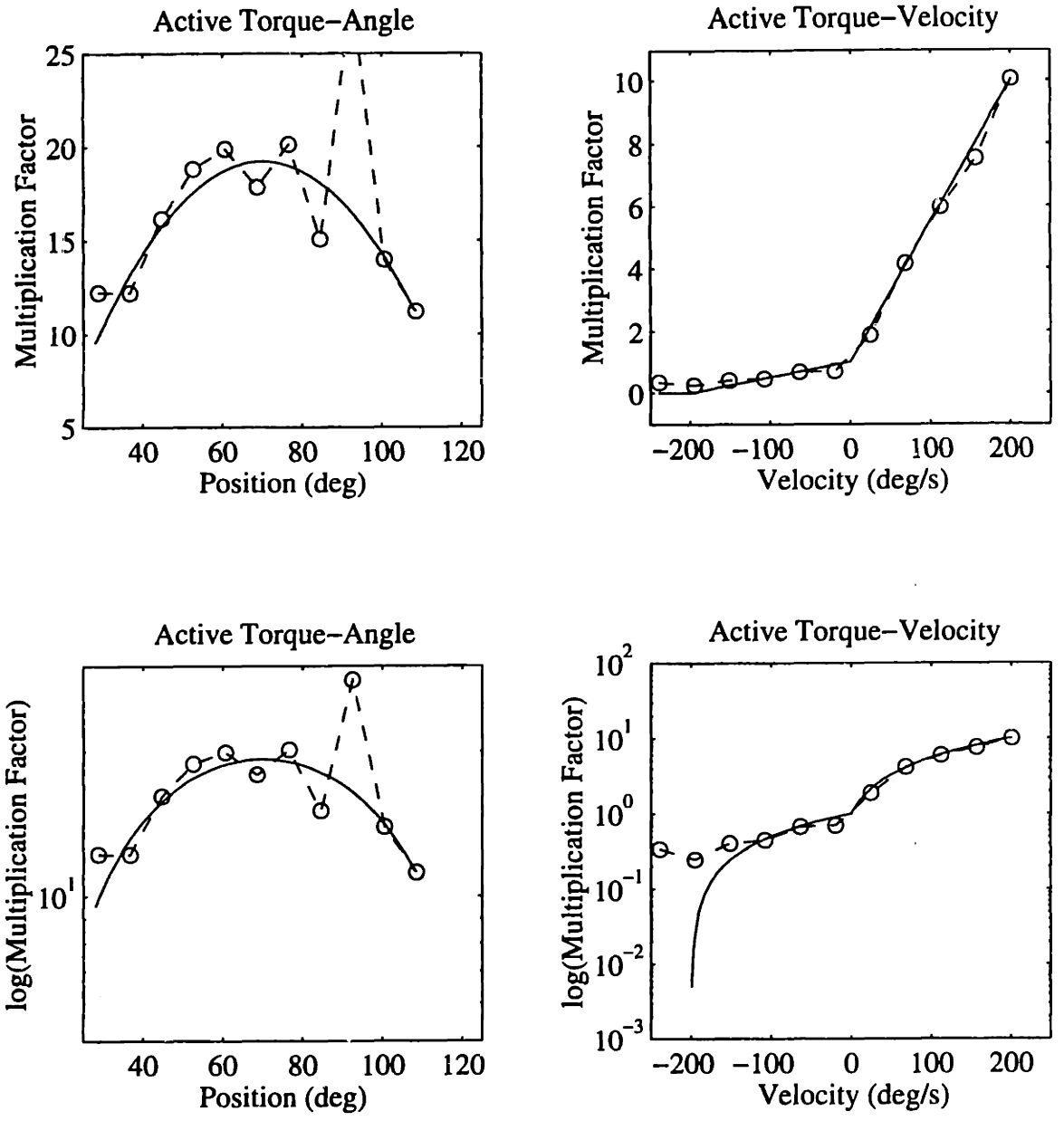

Figure 6-29: Active properties (−) Simulated and (−o−) estimated with active linear estimation procedure. White noise was added to the signal in the real domain. The top and bottom rows show the same curve in the real and log domains. The noise produced some error in both active curves.

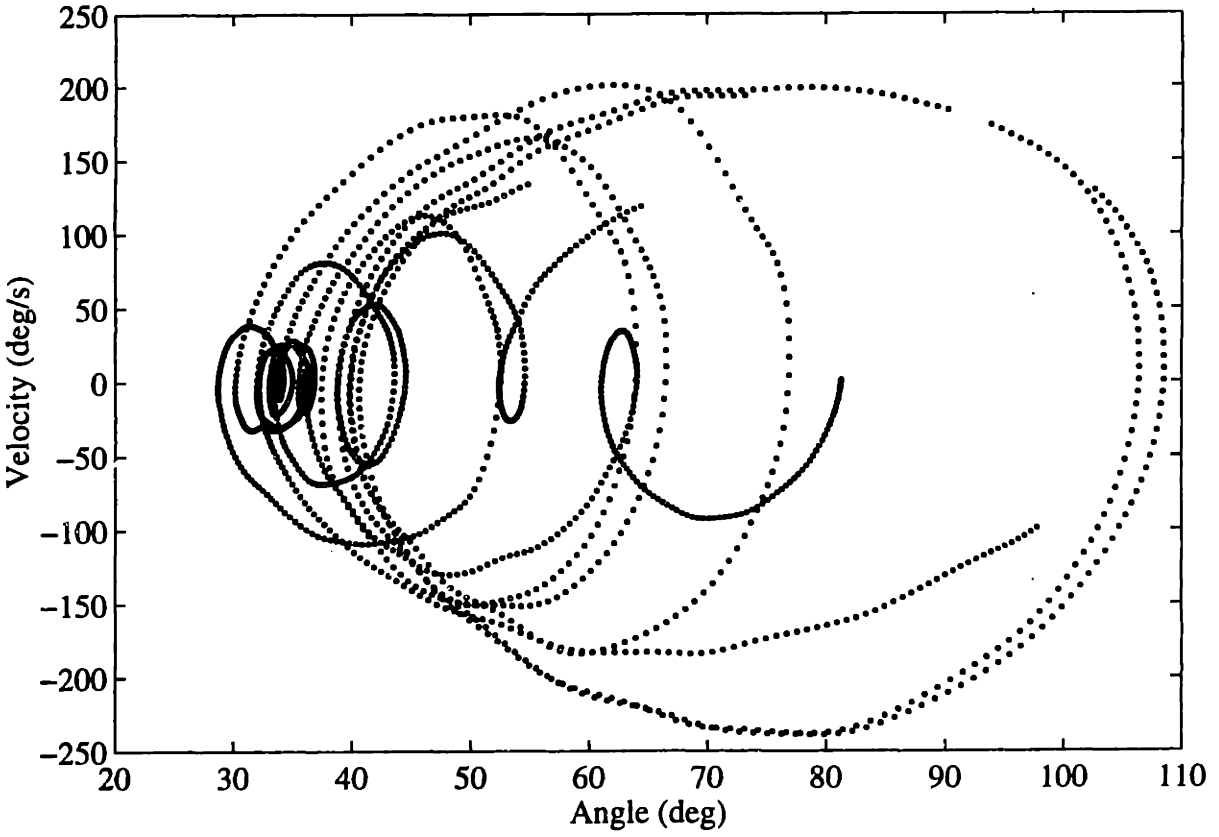

Figure 6-30: Kinematic simulated data used to test active identification algorithm. Prediction errors occur where the phase plane in not well covered.

contraction dynamics and passive dynamics are included in the signal noise. These simulated results point out the importance of a well distributed kinematic trajectory for active identification, and explain the somewhat noisy curves that are produced by the estimation algorithm.

6.9 Prediction of Knee Angle

Simulations of the parameters identified for the muscle-tendon-joint models predicted the joint angle response of the system to the prescribed inputs as shown in Figure 5-12. Figures 6-31 through 6-34 show the predictive ability of each parameter set derived for a single subject. The parameter sets are designated by the identification method which determined the passive dynamic properties.

Figure 6-31 shows the response predicted by the three parameter sets to a step in stimulation amplitude. For this subject, the free swing parameters produced a good estimate of the steady-state response to the step input. The sequential parameters predicted large oscillations in the region where the experimental system showed steady-state. Although this did not happen for every subject, oscillations in the steady-state region were a common feature found in the step response of the sequential parameters. The oscillations result from inaccurate prediction of the active damping.

The last 1.5s of the graph represents free fall where only the passive dynamics were used. For this subject, the sequential parameters predicted a much more damped response than that observed experimentally. For many subjects (see Figure J-1), the sequential parameters predicted a large overshoot during the initial downswing of the leg. On the return oscillation, the response became overdamped. Recall the asymmetric passive torque-velocity curves produced by sequential identification (Figure 6-20). This curve had little damping in the positive velocity region, which corresponds to the downswing of the leg and accounts for the very large overshoot. In the negative velocity region, the comparatively large damping resulted in the overdamped response seen on the return oscillation. The free swing parameters matched

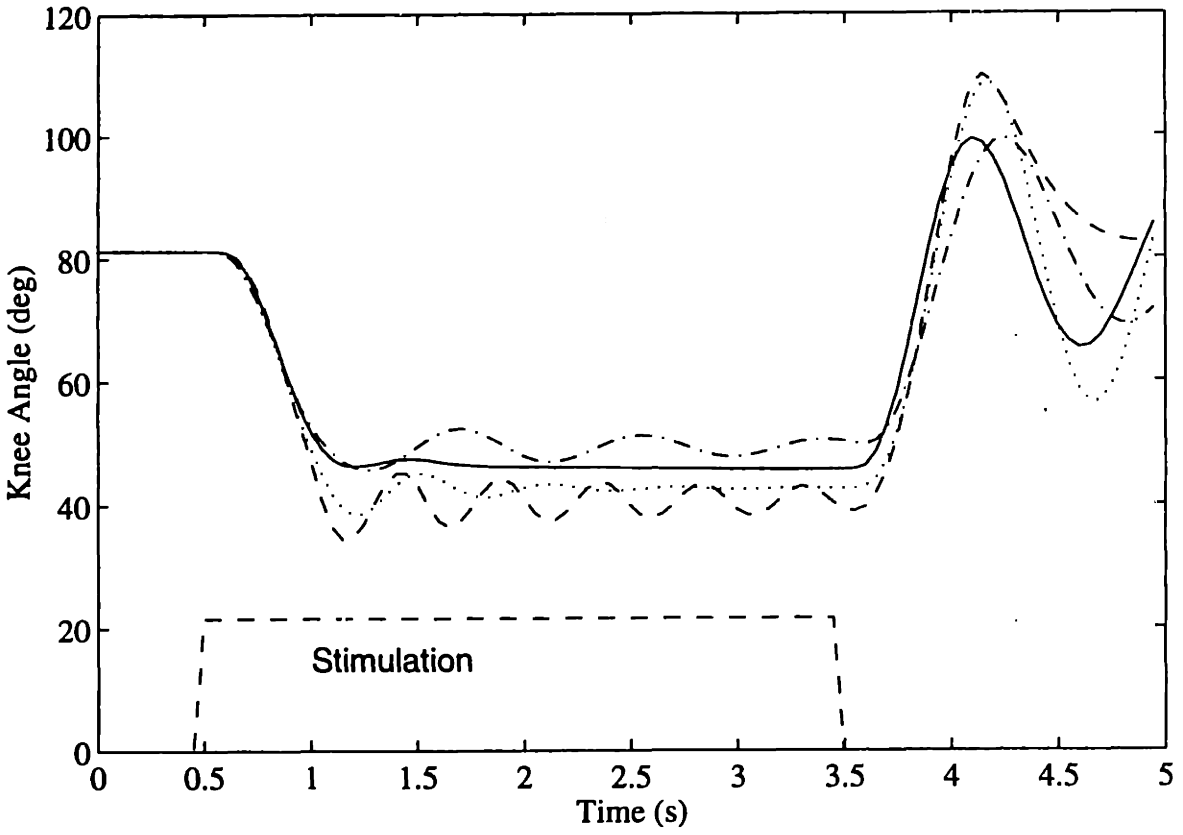

Figure 6-31: Step response: (−) Experimentally measured response and predictions with (−−) sequential parameters, (− · −) simultaneous parameters and (···) free swing parameters. (−−) Stimulation input ($\frac{1}{2}$ amplitude).

Linearized System	ζ	ω_n [rad/s]	0.5T [s/$\frac{1}{2}$ cycle]	M_2/M_1
Sequential (neg. velocity)	0.979	6.656	0.47	-
Simultaneous	0.137	5.190	0.61	0.64
Free Swing	0.021	6.416	0.49	0.80
Experimental System	-	-	0.50	0.84

Table 6.4: The different parameter sets were linearized about 0.0 $\frac{deg}{s}$ and 81 deg of flexion. The damping ratio ζ, natural frequency ω_n, oscillation period T, and the ratio between oscillation peak magnitudes M_2/M_1 for the experimental system were estimated from the last 1.5s of the step response (Figure 6-31). The linearized free swing parameters best approximate the dynamic characteristics of the experimental system.

the oscillation frequency of the passive response best. For this subject, the magnitude of the oscillations was somewhat off. In general the free swing parameters predicted the oscillation frequency during purely passive portions of the response better than the other two parameter sets and the free swing parameters were better able to predict magnitude as well. To look more closely at the dynamic response characteristics, these passive curves were linearized about the operating point, 0.0 $\frac{deg}{s}$ and 81 deg, the steady-state position of this particular passive system. Table 6.4 compares the linearized systems to properties measured from the final 1.5s of the experimental step response (Figure 6-31). The linearized free swing parameters matched the dynamic characteristics of the real system better than the other linearizations.

Figure 6-32 shows the predicted responses to a ramp of stimulation amplitude. All of the parameter sets showed some prediction error near threshold, which corresponded to the threshold error in the IRC. As with the step response, the sequential parameters produced large oscillations in the active region which were not seen with the other parameter sets. None of the predictions were particularly well matched to the ramp response. This was true for most of the subjects (see Figure J-3). The sequential parameter set produced a ramp response with oscillations in the active region of the response. These oscillations were typical across subjects for this parameter set, although oscillations were never seen in the experimental response. The free swing

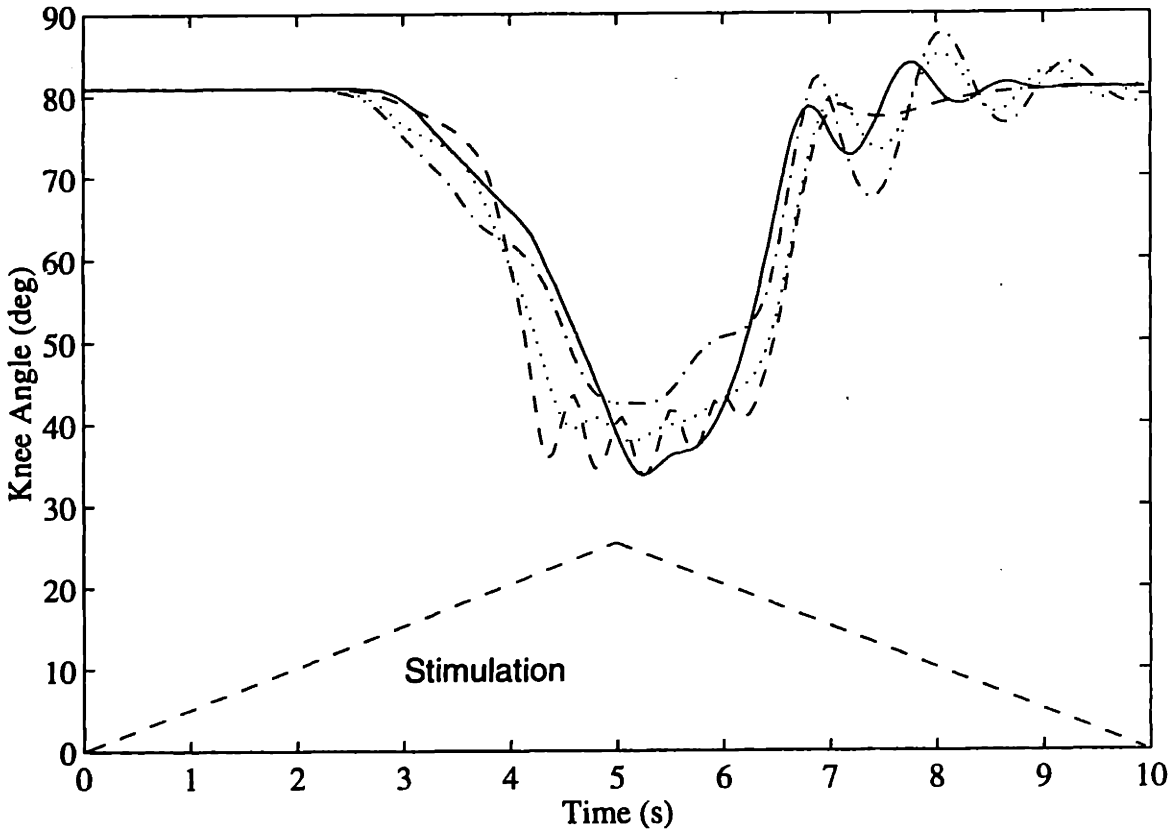

Figure 6-32: Ramp response: (−) Experimentally measured response and predictions with (−−) sequential parameters, (− · −) simultaneous parameters and (···) free swing parameters. (−−) $\frac{1}{2}$ stimulation amplitude.

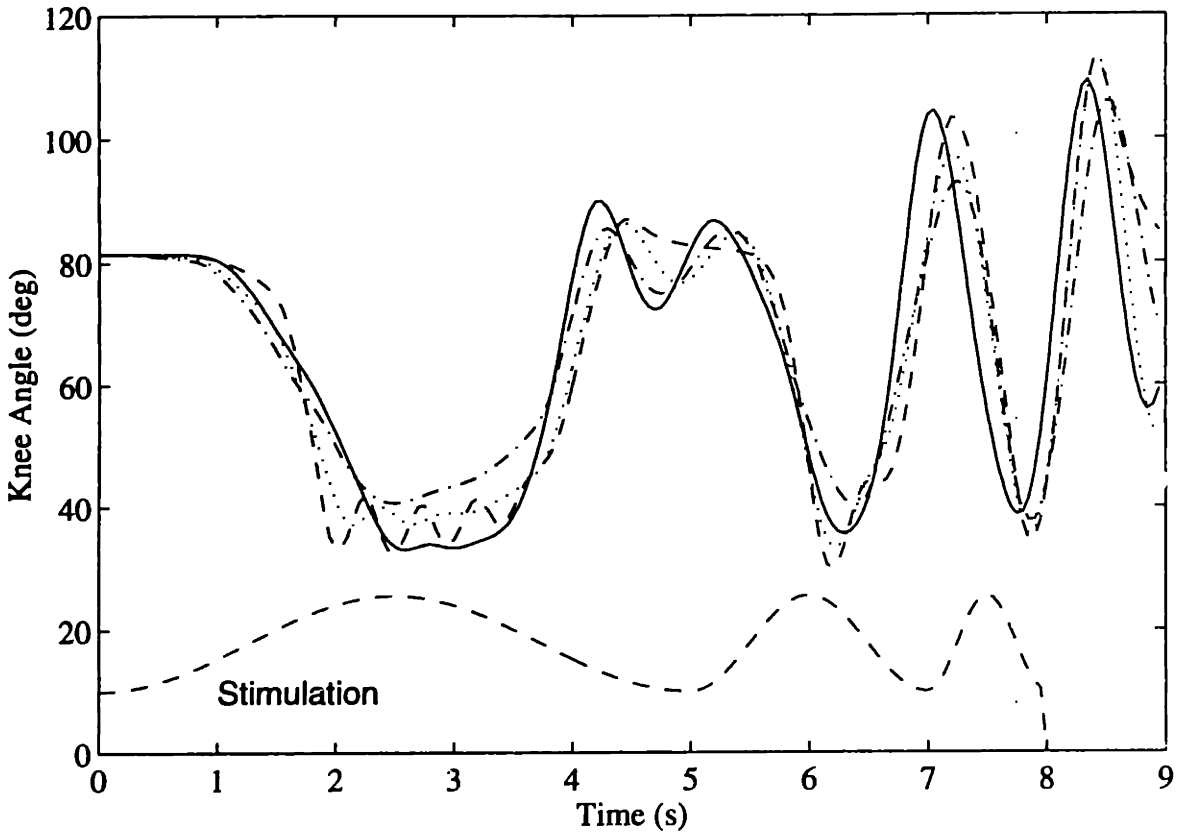

Figure 6-33: Sinewave response: (−) Experimentally measured response and predictions with (− −) sequential parameters, (− · −) simultaneous parameters and (· · ·) free swing parameters. (− −) $\frac{1}{2}$ stimulation amplitude.

parameters and the simultaneous parameters both predicted the general response to the ramp input, but neither matched the magnitude of the response. The quality of ramp response prediction varied widely between subjects. In general, prediction of this input type was not very good, although the overall errors tended to be small. The ramp response prediction was highly dependent on the IRC which played little role in the step response other than determining the overall magnitude of the steady-state step. Since this ramp input was relatively slow, the response may have been more affected by the noise in the active torque-angle and torque-velocity curves than some of the other inputs.

Figure 6-33 shows the response to the swept-sinewave input. In general, prediction in the slow frequency portion of the response suffered from the same problems

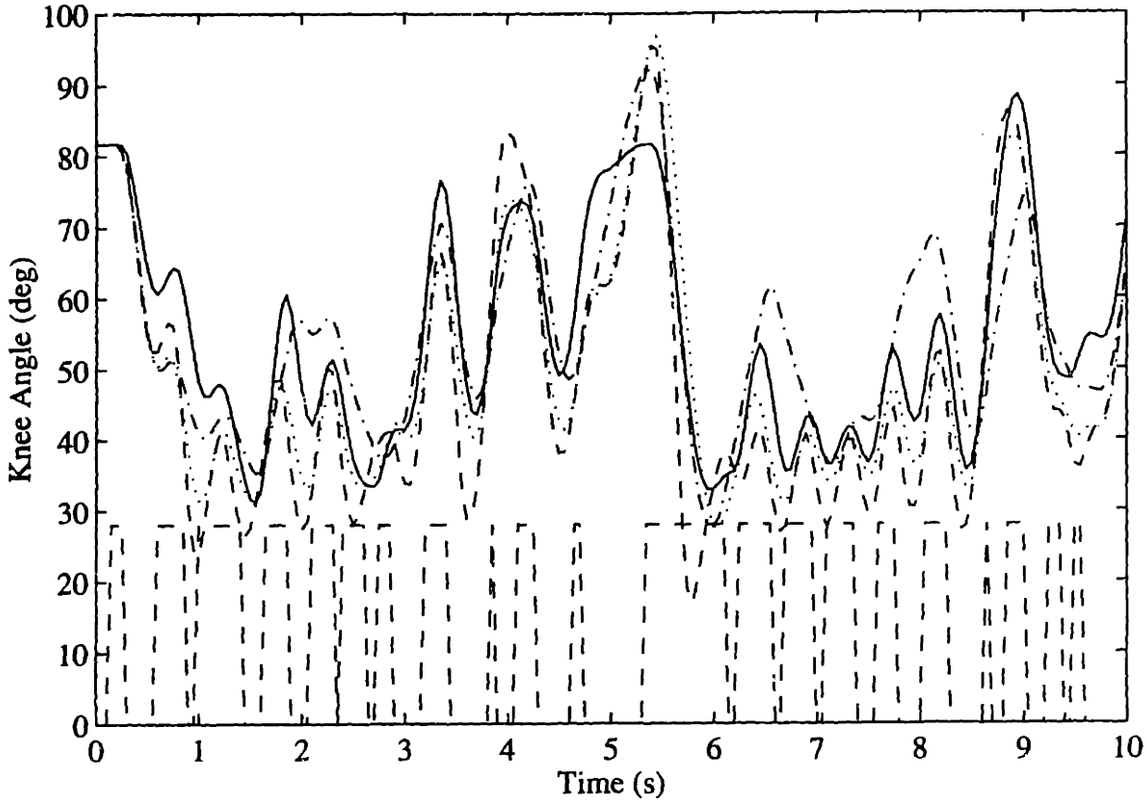

Figure 6-34: Response to a pseudo random binary stimulation train: (−) Experimentally measured response and predictions with (− −) sequential parameters, (− · −) simultaneous parameters and (· · ·) free swing parameters. (− −) $\frac{1}{2}$ stimulation amplitude

as the ramp response. Prediction was not consistently good or bad for any parameter set across subjects. In the more dynamic portion of the response, all three parameter sets predicted the general behavior of the response, with some phase shift and varying amounts of magnitude error. The free swing parameters were slightly better at predicting the phase of the response for most subjects, although there was not a noticeable difference for this particular subject.

Figure 6-34 shows the predicted responses to a random binary stimulation train. No obvious features distinguish between the predictive ability of the different parameter sets.

The average RMS error and the average absolute error (Equations (6.9) and (6.10)

respectively) were computed for each parameter set and each input.

$$E_{RMS} = \sqrt{\frac{\sum_1^N (prediction - data)^2}{N}}. \tag{6.9}$$

$$E_{ABS} = \frac{\sum_1^N |prediction - data|}{N}. \tag{6.10}$$

A t-test (Equation (6.3)) determined the significance of the difference between the prediction error of the various parameter sets for each of the tested inputs. In this case, $\bar{d}$ was the average difference between the prediction error of any two parameter sets and $n = 16$. The critical t value for 95 % confidence is 2.4889. Tables 6.5 through 6.8 show the average difference of errors and t values for each comparison.

For prediction of knee angle response to step and sinewave stimulation patterns, the t-test showed that both the free swing and simultaneous parameter sets were significantly better than the sequential parameters. The sequential parameters also produced significantly more error than other parameter sets when predicting knee angle response to a random binary stimulation pattern. Very few of the comparisons showed a difference between errors for prediction of the ramp response. This may be because a large portion of the ramp response was zero, and all the parameter sets perform well in predicting zero response.

None of the comparisons between the free swing parameters and the simultaneous parameters showed a significant difference in the errors. In most cases the free swing parameters did produce a smaller error; however, the differences were not statistically significant.

6.10 Simplified Models

The random stimulation trials were used to parameterize the torque generator and single-segment models described in Section 5.5.1. Simulations of these simplified models for step, ramp, swept-sine, and random binary inputs were compared to the

Comparison of Step Response	$\bar{d}$ RMS	t value RMS	Level of Significance	$\bar{d}$ AVE ABS	t value AVE ABS	Level of Significance
SEQ1-FS1	4.8691	3.2797	99%	3.1009	3.1151	99%
SEQ2-FS2	7.8915	4.4651	99.5%	5.7171	5.1351	99.5%
SEQ1-SIM1	3.9748	2.0634	90%	2.3797	1.7545	90%
SEQ2-SIM2	6.2515	3.3205	99.5%	4.3682	3.5768	99.5%
SIM1-FS1	0.8943	0.9259	<90%	0.7212	0.9132	<90%
SIM2-FS2	1.6400	1.8235	90%	1.3489	1.8934	90%

Table 6.5: The table shows the average difference between step response prediction errors $\bar{d}$ for the (SEQ) sequential,(FS) free swing, and (SIM) simultaneous parameter sets. The number (1 or 2) indicates the binary stimulation train used for identification of the active parameters. The t values from a comparative t-test are given along with the level of significance of the difference. A positive $\bar{d}$ and t indicate the second parameter set produced less error.

Comparison of Ramp Resp.	$\bar{d}$ RMS	t value RMS	Level of Significance	$\bar{d}$ AVE ABS	t value AVE ABS	Level of Significance
SEQ1-FS1	0.8216	2.5564	97.5%	0.1273	0.8360	<90%
SEQ2-FS2	1.1443	1.8922	90%	0.3581	1.2341	<90%
SEQ1-SIM1	0.5328	1.0824	<90%	0.0640	0.3520	<90%
SEQ2-SIM2	0.3018	0.5892	<90%	0.0080	0.0351	<90%
SIM1-FS1	0.2887	0.7736	<90%	0.0633	0.2715	<90%
SIM2-FS2	0.8425	1.7963	90%	0.3500	1.5380	<90%

Table 6.6: The table shows the average difference between ramp response prediction errors $\bar{d}$ for the (SEQ) sequential,(FS) free swing, and (SIM) simultaneous parameter sets. The number (1 or 2) indicates the binary stimulation train used for identification of the active parameters. The t values from a comparative t-test are given along with the level of significance of the difference. A positive $\bar{d}$ and t indicate the second parameter set produced less error.

Comparison of Sine Response	$\bar{d}$ RMS	t value RMS	Level of Significance	$\bar{d}$ AVE ABS	t value AVE ABS	Level of Significance
SEQ1-FS1	5.0130	3.4210	99.5%	3.1270	4.0541	99.5%
SEQ2-FS2	6.8067	4.4554	99.5%	4.2478	4.6004	99.5%
SEQ1-SIM1	3.9948	2.6736	97.5%	2.2559	2.8228	97.5%
SEQ2-SIM2	5.5209	3.4620	99.5%	3.3162	3.5066	99.5%
SIM1-FS1	1.0181	2.3185	95%	0.8711	2.4567	95%
SIM2-FS2	1.2859	2.3930	95%	0.9316	2.3491	95%

Table 6.7: The table shows the average difference between swept-sinewave response prediction errors $\bar{d}$ for the (SEQ) sequential,(FS) free swing, and (SIM) simultaneous parameter sets. The number (1 or 2) indicates the binary stimulation train used for identification of the active parameters. The t values from a comparative t-test are given along with the level of significance of the difference. A positive $\bar{d}$ and t indicate the second parameter set produced less error.

experimental results and to the results predicted by the full model with the free swing parameter set. Figure 6-35 shows the step response from a single subject. The full model predicted the step response much better than either of the simplified models. The torque generator model displayed significant oscillations in the active region of the response because there was no additional active damping in this model structure. The single-segment model overestimated the magnitude of the steady state response. These same characteristics were seen in the ramp response (Figure 6-36). The single-segment model overestimated the magnitude of the response, while the torque generator oscillated and under estimated the response magnitude. The simplified models did not predict the response to a random binary stimulation train very well either (see Figure 6-37). The torque generator model drastically overshoots the knee angle response in the passive region on the downward swings and the single-segment model overshoots the response on the upward swing in the active region.

The torque generator error was caused by insufficient damping or energy dissipation during muscle activation. In both the single-segment model and the full model, the active damping prevents oscillations in the active regions of the curves. The single-

Comparison of SRB Response	$\bar{d}$ RMS	t value RMS	Level of Significance	$\bar{d}$ AVE ABS	t value AVE ABS	Level of Significance
T1: SEQ1-FS1	3.3080	2.0616	90%	2.1457	2.3415	95%
SEQ2-FS2	5.5130	3.1287	99%	4.1263	3.3505	99.5%
SEQ1-SIM1	3.2309	2.0780	90%	2.0383	2.1970	90%
SEQ2-SIM2	5.0652	3.2093	99%	3.7170	3.4905	99.5%
SIM1-FS1	0.0771	0.1551	<90%	0.1075	0.2691	<90%
SIM2-FS2	0.4478	0.6126	<90%	0.4092	0.7374	<90%
T2: SEQ1-FS1	3.0050	1.7379	<90%	2.3061	2.2017	95%
SEQ2-FS2	8.2810	3.3689	99.5%	5.9272	3.8051	99.5%
SEQ1-SIM1	3.8973	3.3387	99.5%	2.5849	3.2638	99%
SEQ2-SIM2	8.1689	3.3793	99.5%	5.8155	3.6962	99.5%
SIM1-FS1	0.8924	0.7359	<90%	0.2788	0.3639	<90%
SIM2-FS2	0.1122	0.1298	<90%	0.1117	0.2036	<90%

Table 6.8: The table shows the average difference between random binary response prediction errors $\bar{d}$ for the (SEQ) sequential,(FS) free swing, and (SIM) simultaneous parameter sets. The number (1 or 2) indicates the binary stimulation train used for identification of the active parameters, and the symbols (T1 and T2) indicate the prediction trajectory. The t values from a comparative t-test are given along with the level of significance of the difference. A positive $\bar{d}$ and t indicate the second parameter set produced less error.

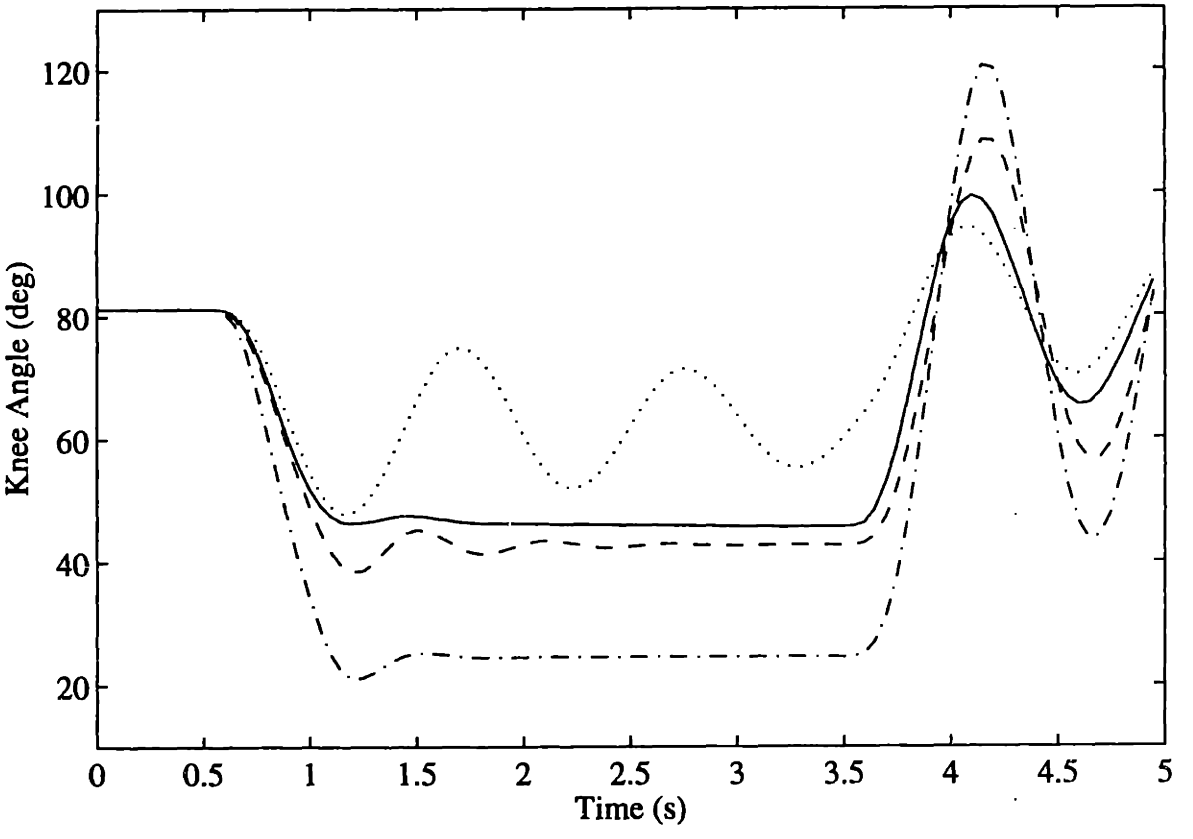

Figure 6-35: Step response: (−) Experimental response and predictions with (−−) full model, (− · −) single-segment model and (· · ·) torque generator model. The full model predicted the step response better than either simplified model.

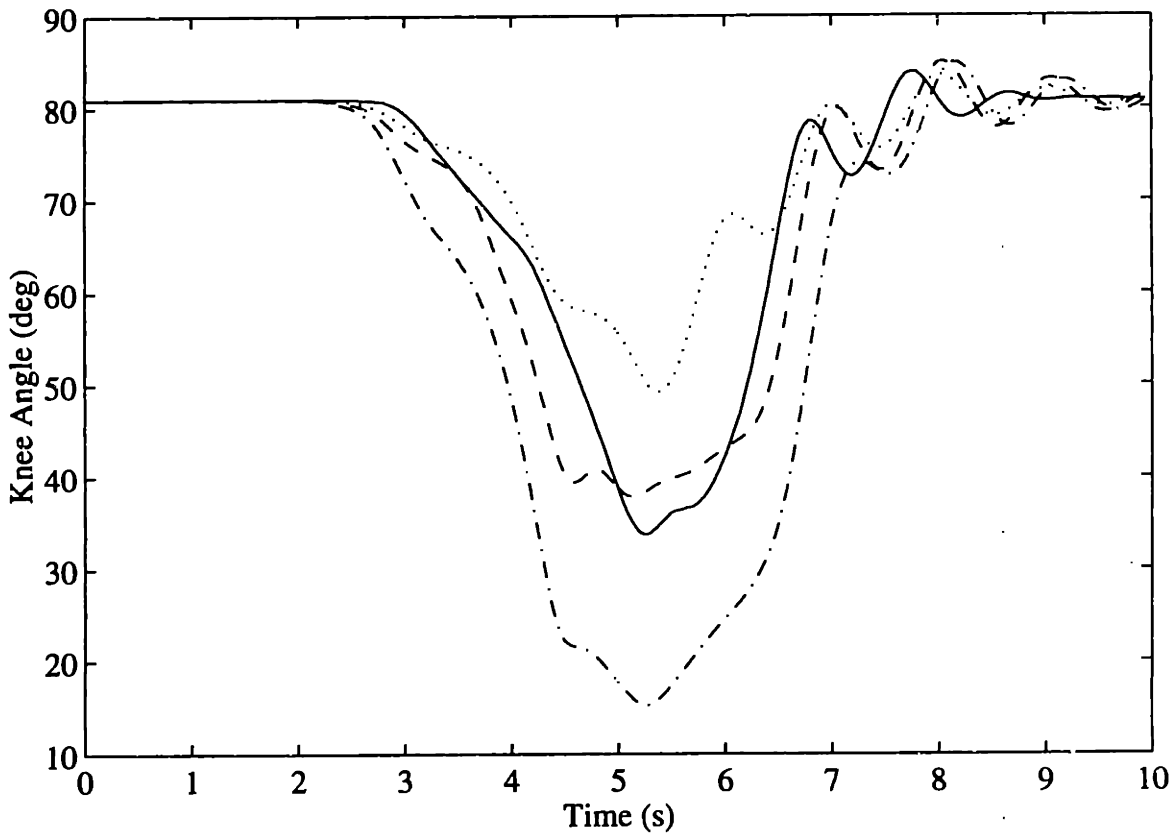

Figure 6-36: Ramp response: (−) Experimental response and predictions with (−−) full model, (− · −) single-segment model and (· · ·) torque generator model. The full model predicted the ramp response better than either simplified model.

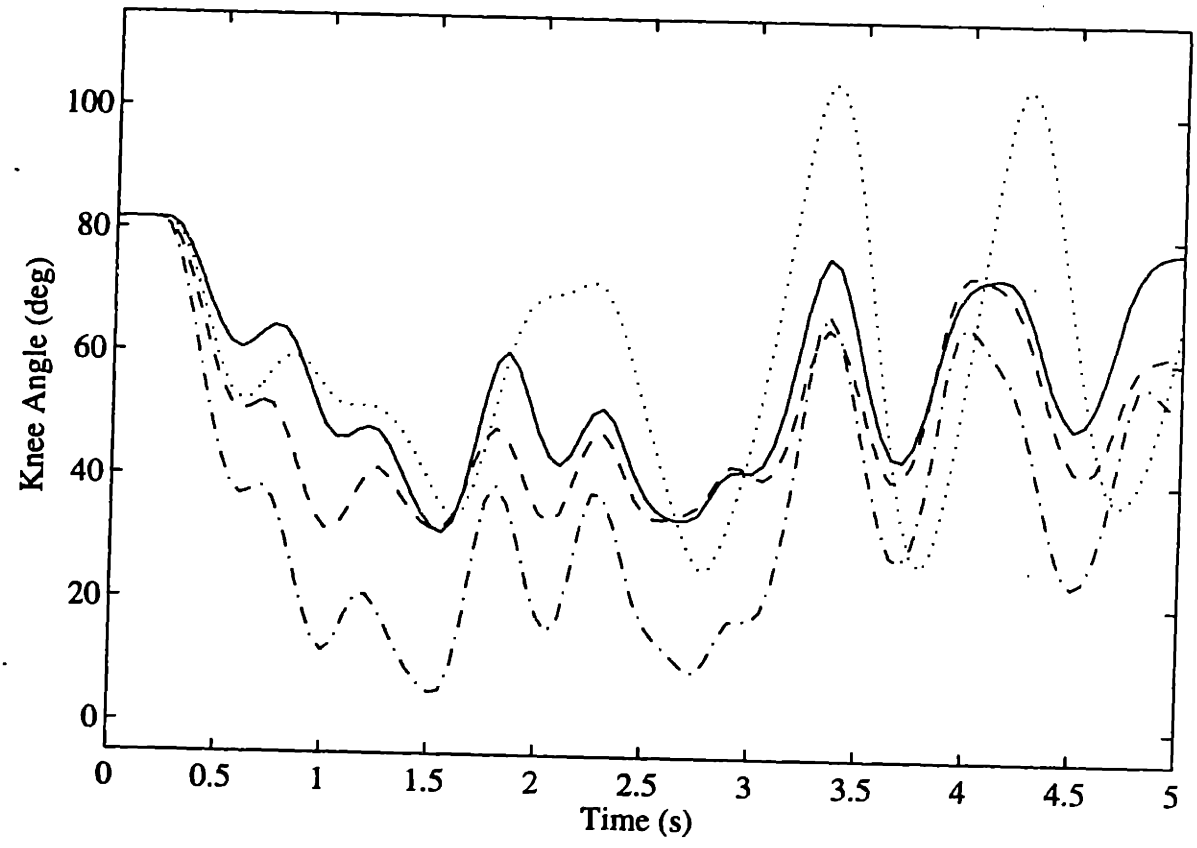

Figure 6-37: Response to random binary input: (−) Experimental response and predictions with (−−) full model, (− · −) single-segment model and (···) torque generator model. Both simplified models displayed large prediction errors in response to a random binary stimulation train.

	Torque generator-Full model				Single-segment-Full model			
	Trial 1		Trial 2		Trial 1		Trial 2	
	t-value	sign.	t-value	sign.	t-value	sign.	t-value	sign.
Step	3.53	99.5%	2.31	95%	6.04	99.5%	7.74	99.5%
Ramp	3.93	99.5%	2.96	99.0%	3.96	99.5%	5.20	99.5%
Sine	4.72	99.5%	3.37	99.5%	5.69	99.5%	7.32	99.5%
PSRB1	1.21	<90%	1.09	<90%	5.90	99.5%	7.64	99.5%
PSRB2	1.24	<90%	1.05	<90%	6.43	99.5%	7.53	99.5%

	Single-segment-Torque generator			
	Trial 1		Trial 2	
	t-value	sign.	t-value	sign.
Step	2.23	95%	4.51	99.5%
Ramp	1.69	<90%	4.23	99.5%
Sine	1.15	<90%	3.78	99.5%
PSRB1	-1.04	<90%	-0.99	<90%
PSRB2	-1.06	<90%	-1.00	<90%

Table 6.9: Summary of t-tests to compare the prediction errors of the various models for all five test inputs. The full model produced significantly less prediction error than the two simplified models for nearly every trajectory tested.

segment model error resulted from the line approximation of the active torque-angle curve. The actual torque-angle curve was clearly bell or hump shaped for virtually all subjects. By approximating this curve as a line, it became impossible for both low and high angle regions to decay to zero. This forced errors in either the high or low angle region, or as in most cases produced some error across the entire angle range.

The average RMS error and average absolute error (Equations 6.9 and 6.10) were computed for the predictions made by each of the simplified models. These errors were compared to the full model with a t-test. The results of the t-test are summarized in Table 6.9.

6.11 Summary of Results

The first isometric experiment compared improved methods for identifying the isometric recruitment curve to the traditional step response method. The results showed that all the ramp methods produced similar IRC estimates when compared to the step response method, and each method produced some error near threshold. Because correlation processing is simple and not susceptible to numerical divide-by-zero problems which effect the deconvolution methods, the ramp correlation method was selected for closer examination and comparison to the step response method. The second isometric experiment looked at the estimated IRC's ability to predict isometric torque output. The results showed no prediction difference between the ramp correlation IRCs and the step response IRCs. In this same experiment, the contraction dynamics were matched to second- and third-order linear systems. The third-order system produced a significantly better fit to the impulse response, but it did not predict a more accurate isometric torque response to the test input.

Computer simulations explored the theoretical accuracy of the ramp correlation method. The IRC estimate obtained with this method contained some error near threshold. For sharp threshold slope discontinuities the error was worse than for IRCs with smooth transitions. Non-linear contraction dynamics did not effect the accuracy of the identification.

The final experiment identified the full non-isometric model. The three passive identification methods produced significantly different passive torque-velocity curves. Computer simulations confirmed that the passive linear estimation algorithms work even for identification of systems which included effects of hysteresis, friction and noise. Each set of passive parameters produced a different set of active parameters, since the active identification algorithm depended on the passive functions. The free swing passive identification method produced a complete parameter set which predicted knee angle output better than the parameter sets produced by the sequential or simultaneous methods. The full model predicted knee angle output better than the simplified torque generator and single-segment models described in the literature.

Chapter 7

Discussion

This thesis contributes to the long-term research goal of providing FES-assisted standing and gait to SCI paraplegics at a level comparable to able-bodied function. Eventually, FES-aided gait which takes advantage of the ballistic characteristics of dynamic walking will replace the FES-assisted shuffling which now exists. To cross the bridge between present day reality and future success, major advances are needed. The model described in this thesis is an important step towards realizing the goals of FES gait research. As it has been studied so far, the model has applications to two major phases of the gait cycle, the stance and swing phases.

The isometric model (Figure 3-6) will be important for control of stance. During gait, stance phase occurs between swing phases and before gait initiation. Even disregarding gait, FES-aided stance provides an SCI individual with dramatically increased mobility. Hard to reach areas, like kitchen cupboards and high shelves in the grocery store are not accessible from a wheel chair. Standing, without walking, brings these items within reach. Transfering, from a bed to a wheel chair or a wheel chair to a car, takes amazing upper body strength and often the help of an assistant. Controlled stance with FES can make these transfers less taxing and less awkward. The social and psychological implications of stance cannot be over looked either. The ability to stand at parties, during a presentation, or during a one-on-one conversation brings the SCI individual to eye level with the world, which psychologically makes their ideas and endeavors equal to others. Stance requires isometric control of joint

torques to support the body's load and keep the subject upright.

The swing phase of gait propels the individual forward to allow progression across a room, down a hallway, across a street, or along a beach. During swing phase, the hip, knee and ankle joints follow consistent trajectories. To achieve reasonable walking speeds, trajectory tracking will be needed to control this dynamic phase of gait.

Neither the full nor the isometric model in present form can be directly implemented in controllers for FES-aided gait. The following sections discuss the results presented in Chapter 6, how the models are useful, and what additional studies are needed to realize the goals of FES-aided gait research.

7.1 The Isometric Model

This study is consistent with a multitude of previous studies [7, 34] which found that a Hammerstein structure can reasonably predict the isometric response of a muscle system. For the isometric twitch response, the form of the linear dynamic block appears to be important. A third-order, repeated poles model of the system response produced a better estimate of the impulse response than a second-order, critically-damped model (Figure 6-8). Higher order repeated poles models did not produce better results, but other more complex linear models were not explored. For most subjects, the impulse response showed some oscillations before decaying to zero. These oscillations cannot be modeled by a simple repeated-poles model of any order. If exact representation of the impulse response were needed, higher order fits would certainly produce more exact results. However, it was not the goal of this thesis to represent the impulse response exactly. It was necessary to trade off accuracy for simplicity in both model form and identification procedures. In general, isolated impulses or twitches are not used for FES. For stance, constant stimulation would be used to lock the joints, or bursts of stimulation could be used to maintain monitored stability of the joints. The overall reaction time of the model to stimulation inputs is important. The actual transients are not as critical, since they tend to die out

quickly. Third-order dynamics reasonably predict both the rise and fall times of the isometric torque for bursts of stimulation (Figure 6-9). More dynamic inputs should be tested to determine if a third-order estimate is significantly better than a second-order estimate. Until then, a third-order, repeated-poles model of the contraction dynamics of quadriceps muscle is recommended.

7.2 The Passive Joint Properties

The results of the passive identification experiments showed dramatic differences in the passive torque-velocity curves measured with different methods (Figure 6-20). The difference between experimental methods which accounts for these differing results is not obvious. Voluntary activity and reflexes may contribute to the difference.

Although voluntary activity is a potential source of error in the experiments, it is unlikely that this is the reason for such large and consistent differences in the results. The experiments were performed on able-bodied subjects who cannot maintain completely relaxed muscles at all times. It may be harder to relax during the slow (sequential) experiment than during the other two experiments, but the consistency of the result across subjects indicates that there is a more basic mechanism producing the difference. If cocontraction were responsible, you would expect to see a big difference for some subjects and little or no difference for the occasional subject who was able to stay relaxed. EMG monitoring did not detect any difference in contraction levels for the muscle, and the subjects did not report that it was more difficult to relax during the sequential experiment.

Varying levels of reflex activity may have influenced the perceived torque-velocity curve. To explain these differences, the muscle model would need to include a parallel reflex pathway between kinematic input and torque output which produces large resistive torques for low frequency velocity inputs, and little or no torque response to high frequency velocity inputs. Figure 7-1 shows a block diagram for such a proposed mechanism. Simulations of such a structure are required to show if the reflex response could be responsible for the measured differences in passive torque-velocity at the knee

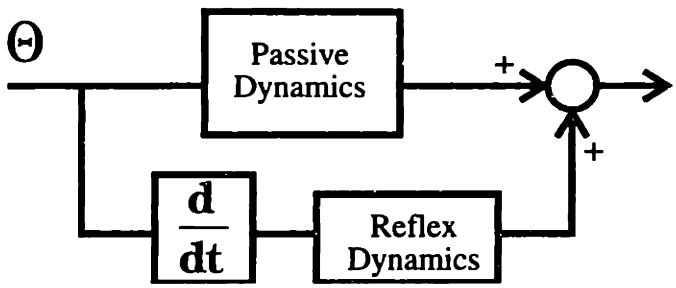

Figure 7-1: A proposed model for including the reflex pathway in parallel with the active muscle properties.

joint. Certainly, reflexes exist and contribute to the overall dynamic response of a muscle-joint-limb. Kearney and Stein looked at the non-linear response of muscle reflexes at the ankle joint [53] and found that the reflex has no effect at frequencies above 10 Hz. The three identification experiments used kinematic trajectories which are quite different in frequency content, but none of the kinematic trajectories had significant frequency content near 10 Hz. Neither the reflex pathway nor voluntary contractions satisfactorily explain these results.

The magnitude of damping in the negative velocity region appears to be inversely proportional to the kinematic frequency of motion. Higher frequency inputs produce a lightly damped torque response, while low frequency inputs produce a highly damped response. Even more puzzling is the fact that these same differences are not seen in the positive velocity region.

Although the difference in measured passive torque-velocity is of concern, it appears that both the free swing and the simultaneous methods produce parameter sets which are appropriate for prediction of joint angle over a wide range of inputs (Figures 6-31-6-33 and Tables 6.5-6.8). The torque-velocity curves produced by these two methods are significantly (and consistently) different; however, the relative torque contribution from this function is small and perhaps any arbitrarily selected low level damping would give a sufficiently accurate estimate of the system. Both Franken [38, 39] and Shue [70] assumed linear passive damping properties, and Veltink [77, 80] neglected the passive damping altogether, when the limb was attached to a known

external load with second-order dynamics. The constant velocity measurements obtained through sequential estimation do not produce an appropriate passive parameter set for joint angle prediction. Presumably these parameters can at least predict response under constant joint velocity kinematics; although none of the inputs tested produced such a response. Since gait does not consist of constant velocity trajectories, this would not be a useful prediction regime regardless.

7.3 Comparison to Simplified Models

The single-segment model described in Section 5.5.1 was used by Shue, Crago and Chizeck [70] to fit data sets obtained from the ankle joint of a cat. Shue controlled the kinematic trajectory of the joint, stimulated the limb with a pseudo-random binary stimulation train and measured the net joint torque. Shue found that the parameter values depended strongly on experimental conditions, primarily the size of the kinematic perturbation. An adaptive algorithm produced excellent fits over the full range of data, but the single-segment, fixed parameter model did not fit the data as well. For a better fixed parameter model, Shue proposed coupling between activation and the velocity dependent term. Shue did not explore more complex shapes for the active torque-angle curve. The results of this thesis agree with Shue's basic conclusion that a single-segment fixed parameter model does not adequately describe the muscle-joint system.

Franken and Veltink [37] looked at the single-segment model applied to the quadriceps muscle of SCI subjects. They were the first to use a free swing method to parameterize the passive system and they used similar methods to identify the active dynamics. Franken's models were expressed in discrete time and his predictions depended on prediction interval. This differs in form from the model used in this thesis, but the basic dynamics of the models were the same. Franken tested his models for prediction of knee angle in response to pseudo-random binary stimulation trains lasting 10 s and he examined the prediction error for various prediction intervals. For the longest prediction interval (1s) the RMS errors were 6.7, 7.5, and 6.3. The

different values were produced by stimulation trains of varying relative magnitude. In comparison, the prediction errors over a full 10s simulation with the free swing parameters and full model from this thesis were 8.1, 7.7, 6.5, and 7.9. These slightly larger errors are primarily due to the difference in prediction method used in the two studies. Franken's predictions were performed for 1s intervals of his 10s data trials, while this study predicted the response continuously over the full 10s. Another potential source of difference may be the random binary pulse train used in the two studies, since Franken's pulse train contained fewer stimulation pulses.

The single-segment model presented in Section 5.5.1 produced much worse prediction than Franken reported with his equivalent model. This is further indication that the error differences between Franken's model and the full model parameterized by the free swing method are due to experiment and prediction method differences.

In the same study, Franken also looked at two torque generator models, which neglected active torque-angle and torque-velocity properties. The first consisted of recruitment characteristics with a time delay to model the contractile dynamics. The second included second-order contractile dynamics. He found that both of these models were as good as his single-segment model for prediction over short time intervals (100 ms), but the torque generators were inadequate for prediction over longer intervals.

The results from Chapter 6 showed that the torque generator model predicted output more accurately than the single-segment model based on rms tracking error, which contradicts Franken's results (Table 6.9). If overall response shape (to step, ramp, and sine input) is examined qualitatively, the single-segment model seems to perform better (Figures 6-35-6-37). The torque generator model had no active damping, so the dynamic response to steps and ramps contained oscillations which were not present in the experimental response. For one subject, the torque generator model was unstable in response to the random binary stimulation train (see Figure K-4 jadr1 and jadl1). This instability was cause in part by poor identification of the passive system damping. The full model and the single-segment model were both able to overcome the deficiencies of the passive system, but the torque generator had

no mechanism to produce active damping, so the simulation became unstable.

Because torque generators contain a structural flaw (no active damping), they are inappropriate for fixed parameter prediction of joint angle output or open-loop control. The torque generator model may be useful, however, with on-line adaptive algorithms. Adaptation on the single active gain parameter, τ_{scale}, may compensate for errors in the prediction output and is simple enough to perform in real-time.

The single-segment model cannot produce an appropriate active torque-angle relationship. This model is structurally better than the torque generator model because it includes active damping, but it is still prone to large steady-state errors due to the active torque-angle approximation. A compromise between these two simple models could approximate the torque-angle relationship as a static gain, but retain the multiple line segment-model for active damping. This removes the structural deficiencies of the torque generator model and retains the only real benefit of the single-segment model. This simplification reduces the number of active parameters which simplifies identification and may have some benefit for adaptive applications.

For fixed parameter needs, the full model with free swing parameters is the most appropriate. The results demonstrate that this model can predict the muscle-joint response to a wide range of stimulation inputs including patterns different from those used for identification.

7.4 Parameterization

The parameterization procedures explored in this research were chosen in hopes of finding rapid means to parameterize the muscle-tendon-joint model. To implement the model in controllers for FES walking systems, each joint under FES control must be calibrated. It may be possible to identify some of the parameters only once, but other parameters must be measured at least once a day and possibly more frequently. For multiple joints and multiple muscles, the number of parameters, frequency of parameterization and parameterization time must be minimized.

7.4.1 Rapid Parameterization Routines

The ramp correlation method for IRC identification, in conjunction with the free swing identification routine for both passive and active properties represents a rapid parameterization protocol. The IRC and contraction dynamics were identified with a 7 s stimulation and data acquisition routine. It took only 10 s each for the passive and active identification routines, but it took almost 5 minutes to calibrate the accelerometer with respect to gravity and measure the passive torque-angle curve with the sequential method. The torque-angle curve can be estimated from the free swing method if the inertia is already known. Since limb inertia does not change much from day-to-day or month-to-month, a slow but accurate method could be used on an infrequent basis to identify the system inertia. Then, it would not be necessary to determine the inertia explicitly during daily identification sessions. If the accelerometer is not needed for control, the position signal could be double differentiated off-line to produce a reasonable estimate of the acceleration. This would eliminate the need to calibrate the accelerometer with respect to gravity. With these two minor changes, the total parameterization time could be reduced to less than 30 s per joint/muscle. In contrast, the traditional step response method for IRC identification required 30 s to gather a single data point. To maintain reasonable resolution, 10 IRC points were measured for a total of 300 s. The sequential method required five minutes (300 s) to measure 20 points on the torque-angle curve and four minutes (240 s) to measure 16 torque-velocity points. The total identification using traditional methods took 12.5 minutes. The free swing method can save 12 minutes, or 96 % of the identification time.

7.4.2 Alternate Inertia Measurements

There are at least two possible methods for obtaining accurate inertia estimates. A quick release experiment can be used to calculate the inertia from measurements of acceleration [84]. The leg must be restrained in a fixed angular position, while a known force, F is applied at a known distance y_f from the joint center. An accelerometer is

placed a distance y_a from the joint center. The restraining force is released, causing the limb to move in reaction to the applied force F. The initial acceleration a is measured and the inertia, J_{limb} is calculated from the following equation:

$$J_{limb} = \frac{F\ y_f\ y_a}{a}. \tag{7.1}$$

This quick-release method was used by Franken and Veltink [38].

Another possible method for identifying the limb inertia is through MRI or other imaging techniques which can distinguish tissue properties based on density. The image pixels, or volume elements, can be assigned a mass, m_i based on the density of the tissue. The overall inertia can be calculated:

$$J_{limb} = \sum i = 1 N m_i x_i^2, \tag{7.2}$$

where x_i represents the distance in the radial direction between the joint center and the mass particle.

7.4.3 Minimizing Daily Parameterization

At this time it is unclear which parameters actually change with time. Those parameters that are stationary over long time periods (days, weeks, or months) do not need to be identified each day. By eliminating these measurements, a multi-joint parameterization routine can be much quicker.

It is logical to assume that the passive parameters do not vary much with time. In addition, it may also be true that the active parameters do not change much with time. For this study, a muscle was defined as whatever contractile tissue was activated by a single stimulation channel. This means that the electrodes which deliver the stimulation are integrated into the system model. For stimulation with surface electrodes, the position of the electrodes is a critical part of the system. When the electrodes are carefully placed in the exact same location from day to day, the isometric model characteristics (IRC and the twitch response) are surprisingly repeatable.

In contrast, small changes in electrode placement can produce dramatic changes in the IRC and contraction dynamics [75]. Presumably, implanted electrodes control coupling to the motor point better than surface electrodes. If so, the stability of an implanted system over several days or even weeks may be quite high. There is some evidence that the active torque-angle and torque-velocity properties do not change significantly over time. McNeal used the same stimulation pattern on different days to produce similar joint trajectories in paraplegic subjects [63] by simply scaling the magnitude of the stimulation input. This study seems to indicate that the dynamic properties of the muscle are constant, even though the recruitment properties change. If both the active and passive parameters are stable with time, it would not be necessary to recalibrate the entire muscle prior to each stimulation session. Instead, simple measurement of the IRC for each muscle of interest may be all that is needed.

The reliability of the experimentally measured parameters needs to be tested over both long and short time periods to determine which parameters change with time. In these experiments, the primary goal was to quickly identify a set of parameters and then determine whether or not that particular combination of model structure and parameters could be used to predict the response of the joint. The experiments did not try to identify fundamental properties of the muscle, and multiple identification trials on a single individual were not performed. Additional trials would help determine which parameters are subject to variation with time and would establish statistical error bounds on each of the parameters.

7.4.4 Parameter Reduction

Future studies should explore the possibility of reducing the number of model parameters. For models which will be used in control, it is important to use the simplest model possible for the task. A simple model often means a model with few parameters. The free swing model presented in this thesis has 11 passive torque-angle parameters, 4 passive torque-velocity parameters, 1 inertia parameter, 11 active torque-angle parameters, 11 torque-velocity parameters, and 1 active gain parameter. Many parameters were used to fit the data to piece-wise linear curves since a large number of

small line segments can describe any shape. If there were some prior knowledge of the expected curve shape, the number of parameters could be reduced.

The passive torque-angle curve is produced by gravity acting on the limb and the compliance of the tissue traversing the joint. Franken [38] modeled these properties in the following way:

$$\tau_{pta}(\theta) = mglsin(\theta) + k_1 e^{k_2 \theta}. \tag{7.3}$$

Use of this equation reduces the 11 torque-angle parameters to 3. It can also make a distinction between the gravity terms, which are dependent on the global orientation of the limb, and the compliance torques, which are dependent on internal joint angle. Separation of the two terms was not important for the identification and prediction experiments in this research, but it will be important for multi-joint experiments where the relative position of the joint changes with respect to gravity.

The active torque-velocity curve appears to be well modeled by two line segments, one for the positive velocity region and one for the negative velocity region. This would reduce the active torque-velocity parameters to two.

It may be possible to match the active torque-angle curve to a simple function with a limited number of parameters. Some possible function candidates are gaussians, quintic splines, and parabolas. All of these shapes can be parameterized with two variables.

7.5 Equipment

The experimental set up used in this study was necessary to explore all of the varying identification algorithms. Based on the results of these experiments, the essential equipment list can be reduced. As discussed in Section 7.4.1, if the inertia can be identified separately, the free swing protocol can be used to identify the passive and active, joint angle and angular velocity dependent properties. For this identification protocol the motor is not needed, since the leg is induced to move on its own. The IRC ramp correlation protocol requires a means to lock the joint at a fixed angle and a transducer to measure the net joint torque. A sensor is needed to measure joint

position. This position signal can be differentiated to produce a velocity measurement and double differentiated to produce the acceleration signal. Therefore, two sensors and a locking mechanism, along with a stimulator are all that is needed to identify all of the model parameters.

To extend this work to the hip and ankle joints, somewhat different experimental set-ups would be needed. A device similar to the knee bench could be easily built for the ankle joint. Because the foot is a very low inertia segment, special care would need to be taken to produce an experimental rig with low inertia, so that the natural dynamics of the joint were not distorted during the experiments. Several investigators have experimental set-ups to investigate the dynamics of the ankle joint [1]. A completely different type of experimental set-up is needed to test the hip joint.

One way to perform these experiments on all three joints would be to use a set of leg braces with position sensors and torque transducers at each of the joints. A mobile measurement rig like a brace has advantages even for single joint experiments, since it allows alteration of the joint orientation relative to gravity. This would help distinguish gravity and joint compliance effects, which was not done in this study. An experimental brace must be adjustable to accommodate subjects of different sizes. Each joint needs a locking mechanism to isolate the motion of each joint and to measure the isometric muscle properties. For realistic motion, the hip joint needs to accommodate several degrees of freedom. Golfarb and Durfee [33, 42] built such a brace for the knee and hip joints.

Hip joint experiments could be performed with the subject standing on a single leg. A support structure might be needed to keep the subject's torso fixed. By locking the knee and stimulating either the hip flexors or the hip extensors of the freely swinging leg, a single muscle, single joint experiment with a protocol similar to the one in this study could be performed. In a similar standing position, locking the hip joint and stimulating the hamstrings would allow identification of the knee flexors. Both of these potential experiments may be difficult to perform with able-bodied subjects because the muscles are hard to recruit with surface electrodes; however they can be performed with SCI subjects.

Multiple joint experiments using biarticular muscles (like the quadriceps) could also be performed in such a rig.

7.6 Future Work

Many questions were answered by this research, but more questions remain. In addition to parameter reduction and identification repeatability experiments suggested in Section 7.4.4, the following sections suggest future experiments to complement the work presented in this thesis and point out potential difficulties and solutions which may be encountered along the way.

7.6.1 Tests with Spinal Cord Injured Subjects

These experiments were performed only on able-bodied subjects. The experiments should be repeated with spinal cord injured subjects to validate the application of this study to SCI rehabilitation. On a gross level, the muscles of SCI and able-bodied subjects are the same. The SCI muscles may be weaker, due to insufficient use, and possibly slower since many of the fast muscle fibers convert to slow fibers when they are not used sufficiently. With SCI subjects there will be no voluntary activity, which was a possible source of error with able-bodied subjects. Reflex activity is a problem with SCI subjects, since spasticity is a common side effect of SCI. Subjects with severe spasticity are often on medication to control the spasticity, in which case the spasticity may be less of a problem. Highly spastic subjects would not be candidates for an FES walking prosthesis and would not be appropriate for such a study.

7.6.2 Load Transitions and Weight Bearing

This study examined the model prediction performance under free swinging conditions which are similar to the swing phase of gait. Other significant parts of the gait cycle also need to be controlled. The model should be tested under conditions which simulate weight bearing and load transitions. Weight bearing occurs during both

single and double leg stance while load transitions occur at toe off and heel strike. The isometric model may be appropriate for prediction during stance, however, it has not been tested under loaded conditions.

A experimental brace, like the one proposed in Section 7.5, may be appropriate weight bearing experiments. Veltink [77] used a controlled motor to simulate known dynamics loads and similar equipment could be used to simulate load transitions.

7.6.3 Using the Model for Control

This modeling project was undertaken to lay the foundation for model based control. The model is appropriate if a controller can be designed to compensate for any existing errors. In general, modeling and controller design are iterative processes. This research represents only one pass at the modeling iteration. The next step must be to use the model for design of a controller. The controller must be tested for robustness. Based on these results further recommendations will be made for model simplification or improved accuracy.

A multitude of potential control strategies exist. Non-linear open-loop control can be tested by inverting the non-linear dynamic model. A PID loop around this non-linear compensator could help correct modeling errors and improve disturbance rejection. A simple adaptive scheme which updates the active gain parameter τ_{scale} based on the system response maybe enough to compensate for short term fatigue or potentiation effects. Other more complex adaptive controllers maybe needed if the active torque-angle and torque-velocity properties also vary with time.

7.6.4 Parameter Bounds

To guarantee the stability and robustness of non-linear controllers, it is important to place bounds on potential modeling errors. As discussed in Section 6.3, the correlation method produces some systematic error when estimating the threshold of the IRC. This error can be overcome by good controller design, because the limits of the error magnitude are known. Error bounds need to be estimated for all the model

parameters. The repeatability experiments suggested in Section 7.4.3 would establish these error bounds as well as determining which parameters vary with time.

7.6.5 The Effect of Time on Prediction

From this study, it is unclear how important time is for prediction accuracy. All the data used to identify the full model was collected within a half hour period of time. In addition, the active identification experiments were performed immediately before data was collected for the step, ramp, and swept-sine test inputs. Less that five minutes passed between collection of the modeling data and collection of the prediction data. The longest prediction trials required from these models were 10 s. These conditions were chosen to minimize the time varying effects of fatigue and potentiation, since the model cannot compensate for these time dependent changes. Future research must establish the magnitude of the fatigue problem under stimulation paradigms which might be used for FES gait. If fatigue is an issue which cannot be ignored, then two possible solutions exist. The model could be modified to include time varying effects by incorporating a slowly decaying multiplicative term into the active torque block. This would require an accurate model of both fatigue and potentiation effects and maybe a formidable task, since the underlying causes of both fatigue and potentiation are not yet understood. Alternately, real-time adaptive algorithms incorporated into a controller structure could compensate for changes in the system.

7.6.6 Expansion to Multi-joint Applications

The model used for this study needs to be modified and extended for applications which include multiple muscles, joints, and degrees of freedom. The knee is a relatively simple joint, since the primary action of the quadriceps muscle produces motion along a single degree of freedom. The quadriceps muscle is a two joint muscle which acts across both the hip and the knee. The biarticular nature of the quadriceps muscle means that the length of the muscles (hence the position and velocity dependent terms

of the model) depends on the joint angle of both the hip and the knee. Preliminary experiments showed that torque at the knee depends heavily on the hip angle, so the biarticular nature should not be neglected.

One possible approximation assumes the active and passive dependence of the model for each joint can be expressed by separable functions. In this case the following equation would model the passive property at the knee:

$$\tau_{pta\_knee}(\theta_{knee}, \theta_{hip}) = \tau_{pta_{knee}}(\theta_{knee}) + \tau_{pta_{hip}}(\theta_{hip}), \tag{7.4}$$

and Equation (7.5) could model the active torque-angle property.

$$\tau_{ata\_knee}(\theta_{knee}, \theta_{hip}) = \tau_{ata_{knee}}(\theta_{knee}) \times \tau_{ata_{hip}}(\theta_{hip}), \tag{7.5}$$

Likewise, the velocity properties may also be separable. If separability is not feasible, the functions will have to be defined for multi-variable inputs.

Multiple single-joint muscles are easy to add to the model structure. Each additional stimulation channel activates a parallel active muscle structure with its own active torque-angle and torque-velocity properties (see Section 3.1).

In addition to acting across multiple joints, many muscles also act to move those joints in multiple directions. This study looked at flexion-extension of the knee joint which is the primary direction of knee motion. The hip, which is best modeled by a ball and socket joint [60], has multiple degrees of freedom which include flexion-extension and abduction-adduction. Each stimulation channel must be characterized for the motions it produces in each of the primary degrees of freedom, and the model must accommodate the changes in muscle activity with joint configuration.

Chapter 8

Conclusions and Contributions

The goal of this research was to select an appropriate model structure of a muscle-tendon-joint system, to develop rapid parameterization procedures for the model and to provide insight into the underlying behavior of intact muscle systems.

8.1 Conclusions

The model developed in Chapter 3 adequately describes the performance of the quadriceps muscle-knee joint system for a wide variety of inputs, including step, ramp, swept-sine and random binary stimulation patterns. This simple model does not capture the full complexity of the joint system, since the passive damping and stiffness properties are dependent on measurement techniques. The model parameterized with the free swing techniques does capture the essential behavior of the limb under conditions which would be encountered during the swing phase of FES controlled gait. The prediction accuracy seems sufficient for simulation studies and at least preliminary investigation of model based controllers, but it is not accurate enough for use in open-loop control.

The free swing method is recommended for identification of the passive joint-limb properties. Models identified with this method are best able to predict the passive behavior of the system during free swing. The free swing method is fast and does not require a motor to move the limb, if the inertia is known. The sequential method is

much slower and identifies a torque-velocity curve which is very different from those identified with the other two methods. The simultaneous method is an acceptable alternative to the free swing method although it requires the use of a motor. The free swing method requires the least amount of equipment and produced the best estimate of behavior over all the inputs.

The free swing method for active identification is also recommended. This was the only method tested and described in this thesis. Other methods, equivalent to the sequential and simultaneous passive methods, but including stimulation, were tested in preliminary experiments. Forcibly stretching stimulated muscle can cause damage to the muscle, so these potential methods were rejected due to safety concerns. It would be possible to safely measure the active torque-angle curve with the sequential method; however, it would still be necessary to measure the active torque-velocity curve with the method used here.

The model chosen for this work is better than simplified models described in Section 5.5.1 for prediction of joint angle output. The simplified models are not appropriate for fixed parameter applications, but they may be useful in adaptive control, since parameter adaptation may compensate for modeling inadequacies.

8.2 Contributions

The contributions of this thesis are listed below:

1. An appropriate model structure was chosen for development of a fully parameterized, non-linear, non-isometric model of an intact human muscle under FES.

2. Rapid parameterization techniques were developed which are 25 times faster than traditional identification routines.

3. The model structure was found to appropriately describe the muscle-tendon-joint system under conditions that would be encountered during the swing phase of gait.

4. The results suggest common underlying shapes for the model functions which may be used to simplify parameter identification. The passive torque-angle curve resembles a sine function in summation with an exponential. The passive torque-velocity curve can be modeled by two line segments with a discontinuity at zero. The active torque-velocity curve appears as a straight line, or at most two line segments with a discontinuity at zero. The active torque-angle curve is shaped like a bump or a hill with a high point in the middle of the angle range and low points on both ends. It may be possible to parameterize this shape with a gaussian, quintic spline, parabola or other such profile.

5. The results demonstrate that the proposed model predicts knee angle better than simplified versions of the model which were published in the literature. Analysis explained where the deficiencies arose in the simplified models.

The contributions of this research are many, but additional research is needed in several areas. Section 7.6 describes some of the questions that still need to be addressed. The most important ones are summarized here:

- Test the model with SCI subjects who have heightened reflexes.
- Examine the model under conditions which simulate load transitions and weight bearing.
- Extend the model to include multiple muscles and multiple joints.
- Demonstrate that the model is useful for model based control.

Bibliography

[1] G.C. Agarwal and G.L. Gottlieb. Compliance of human ankle joint. *J. Biomech. Eng.*, 99:166–170, 1977.

[2] J. Allin and G. Inbar. Fns control schemes for the upper limb. *IEEE Trans. Biomed. Eng.*, 33(9):818–828, 1986.

[3] J. Allin and G. Inbar. Fns parameter selection and upper limb characterization. *IEEE Trans. Biomed. Eng.*, 33(9):809–817, 1986.

[4] T. Bajd et al. The use of a four-channel electrical stimulator as an ambulatory aid for paralegic patients. *Phys. Ther.*, 63(7):116–1120, 1983.

[5] T. Bajd, A. Krajl, R. Turk, and H. Benko. Symmetry of fes response in the lower extremities of paraplegic patients. *J. Biomed. Eng.*, 12:415–418, 1990.

[6] T. Bajzek and R. Jaeger. Characterization and control of muscle response to electrical stimulation. *Ann. Biomed. Eng.*, 14:485–501, 1987.

[7] R. Baratta and M. Solomonow. The dynamic response model of nine different skeletal muscles. *IEEE Trans. Biomed. Eng.*, 37(3):243–251, 1990.

[8] R. Baratta and M. Solomonow. Dynamic performance of a load-moving skeletal muscle. *Journal of Applied Physiology*, 71:749–757, 1991.

[9] R. Baratta and M. Solomonow. The effect of tendon viscoelastic stiffness on the dynamic performance of isometric muscle. *J. Biomechanics*, 24:109–116, 1991.

[10] R. Baratta, B H. Zhou, and M. Solomonow. Frequency response model of skeletal muscle: effect of perturbation level, and control strategy. *Med. & Biol. Eng. & Comput.*, 27:337–345, 1989.

[11] P. Bawa, A. Mannard, and R. Stein. Effects of elastic loads on the contractions of cat muscles. *Biol. Cybern.*, 22:129–137, 1976a.

[12] P. Bawa, A. Mannard, and R. Stein. Predictions and experimental tests of a visco-elastic muscle model using elastic and inertial loads. *Biol. Cybern.*, 22:139–145, 1976b.

[13] L. Benton, L. Baker, B. Bowman, and R. Waters. *Functional Electrical Stimulation: A Practical Guide, 2nd edition.* Professional Staff Association, Rancho Los Amigos Rehabilitation Engineering Center, Rancho Los Amigos Hospital, Downey CA, 1981.

[14] L. Bernotas, P. Crago, and H. Chizeck. A discrete-time model of electrically stimulated muscle. *IEEE Trans. Biomed. Eng.*, 33(9):829–838, 1986.

[15] L. Bernotas, P. Crago, and H. Chizeck. Adaptive control of electrically stimulated muscle. *IEEE Trans. Biomed. Eng.*, 34(2):140–147, 1987.

[16] G. Brown and U. von Euler. The after effects of a tetnus on mammalian muscle. *J. Physiology*, 93:39–60, 1938.

[17] G. L. Brown and D. B. Burns. Fatigue and neuromuscular block in mammalian skeletal muscle. *Roy. Soc. Lon. Proc. Ser. B*, 136:182–195, 1949.

[18] R. Burke, P. Rudomin, and F. Zajac. The effect of activation history on tension production by individual muscle units. *Brain Res.*, 109:515–529, 1976.

[19] N. Chesler. Emg as an indicator of fatigue during FES-aided standing of paraplegics. Master's thesis, Massachusetts Institute of Technology, May 1991.

[20] J. Chiou. Modelling and simulation of paraplegic gait induced by functional electrical stimulation. Master's thesis, Massachusetts Institute of Technology, May 1993.

[21] H. J. Chizeck, R. Lalonde, C. W. Chang, J. A. Rosenthal, and E. B. Marsolais. Performance of a closed-loop controller for electrically stimulated standing in paralyzed patients. In *Proceedings of the RESNA 8th Annual Conference*, pages 231–233, 1985.

[22] H.J. Chizeck, P.E. Crago, and L.S. Kofman. Robust closed-loop control of isometric muscle force using pulsewidth modulation. *IEEE Trans. Biomed. Eng.*, 35:510–517, 1988.

[23] H.J. Chizeck, N. Lan, L. S. Palmieri, and P. E. Crago. Feedback control of electrically stimulated muscle using simultaneous pulse width and frequency modulation. *IEEE Trans. Biomed. Eng.*, 38(12):1224–1234, 1991.

[24] P. Chow and H. J. Chizeck. Nonlinear recursive identifcation of electrically stimulated muscle. In *Proceedings of the IEEE Eleventh Annual Conference of the Engineering in Medicine and Biology Society*, pages 965–966, 1989.

[25] P. Crago, J. Mortimer, and P. Peckham. Closed-loop control of force during electrical stimulation of muscle. *IEEE Trans. Biomed. Eng.*, 27:306–311, 1980.

[26] P. Crago, P. Peckham, and G. Thrope. Modulation of muscle force by recruitment during intramuscular stimulation. *IEEE Trans. Biomed. Eng.*, 27(12):679–684, 1980.

[27] P.E. Crago, R.J. Nakai, and H.J. Chizeck. Feedback regulation of hand grasp opening and contact force during stimulation of paralyzed muscle. *IEEE Trans. Biomed. Eng.*, 38:17–28, 1991.

[28] W. Crochetiere, L. Vodovnik, and J. Reswick. Electrical stimulation of skeletal muscle - a study of muscle as an actuator. *Med. Biol. Eng.*, 5:111–124, 1967.

[29] C.R. Dohrmann, H.R. Busby, and D.M. Trujillo. Smoothing noisy data using dynamic programming and generalized cross-validation. *Journal of Biomechanical Engineering*, 110:37–41, 1988.

[30] W. Durfee. *Task Control with an electrically stimulated antagonist muscle pair.* PhD thesis, Massachusetts Institute of Technology, June 1985.

[31] W.K. Durfee. Graph user's guide: a c library for pc line plots. *Copyright WK-Durfee*, 1989.

[32] W.K. Durfee. Task-based methods for evaluating electrically stimulated antagonist muscle controllers. *IEEE Trans. Biomed. Eng.*, 36(3):309–321, 1989.

[33] W.K. Durfee, M. Goldfarb, A.W. Wiegner, and N. Walsh. Preliminary evaluation of a controlled-brake orthoses for regulating FES-aided gait. In *Proceedings of the Annual International Conference of the IEEE Engineering in Medicine and Biology Society*, volume 15, 1993.

[34] W.K. Durfee and K.E. MacLean. Methods for estimating isometric recruitment curves of electrically stimulated muscle. *IEEE Trans. Biomed. Eng.*, 36(7):654–667, 1989.

[35] W.K. Durfee and K.I. Palmer. Estimation of force-activation, force-length and force-velocity properties in isolated, electrically stimulated muscle. *IEEE Trans. Rehab. Eng.*, 41:205–216, 1994.

[36] George E. Forsythe, Michael A. Malcolm, and Cleve B. Moler. *Computer Methods for Mathematical Computations.* Prentice-Hall, Inc., 1977.

[37] H.M. Franken, P.H. Veltink, G. Baardman, R. A. Redmeyer, and Herman B.K. Boom. Cycle-to-cycle control of the swing phase of paraplegic gait induced by surface electrical stimulation. In Press *Med. & Biol. Eng. & Comp.*, 1994.

[38] H.M. Franken, P.H. Veltink, R. Tijsmans, Henk Nijmeijer, and Herman B.K. Boom. Identification of passive knee joint and shank dynamics in paraplegics using quadriceps stimulation. *IEEE Trans. Rehab. Eng.*, 3:154–164, 1994.

[39] H.M. Franken, P.H. Veltink, R. Tijsmans, Henk Nijmeijer, and Herman B.K. Boom. Identification of quadriceps - lower leg dynamics in paraplegics using randomized interpulse interval stimulation. Submitted *IEEE Trans. Rehab. Eng.*, 1994.

[40] Y. C. Fung. *Biomechanics: Mechanical Properties of Living Tissue.* Springer-Verlag, second edition, 1993.

[41] H. Gareis, M. Solomonow, R. Baratta, R. Best, and R. D'Ambrosia. The isometric length-force models of nine different skeletal muscles. *J. Biomechanics*, 25:903–916, 1992.

[42] M. Goldfarb. *A Controlled Brake Orthosis for FES Aided Gait.* PhD thesis, Massachusetts Institute of Technology, June 1994.

[43] Gene H. Golub and Charles F. VanLoan. *Matrix Computations.* The Johns Hopkins University Press, second edition, 1989.

[44] P. Grandjean and J. Mortimer. Recruitment properties of monopolar and bipolar epimysial electrodes. *Ann. Biomed. Eng.*, 14:53–66, 1986.

[45] J. Hausdorff. Gait orthosis combining controllable damping and muscle stimulation. Master's thesis, Massachusetts Institute of Technology, August 1988.

[46] J. Hausdorff and W. Durfee. Open-loop position control of the knee joint using electrical stimulation of the quadriceps and hamstrings. *Med. & Biol. Eng. & Comput.*, 29:269–280, 1991.

[47] I. Hunter and M. Korenberg. The identification of nonlinear biological systems: Wiener and hammerstein cascade models. *Biol. Cybern.* 55:135–144, 1986.

[48] R. Jaeger, G. Yarkony, and R. Smith. Standing the spinal cord injured patient by electrical stimulation: refinement of a protocol for clinical use. *IEEE Trans. Biomed. Eng.*, 36(7), 1989.

[49] D. Jones, B. Bigland-Ritchie, and R. Edwards. Excitation frequency and muscle fatigue: Mechanical responses during voluntary and stimulated contractions. *Expt. Neurol.*, 54:401–413, 1979.

[50] G. Joyce, P. Rack, and D. Westbury. The mechanical properties of cat soleus muscle during controlled lengthening and shortening movements. *J. Physiol.*, 204:461–474, 1969.

[51] G. Kang and F. E. Zajac. Simulation of paraplegic postural control induced by functional neuromuscular stimulation. In *Proceedings of the RESNA 10th Annual Conference*, pages 636–638, 1987.

[52] Z. Karu. Optimization of force and fatigue properties of electrically stimulated human skeletal muscle. Master's thesis, Massachusetts Institute of Technology, May 1992.

[53] R.E. Kearney, R.B.Stein, and L. Parmeswaran. Differential identification of passive and reflex mechanisms in human ankle stiffness dynamcis. In *Proceedings of the Annual International Conference of the IEEE Engineering in Medicine and Biology Society, Volume 16:1994*, pages 430–431, 1994.

[54] E.J. Kennedy. *Spinal Cord Injury: The Facts and Figures.* The University of Alabama at Birmingham Press, second edition, 1986.

[55] A. Krajl and T. Bajd. *Functional Electrical Stimulation: Standing and Walking after Spinal Cord Injury.* CRC Press, Boca Raton, Florida, 1989.

[56] A. Kralj et al. Results of FES application to 71 sci patients. In *Proceedings of the RESNA 10th Annual Conference*, pages 645–647, 1987.

[57] N. Lan and P. E. Crago. Optimal control of muscle stiffnesses for fns induced arm movements. In *Proceedings of the Annual International Conference of the IEEE Engineering in Medicine and Biology Society, Volume 13:1991*, pages 920–921, 1991.

[58] N. Lan, P. E. Crago, and H. J. Chizeck. Feedback control methods for task regulation by electrical stimulation of muscles. *IEEE Trans. Biomed. Eng.*, 38(12):1213–1223, 1991.

[59] Charles L. Lawson and Richard J. Hanson. *Solving Least Squares Problems.* Prentice-Hall, Inc., 1974.

[60] P.J. Lord. *Computer Aided Intertrochanteric Osteotomy Planning and Surgery Simulation.* PhD thesis, Massachusetts Institute of Technology, June 1994.

[61] K. MacLean. Estimation of isometric recruitment curves of electrically stimulated muscle. Master's thesis, Massachusetts Institute of Technology, August 1988.

[62] A. Mannard and R. Stein. Determination of the frequency response of isometric soleus muscle in the cat using random nerve stimulation. *J. Physiol.*, 229:276–296, 1973.

[63] D.R. McNeal, R.J. Nakai, P. Meadows, and W. Tu. Open-loop control of the freely-swinging paralyzed leg. *IEEE Trans. Biomed. Eng.*, 36(9):895–905, 1989.

[64] K. Palmer. Modeling and identification of electrically stimulated muscle. Master's thesis, Massachusetts Institute of Technology, August 1990.

[65] Eric Young Park. Design of a mechanical orthosis for evaluating a novel hybrid gait system. BSME Thesis, Massachusetts Institute of Technology, June 1987.

[66] W. Press et al. *Numerical Recipies in C: The Art of Scientific Computing.* Cambridge University Press, second edition, 1992.

[67] P. Rack and D. Westbury. The effects of length and stimulus rate on tension in the isometric cat soleus muscle. *J. Physiol.*, 204:443–460, 1969.

[68] C. A. Sacher, M. S. Hatwell, and G. F. Inbar. A discrete model of the paraplegic knee joint under electrical stimulation. In *Proceedings of the IEEE Eleventh Annual Conference of the Engineering in Medicine and Biology Society*, pages 837–838, 1989.

[69] Spinal cord injury statistics. Publication of the National Spinal Cord Injury Statistics Center, 1988.

[70] G. Shue, P. E. Crago, and H. J. Chizeck. Muscle-joint models incorporating activation dynamics, moment-angle and moment-velocity properties. *IEEE Trans. Biomed. Eng.*, 42:212–223, 1995.

[71] M. Solomonow. External control of the neuromuscular system. *IEEE Trans. Biomed. Eng.*, 31:752–763, 1984.

[72] U. Stanic and A. Trnkoczy. Closed-loop positioning of hemiplegic patient's joint by means of functional electrical stimulation. *IEEE Trans. Biomed. Eng.*, 21:365–370, 1974.

[73] J. Stephens, R. Reinking, and D. Stuart. The motor units of cat medial gastrocnemius: Electrical and mechanical properties as a function of muscle length. *J. Morph.*, 146:485–512, 1975.

[74] L.A. Streeter, H. Chizeck, and R. Kobetic. Input-output response of the quadriceps muscle in paraplegic patients. In *Proceedings of the RESNA 8th Annual Conference*, pages 240–242, 1985.

[75] A. Trnkoczy. Variability of electrically evoked muscle contraction with special regard to closed-loop controlled orthosis. *Annals Biomed. Eng.*, 2:226, 1974.

[76] W. Tu, D. R. McNeal, and L. L. Baker. A computerized system to generate recruitment data for neuromuscular electrodes. In *Proceedings of the IEEE Eleventh Annual Conference of the Engineering in Medicine and Biology Society*, pages 973–974, 1989.

[77] P. H. Veltink, A. El-Bialy, H. J. Chizeck, and P. E. Crago. Nonlinear control of an artificially stimulated muscle-skeleton-load system. In *Proceedings of the IEEE Eleventh Annual Conference of the Engineering in Medicine and Biology Society*, pages 969–970, 1989.

[78] P. H. Veltink et al. Optimal control of fes-induced cyclical leg movements. In *Proceedings of the Annual International Conference of the IEEE Engineering in Medicine and Biology Society, Volume 13:1991*, pages 922–923, 1991.

[79] P.H. Veltink. Control of fes-induced cyclical movements of the lower leg. *Med. & Biol. Eng. & Comput.*, 29:NS8–NS12, 1991.

[80] P.H. Veltink, H.J. Chizeck, and P.E. Crago. Nonlinear joint angle control for artificially stimulated muscle. *IEEE Trans. Biomed. Eng.*, 39:368–380, 1992.

[81] W. Crochetiere Vodovnik, L. and J. Reswick. Control of a skeletal joint by electrical stimulation of antagonists. *Med. Biol. Eng. Comput.*, 5:97–109, 1967.

[82] G. Wilhere, P. Crago, and H. Chizeck. Design and evaluation of a digital closed-loop controller for the regulation of muscle force by recruitment modulation. *IEEE Trans. Biomed. Eng.*, 32(9):668–676, 1985.

[83] J.H. Wilkinson and C. Reinsch. *Linear Algebra.* Springer-Verlag, 1971.

[84] D.A. Winter. *Biomechanics and Motor Control of Human Movement.* John Wiley & Sons, second edition, 1990.

[85] J.M. Winters and S.L. Woo. *Multiple Muscle Systems.* Springer-Verlag, 1990.

[86] H.J. Woltring. A fortran package of generalized, cross-validatory spline smoothing and differentiation. *Advanced Engineering Software*, 8(2):104–113, 1986.

[87] G.T. Yamaguchi and F.E. Zajac. Restoring unassisted natural gait to paraplegics via functional neuromuscular stimulation: a computer simulation study. *IEEE Trans. Biomed.*, 37(9):886–902, 1990.

[88] F. E. Zajac, E. L. Topp, and P. J. Stevenson. A dimensionless musculotendon model. In *Proceedings of the IEEE Eighth Annual Conference of the Engineering in Medicine and Biology Society*, pages 601–604, 1986.

[89] F.E. Zajac. Muscle and tendon: properties, models, scaling, and application to biomechanics and motor control. *CRC Crit. Rev. Biomed. Eng.*, 17(4):359–411, 1989.

[90] M. Zefran, T. Bajd, and A. Krajl. Parallel structure model of paraplegic patient's gait. In *Proceedings of the Annual International Conference of the IEEE Engineering in Medicine and Biology Society, Volume 13:1991*, pages 924–925, 1991.

[91] B. Zhou and R. Baratta. Manipulation of muscle force with various firing rate and recruitment control strategies. *IEEE Trans. Biomed. Eng.*, 34(2):128–139, 1987.

Appendix A

Schematics

This appendix contains schematics to all the electronic hardware which was developed or modified during the course of this project. For a full schematic of the stimulator and EMG processor electronics see [19]. The following schemaics are included:

- Motion control system electronics
- Motor controller box panel layout
- Stimulator/EMG Processor modifications which include the following changes:
    1. U2A (stimulator card) replaced with DG308A SPST CMOS Analog switch from Siliconix
    2. U4 (EMG card) replaced with PVR3301 from International Rectifier

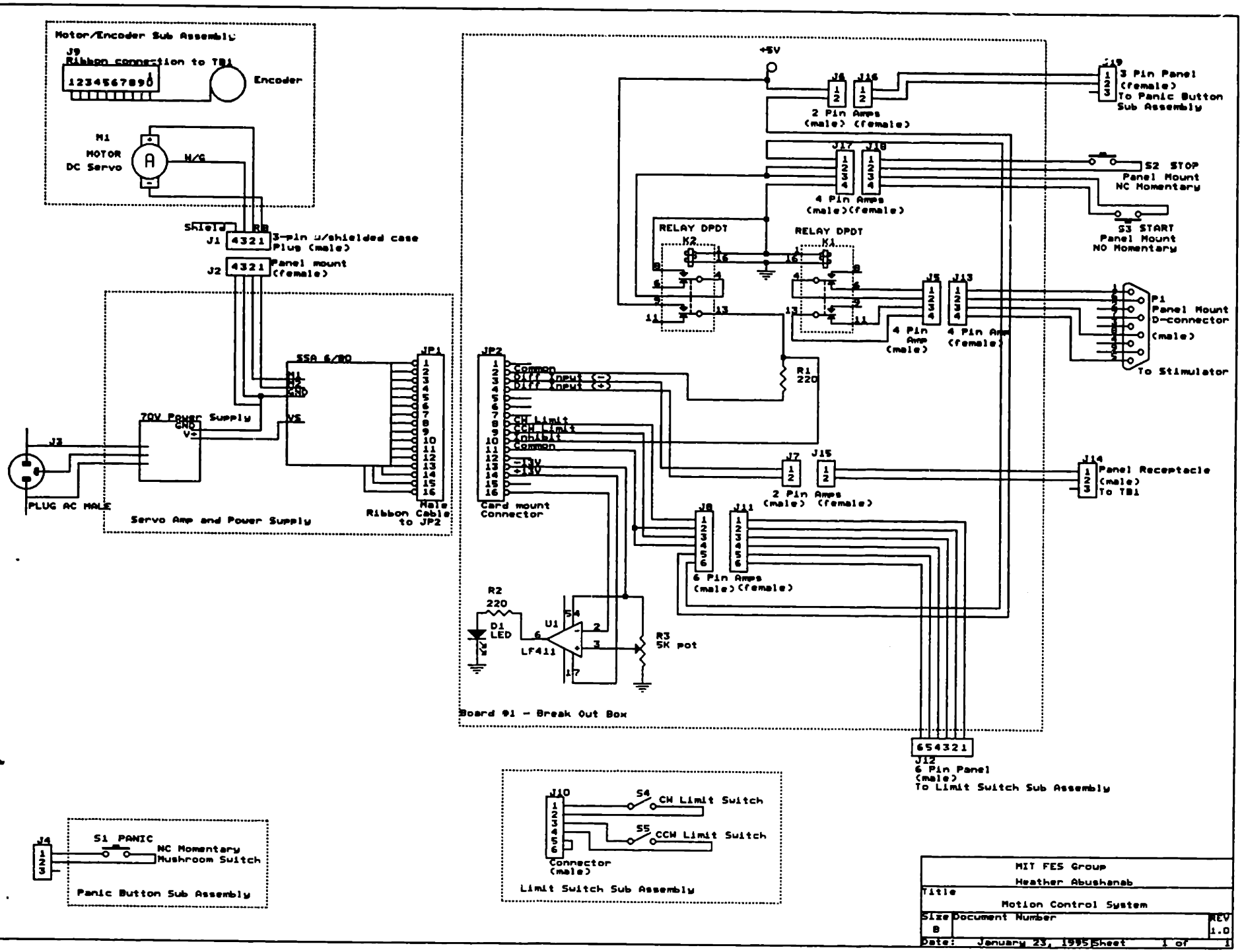
Motor/Encoder Sub Assembly
J9
Ribbon connection to TB1
1 2 3 4 5 6 7 8 9 10
Encoder
M1
MOTOR
DC Servo
H/G
Shield
J1 4321
3-pin u/shielded case
Plug (male)
J2 4321
Panel mount
(female)
SSA 6/80
JP1
M1
M2
GND
VS
70V Power Supply
GND
V+
J3
PLUG AC MALE
Servo Amp and Power Supply
Male
Ribbon Cable
to JP2
+5V
J6
J16
2 Pin Amps
(male) (female)
J19
3 Pin Panel
(female)
To Panic Button
Sub Assembly
J17
J18
4 Pin Amps
(male)(female)
S2 STOP
Panel Mount
NC Momentary
S3 START
Panel Mount
NO Momentary
RELAY DPDT
K2
RELAY DPDT
K1
J5
J13
4 Pin
Amp
(male)
4 Pin Amp
(female)
P1
Panel Mount
D-connector
(male)
To Stimulator
JP2
Common
Diff Input (-)
Diff Input (+)
CW Limit
CCW Limit
Inhibit
Common
-15V
+15V
Card mount
Connector
R1
220
J7
J15
2 Pin Amps
(male) (female)
J14
Panel Receptacle
(male)
To TB1
J8
J11
6 Pin Amps
(male)(female)
R2
220
D1
LED
U1
LF411
R3
5K pot
Board #1 - Break Out Box
654321
J12
6 Pin Panel
(male)
To Limit Switch Sub Assembly
J4
S1 PANIC
NC Momentary
Mushroom Switch
Panic Button Sub Assembly
J10
S4
CW Limit Switch
S5
CCW Limit Switch
Connector
(male)
Limit Switch Sub Assembly
MIT FES Group
Heather Abushanab
Title
Motion Control System
Size
B
Document Number
REV
1.0
Date: January 23, 1995
Sheet 1 of 1

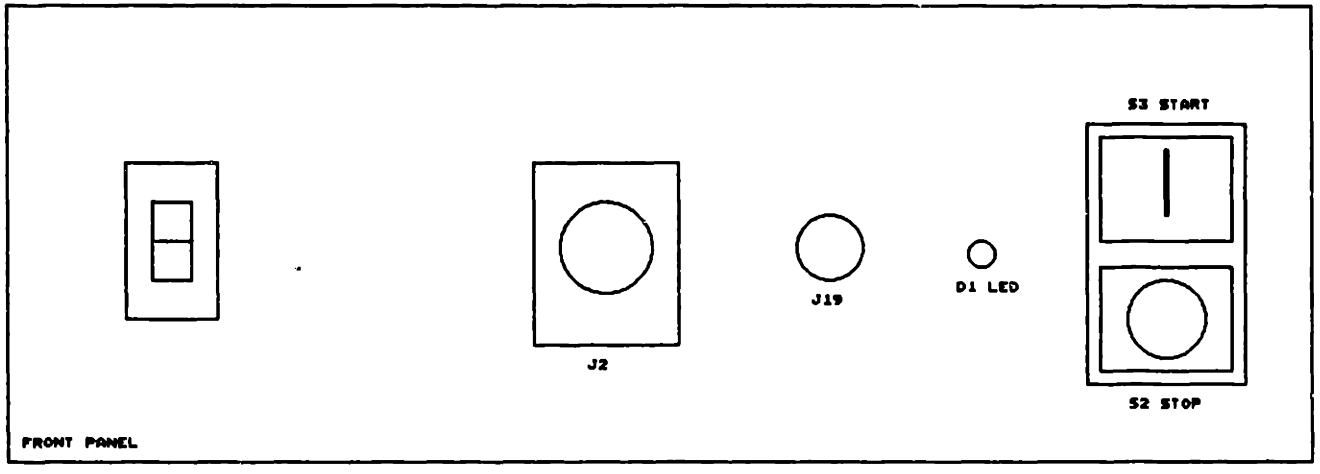

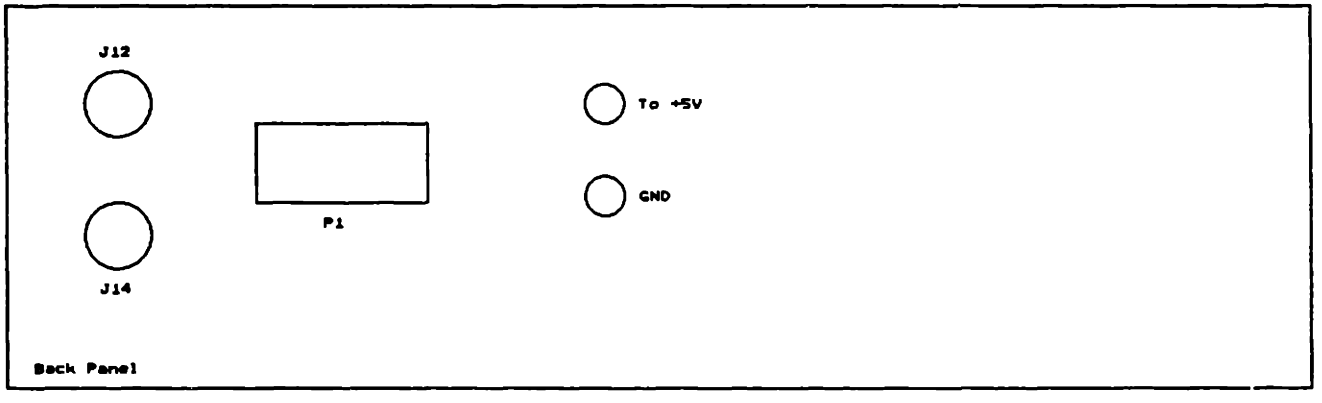

Heather Abushanab MIT FES GROUP		
Title Motion Control System - Panel Schematic		
Size B	Document Number	REV 1.0
Date: January 23, 1995	Sheet 1 of 1	

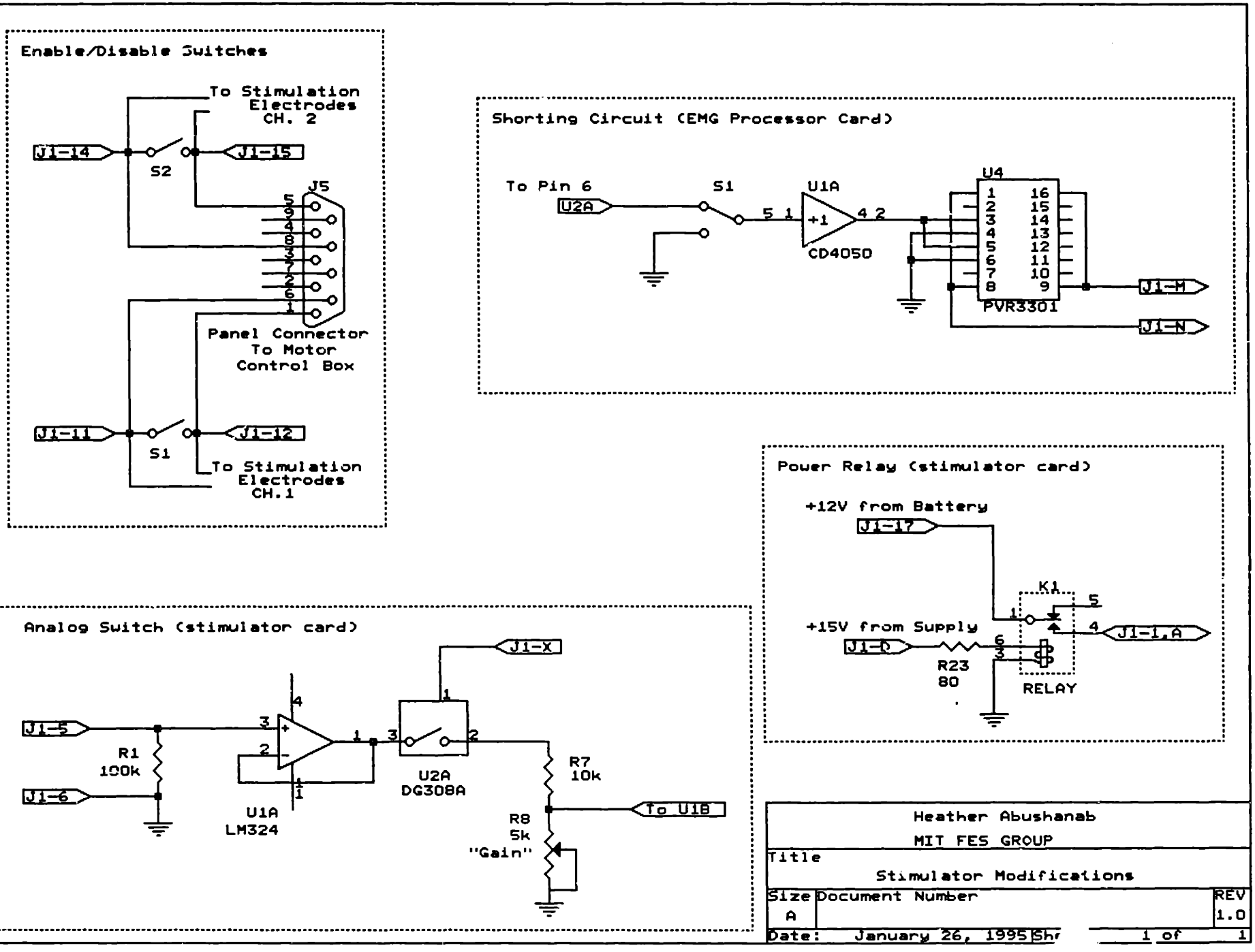
Enable/Disable Switches
To Stimulation Electrodes CH. 2
J1-14
S2
J1-15
J5
Panel Connector To Motor Control Box
J1-11
S1
J1-12
To Stimulation Electrodes CH.1
Shorting Circuit (EMG Processor Card)
To Pin 6
U2A
S1
U1A
+1
CD4050
U4
PVR3301
J1-M
J1-N
Power Relay (stimulator card)
+12V from Battery
J1-17
K1
+15V from Supply
J1-D
R23
80
RELAY
J1-1,A
Analog Switch (stimulator card)
J1-X
J1-5
R1
100k
J1-6
U1A
LM324
U2A
DG308A
R7
10k
R8
5k
"Gain"
To U1B
Heather Abushanab
MIT FES GROUP
Title
Stimulator Modifications
Size
A
Document Number
REV
1.0
Date: January 26, 1995
Sh
1 of 1

Appendix B

Selected Vendors

Company (Distributor)	Contact	Address	Phone
Omnitech Robotics, Inc	Dave Parrish	2640 Raritan Circ., Englewood, CO 80110	(303) 922-7773
Sensotec, Inc	Kevin Westhora	1200 Chesapeake Ave, Columbus, OH 43212-2288	(800) 848-6564 ext 229
Underwood Sales (Stock Drive Products)	Bill Underwood		(516) 599-5010
Hamilton Hallmark (Analog Devices)	Matt	10M Centennial Dr., Peabody, MA	(800) 332-8638 ext 3505
A/D Nova (International Rectifier)	Steve Colino		(516) 878-0664
Burr Brown			(617) 229-0300
Nevada Computer (Western Digital)	Mark Powers	684 Wells Road, Boulder City, NV 89005	(702) 294-1168
Northgate Computer Systems, Inc.	Mary Novakowski	141 N. Jonathan Blvd., Chaska, NM 55318	(800) 548-1993 ext 7910

Appendix C

Sensor Calibration

This appendix contains calibration curves for the various sensors.

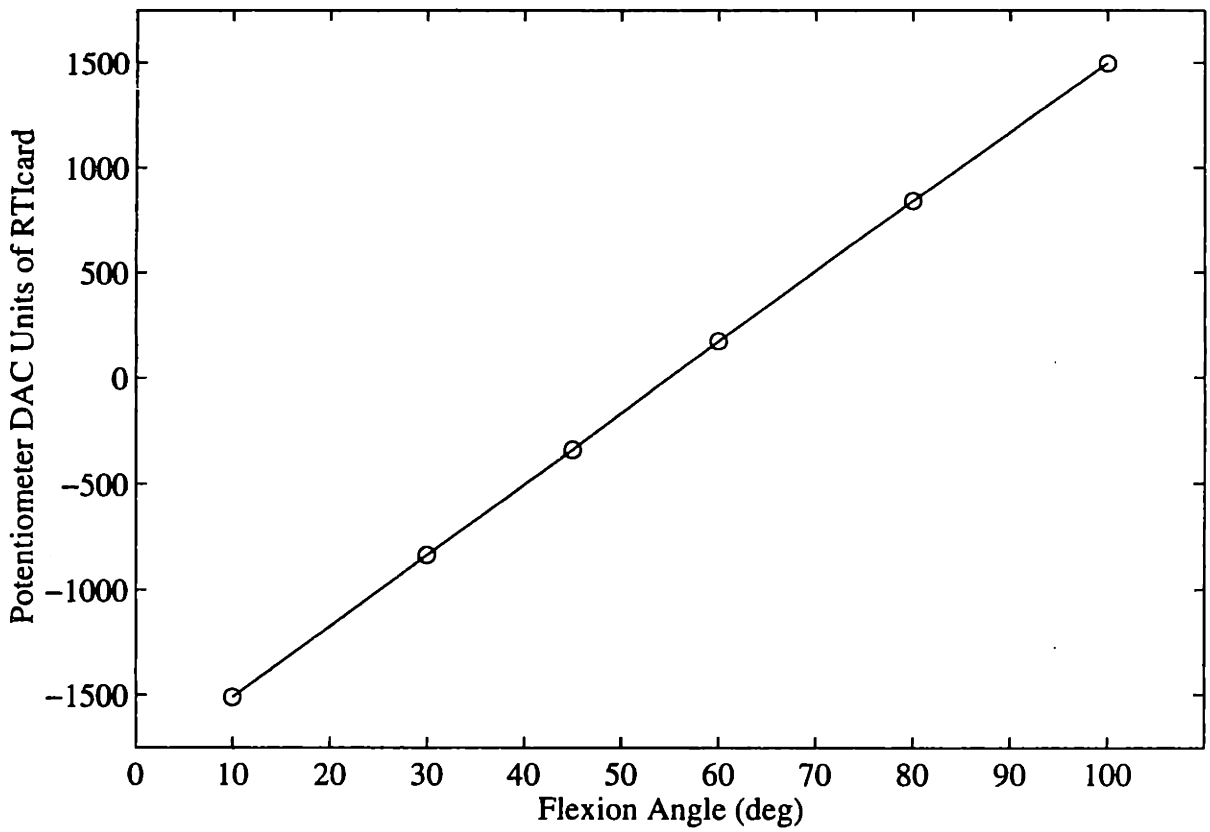

Figure C-1: Calibration curve for Potentiometer

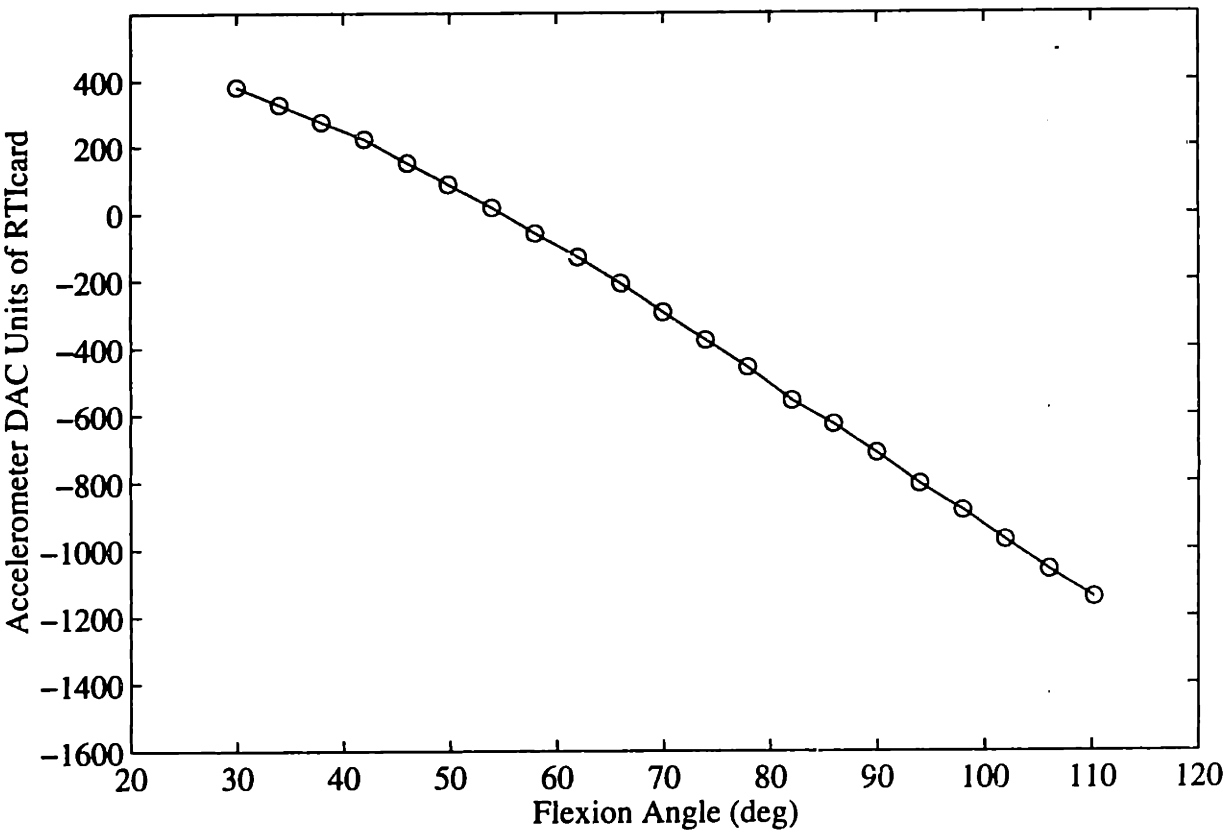

Figure C-2: A typical accelerometer reading vs position curve. This curve was recalibrated before each experiment and was used to remove the effect of gravity from the accelerometer signal.

Appendix D

Informed Consent Form

This form was given to each subject at the beginning of the first experimental session. The subject read the form and the investigator answered all of the subject's questions. The subject signed the form, indicating his understanding of the experiment and his consent to participate. The subject was allowed to ask additional questions during the experiment.

INFORMED CONSENT STATEMENT

Muscle Modeling and Parameterization for Control with FES

Functional electrical stimulation (FES) is a promising means of restoring function to paralyzed limbs and has been used with limited success to achieve assisted standing and walking. The goal of this research project is to develop models and methods for parameterization that will help customize FES control systems for individuals.

During this experiment, your leg will be stimulated and a motor will move the leg through fixed trajectories. The experimental apparatus consists of a bench for you to sit on. A light weight orthosis or brace is fixed to the bench and will be strapped to your leg. A pair of surface stimulation electrodes will be placed over the quadriceps muscle. Your leg will move under the control of both electrical stimulation and the motor. An EMG electrode and ground strap will also be placed on the leg to monitor muscle activity during the experiment. Conductive gel will be applied between your skin and the EMG electrodes to achieve good contact. The gel wipes off easily after the experiment.

You will be asked to sit on the bench with your leg in the brace. During the actual experiment, you will be asked to recline on the bench, so that your hip is held in a fixed position through out the experiment. You will be asked to relax your leg muscles as much as possible to minimize the possibility of voluntary contractions contaminating the results.

Exp I: Your leg will be held at a fixed flexion angle and stimulated for short periods of time.
Exp II: Your leg will be moved through a series of trajectories, but will not be stimulated.
Exp III: Your leg will be moved to fixed positions and held. The leg will be stimulated at each fixed position. Then the leg will be stimulated and moved at a slow angular velocity for short angular distances.
Exp IV: The brace will be decoupled from the motor. A random stimulation pattern will be applied to the leg and the motion of the leg will be recorded. The stimulation patterns include: pseudo-random binary signals, step signals, ramp signals and sinusoids of varying frequency.

Stimulating electrodes are used routinely by therapists for rehabilitation. The current levels you will receive have been shown to be harmless. Although you may feel some discomfort due to the current when the stimulation is initiated, this feeling usually does not persist. In addition, there may be some temporary irritation of the skin which will disappear with time. There are essentially no other risks or discomforts associated with the procedure. It is understood that you may withdraw from this experiment at any time and for any reason. Individuals with a history of cardiac, vascular or neurologic problems should not participate in these experiments.

Any questions you have regarding the procedure (before, during or after the experiments) will be answered. You will not benefit directly from this project, but your participation will help advance surface FES techniques for the restoration of gait to paraplegics.

CONSENT:

I have fully explained to _____ the nature and purpose of the above procedure and will answer all questions to the best of my ability.

_____
Investigator's Signature

I have read and understood this Informed Consent Statement and have had the procedures for these experiments fully explained to me. I give my consent to participate in the procedures as a volunteer. I understand that I am free to withdraw at any time for any reason with no penalty.

In the unlikely event of physical injury resulting from participation in this research, I understand that medical treatment will be made available from the MIT Medical Department, including first aid, emergency treatment and follow-up care as needed, and that my insurance carrier may be billed for the cost of such treatment. However, no compensation can be provided for medical care apart from the foregoing. I further understand that making such medical treatment available, or providing it, does not imply that such injury is the investigator's fault. I also understand that by my participation in this study I am not waiving any of my legal rights. (Further information on these rights may be obtained by calling the Insurance and Legal Affairs department in the MIT Treasurer's Office at 253-2822.)

I understand that I may also contact the Chairman of the Committee on the Use of Humans as Experimental Subjects, MIT 253-6787, if I feel I have been treated unfairly as a subject.

_____
Signature of Subject/Parent/Guardian

_____
Signature of Witness

_____
Date

Appendix E

Experimental Data Sheet

Data sheets for both the isometric experiment and the full model identification experiment are given in this appendix.

IRC Experiment: Data Sheet

Subject name_____ Initials____ Date_____

First Leg_____

Maximum Stimulation_____mA

Threshold_____mA

Ramp IRC:

Maximum Stimulation_____mA

Minimum Stimulation_____mA

Filename_____.dat

Step IRC:

Maximum Stimulation_____mA

Minimum Stimulation_____mA

Filename_____.dat

Prediction:

Maximum Stimulation_____mA

Minimum Stimulation_____mA

Filename_____.dat

Comments:_____

_____

_____

_____

_____

Processing:

system poles:_____

system delay_____s

Error Analysis:

RMS error_____

Second Leg_____

Maximum Stimulation_____mA

Threshold_____mA

Ramp IRC:

Maximum Stimulation_____mA

Minimum Stimulation_____mA

Filename_____.dat

Step IRC:

Maximum Stimulation_____mA

Minimum Stimulation_____mA

Filename_____.dat

Prediction:

Maximum Stimulation_____mA

Minimum Stimulation_____mA

Filename_____.dat

Comments:_____

_____

_____

_____

_____

Processing:

system poles:_____

system delay_____s

Error Analysis:

RMS error_____

Data Sheet Record for Muscle-Joint Model Identification Experiments

Subject_____Initials_____Leg____Session___
Date_____Data dir_____File stub_____
Subject data:
Age_____yrs Sex_____
Height_____m Weight_____lb_____kg
Knee to Ankle _____m Calf circumference _____m
Accelerometer placement_____m

I. Isometric Identification (IRC.exe) Comments:
Max. Stim Tolerance_____mA
Stim Threshhold_____mA
Knee angle_____deg
Data_____.iso _____e.iso
max_____mA min _____mA
Processed file _____.irc
poles: _____s^{-1} delay: _____ms

II. Passive Identification #1: Comments:
Maximum Knee Angle_____deg
Minimum Knee Angle _____deg
A. Sequential Identification (PASSIVE.exe)
Max Angle_____deg Min Angle_____deg
position_____.pos_____pe.pos
velocity _____.vel _____pe.vel
processed data_____.mat
Inertia_____$N \cdot m \cdot s^2$_____$N \cdot m \cdot s^2/deg$
$0.0277(m\,[\text{lb}])(0.01867\ell\,[\text{in}])^2\pi/180$
B. Simultaneous Identification (TRAJEXP.exe)
Max Angle_____deg Min Angle_____deg
Traj #1_____p1.dat _____e.p1
processed data _____p1.mat
Traj #2_____p2.dat _____e.p2
processed data _____p2.mat

III. Active Identification Comments:

Simultaneous Identification (ACT2.exe):

Trial #1 _____q.tr1 _____e.tr1

Stim _____mA TRJ:_____Hz

processed w/_____p__.mat

full model_____q__1.mat

Trial #2 _____q.tr2 _____e.tr2

Stim _____mA TRJ:_____Hz

processed w/_____p__.mat

full model_____q__2.mat

IV. Passive Identification #2 (ACT2.exe):

Trial #1_____p.1 _____e.tr1

Stim _____mA

processed_____p__.mat

Trial #2_____p.2 _____e.tr2

Stim _____mA

processed_____p__.mat

Trial #3_____p.3 _____e.tr2

Stim _____mA

processed_____p__.mat

V. Prediction experiments (ACT2.exe): Comments:

A. Step_____q.stp _____e.stp

Stim_____mA

B. Ramp_____q.rmp _____e.rmp

Max. Stim_____mA

C. Sine_____q.sin _____e.sin

Max. Stim_____mA Min. Stim_____mA

Appendix F

Experimental Protocol

This appendix contains explicit item by item protocols for the isometric experiments and the full model experiments.

Protocol -Comparing IRC methods (Revised Protocol - March 25,1994)
Heather Beck Abushanab

I. Preparation -(before subject arrives)

A. Set-Up Stimulator

1. Turn on Power
2. Set Frequency Control to External
3. Set Amplitude Control to Internal
4. Make sure BLANK and SHORT are off (EMG Processor Module)
5. Make sure Break Out Box is disconnected (9 pin D-connector on back)
6. Make sure Channel 2 Amplitude is off (Counter Clockwise)
7. Measure battery voltage w/volt meter
    a. Should read 12 V
    b. If needed, borrow battery from Michael's setup; Recharge battery
8. Plug-in electrode leads to Channel 1 of Stimulator and Meter Box
9. Enable Channel 1
10. Put Meter Box switch on METER
11. Run program IRC_3; Select Test Tolerance
12. Make sure meter reading is approximately the same as computer reading
13. Lower amplitude to zero and disable Channel 1.

B. Set-Up Bench

1.Turn on Power to Bench (A/C Power On).
2. Disconnect the Panic Button from the Motor Control Box (this will insure that the motor cannot be turned on).
3. Make sure Pot and Torque 2 Connectors are plugged in.
4. Run program IRC_3; Select Test Tolerance
5. Check position readout. Lock the brace at approx. 90 degrees with the bolts/plate.
6. Test torque transducer by tugging on the brace strut.
7. Make sure the bench is located so that the subject can reach the stimulator enable switch and the amplitude dial.

II. Preparation (after subject arrives)

A. Explain the basic experiment to the subject
B. Give them the information sheet to read.
C. Ask them to sign the informed consent sheet.
D. Place Subject's name and initials on data sheet.
E. Position subject on the bench so the knee is aligned with the joint of the brace.
F. Strap the calf to the brace with velcro strap. (Make this as tight as is comfortable for the subject).
G.. Wet electrodes and place them on the leg.
H. Strap down upper thigh with velcro.
I. Explain to the subject what the stimulation feels like (tingling, pins and needles)
J. Run IRC_3; Select Test Tolerance
K. Determine Subjects Maximum Tolerance and Threshold.

1. Ask subject to enable Channel 1.
2. Ask subject to slowly increase stimulation and allow time for the subject to get used to the feeling. Encourage the subject to relax and to increase stimulation as much as is comfortable.
3. Make sure the subject produces at least 6 N-m of Torque at maximum.
    If you cannot get this torque:
    a. Encourage higher stimulation
    b. Try moving the electrodes a bit.
    c. Try reversing the electrode leads.
    d. If none of this works, thank the subject and explain that we will not be able

to use them as a subject.

4. Record maximum comfortable stimulation level.
5. Record threshold stimulation level.

II. Ramp IRC Experiment: Run IRC_3

A. Change amplitude control to external (Switch Up)
B. Set Maximum Stimulation to Subject maximum tolerance.
C.. Set Minimum Stimulation to 5 mA **below** threshold.
D.. Enter filename for ramp experiment (ex hlbrampr, where hlb are subject initials and r indicates the right leg).
E. Record max,min and filename on data sheet.
F. Select Run IRC Experiment.
G. Explain this portion of the experiment to the subject. (There will be a conditioning pulse lasting 3 seconds followed by two impulses and two ramps)
H. Have the subject recline, so the hip is fully extended.
I. Ask the subject if they are ready to begin. Tell them to relax and to remain still through out the experiment.
J. Look at the data run. (Does it look good? Does the force record start and end at zero N-m? Does the ramp in force cover most of the data run?).
K. Repeat the experiment if the data is not good. Save the data if it is good and exit the program.

III. Step IRC Experiment: Run StepIRC

A. Ask the subject to remain in the same position while you prepare for the next experiment.
B. Set the Maximum Stimulation to same as part IIIA.
C. Set the Minimum Stimulation to threshold.
D. Enter filename (ex. hlbstepr, where hlb are subject initials and r refers to right leg).
E. Record Max, Min and filename on data sheet.
F. Explain this part of the experiment to the subject (There will be 10 ramps of increasing stimulation amplitude. Each one lasts 3 seconds followed by 30 seconds of rest.)
G. Ask the subject if they are ready to begin. Tell them to relax through out the experiment.
I. Look at the data. Is it okay?
J. Save the data and exit the program.

IV. Prediction Experiment: Run IRC_3

A. Ask the subject to remain in the same position while you prepare for the next experiment.
B. Set the Maximum Stimulation to same as part IIIA.
C. Set the Minimum Stimulation to 5 mA **above** threshold.
D. Enter filename (ex. hlbpr, where hlb are subject initials and r refers to right leg).
E. Record Max, Min and filename in data sheet.
F. Explain this part of the experiment to the subject (This is a stimulation profile which lasts 11 seconds. The stimulation will ramp and hold to various levels. Please try to relax.)
G. Ask the subject if they are ready to begin. Tell them to relax.
H. Look at the data. Is it okay?
I. Save the data.

V. Backup Data

Let the subject rest, or go to the bathroom if needed. Explain that you will repeat the same experiments on the other leg and that they will need to remain still for the duration of the experiments. If the subject needs a rest period, use this time to process the data and run the simulations (part VII and VIII).

VI. Repeat the experiment with the second leg beginning from part IIE.

VII. Process Ramp Data: Run IRC_3

A. Enter filename for processing
B. Select Process Data
C. Smooth and Average IRCs
D. Look at processed data. Note any thing that looks unusual.
E. Record system poles and system delay on data sheet.

VIII. Simulations: Run Isosim

A. Enter subject initials
B. Enter right or left leg
C. Choose to Automatically update filenames
D. Enter poles from data sheet. Choose 2nd order system
E. Choose to simulate with both the ramp and step irc → Enter min. & max. stim. levels.
F. Begin simulation
G. Look at output. Note anything unusual.
H. Record output filename on data sheet.
I. Exit program.
J. Convert data to matlab binary format: Run sim2mat and enter filename at the prompt.
K. Plot data using the matlab .m file plotdata.

Protocol for Full Muscle-Joint Model Identification

(Prepared by H. Abushanab; September 1994)

I. Pre-Experiment Set-Up (before subject arrives)

A. Power On

1. Stimulator
2. Motor Control Box
3. Bench Box
4. Re-boot computer

B. Check all cable and motor connections.

1. Stimulator
   - Power
   - Break out cable to motor control box
   - Ribbon cable to jumper box; jumper box to computer
   - Stimulation leads to test box
   - EMG electrode
   - BNC from EMG to Oscilloscope
2. Motor Control Box
   - Power
   - Panic Button
   - Motor Cable
   - Motor command input to motor jumper box
   - Limit switches
   - Break out cable to stimulator
   - 5v/GND from Bench electronics
3. Bench Electronics
   - Power
   - Ribbon cable to jumper box; jumper box to computer
   - 5v to motor control box
   - Sensors: Pot, Acc, Strain gauges
4. Computer
   - Rticard ribbon cable to jumper box
5. Motor
   - Motor Cable to motor control box
   - Encoder to Jumper Board
6. Jumper Board
   - Encoder connection
   - Motor control connection
   - Ribbon cable to Omnitech Controller Board in computer

C. Test Equipment

1. Stimulator
   - run program irc.exe; choose toltest
   - hit green button on motor control box to enable equipment
   - make sure enable switch for channel 1 is enabled.
   - put freq. switch to computer control; amp to manual
   - test stimulation
   - test EMG by placing on hand muscle and looking at oscilloscope

2. Bench Electronics
   - run irc.exe; choose toltest
   - move knee brace and note position reading
   - make sure strain gauge and accelerometer are registering.
3. Calibrate accelerometer (use IRC.exe and lock command)
   - place accelerometer at +/-g and 0g.
   - look at DAC output. Make sure conversions are still correct.

II. Set-up (with subject)

A. Paper Work

- Explain basics of experiment to subject.
- Have subject read and sign consent form.
- Fill out subject data in record sheet.

B. Physical Set-Up

- Place electrodes on quadriceps.
- Put EMG ground strap on leg.
- Make sure motor and stimulator are disabled.
- Place subject on bench, adjust brace and secure leg with Velcro straps.
- Strap Accelerometer to subject ankle.
- Measure distance from joint to accelerometer. Record. Update file "filename.dat".
- Have subject move leg and note full range of motion. Record this as maximum and minimum knee angle under passive identification.
- Plug electrode leads into electrodes.
- Give Panic Button to subject and explain that it will shut off the stimulation and the motor any time during the experiment.
- Have subject recline on the bench. Stress importance of remaining relaxed during the experiment and remaining in the same posture.

C. Test EMG

- Place EMG electrode on leg. Secure with surgical tape.
- Look at signal on Osciloscope.
- Adjust electrode placement so that there is a distinct difference between the relaxed and contracted states.

D. Determine Stimulation Levels

- Enable stimulator by hitting green button on motor controller.
- Run irc.exe; Lock knee at 90 deg.
- Choose toltest; freq. - computer; amp - manual.
- Let the subject adjust the stimulation.
- Record max. stimulation and stim threshold.

III. Isometric Identification Experiment:

A. Setup Program

- Run IRC.exe;
- Switch Amplitude control to computer.
- Enter datafile name.
- Change max. stimulation to subject's maximum. Record on data sheet.
- Change minimum stimulation to 5 ma less than subject's threshold. Record on data sheet.
- Explain details of this portion of the experiment to the subject
(2 impulses; 2 ramps; remain relaxed).

B. Run experiment - (make sure subject is ready before beginning).

C. Results

- Look at EMG and Force record. If there are signs of co-contraction, repeat experiment. If the full IRC range was not covered, adjust minimum stimulation and repeat experiment.
- Process data while allowing subject to rest. Note poles and delay time.

IV. Passive Identification

A. Sequential

1. Set-up

- Disable stimulator channel 1.
- Run PASSIVE.exe
- Enter subject information
- Explain Position experiment to subject (10 positions, each measured 4 times, stay relaxed).

2. Run Experiments and Examine Results

- Run Passive T-A identification experiment, when subject is ready.
- Look at curve and repeat if it is unreasonable.
- Look at EMG record. Repeat if there are signs of co-contraction.
- Explain Velocity experiment to subject (6 speeds; both directions, stay relaxed).
- Run Passive T-V identification experiment, when subject is ready.
- Look at curve and repeat if it is unreasonable.
- Look at EMG record. Repeat if there are signs of co-contraction.

B. Simultaneous

1. Set-up

- Run TRAJEXP.exe
- Enter subject information.
- Enter maximum and minimum knee angle for testing.
- Choose trajectory #1.
- Explain experiment (Random trajectory, may be a little disconcerting, stay relaxed).

2. Run Experiments and Examine Results

3. Repeat for Trajectory 2.

V. Active Identification- Simultaneous Experiment.

1. Set-up

- Disable motor (red switch or panic button).
- Disconnect coupler between motor and transmission.
- Re-enable motor (green switch)
- Run ACT2.exe
- Choose toltest; put stim amp on manual.
- Increase stim until leg reaches full extension. Note level.
- Put stim on computer control.
- Enter subject info into program.
- Explain experiment to subject (random stimulation pattern, leg will move on its own, try to relax).

2. Run Experiment and Examine Results

- Look at phase plane covered by this experiment.
- Raise or lower stim level if needed. Repeat experiment.

VI. Prediction Experiments (ACT2.exe)

A. Step Response

-max stim: 75% of IRC range; record in data sheet.
- explain experiment (3 s constant stimulation; leg will move; stay relaxed).

B. Ramp Response

- max stim: max. of tolerance
- explain experiment (10 s; ramp up, then down; leg will move; stay relaxed).

C. Sine Response

- max. stim: max. of tolerance
- min. stim: just below threshold.
- explain experiment (10s sine stimulation; increasing frequency; leg will move; stay relaxed).

VII. Repeat Full Experiment with second leg.

Appendix G

The Hill Model and Coordinate Transformation

The Hill muscle model was developed to explain the behavior of muscle in an isolated environment. The original equations were written in terms of muscle length and velocity. The follwing equation shows the contractile force of muscle in terms of the origial Hill cooridinates where x represents the muscle length and $\dot{x}$ represents the muscle velocity.

$$F_{CE} = f_{STIM} \times f_x(x) \times f_{\dot{x}}(\dot{x}) \tag{G.1}$$

In an intact human, the muscle acts through a moment arm to produce a torque about the joint. All coordinate transformations like this one are specifed by the Jacobian matrix J, so that

$$dx = Jd\theta. \tag{G.2}$$

and

$$\tau = J^T F \tag{G.3}$$

where J is a function of θ. For this example, the matrix J is a single function describing the non-linear mucsle moment arm, $r(\theta)$, so that

$$J = J^T = r(\theta). \tag{G.4}$$

The torque produced at the joint due to the contractile force is

$$\tau_{CE} = r(\theta) \times F_{CE} = r(\theta) \times f_{STIM} \times f_x(x) \times f_{\dot{x}}(\dot{x}). \tag{G.5}$$

From Equation (G.2) a relationship is defined between muscle length and joint angle, as well as muscle velocity and joint velocity.

$$x = \int dx = \int r(\theta) d\theta. \tag{G.6}$$

$$\dot{x} = \frac{dx}{dt} = \frac{dx}{d\theta}\frac{d\theta}{dt} = r(\theta)\dot{\theta}. \tag{G.7}$$

Note that x is a function of θ, but that $\dot{x}$ is a function of both θ and $\dot{\theta}$. Substituting these relationships into Equation (G.5) results in an equation for contractile element torque with respect to θ and $\dot{\theta}$.

$$\tau_{CE} = r(\theta) \times f_{STIM} \times f_x(\int r(\theta) d\theta) \times f_{\dot{x}}(r(\theta)\dot{\theta}). \tag{G.8}$$

The only part of this equation which is a function of more than one variable is $f_{\dot{x}}$. The separable feature of the Hill structure remains only if $f_{\dot{x}}$ can be separated into independent functions of θ and $\dot{\theta}$. This would be true in cases where the muscle moment arm is linear ($r(\theta) = r$) or the velocity function is limited to powers of x, (for example: $f_{\dot{x}}(\dot{x}) = ax^{1.2}$). In general $f_{\dot{x}}$ is not a separable function.

The preceeding analysis shows that the Hill model, developed for the muscle coordinate frame, cannot be used to justify a similar model in the joint coordinates, since a direct translation puts severe (and unrealistic) constraints on the form of the torque-velocity curve. At this point it is important to remember that the Hill model itself is only a model. It does a reasonable job explaining much of the observed behavior of muscle, but it is by no means an exact or complete description of that behavior. The Hill model did provide some initial motivation for investigation of the multiplicative structure in this study; however, there are more compelling reason to look at the model structure in the context of identification and control. The multi-

plicative structure allows the contractile element torque to change with changes in joint angle and joint velocity, a phenonmenon which is observed and justified by what we know of muscle mechanics. The identification techniques described in Chapter 4 are possible because of the separable model structure and model based controllers are easier to produce for separable models. As always, selection of this model structure was a trade off between accuracy and simplicity.

Appendix H

Isometric Torque Prediction

The table in this appendix contains the error statistics for all 46 data sets from the focused isometric experiment. The normalized RMS error was calculated from the equation:

$$E_{RMS} = \sqrt{\frac{\sum_1^N (\frac{prediction-data}{data})^2}{N}}. \tag{H.1}$$

The average error was given by the following equation:

$$E_{AVE} = \frac{\sqrt{\sum_1^N (prediction - data)^2}}{\sum_1^N data}. \tag{H.2}$$

In the table, simulation order refers to second- or third-order contraction dynamics.

			Normalized RMS Error		Average Absolute Error	
Subject	Leg	Simulation Order	Step Response IRC	Ramp Response IRC	Step Response IRC	Ramp Response IRC
daf	r	2	2.6161	2.4892	0.0129	0.0121
daf	r	3	2.2818	2.0923	0.0134	0.0126
daf	l	2	1.385	0.9091	0.0048	0.0032
daf	l	3	1.1447	0.7183	0.0046	0.003
kbb	r	2	0.6379	0.5548	0.0054	0.0072
kbb	r	3	0.6936	0.5778	0.0056	0.0074
kbb	l	2	1.1224	0.7927	0.0068	0.0067
kbb	l	3	0.7435	0.6169	0.0062	0.006
bmn	r	2	0.4464	0.4148	0.0033	0.0035
bmn	r	3	0.4095	0.3707	0.0024	0.0026
bmn	l	2	0.4944	0.4953	0.0042	0.0045
bmn	l	3	0.5252	0.5255	0.0041	0.0045
ttt	r	2	1.695	2.0854	0.0046	0.0062
ttt	r	3	0.8637	1.1704	0.0031	0.0052
ttt	l	2	2.1337	3.6344	0.0065	0.0061
ttt	l	3	1.6479	3.1294	0.0069	0.0063
alj	r	2	0.4934	0.7622	0.0045	0.0047
alj	r	3	0.5089	0.865	0.0048	0.005
alj	l	2	4.1737	5.5212	0.0018	0.002
alj	l	3	1.5162	2.9493	0.0012	0.0015
tbg	r	2	0.5056	0.6023	0.0043	0.0057
tbg	r	3	0.4432	0.5091	0.003	0.0046
tbg	l	2	0.5062	0.5553	0.0037	0.0035
tbg	l	3	0.5688	0.6248	0.005	0.0047
mec	r	2	0.5763	0.7077	0.0123	0.0126
mec	r	3	0.582	0.7259	0.0128	0.013
mec	l	2	3.8679	4.5328	0.0112	0.0111
mec	l	3	3.6347	4.308	0.0116	0.0114
sob	r	2	0.8883	0.888	0.0031	0.0029
sob	r	3	0.8738	0.8259	0.003	0.0027
sob	l	2	7.0626	3.1323	0.0069	0.0051
sob	l	3	6.8261	2.8454	0.0065	0.0048
mrc	r	2	1.2239	1.3703	0.0065	0.0061
mrc	r	3	0.8095	0.959	0.0063	0.0058
mrc	l	2	1.9769	1.5973	0.0045	0.0047
mrc	l	3	1.3589	0.8218	0.0051	0.0052
rll	r	2	1.7688	1.4865	0.0059	0.0057
rll	r	3	1.1941	1.0032	0.0044	0.0043
rll	l	2	0.5304	0.6022	0.0059	0.0056
rll	l	3	0.5575	0.6471	0.0061	0.0059
smy	r	2	0.8564	1.1645	0.0033	0.0033
smy	r	3	0.8294	1.1513	0.0038	0.0037
smy	l	2	2.8383	2.4805	0.0084	0.0082
smy	l	3	2.7811	2.4166	0.0089	0.0087
kdf	r	2	0.6682	0.6111	0.0045	0.0045
kdf	r	3	0.6416	0.5956	0.0035	0.0035

Continued:			Normalized RMS Error		Average Error	
Subject	Leg	Simulation Order	Step Response IRC	Ramp Response IRC	Step Response IRC	Ramp Response IRC
kdf	l	2	0.8553	1.156	0.0032	0.0029
kdf	l	3	0.5669	0.8124	0.004	0.0037
jeh	r	2	1.8223	2.5073	0.0051	0.0061
jeh	r	3	1.2387	1.9855	0.0032	0.0045
jeh	l	2	0.6926	0.5151	0.0043	0.0044
jeh	l	3	0.6471	0.4851	0.0044	0.0045
slj	r	2	0.5997	0.4356	0.0058	0.0041
slj	r	3	0.6219	0.4554	0.0061	0.0046
slj	l	2	4.0683	1.2923	0.0058	0.0049
slj	l	3	3.8785	1.0046	0.0053	0.0045
knu	r	2	1.3769	0.8692	0.0037	0.0029
knu	r	3	1.7429	1.003	0.0042	0.0037
knu	l	2	1.4815	1.4909	0.0126	0.011
knu	l	3	1.4395	1.4152	0.0124	0.0108
ksb	r	2	1.0128	1.9923	0.0053	0.0046
ksb	r	3	0.5585	1.317	0.0059	0.0052
ksb	l	2	0.7641	1.9899	0.0063	0.0082
ksb	l	3	0.556	1.616	0.0069	0.0085
wrg	r	2	0.4896	0.5705	0.0065	0.0055
wrg	r	3	0.5025	0.6371	0.0067	0.0056
wrg	l	2	7.75	8.5122	0.0044	0.0054
wrg	l	3	7.5146	8.2197	0.0045	0.0054
gea	r	2	2.1315	3.0125	0.0059	0.0068
gea	r	3	1.4625	2.1412	0.0044	0.0056
gea	l	2	3.77	4.8669	0.0044	0.0042
gea	l	3	2.4674	3.7604	0.0033	0.0031
mdt	r	2	1.7564	1.3676	0.0078	0.0079
mdt	r	3	1.4522	1.0594	0.0065	0.0065
mdt	l	2	1.4072	1.1003	0.0066	0.0066
mdt	l	3	1.2221	0.9155	0.0076	0.0077
kon	r	2	3.9625	0.7973	0.0123	0.0064
kon	r	3	3.8435	0.6212	0.0117	0.0054
rpd	r	2	20.1506	11.2243	0.0129	0.0112
rpd	r	3	19.9104	11.2011	0.0123	0.0111
rpd	l	2	0.5209	0.4581	0.0038	0.004
rpd	l	3	0.5734	0.4836	0.0042	0.0044
mdc	r	2	0.4671	0.3991	0.0036	0.003
mdc	r	3	0.471	0.4013	0.0032	0.0025
dgv	r	2	0.5521	0.4928	0.007	0.0067
dgv	r	3	0.5761	0.4992	0.007	0.0067
dgv	l	2	0.4219	0.2785	0.0028	0.0029
dgv	l	3	0.4354	0.2765	0.0025	0.0025
kal	r	2	1.3088	2.5993	0.0024	0.0042
kal	r	3	1.35	2.5649	0.0027	0.0043
kal	l	2	0.9846	1.1639	0.0032	0.0039
kal	l	3	0.5745	0.7054	0.0036	0.0043

Appendix I

Model Parameters

This appendix shows all the parameters sets identified for each subject leg. One set of passive parameters was found with each experimental method: $(-\circ-)$ sequential, $(-\cdot*\cdot-)$ simultaneous, and $(\cdots+\cdots)$ free swing. The two active random binary trajectories were each paired with the three passive parameter sets to determine the active parameters. In this way a total of six active parameter sets were determined for each subject. Each graph is labeled with a subject tag.

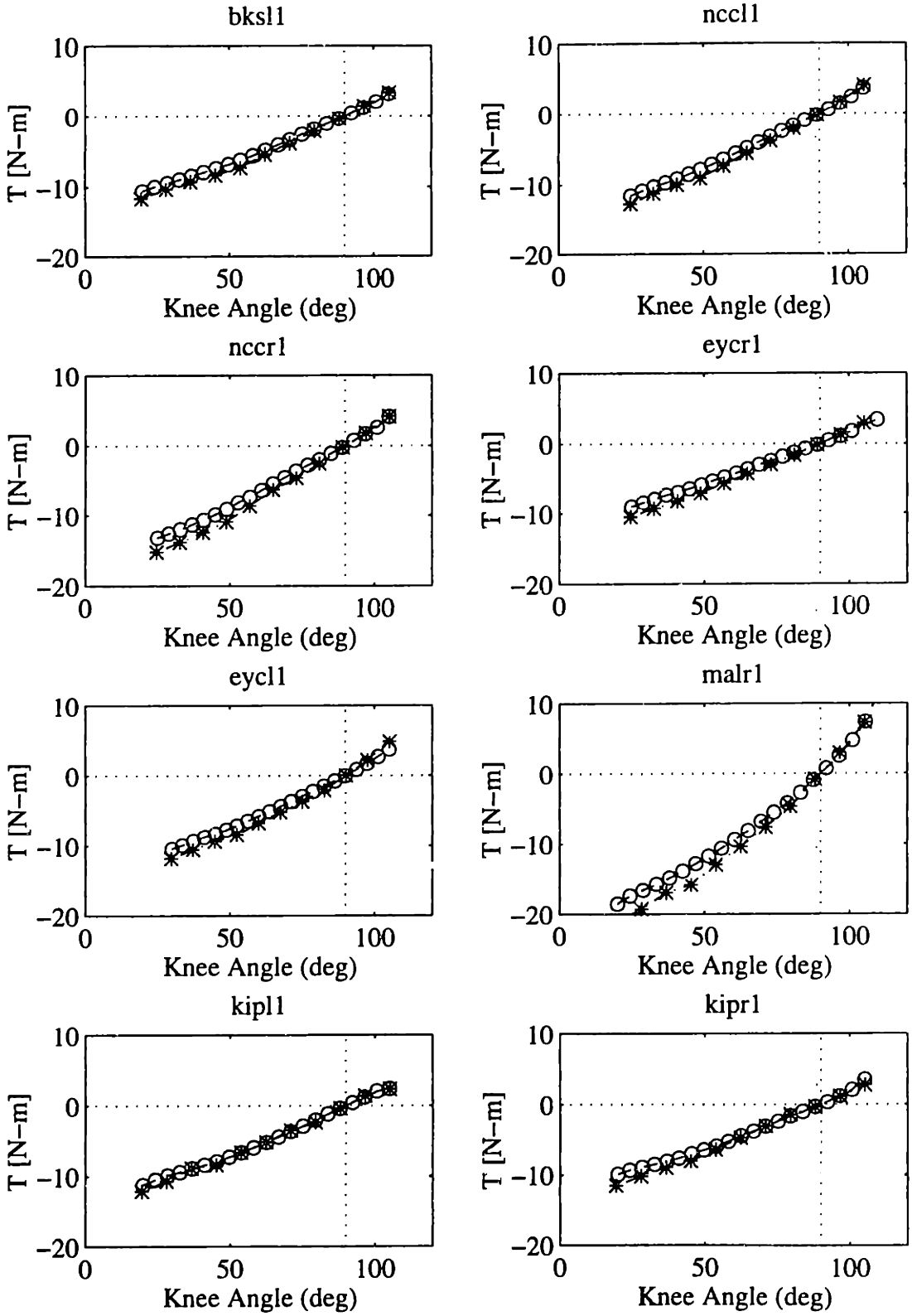

Figure I-1: Passive torque-angle (– o –) sequential and free swing, (– · ∗ · –) simultaneous

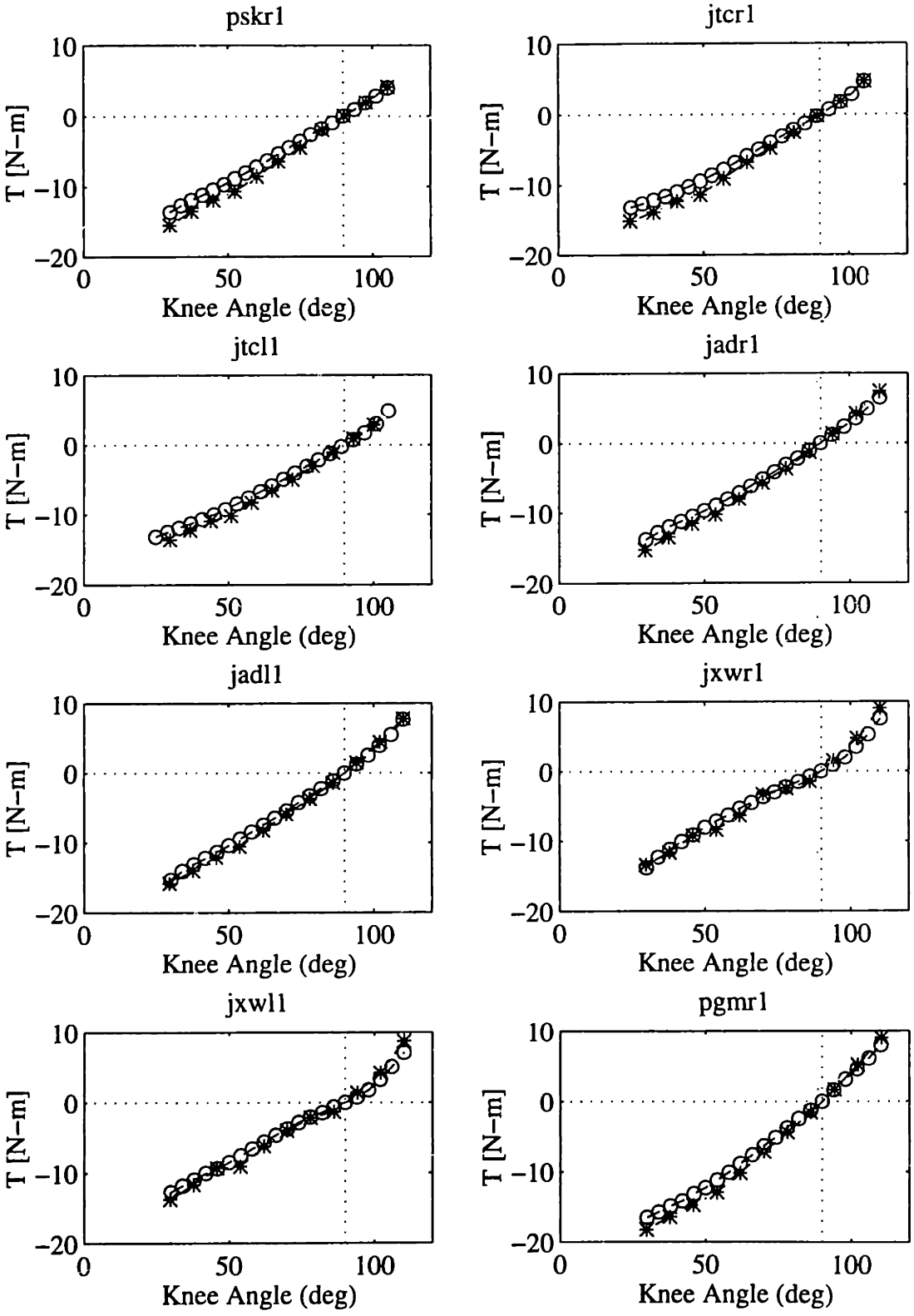

Figure I-1: (continued) Passive torque-angle (−o−) sequential and free swing, (−·∗·−) simultaneous

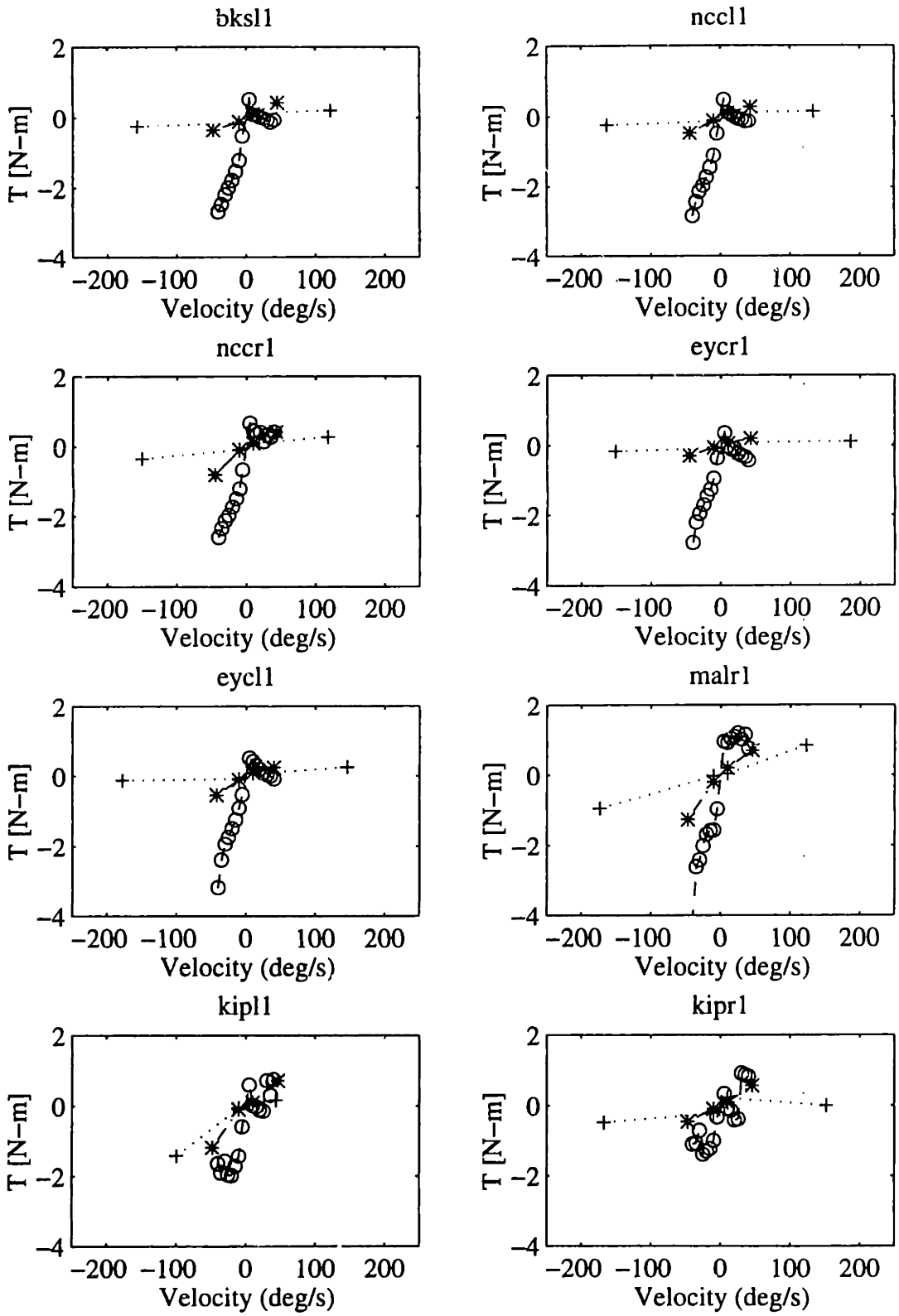

Figure I-2: Passive torque-velocity: (− ∘ −) sequential, (− · ∗ · −) simultaneous, and (· · · + · · ·) free swing

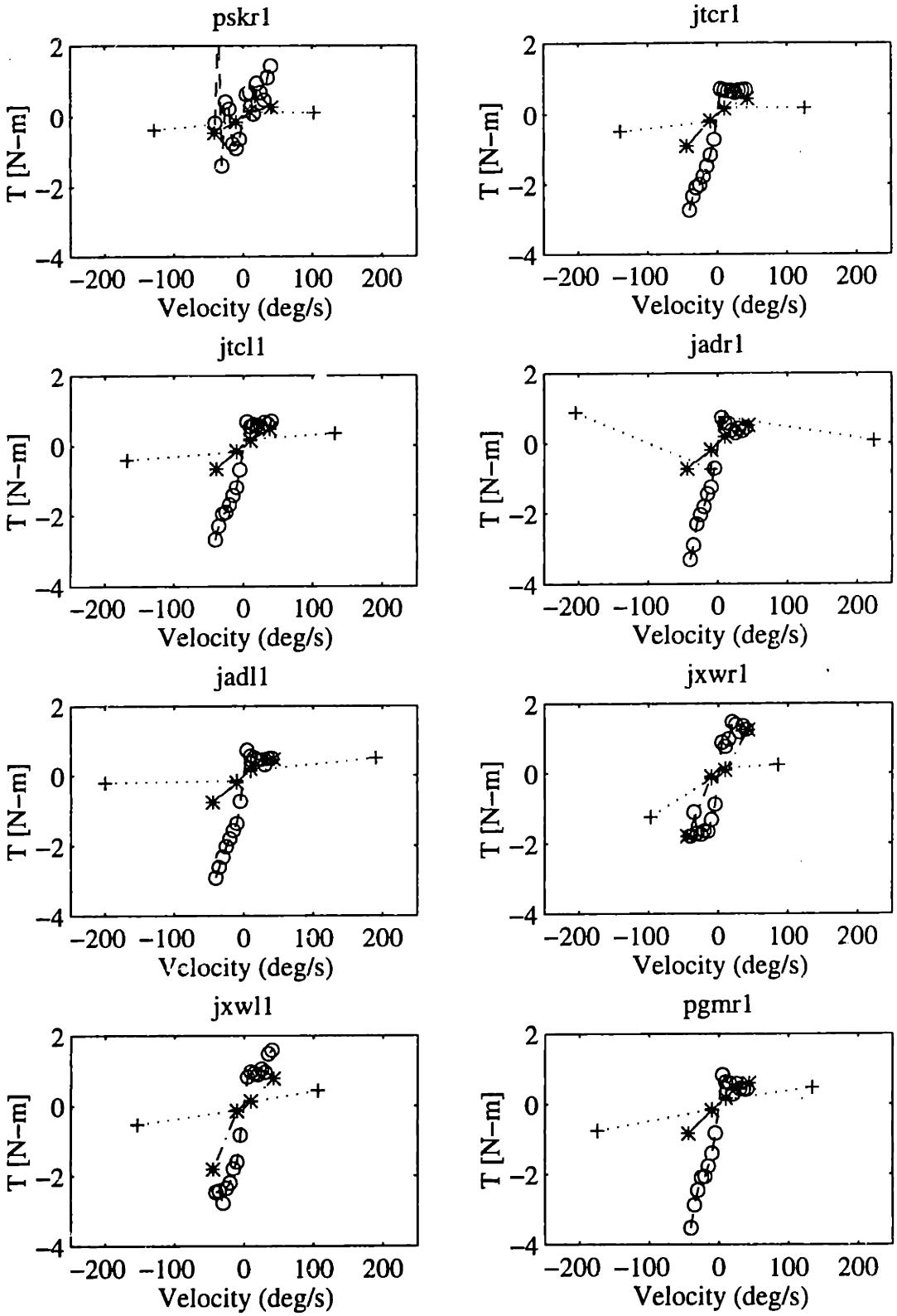

Figure I-2: (continued) Passive torque-velocity (– o –) sequential, (– · ∗ · –) simultaneous, and (· · · + · · ·) free swing

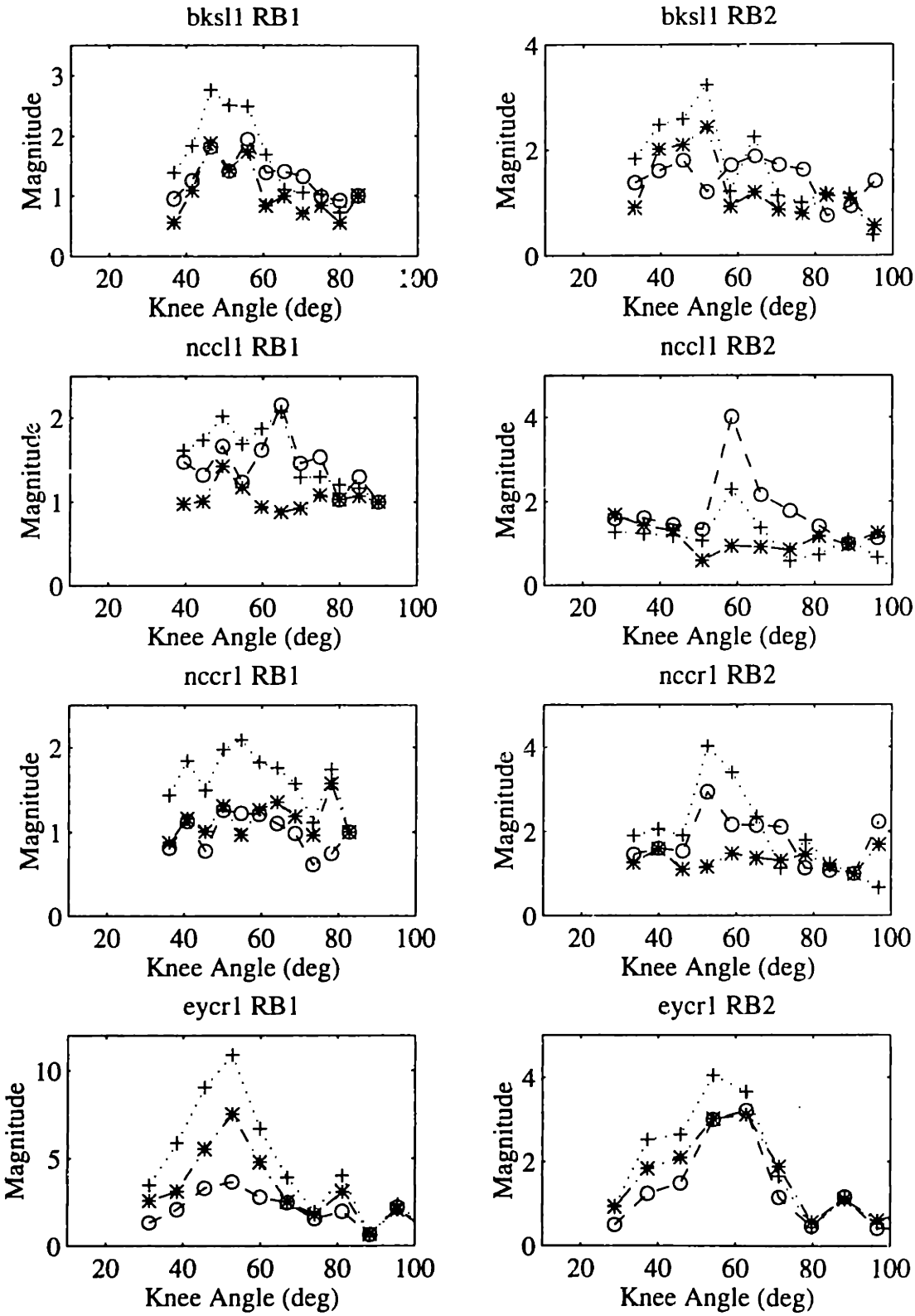

Figure I-3: Active torque-angle curves identified from random binary stimulation 1 (RB1) or 2 (RB2) and $(- \circ -)$ sequential, $(- \cdot * \cdot -)$ simultaneous, or $(\cdots + \cdots)$ free swing passive parameters.

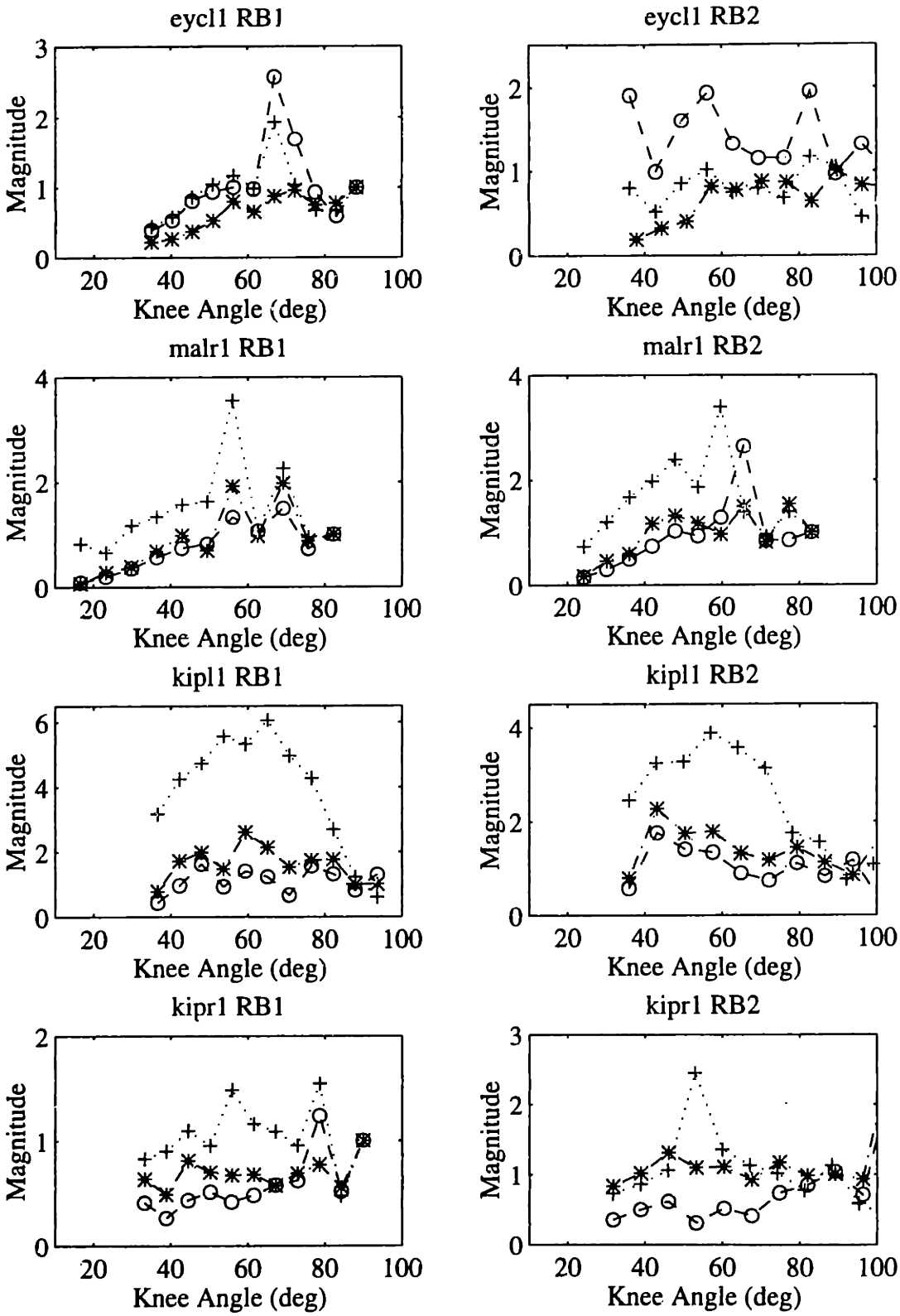

Figure I-3: (continued) Active torque-angle curves identified with $(-\circ-)$ sequential, $(-\cdot*\cdot-)$ simultaneous, and $(\cdots+\cdots)$ free swing parameters

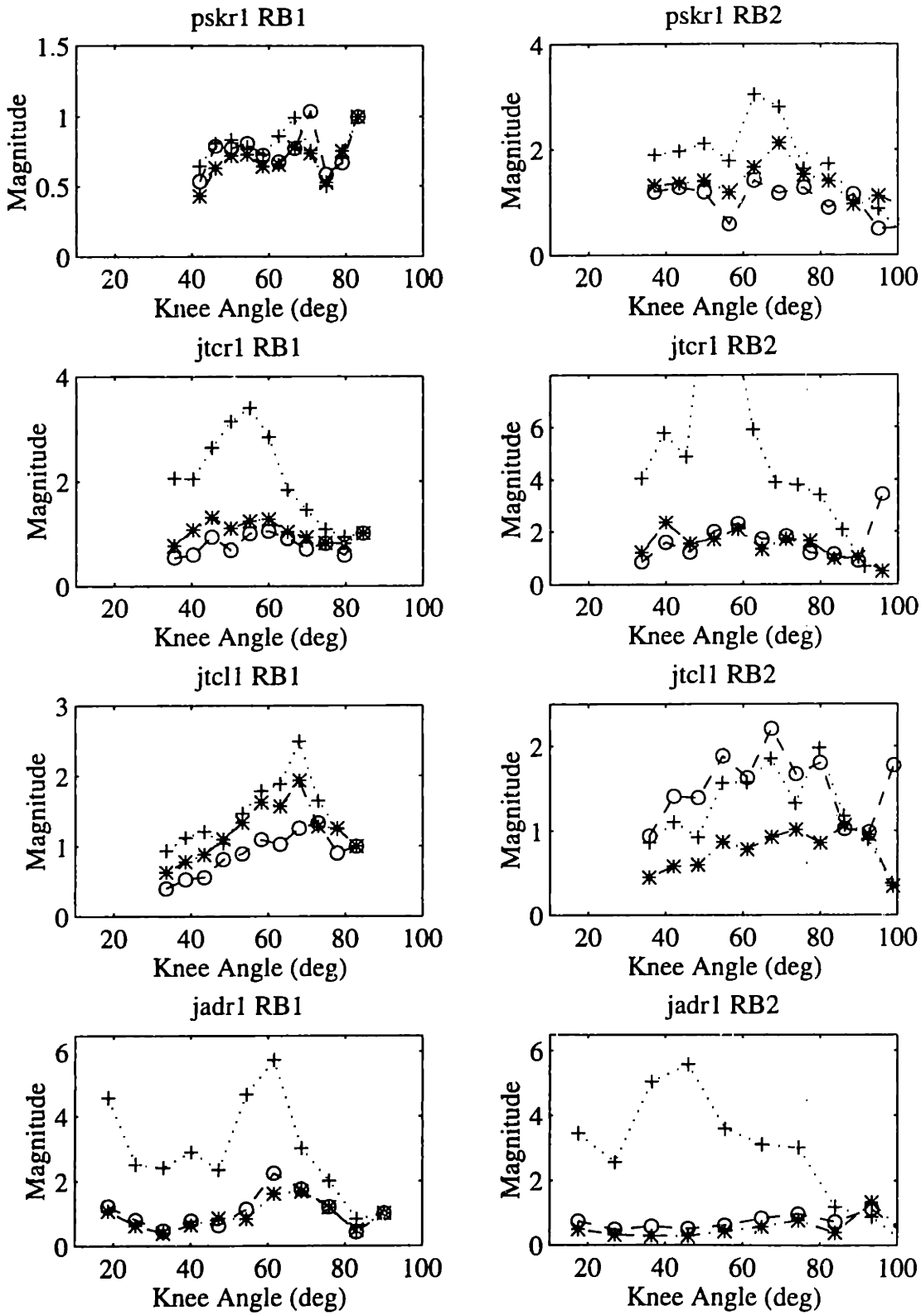

Figure I-3: (continued) Active torque-angle curves identified with $(-\circ-)$ sequential, $(-\cdot*\cdot-)$ simultaneous, and $(\cdots+\cdots)$ free swing parameters

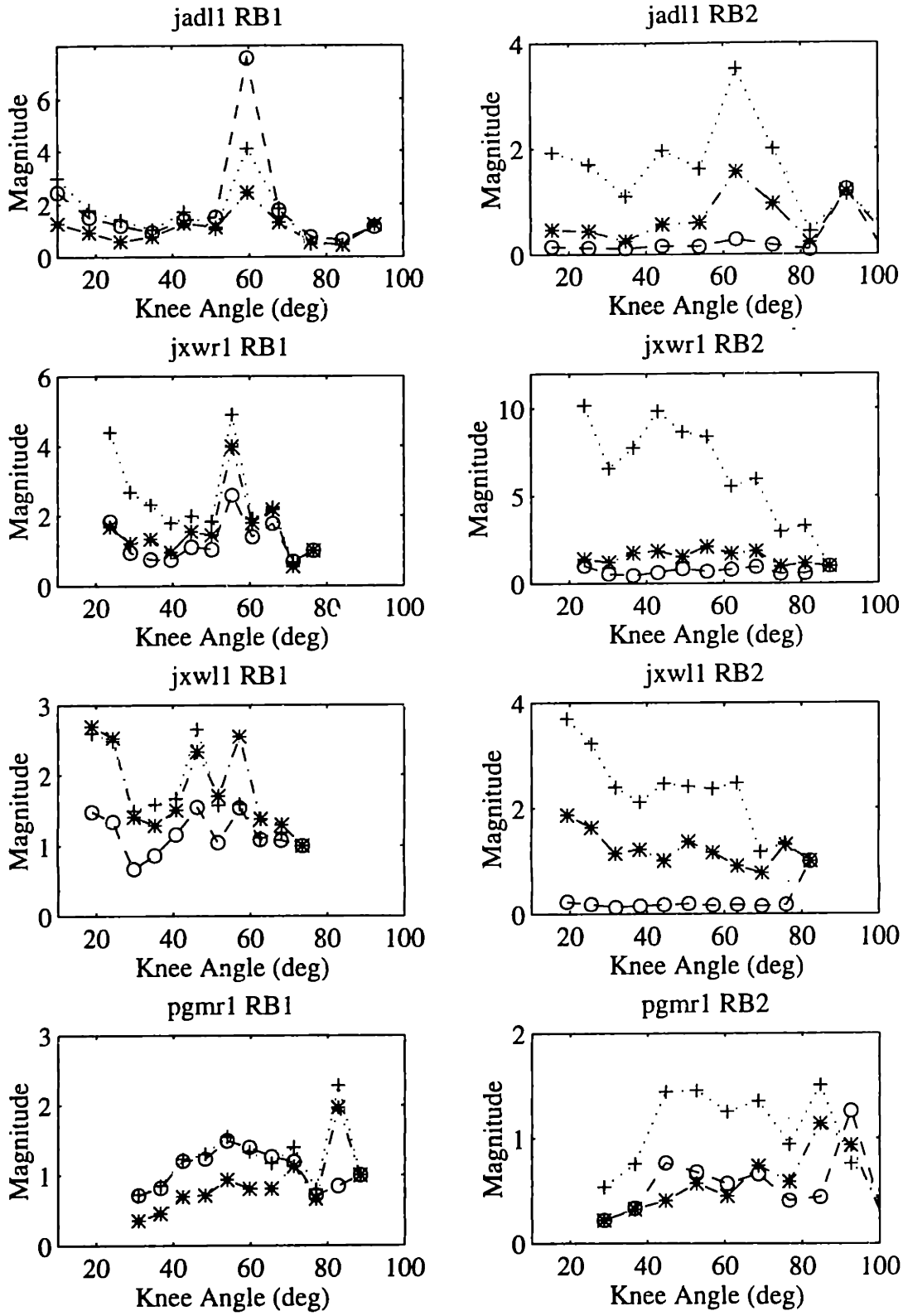

Figure I-3: (continued) Active torque-angle curves identified with $(-\circ-)$ sequential, $(-\cdot*\cdot-)$ simultaneous, and $(\cdots+\cdots)$ free swing parameters

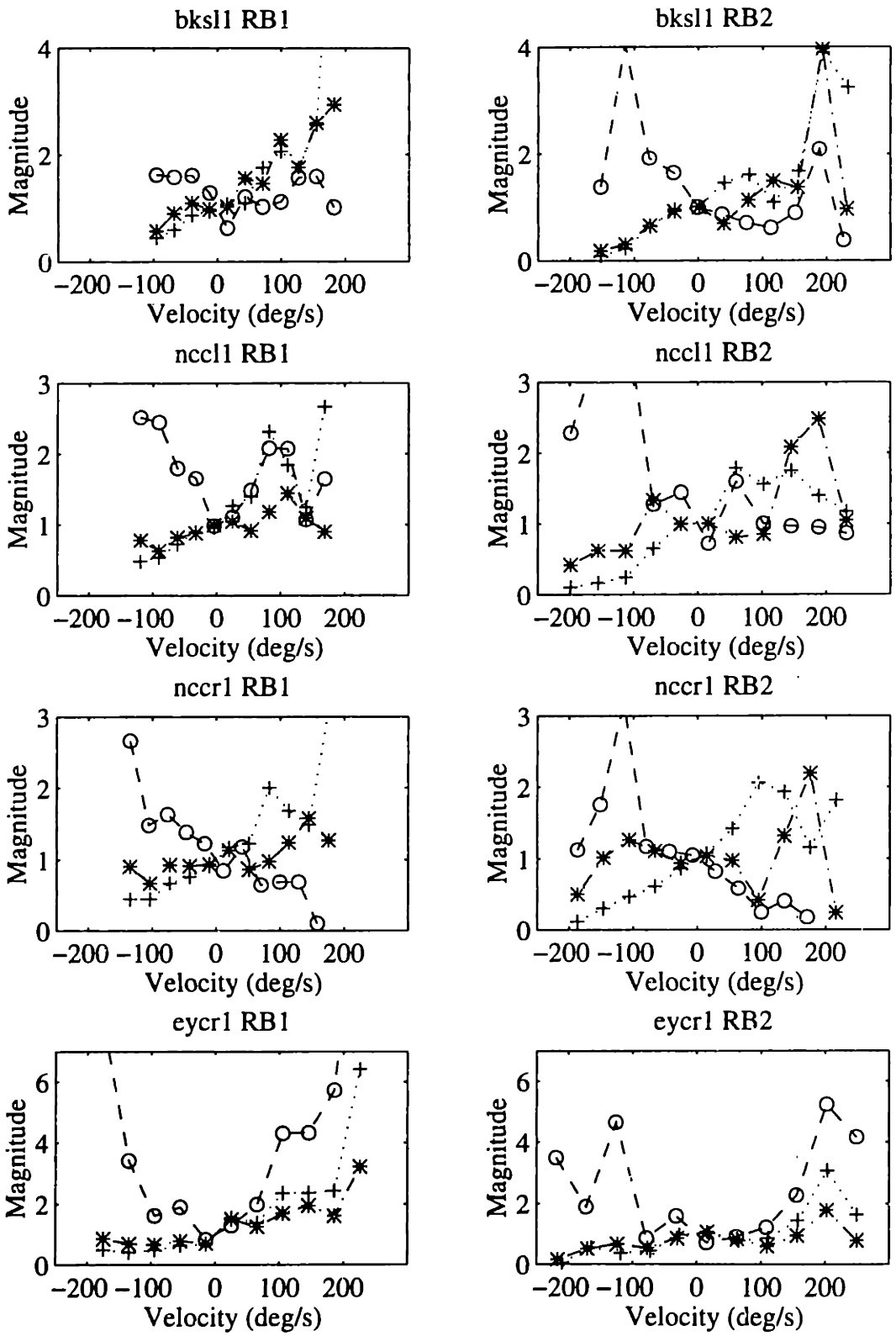

Figure I-4: Active torque-velocity curves identified with (− o −) sequential, (− · ∗ · −) simultaneous, and (· · · + · · ·) free swing parameters

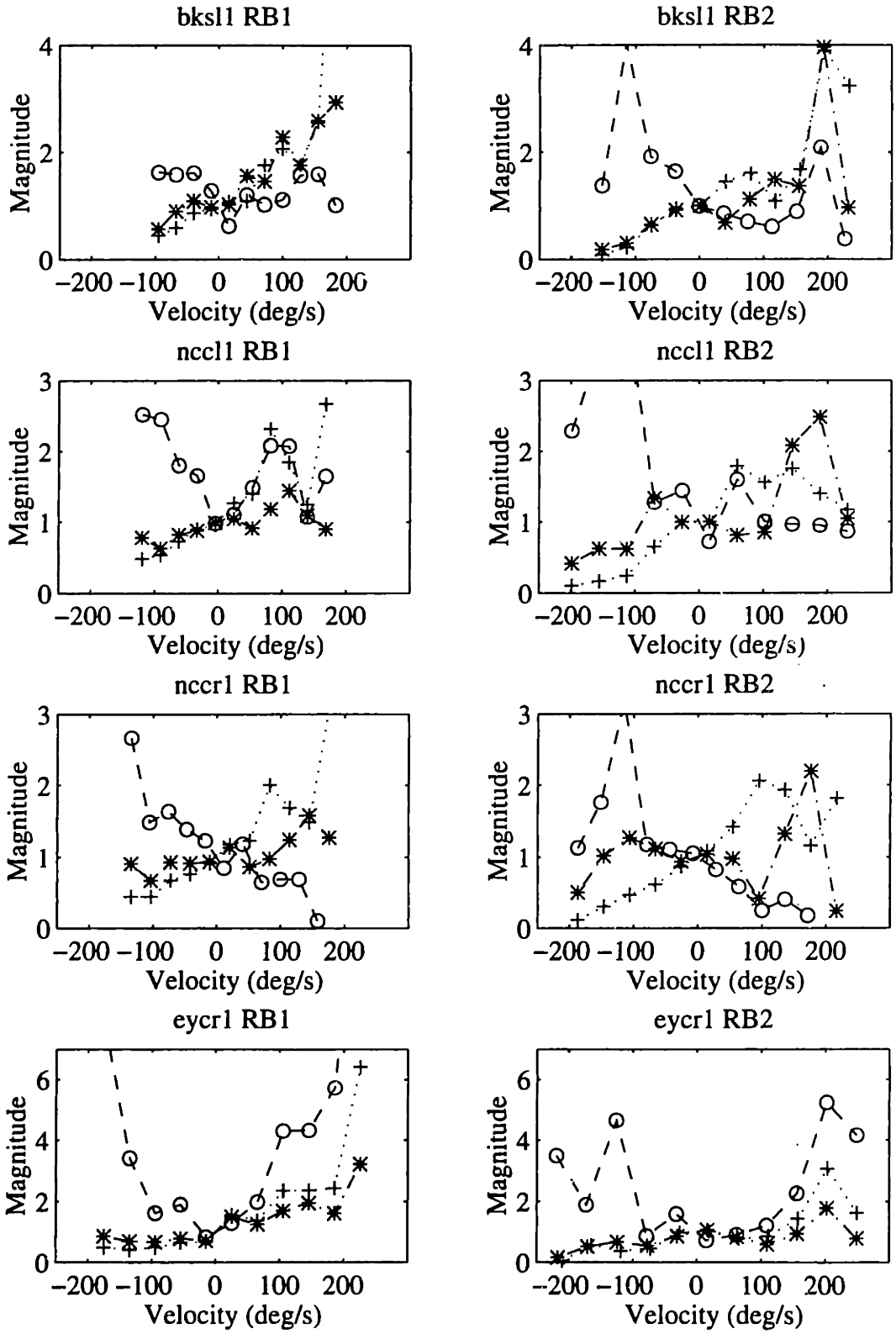

Figure I-4: (continued) Active torque-velocity curves identified with (− o −) sequential, (− · ∗ · −) simultaneous, and (· · · + · · ·) free swing parameters

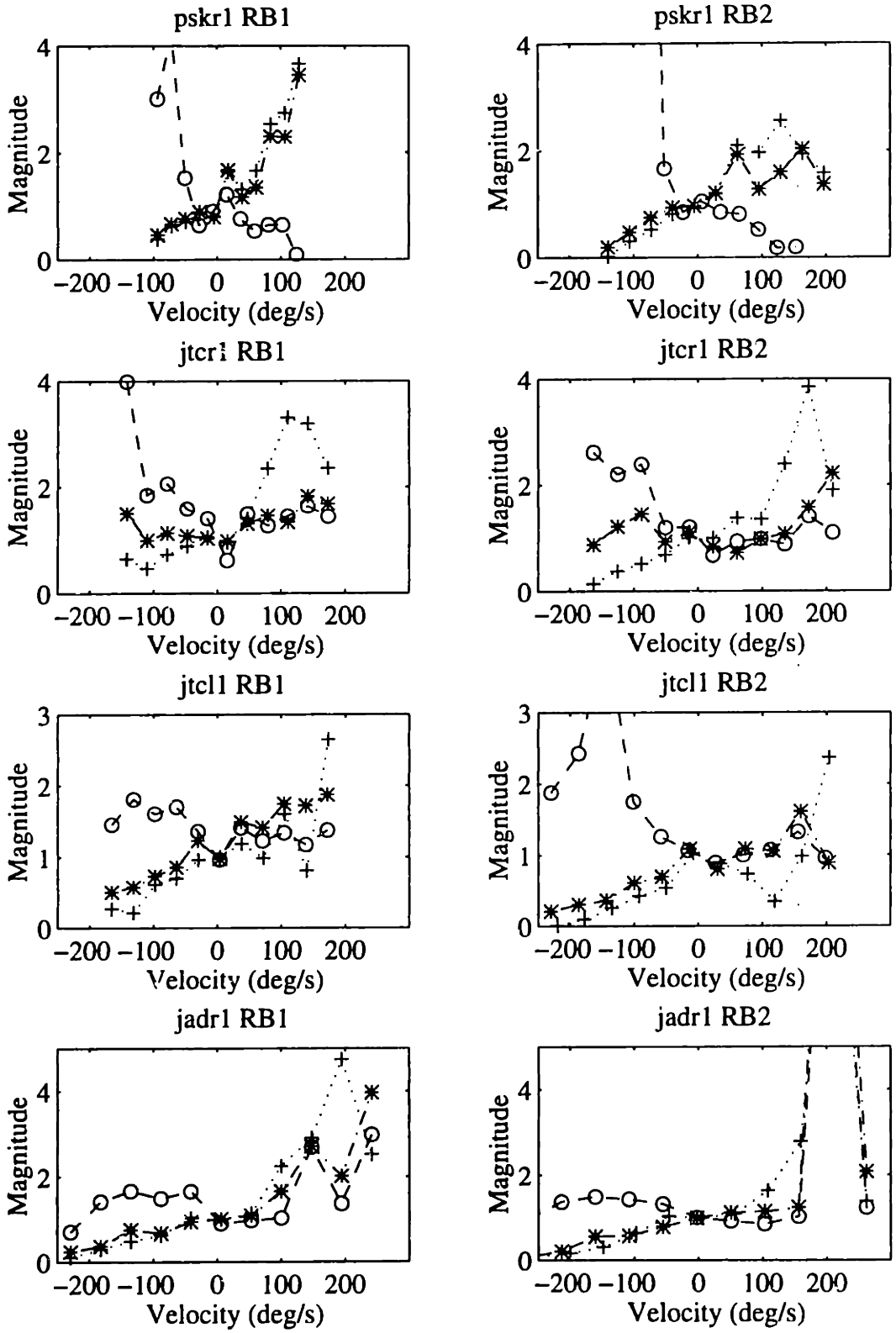

Figure I-4: (continued) Active torque-velocity curves identified with (– ∘ –) sequential, (– · ∗ · –) simultaneous, and (· · · + · · ·) free swing parameters

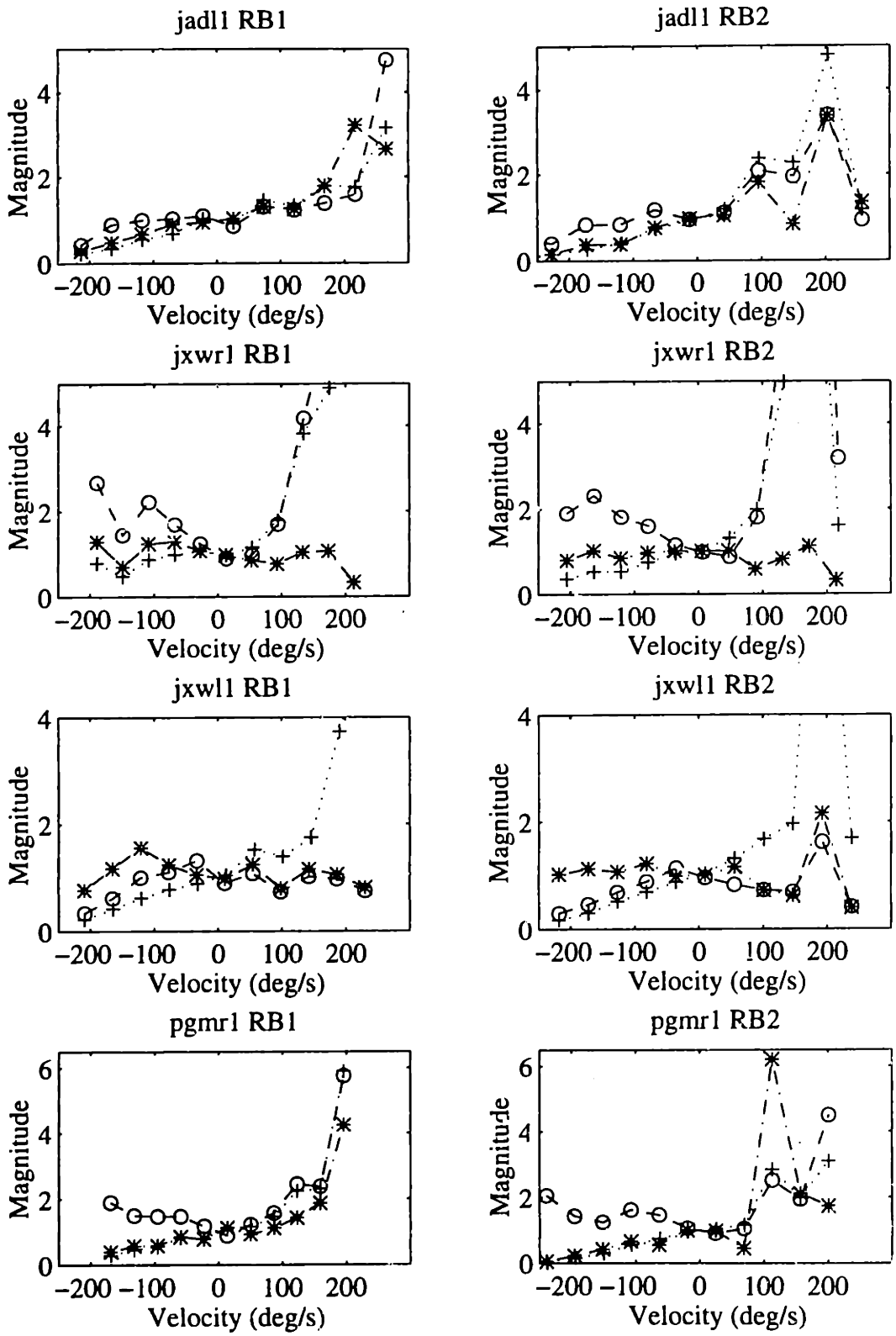

Figure I-4: (continued) Active torque-velocity curves identified with (– o –) sequential, (– · * · –) simultaneous, and (· · · + · · ·) free swing parameters

Appendix J

Knee Angle Prediction: Simulations and Error Calculations

J.1 Comparison of Parameter Sets

The tables in this appendix contain prediction error calculations for each parameter set (sequential, free swing, and simultaneous) for all 16 subjects. The tags RB1 & RB2 refer to the random binary signal used to determine the active parameters, making a total of 6 parameter sets for each subject. The errors for each input (step, ramp, swept-sine, random binary 1, and random binary 2) are shown in separate tables. The RMS error was calculated with the following equation:

$$E_{RMS} = \sqrt{\frac{\sum_1^N (prediction - data)^2}{N}}. \tag{J.1}$$

The average absolute error was calculated by the following equation:

$$E_{ABS} = \frac{\sum_1^N |prediction - data|}{N}. \tag{J.2}$$

Following each table are graphs of the simulations. Each graphs shows the experimentally measure knee angle and predictions with parameter sets derived from the passive sequential, simultaneous or free swing parameters and either RB1 or RB2.

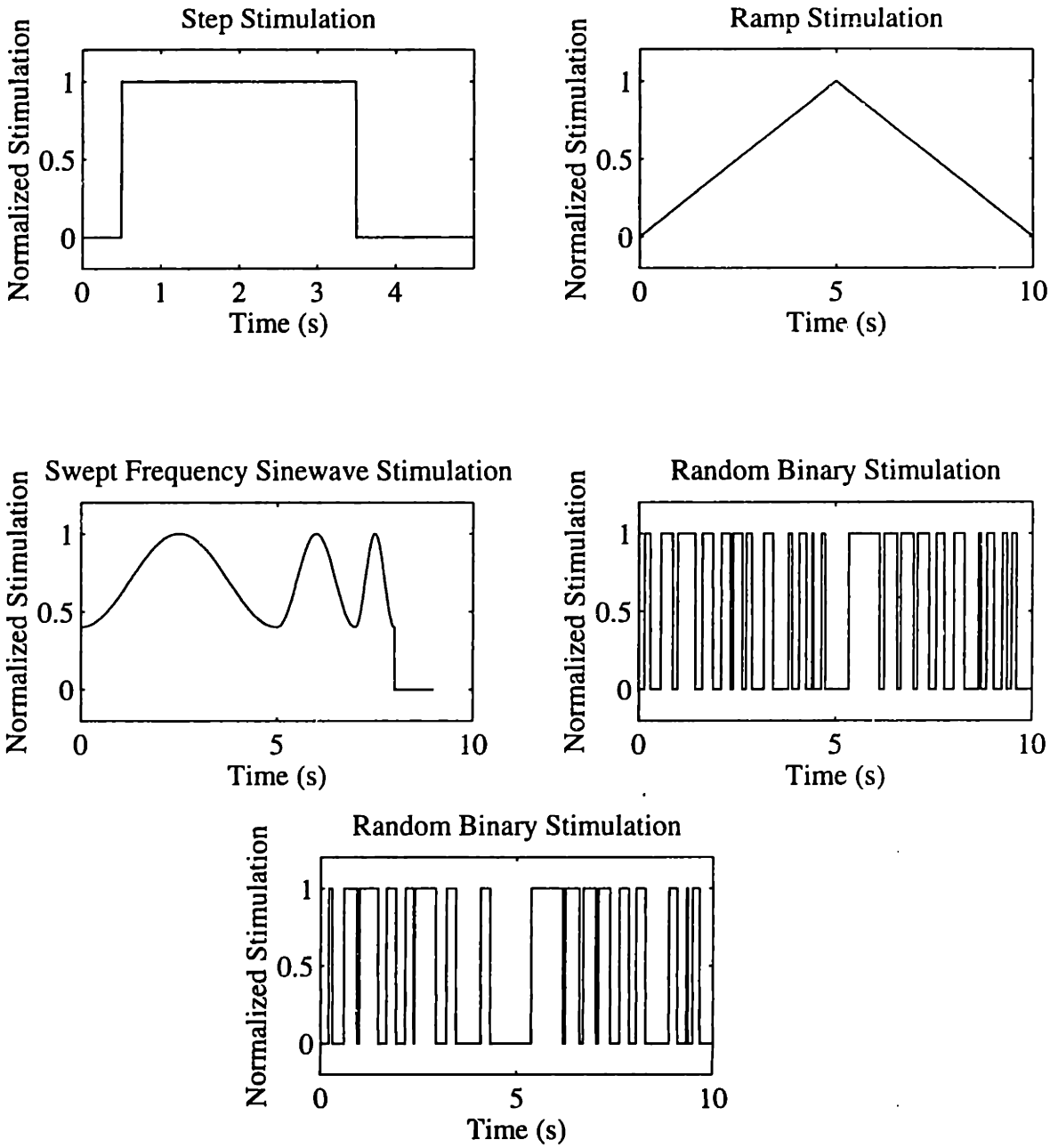

Figure J-1: Stimulation inputs: step, ramp, swept-sinewave, random binary 1, and random binary 2

RMS ERROR for Step Response Prediction

	Parameter Sets					
	Sequential		Free Swing		Simultaneous	
Subject	RB1	RB2	RB1	RB2	RB1	RB2
bksl1	15.358	20.911	6.613	16.336	12.916	20.057
nccl1	7.602	21.579	3.469	3.846	5.752	13.059
nccr1	6.691	17.177	7.242	8.422	3.582	9.276
eycr1	32.542	31.047	12.606	21.969	3.309	16.133
eycl1	10.330	12.667	2.723	2.308	4.822	3.781
malr1	23.536	21.193	7.328	5.872	8.566	8.411
kipl1	7.888	8.551	7.497	5.440	6.492	6.579
kipr1	10.112	12.290	2.971	4.127	8.315	6.644
pskr1	8.182	33.713	7.566	6.826	8.409	5.395
jtcr1	12.128	13.874	7.166	6.573	13.573	15.529
jtcl1	6.746	8.786	3.998	3.052	5.741	4.957
jadr1	14.337	15.509	13.244	13.741	14.790	14.592
jadl1	13.276	13.820	12.091	12.044	11.998	12.032
jxwr1	10.159	9.680	8.678	6.760	8.080	6.344
jxwl1	6.255	5.987	6.809	6.262	5.365	6.248
pgmr1	6.568	8.080	3.804	5.020	6.404	5.801

AVERAGE ABSOLUTE ERROR for Step Response Prediction

	Parameter Sets					
	Sequential		Free Swing		Simultaneous	
Subject	RB1	RB2	RB1	RB2	RB1	RB2
bksl1	11.894	16.362	5.351	12.883	10.226	15.930
nccl1	5.241	17.214	2.708	2.853	4.622	9.710
nccr1	5.710	12.633	6.222	7.213	2.807	7.282
eycr1	23.863	25.107	9.947	18.735	2.695	13.510
eycl1	5.567	7.956	2.220	1.647	4.106	3.042
malr1	14.955	13.416	6.147	4.852	7.264	7.089
kipl1	5.402	6.442	5.557	3.692	4.745	4.972
kipr1	8.195	9.949	2.547	3.250	6.869	5.203
pskr1	6.229	22.628	6.684	5.967	7.497	4.463
jtcr1	9.514	10.938	5.489	5.362	10.727	10.764
jtcl1	4.890	6.407	3.375	2.566	4.871	3.920
jadr1	11.607	12.879	10.418	7.599	12.041	12.097
jadl1	9.469	9.743	7.962	8.127	8.338	9.018
jxwr1	7.715	7.408	6.596	4.600	5.849	3.829
jxwl1	4.699	4.843	5.822	5.242	3.810	5.311
pgmr1	4.831	6.111	3.124	3.975	5.240	4.003

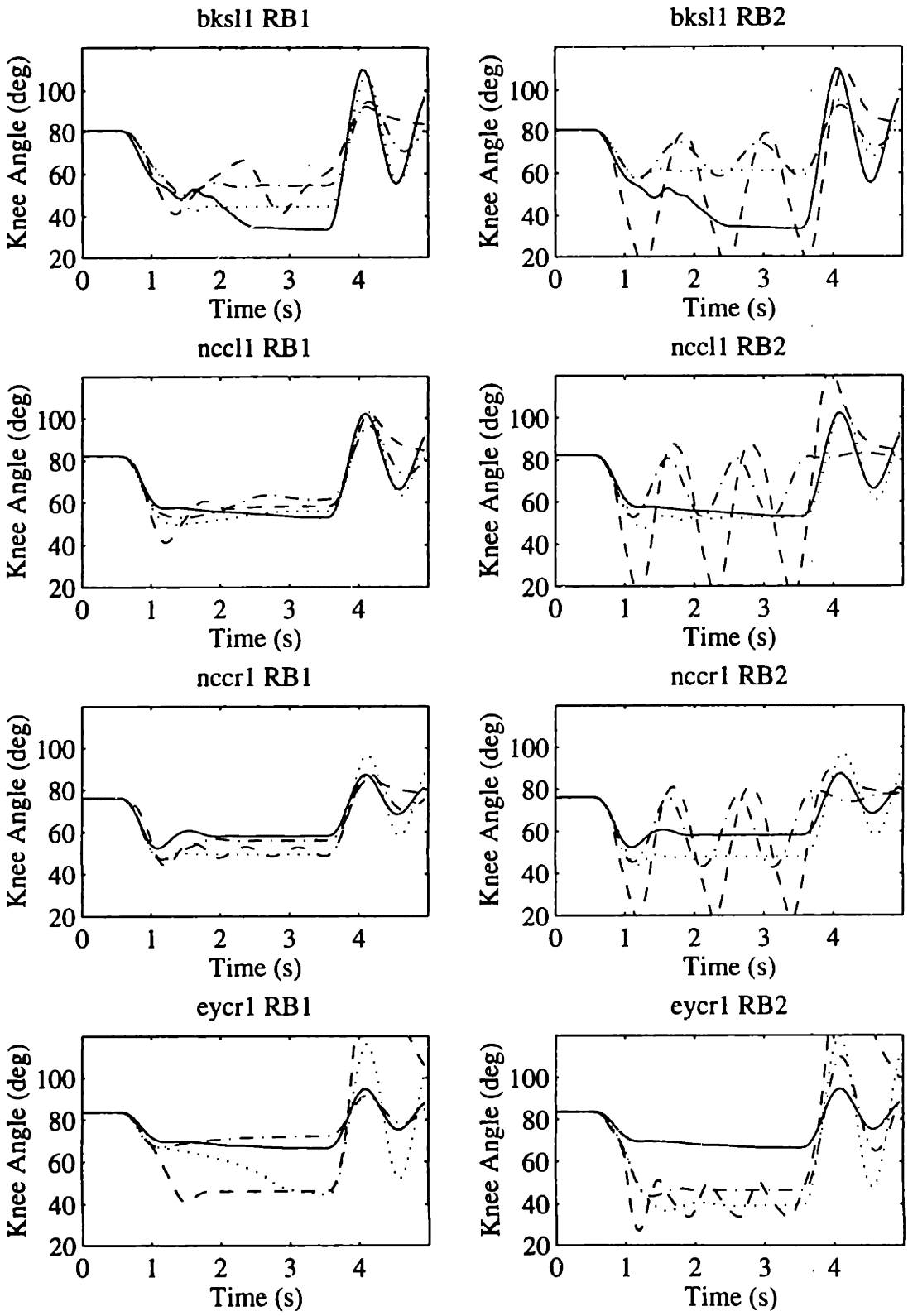

Figure J-2: Step response:(−) Experimental knee angle and predictions with (−−) sequential, (− · −) simultaneous, and (· · ·) free swing parameters.

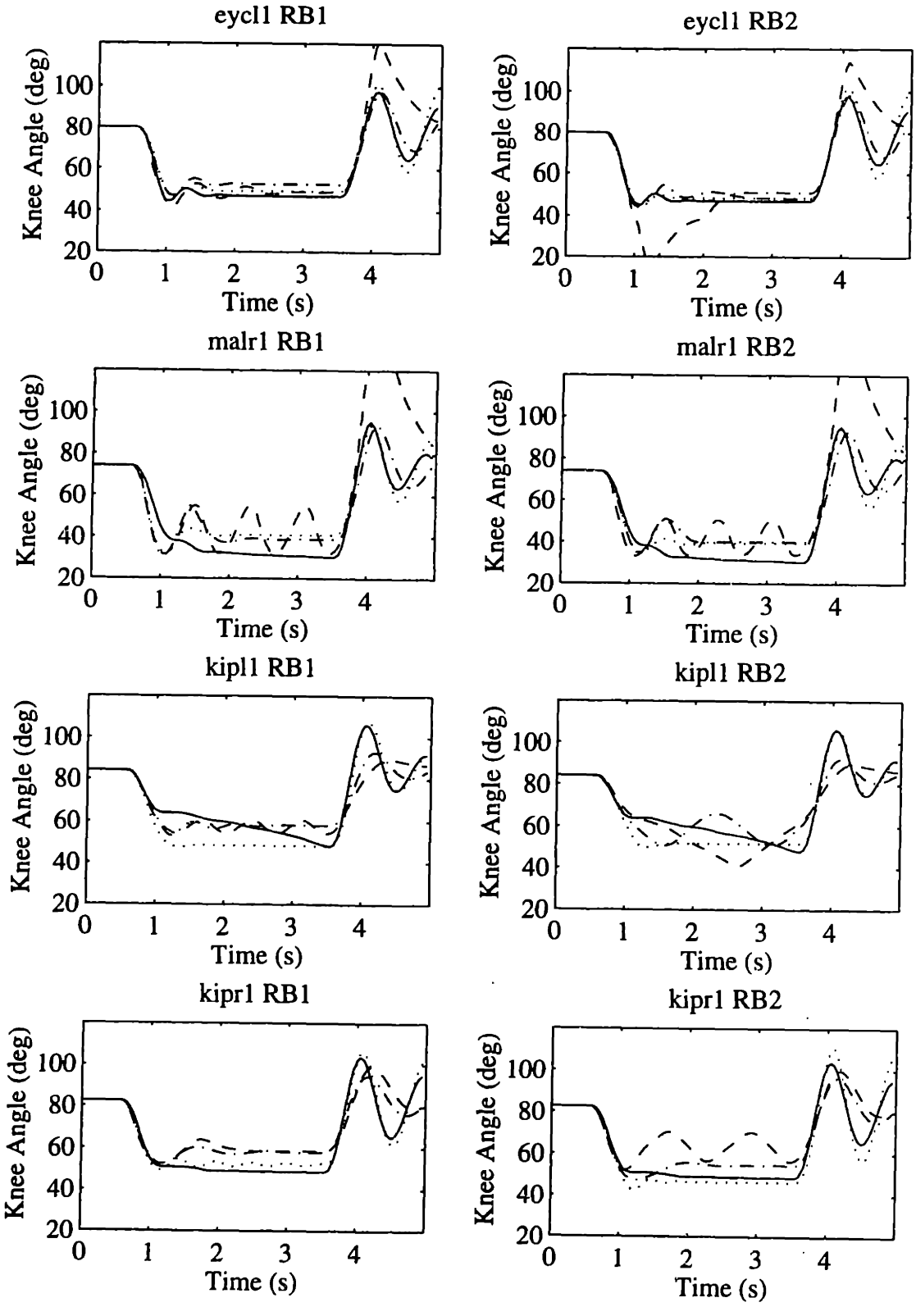

Figure J-2: (continued) Step response:(−) Experimental knee angle and predictions with (−−) sequential, (− · −) simultaneous, and (· · ·) free swing parameters.

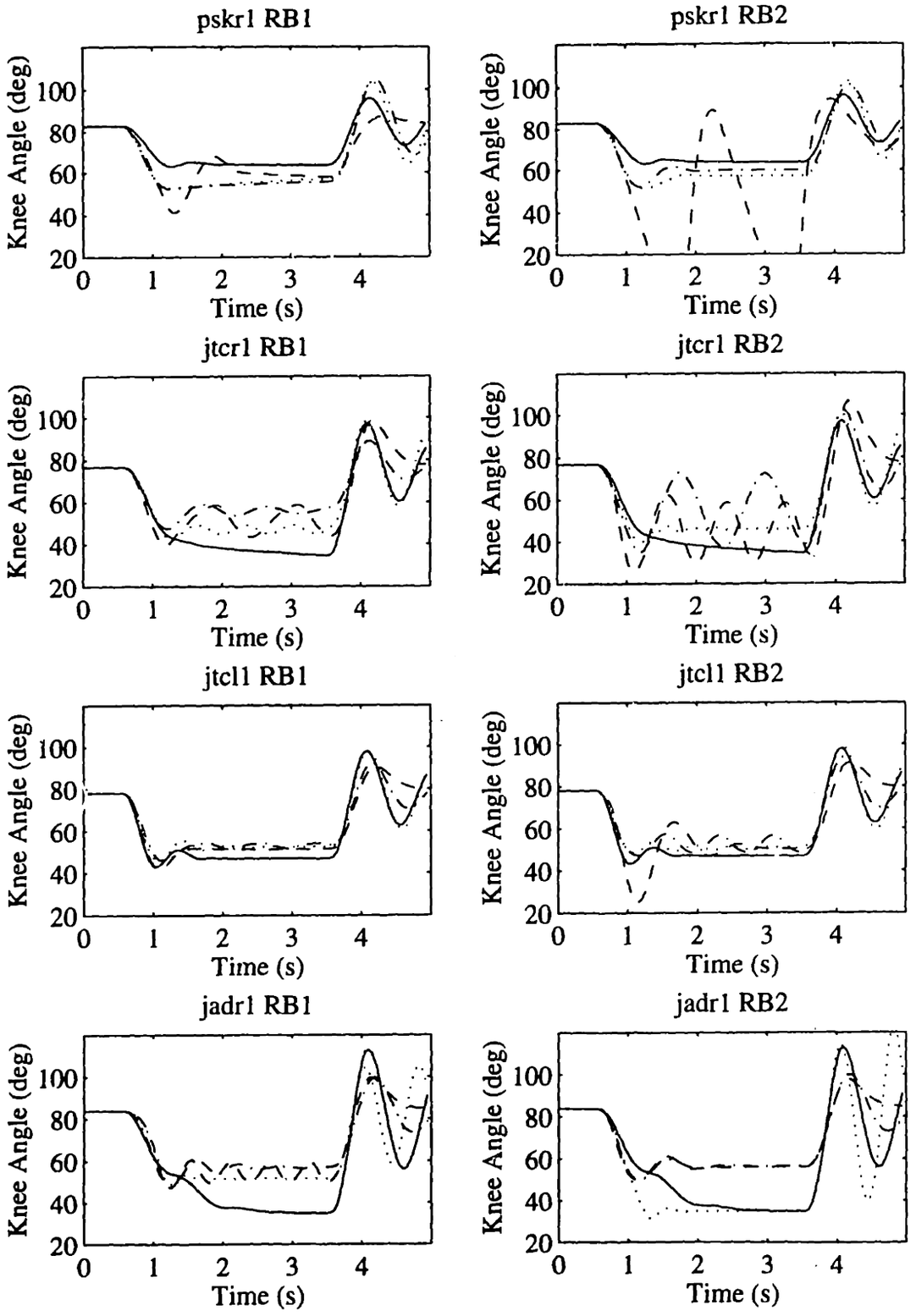

Figure J-2: (continued) Step response:(−) Experimental knee angle and predictions with (−−) sequential, (− · −) simultaneous, and (· · ·) free swing parameters.

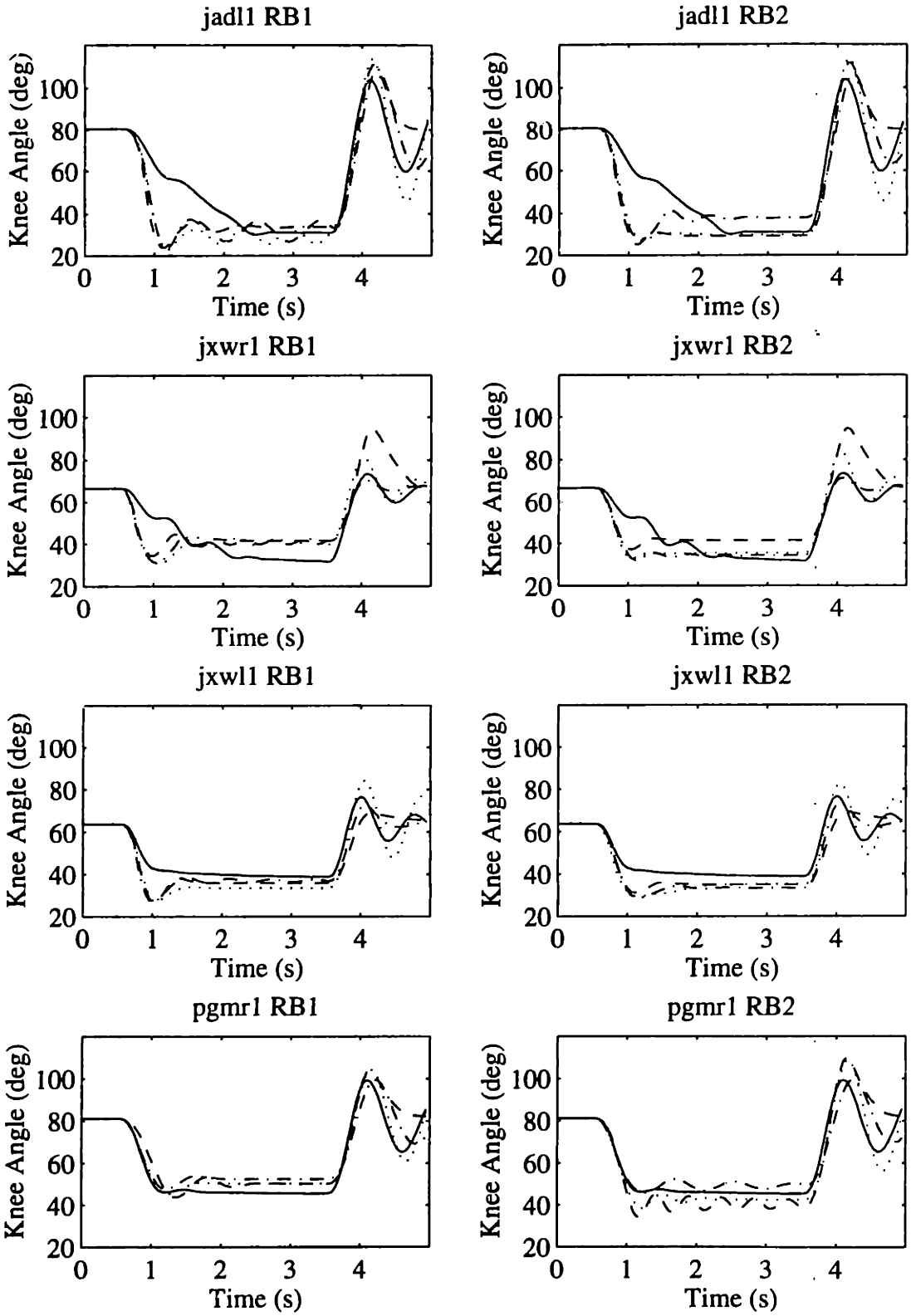

Figure J-2: (continued) Step response:(−) Experimental knee angle and predictions with (−−) sequential, (− · −) simultaneous, and (· · ·) free swing parameters.

RMS ERROR for Ramp Response Prediction

	Parameter Sets					
	Sequential		Free Swing		Simultaneous	
Subject	RB1	RB2	RB1	RB2	RB1	RB2
bksl1	10.427	12.758	9.726	9.886	9.832	10.644
nccl1	5.110	8.349	4.388	6.298	5.651	9.048
nccr1	4.675	3.661	3.697	5.738	1.836	3.630
eycr1	9.535	10.925	5.339	8.205	2.724	9.325
eycl1	5.594	12.244	5.148	4.809	5.195	5.920
malr1	6.997	8.041	6.781	7.649	7.496	7.606
kipl1	10.692	11.054	10.541	12.065	11.604	12.639
kipr1	4.593	6.145	3.713	5.009	5.570	7.342
pskr1	5.269	6.217	4.306	5.408	4.232	4.167
jtcr1	8.559	8.596	5.693	4.406	8.396	10.144
jtcl1	3.882	3.481	5.058	5.541	4.687	4.788
jadr1	8.733	8.187	7.058	6.662	9.267	9.467
jadl1	11.099	9.713	11.301	9.237	9.354	9.760
jxwr1	7.575	6.959	7.843	7.797	8.091	7.915
jxwl1	5.099	3.832	5.318	4.142	5.338	4.258
pgmr1	4.399	5.794	3.180	4.792	4.437	4.472

AVERAGE ABSOLUTE ERROR for Ramp Response Prediction

	Parameter Sets					
	Sequential		Free Swing		Simultaneous	
Subject	RB1	RB2	RB1	RB2	RB1	RB2
bksl1	5.364	6.670	5.377	5.559	5.449	5.538
nccl1	3.181	4.907	3.012	4.111	3.628	4.639
nccr1	2.373	2.047	1.971	2.968	1.111	2.029
eycr1	3.247	4.991	3.552	4.336	1.894	4.712
eycl1	3.374	5.942	3.386	2.797	3.306	3.243
malr1	4.056	4.342	3.985	3.698	4.069	3.952
kipl1	5.038	5.349	4.922	5.574	5.463	5.645
kipr1	2.435	3.105	2.052	2.920	2.442	3.353
pskr1	2.602	2.712	2.363	3.346	2.377	2.361
jtcr1	4.722	4.751	3.028	2.657	4.520	5.208
jtcl1	2.015	2.055	2.838	3.361	2.687	3.019
jadr1	4.680	4.814	3.893	3.720	5.414	5.699
jadl1	5.950	4.731	6.379	4.404	4.442	5.442
jxwr1	5.170	4.557	5.705	5.441	5.833	5.487
jxwl1	2.929	2.294	3.346	2.669	3.544	2.624
pgmr1	2.815	3.086	2.104	3.064	2.748	3.275

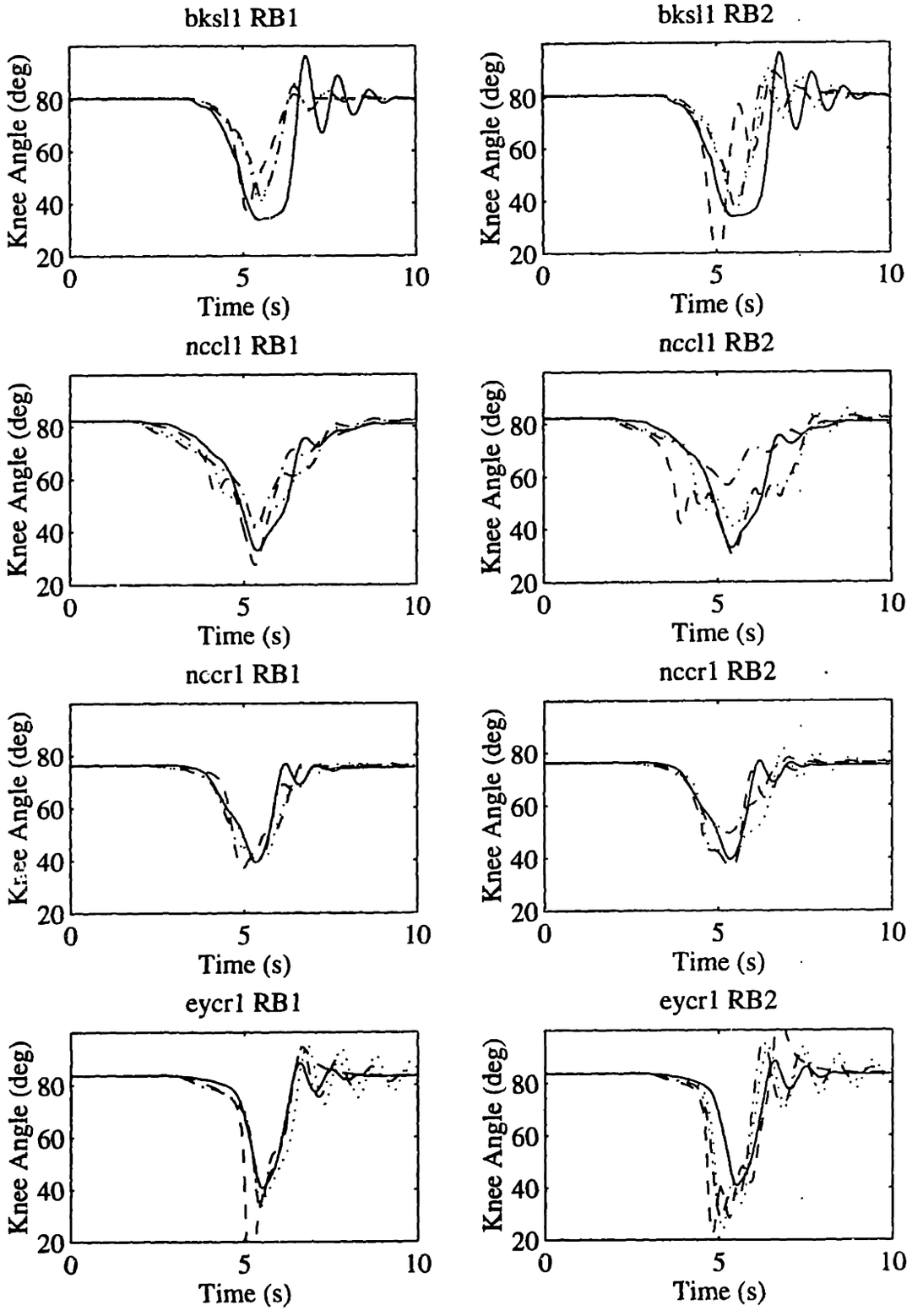

Figure J-3: Ramp response:(−) Experimental knee angle and predictions with (−−) sequential, (− · −) simultaneous, and (· · ·) free swing parameters.

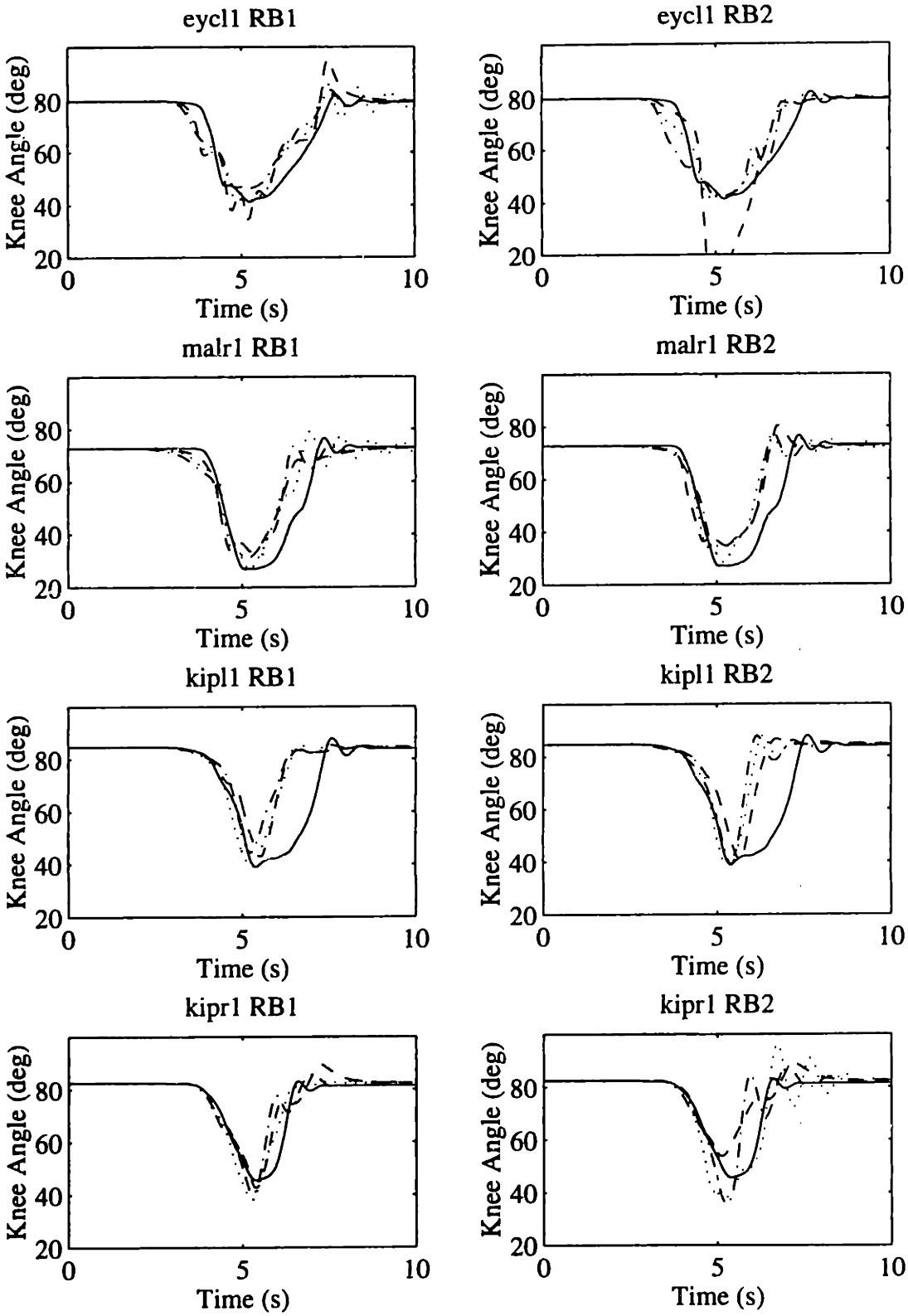

Figure J-3: (continued) Ramp response:(−) Experimental knee angle and predictions with (−−) sequential, (− · −) simultaneous, and (· · ·) free swing parameters.

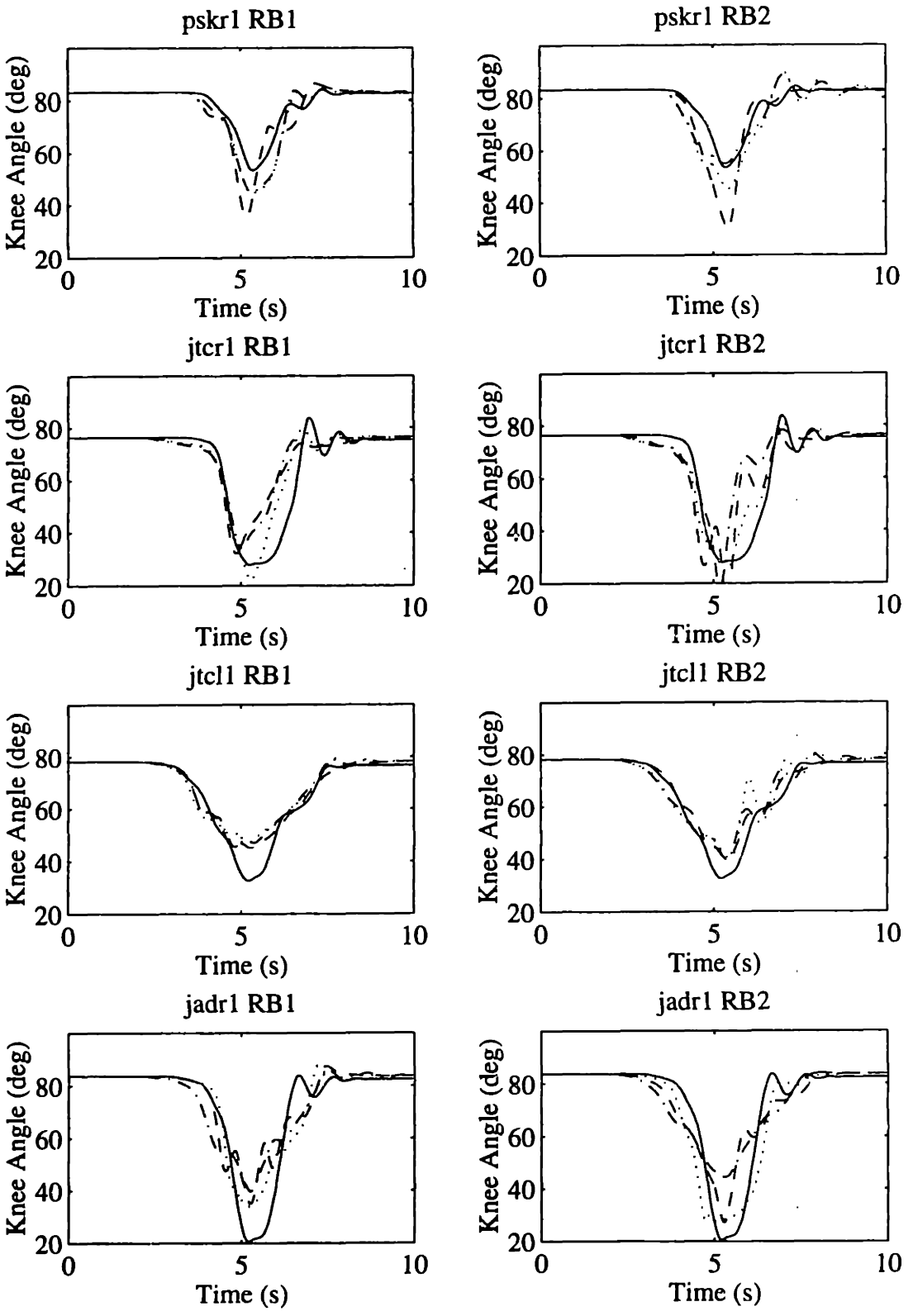

Figure J-3: (continued) Ramp response:(−) Experimental knee angle and predictions with (− −) sequential, (− · −) simultaneous, and (· · ·) free swing parameters.

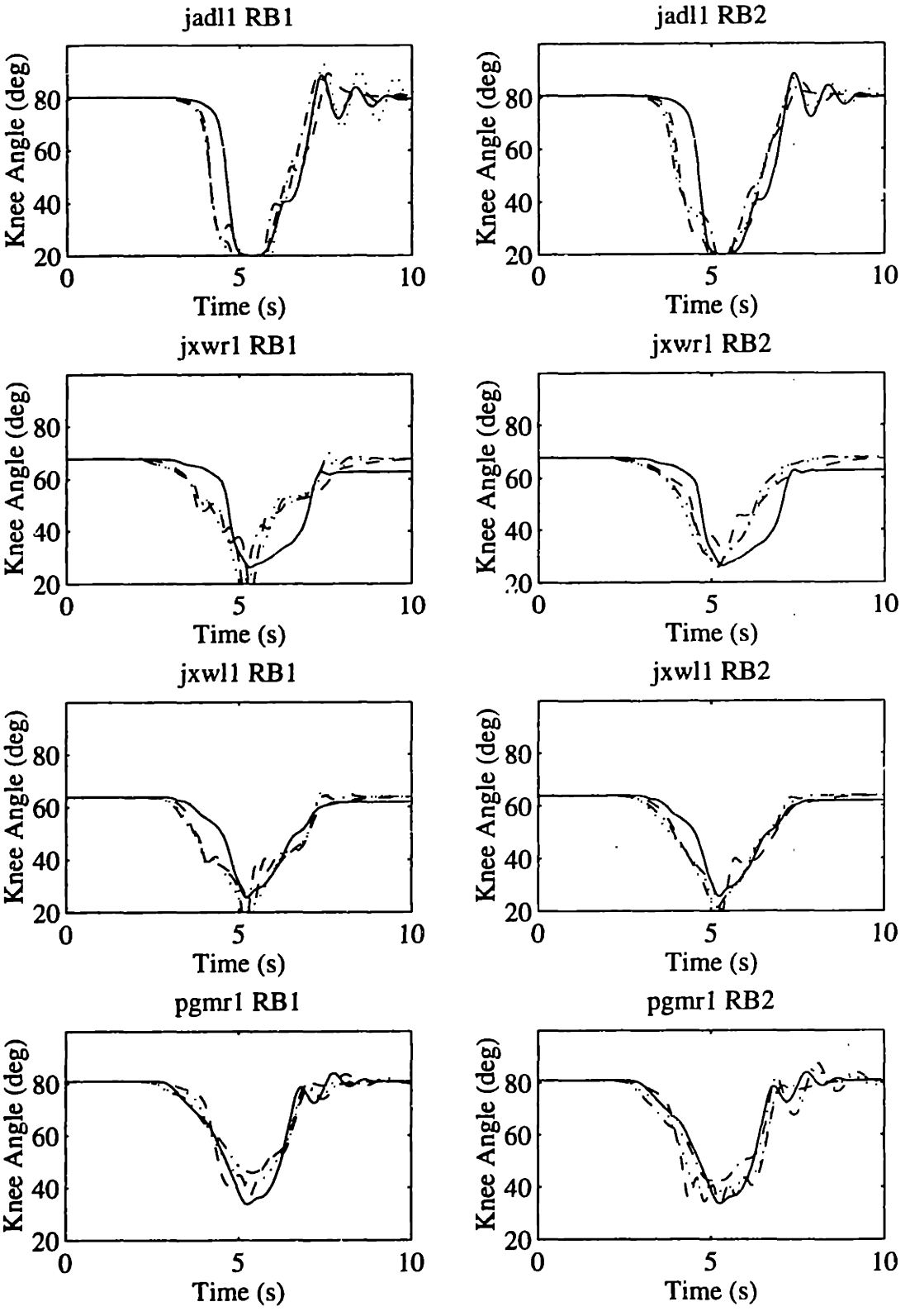

Figure J-3: (continued) Ramp response:(−) Experimental knee angle and predictions with (−−) sequential, (− · −) simultaneous, and (···) free swing parameters.

RMS ERROR for Swept-sine Response Prediction

	Parameter Sets					
	Sequential		Free Swing		Simultaneous	
Subject	RB1	RB2	RB1	RB2	RB1	RB2
bksl1	13.921	20.058	11.785	12.247	13.062	13.463
nccl1	11.600	22.076	9.066	9.730	7.727	12.637
nccr1	10.787	15.770	6.227	8.792	4.964	8.201
eycr1	30.357	32.396	6.548	11.728	6.566	13.704
eycl1	10.546	23.748	5.248	8.818	5.676	6.376
malr1	18.966	17.631	7.285	7.945	9.539	8.830
kipl1	14.621	15.516	14.255	16.441	16.321	16.819
kipr1	10.049	12.486	6.915	5.707	9.844	10.288
pskr1	9.706	21.567	6.886	8.960	7.295	9.003
jtcr1	16.616	14.430	7.314	6.800	11.222	12.724
jtcl1	9.269	9.688	6.499	6.146	8.266	7.456
jadr1	14.936	11.508	11.096	9.588	13.747	13.031
jadl1	14.955	11.950	12.921	10.079	10.592	10.788
jxwr1	8.682	6.868	7.202	7.101	7.851	6.005
jxwl1	6.701	5.581	6.845	5.707	6.831	5.268
pgmr1	10.584	11.657	5.998	8.230	8.877	10.003

AVERAGE ABSOLUTE ERROR for Swept-Sine Response Prediction

	Parameter Sets					
	Sequential		Free Swing		Simultaneous	
Subject	RB1	RB2	RB1	RB2	RB1	RB2
bksl1	9.785	14.618	8.986	8.984	10.029	10.117
nccl1	8.957	16.465	7.162	7.008	5.994	9.075
nccr1	7.744	11.132	4.744	6.409	3.983	6.195
eycr1	17.234	18.647	4.884	7.529	4.810	9.794
eycl1	6.655	16.848	3.937	6.961	4.500	4.726
malr1	12.034	10.786	5.124	5.179	7.270	6.454
kipl1	11.288	11.822	10.121	11.612	12.513	12.126
kipr1	7.408	8.528	4.502	4.575	6.716	6.569
pskr1	7.486	13.370	5.721	7.658	5.972	7.558
jtcr1	12.158	11.472	5.920	5.503	8.792	9.341
jtcl1	6.737	6.404	5.094	4.724	6.275	5.418
jadr1	11.529	9.049	8.423	7.043	11.161	10.601
jadl1	10.938	7.722	9.088	6.592	7.452	7.185
jxwr1	6.858	4.788	5.885	5.384	6.305	4.645
jxwl1	5.118	4.257	5.474	4.856	5.318	4.206
pgmr1	7.827	8.162	4.661	6.087	6.573	6.997

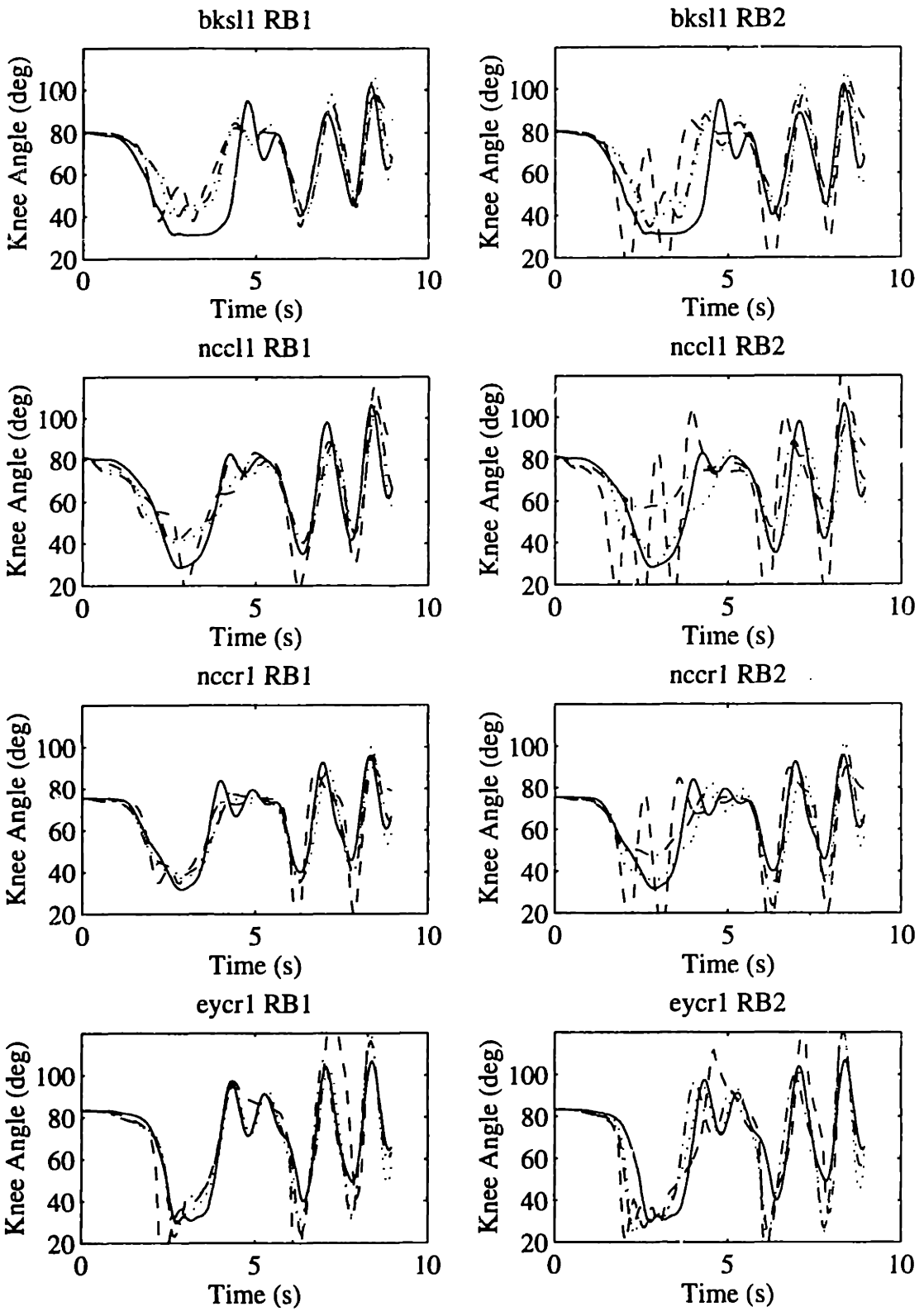

Figure J-4: Swept-sine response:(−) Experimental knee angle and predictions with (−−) sequential, (− · −) simultaneous, and (· · ·) free swing parameters.

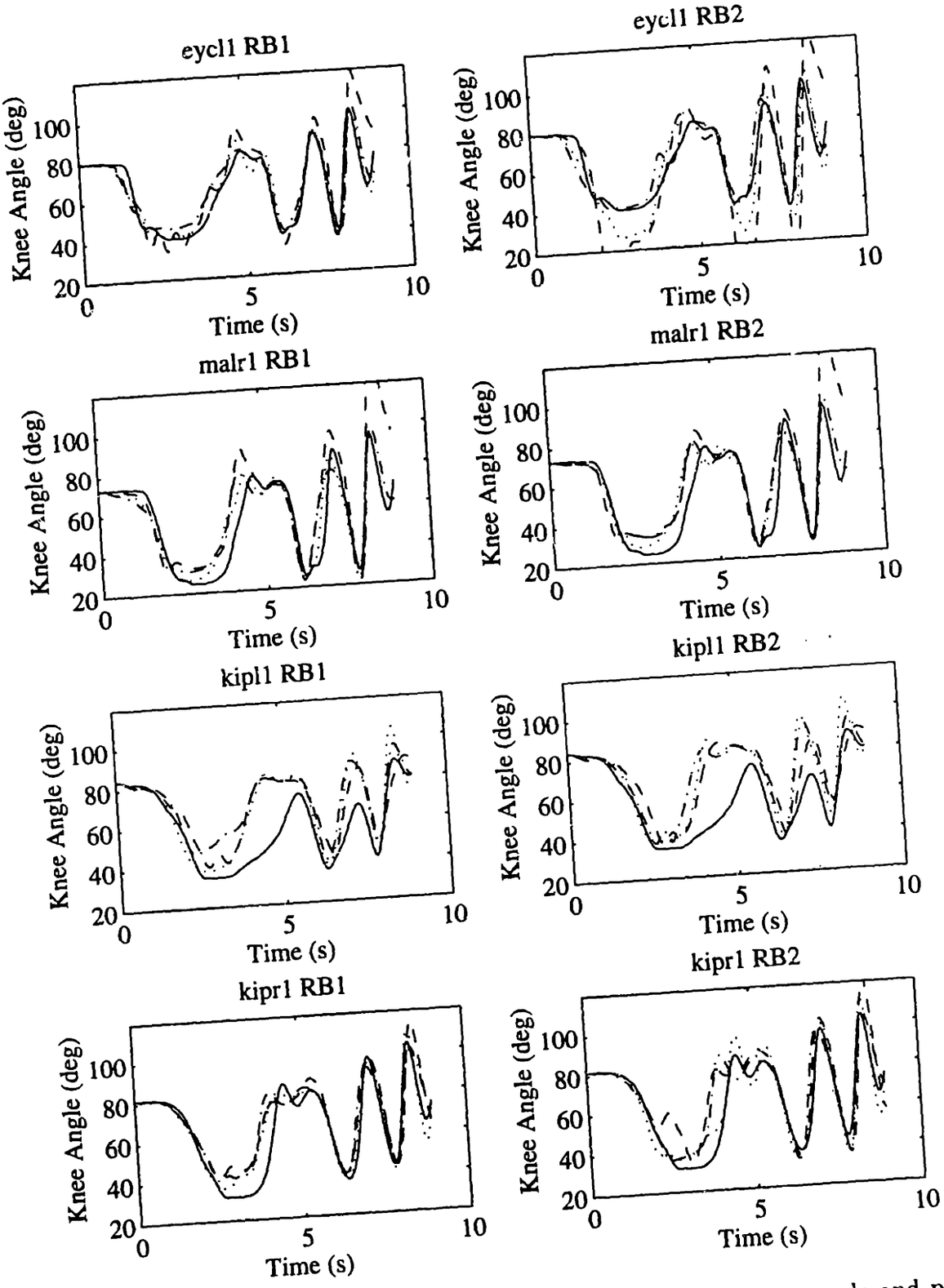

Figure J-4: (continued) Swept-sine response:(−) Experimental knee angle and predictions with (−−) sequential, (−·−) simultaneous, and (···) free swing parameters.

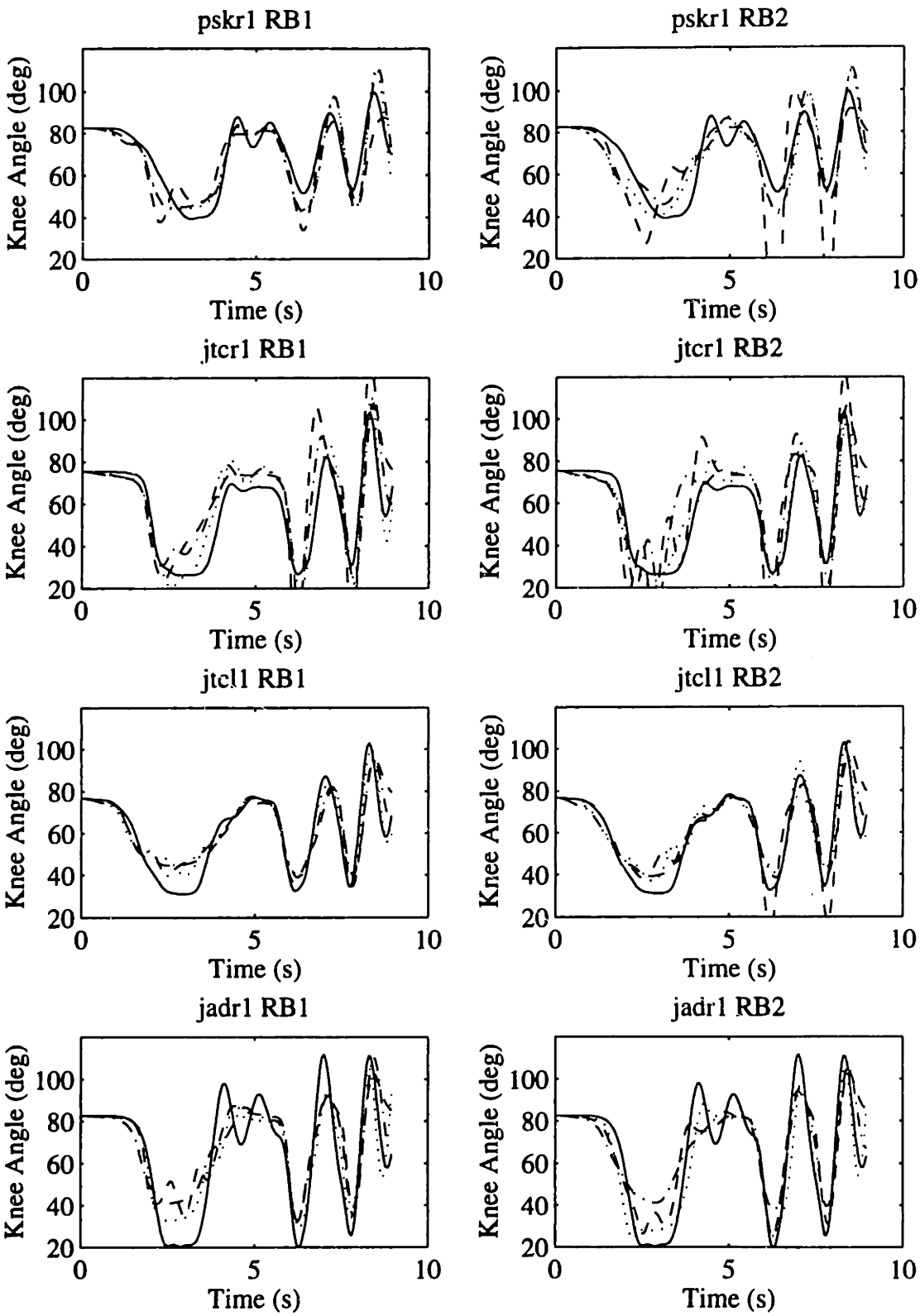

Figure J-4: (continued) Swept-sine response:(−) Experimental knee angle and predictions with (− −) sequential, (− · −) simultaneous, and (· · ·) free swing parameters.

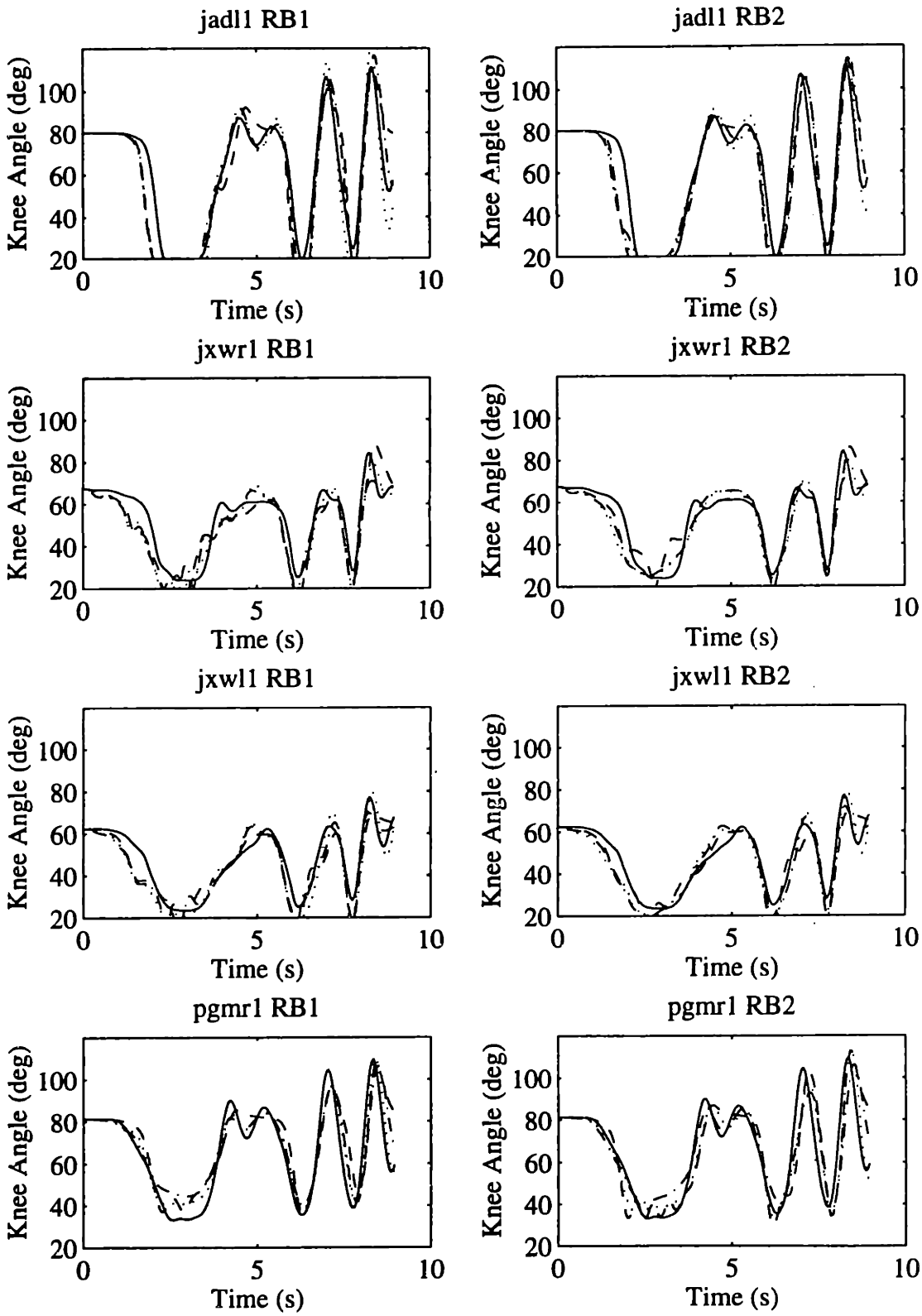

Figure J-4: (continued) Swept-sine response:(−) Experimental knee angle and predictions with (−−) sequential, (−·−) simultaneous, and (···) free swing parameters.

RMS ERROR for Random Binary Trajectory #1 Response Prediction

	Parameter Sets					
	Sequential		Free Swing		Simultaneous	
Subject	RB1	RB2	RB1	RB2	RB1	RB2
bksl1	7.941	15.992	7.396	8.090	9.154	9.178
nccl1	8.604	21.582	3.554	6.346	5.677	12.024
nccr1	12.229	16.188	4.221	7.224	3.191	9.564
eycr1	31.915	23.570	7.188	14.293	7.809	14.231
eycl1	11.025	23.021	4.769	5.912	4.494	4.520
malr1	10.035	12.002	8.359	8.645	9.865	9.499
kipl1	7.355	9.571	4.927	4.653	6.653	9.470
kipr1	5.047	7.894	5.019	8.752	4.413	8.788
pskr1	6.418	25.254	3.945	5.531	3.535	5.932
jtcr1	8.046	11.151	4.467	6.223	6.947	9.783
jtcl1	5.092	8.568	7.503	10.323	6.715	7.539
jadr1	8.876	9.755	12.599	13.726	7.491	7.673
jadl1	18.122	11.157	16.773	11.319	14.453	9.649
jxwr1	9.890	7.025	9.505	7.625	8.153	5.898
jxwl1	6.786	6.898	5.519	5.338	7.260	7.252
pgmr1	5.857	10.409	4.567	7.830	5.737	7.993

AVERAGE ABSOLUTE ERROR for Random Binary Trajectory #1 Response Prediction

	Parameter Sets					
	Sequential		Free Swing		Simultaneous	
Subject	RB1	RB2	RB1	RB2	RB1	RB2
bksl1	5.983	11.268	5.849	5.873	7.491	6.820
nccl1	6.912	16.903	2.530	4.913	4.057	9.153
nccr1	8.373	13.043	3.269	5.784	2.561	7.570
eycr1	18.779	16.703	5.253	10.427	5.093	10.310
eycl1	7.427	17.624	3.221	4.207	3.611	3.270
malr1	8.222	8.571	6.001	6.230	7.707	7.422
kipl1	5.723	7.018	3.821	3.435	5.200	6.914
kipr1	4.106	6.529	3.933	6.795	3.233	6.397
pskr1	4.605	15.941	3.260	4.542	2.918	5.010
jtcr1	5.910	9.691	3.401	4.792	5.581	7.746
jtcl1	4.047	7.193	6.381	8.568	5.726	6.563
jadr1	7.136	8.039	9.148	11.119	6.448	6.329
jadl1	13.874	8.085	12.834	7.681	9.839	6.976
jxwr1	7.740	5.555	7.492	5.497	6.035	4.401
jxwl1	5.470	5.334	4.205	4.054	5.881	5.584
pgmr1	4.332	8.647	3.709	6.208	4.642	6.209

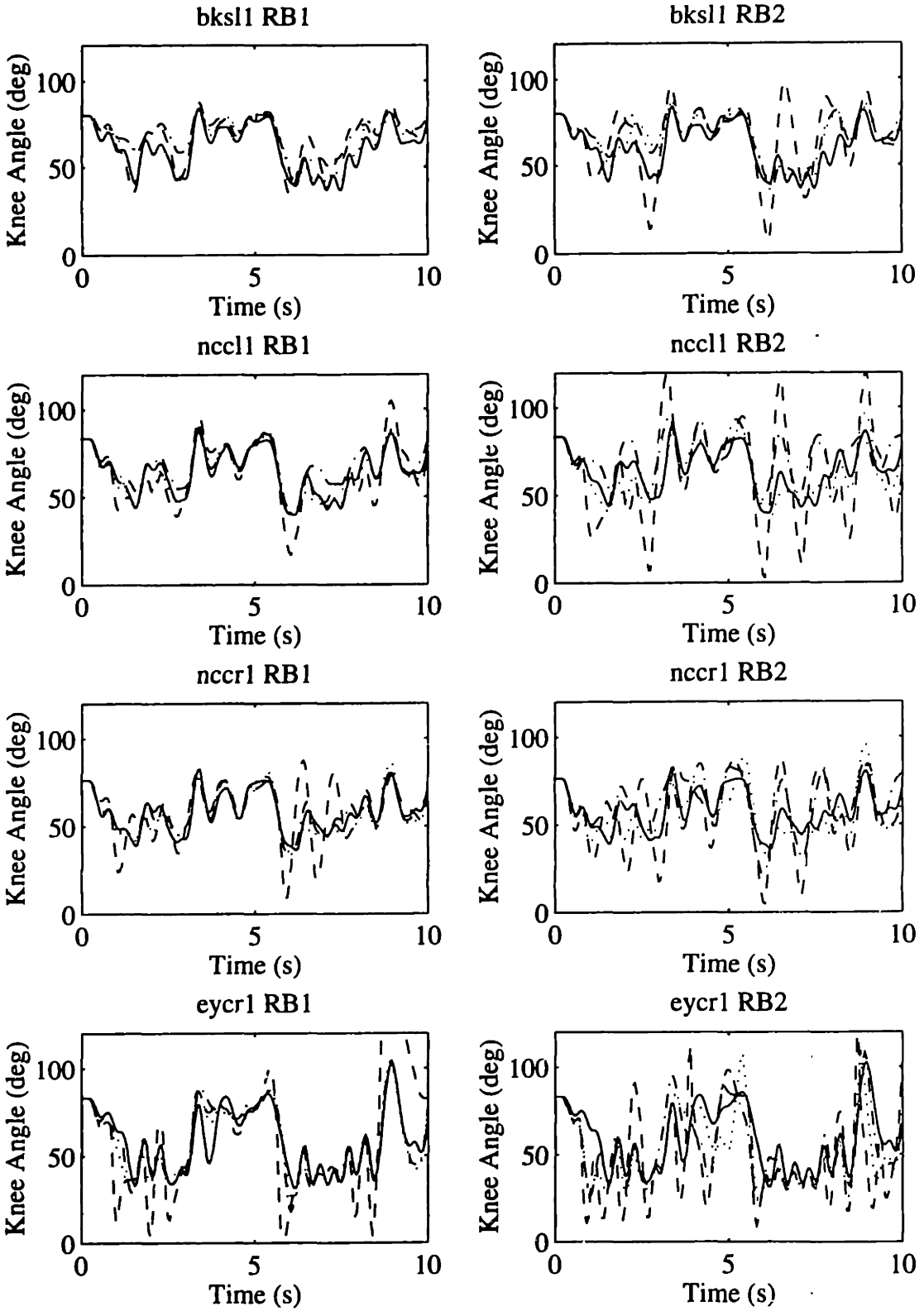

Figure J-5: Random binary 1 response: (−) Experimental knee angle and predictions with (−−) sequential, (− · −) simultaneous, and (· · ·) free swing parameters.

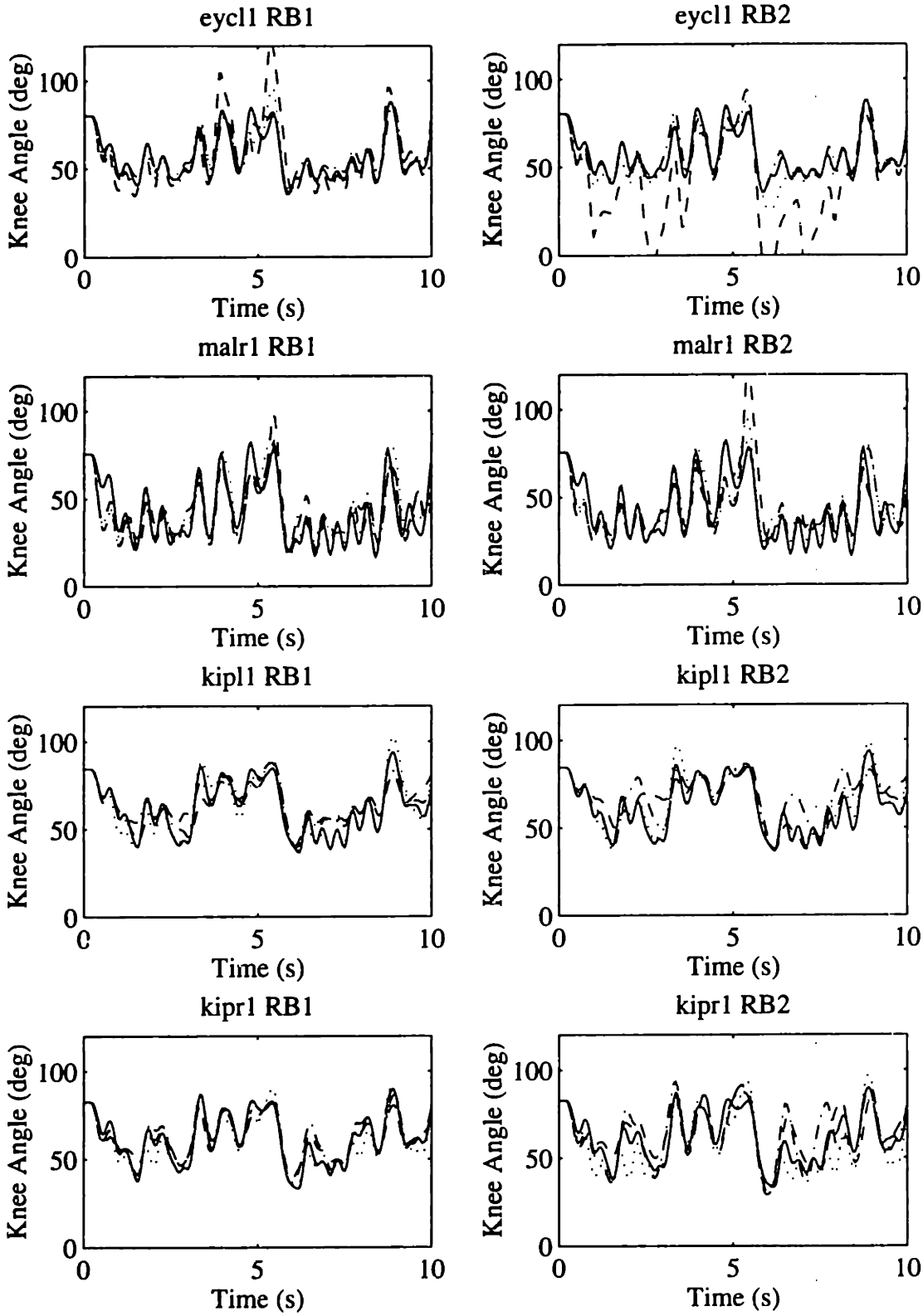

Figure J-5: (continued) Random binary 1 response: (−) Experimental knee angle and predictions with (−−) sequential, (− · −) simultaneous, and (···) free swing parameters.

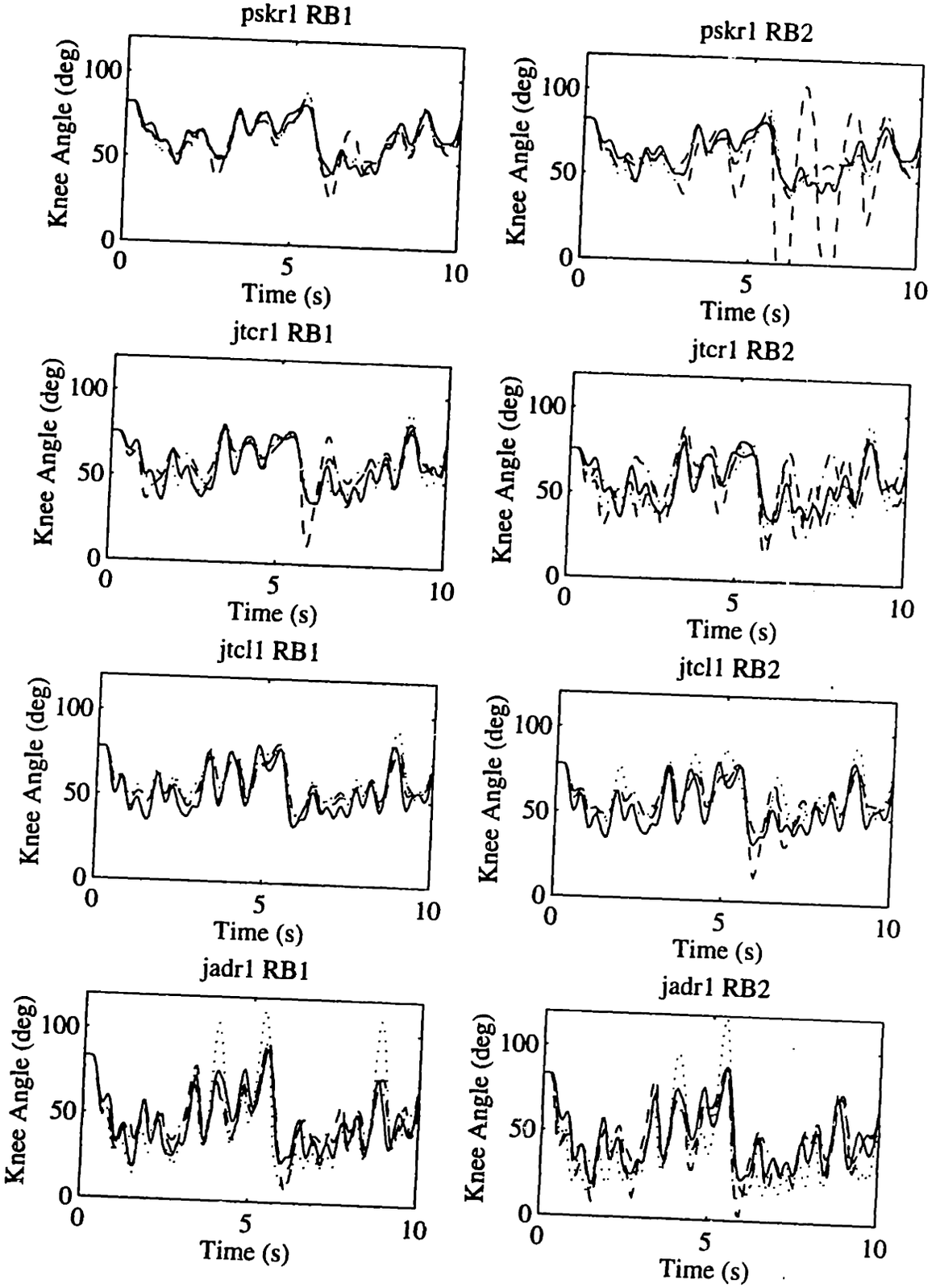

Figure J-5: (continued) Random binary 1 response: (−) Experimental knee angle and predictions with (−−) sequential, (− · −) simultaneous, and (···) free swing parameters.

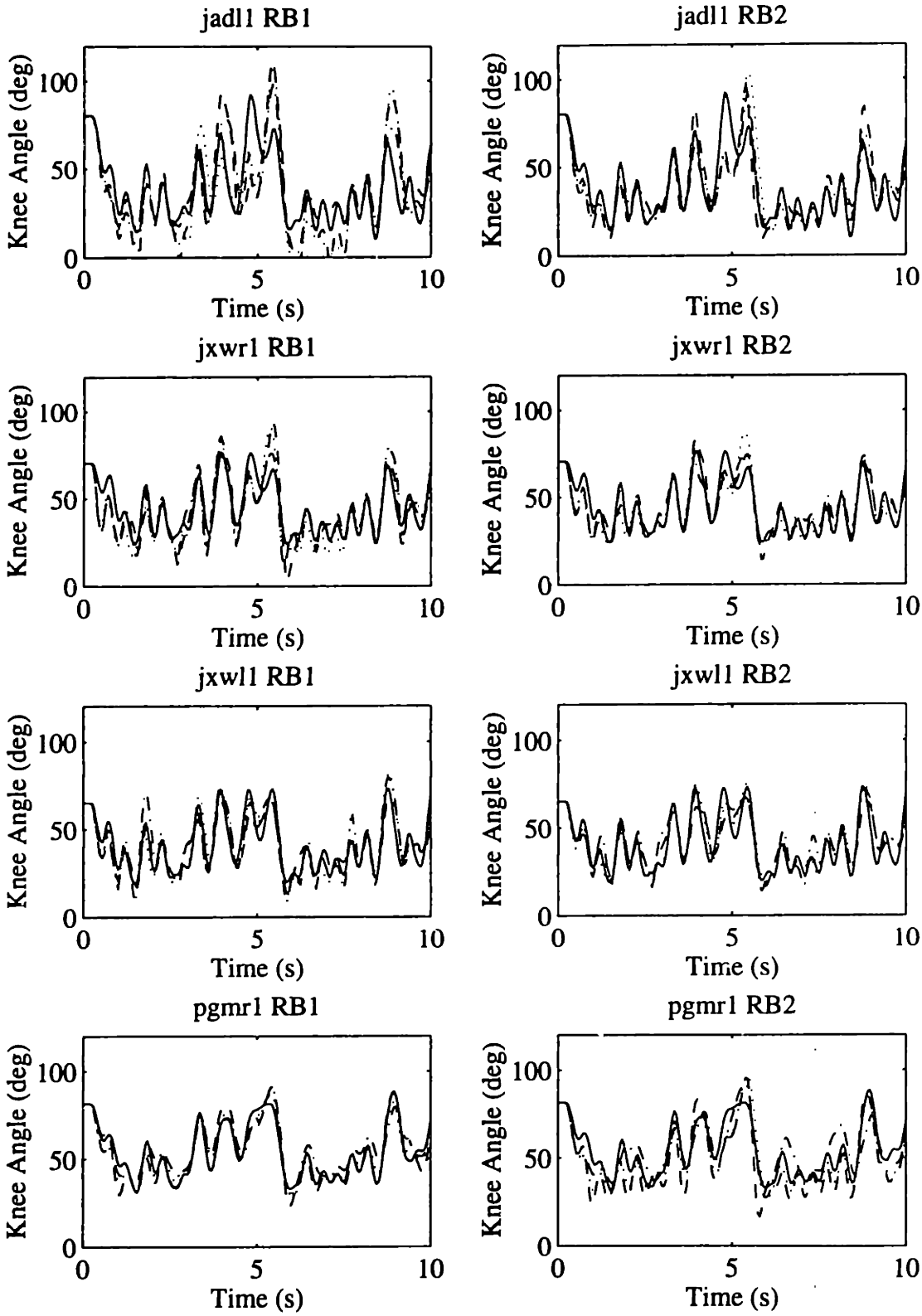

Figure J-5: (continued) Random binary 1 response: (−) Experimental knee angle and predictions with (−−) sequential, (− · −) simultaneous, and (···) free swing parameters.

RMS ERROR for Random Binary Trajectory #2 Response Prediction

	Parameter Sets					
	Sequential		Free Swing		Simultaneous	
Subject	RB1	RB2	RB1	RB2	RB1	RB2
bksl1	8.201	16.017	7.106	7.017	9.123	9.028
nccl1	11.384	23.120	5.915	7.963	7.128	13.534
nccr1	17.379	16.707	5.014	7.146	4.867	7.750
eycr1	25.630	42.429	9.508	12.413	13.078	11.592
eycl1	16.590	22.668	4.912	8.324	4.693	4.216
malr1	8.817	11.239	7.282	7.650	9.649	8.252
kipl1	10.771	11.600	6.744	4.000	8.183	8.297
kipr1	10.008	10.737	9.032	7.991	7.065	9.183
pskr1	9.821	36.333	9.106	7.798	7.167	7.223
jtcr1	10.089	12.455	6.403	5.740	8.163	9.708
jtcl1	7.869	10.335	7.392	9.062	8.026	7.515
jadr1	11.006	8.943	24.605	16.595	10.079	8.496
jadl1	15.855	13.078	21.090	11.000	10.497	9.777
jxwr1	16.137	13.062	10.730	8.468	9.901	5.373
jxwl1	6.857	6.248	5.770	5.040	6.851	4.736
pgmr1	7.794	9.841	5.518	6.108	7.380	9.432

AVERAGE ABSOLUTE ERROR for Random Binary Trajectory #2 Response Prediction

	Parameter Sets					
	Sequential		Free Swing		Simultaneous	
Subject	RB1	RB2	RB1	RB2	RB1	RB2
bksl1	6.405	11.624	5.854	5.766	7.630	7.093
nccl1	9.253	16.702	4.449	5.897	5.595	9.146
nccr1	13.168	12.595	3.974	4.928	3.790	4.934
eycr1	16.986	25.210	6.689	8.165	9.231	8.185
eycl1	10.662	18.207	3.289	6.445	3.816	2.989
malr1	7.171	8.424	5.473	5.238	7.347	6.384
kipl1	7.854	8.444	5.097	3.139	6.619	6.180
kipr1	7.686	8.631	6.682	6.258	5.421	6.359
pskr1	7.697	25.989	6.838	6.036	5.662	5.483
jtcr1	7.898	9.826	5.124	4.467	6.545	6.788
jtcl1	6.178	8.137	6.074	7.231	6.767	6.395
jadr1	8.798	7.149	15.048	10.961	8.050	6.491
jadl1	12.299	8.343	15.685	6.669	7.619	6.563
jxwr1	11.063	8.877	8.680	6.310	7.578	3.876
jxwl1	5.428	4.925	4.378	3.687	5.397	3.800
pgmr1	5.506	7.613	3.820	4.663	5.624	6.983

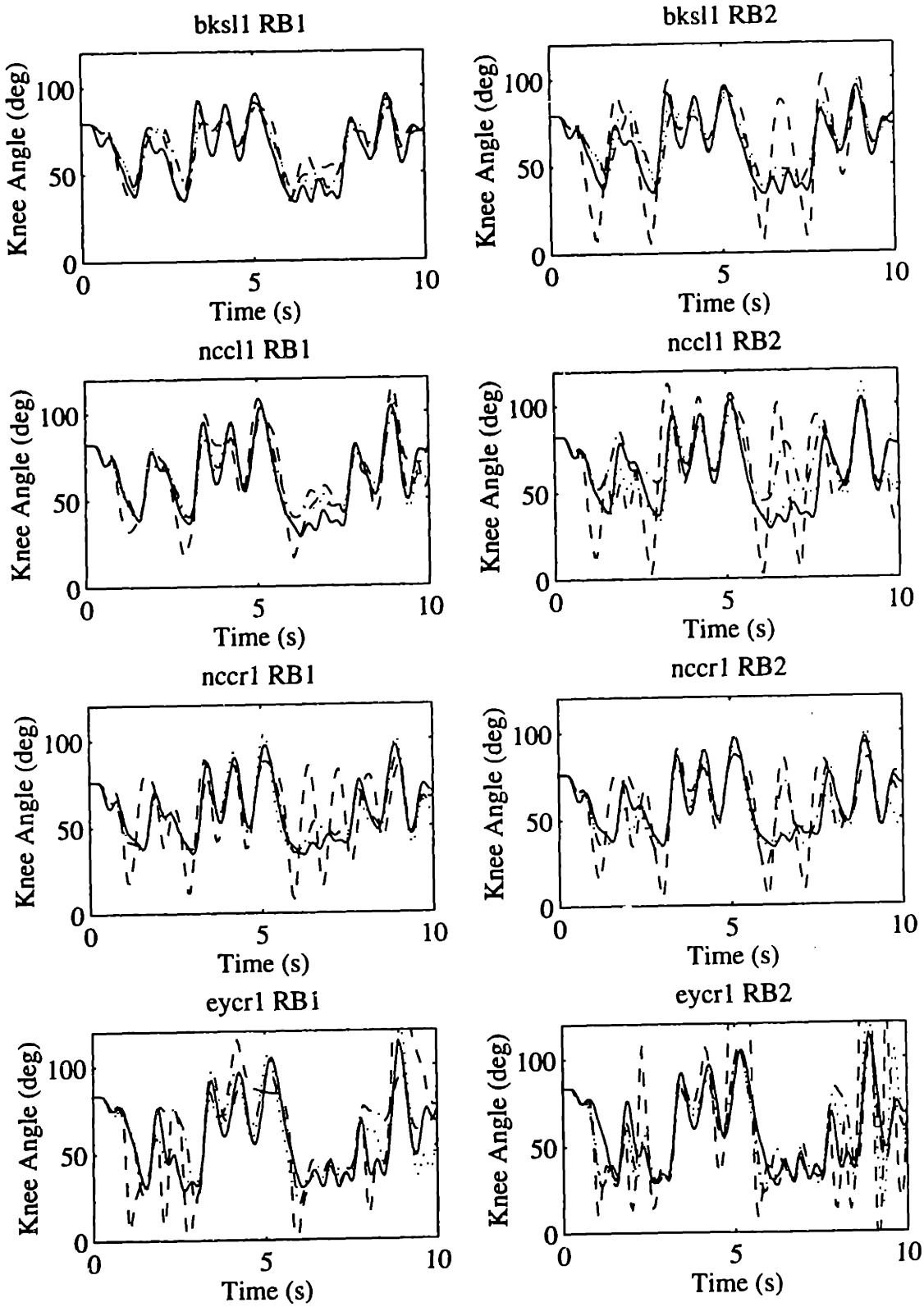

Figure J-6: Random binary 2 response: (−) Experimental knee angle and predictions with (− −) sequential, (− · −) simultaneous, and (· · ·) free swing parameters.

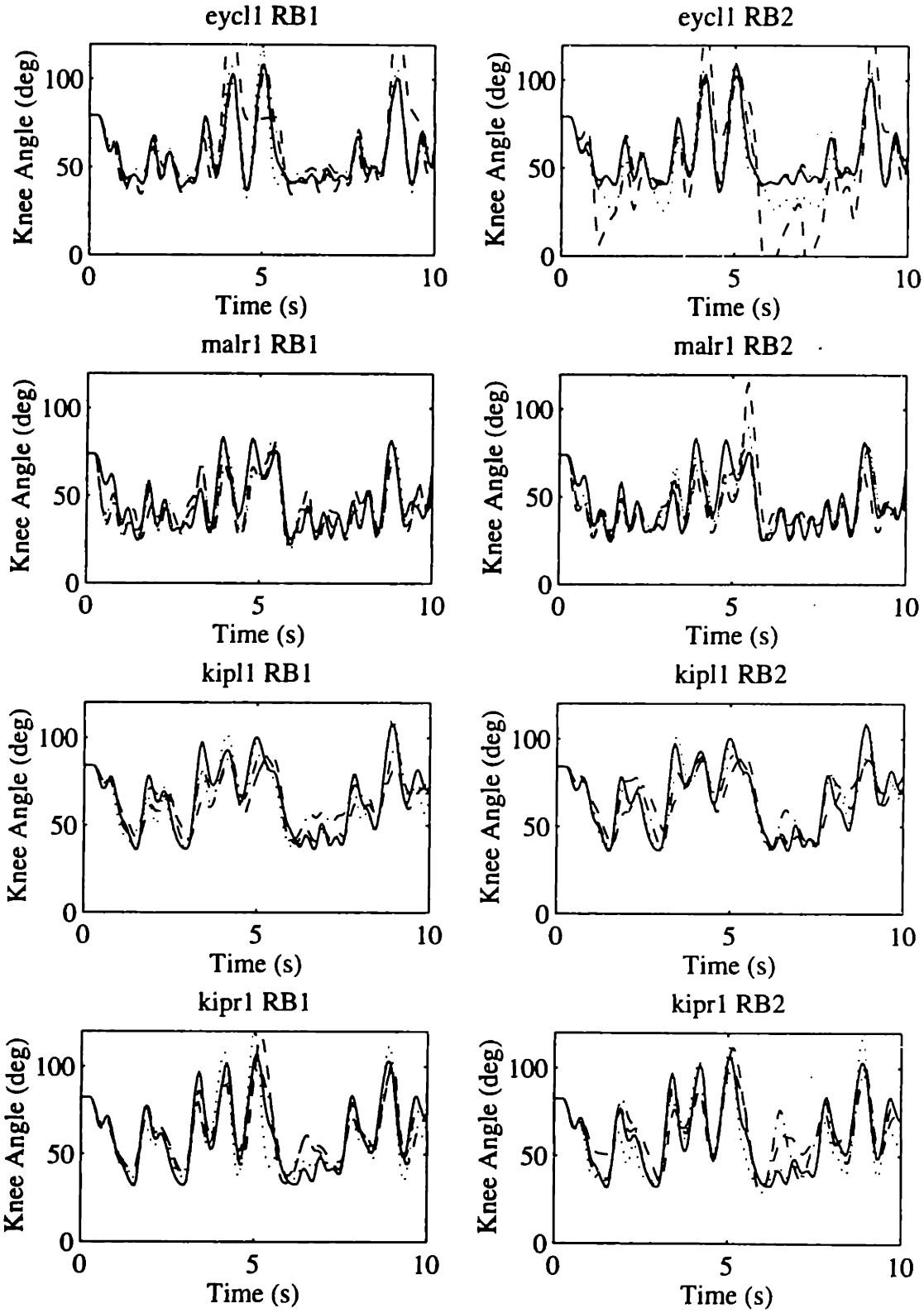

Figure J-6: (continued) Random binary 2 response: (−) Experimental knee angle and predictions with (−−) sequential, (− · −) simultaneous, and (···) free swing parameters.

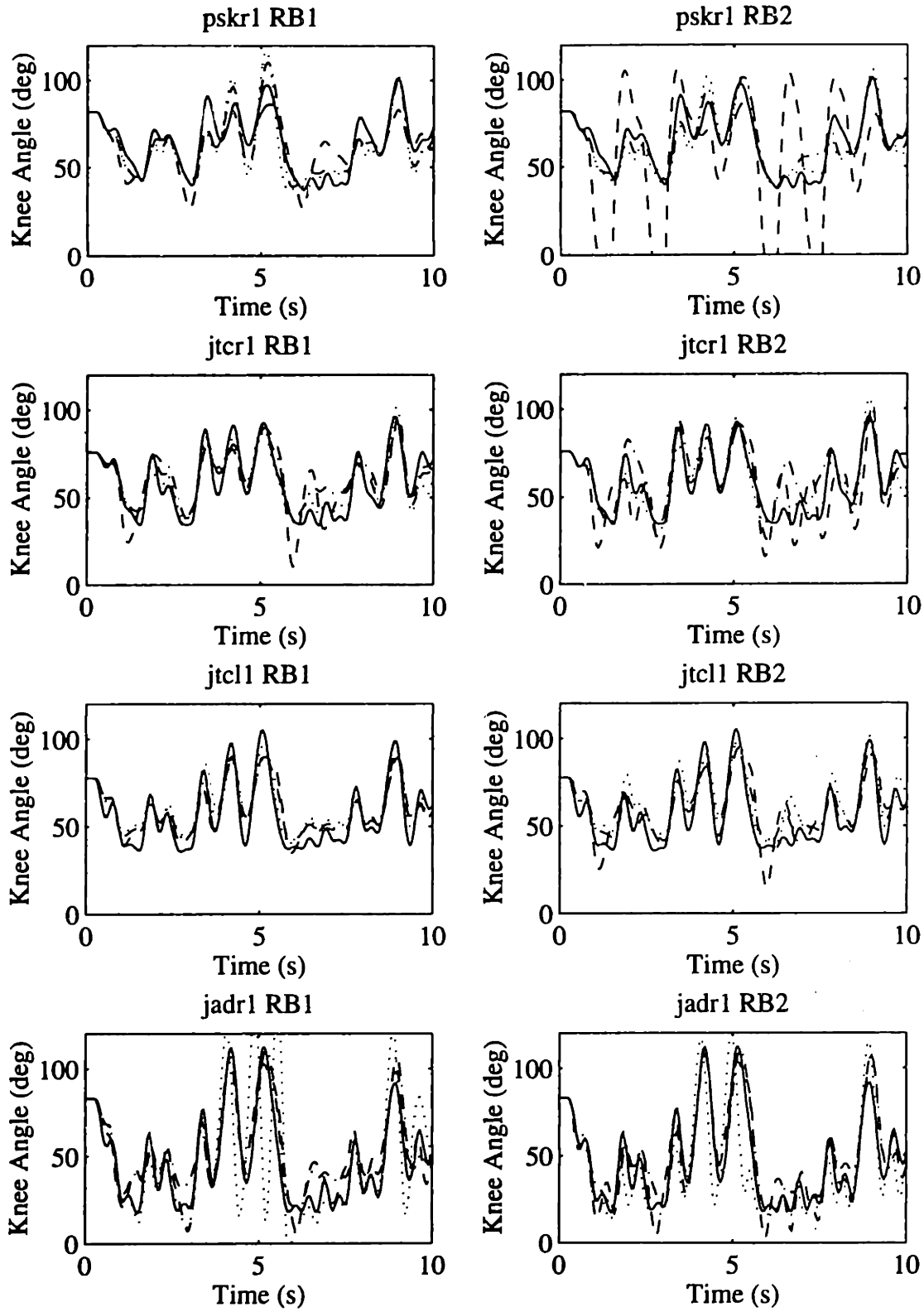

Figure J-6: (continued) Random binary 2 response: (−) Experimental knee angle and predictions with (−−) sequential, (− · −) simultaneous, and (···) free swing parameters.

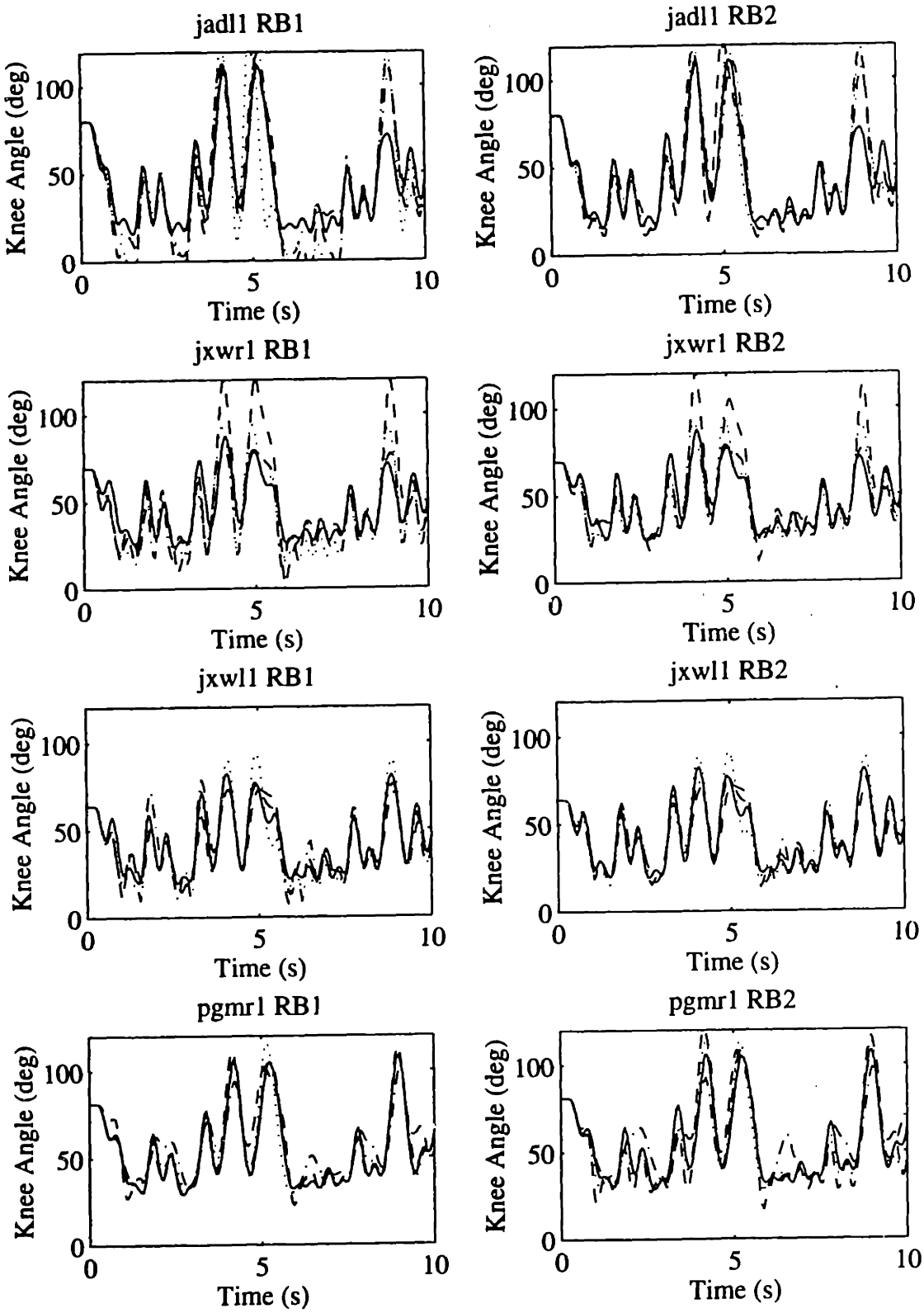

Figure J-6: (continued) Random binary 2 response: (−) Experimental knee angle and predictions with (−−) sequential, (− · −) simultaneous, and (···) free swing parameters.

Appendix K

Comparison to Simplified Models

The tables in this section contain the RMS prediction error calculations obtained with the full model using the free swing parameter set compared to the simplified single-segment and torque generator models. As in the previous section, the error was calculated with Equation (J.1) and the tags RB1 & RB@ refer to the random binary signal used to determine the active parameters. Following each table are graphs of the individual simulations.

RMS ERROR for Step Response Prediction

	Model Type					
	Full		Single-Segment		Torque Generator	
Subject	RB1	RB2	RB1	RB2	RB1	RB2
bksl1	6.613	16.336	14.889	18.155	14.762	14.502
nccl1	3.469	3.846	20.222	27.870	9.417	10.417
nccr1	7.242	8.422	21.420	28.959	4.733	5.613
eycr1	12.606	21.969	38.891	33.951	7.540	7.569
eycl1	2.723	2.308	17.098	24.681	12.546	11.860
malr1	7.328	5.872	10.117	11.375	21.080	19.637
kipl1	7.497	5.440	28.032	21.227	6.652	6.339
kipr1	2.971	4.127	22.648	27.201	11.423	10.865
pskr1	7.566	6.826	22.179	30.608	7.991	9.046
jtcr1	7.166	6.573	17.232	21.259	14.815	14.769
jtcl1	3.998	3.052	2.516	3.653	8.589	8.834
jadr1	13.244	13.741	22.291	29.011	26.333	21.455
jadl1	12.091	12.044	18.754	30.886	18.089	19.336
jxwr1	8.678	6.760	13.128	15.054	10.333	9.765
jxwl1	6.809	6.262	15.239	19.852	5.907	6.487
pgmr1	3.804	5.020	7.745	18.262	12.690	12.688

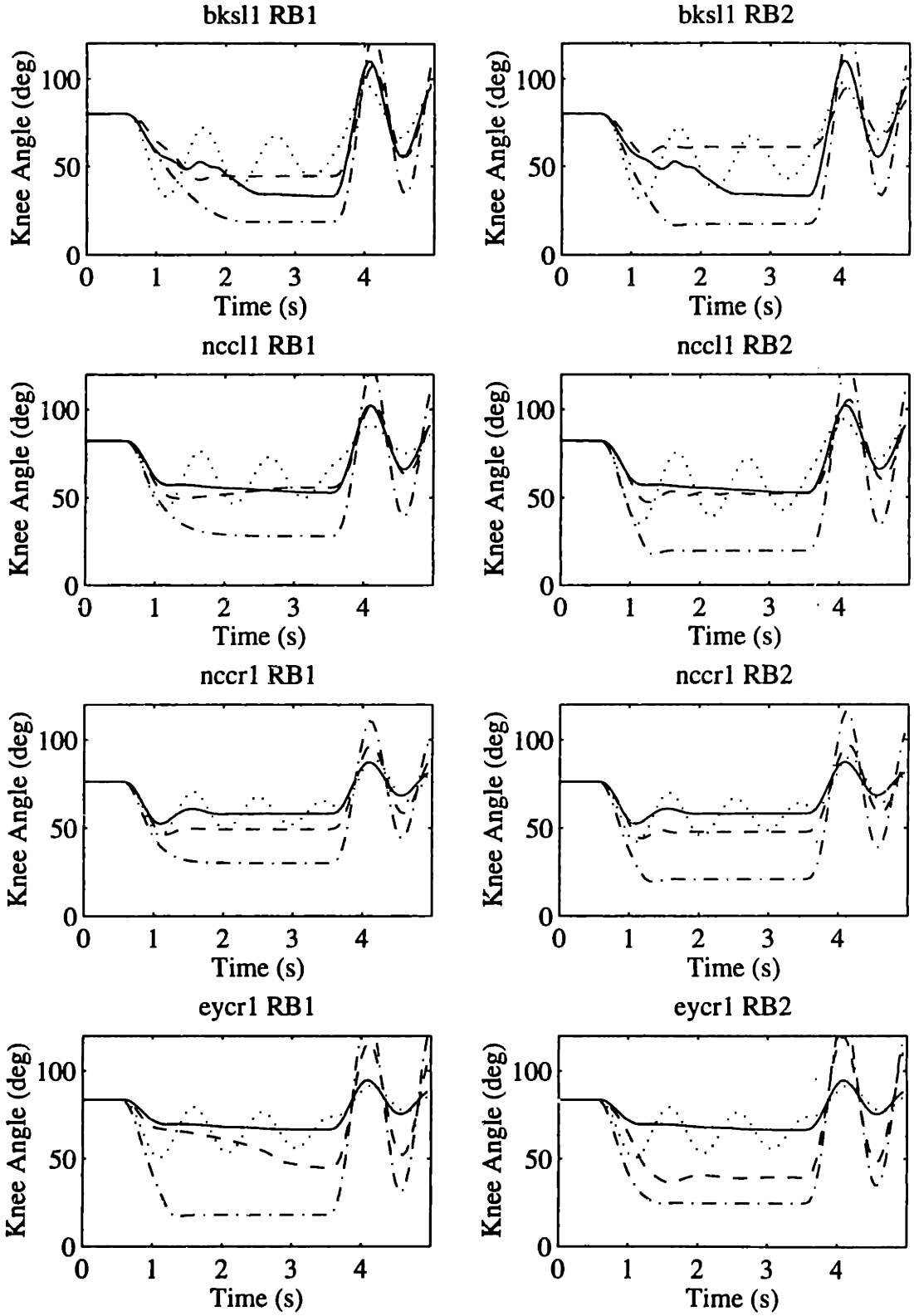

Figure K-1: Step response: (−) Experimental knee angle and predictions with (−−) full model, (− · −) single-segment model and (· · ·) torque generator model.

RMS ERROR for Ramp Response Prediction

	Model Type					
	Full		Single-Segment		Torque Generator	
Subject	RB1	RB2	RB1	RB2	RB1	RB2
bksl1	9.726	9.886	5.485	7.513	10.096	9.999
nccl1	4.388	6.298	11.936	20.617	6.932	6.371
nccr1	3.697	5.738	10.870	15.363	3.208	2.907
eycr1	5.339	8.205	19.533	14.123	10.123	10.149
eycl1	5.148	4.809	11.233	18.870	8.371	7.905
malr1	6.781	7.649	7.515	7.733	12.881	12.147
kipl1	10.541	12.065	12.036	12.214	12.693	12.581
kipr1	3.713	5.009	10.770	14.933	6.103	6.050
pskr1	4.306	5.408	10.366	17.322	5.577	6.163
jtcr1	5.693	4.406	10.928	14.737	9.600	9.564
jtcl1	5.058	5.541	2.258	3.403	4.689	4.392
jadr1	7.058	6.662	12.950	22.602	14.748	9.867
jadl1	11.301	9.237	14.047	22.831	11.188	12.291
jxwr1	7.843	7.797	10.675	13.029	10.207	9.853
jxwl1	5.318	4.142	11.668	15.426	4.319	4.438
pgmr1	3.180	4.792	6.281	13.636	7.859	7.857

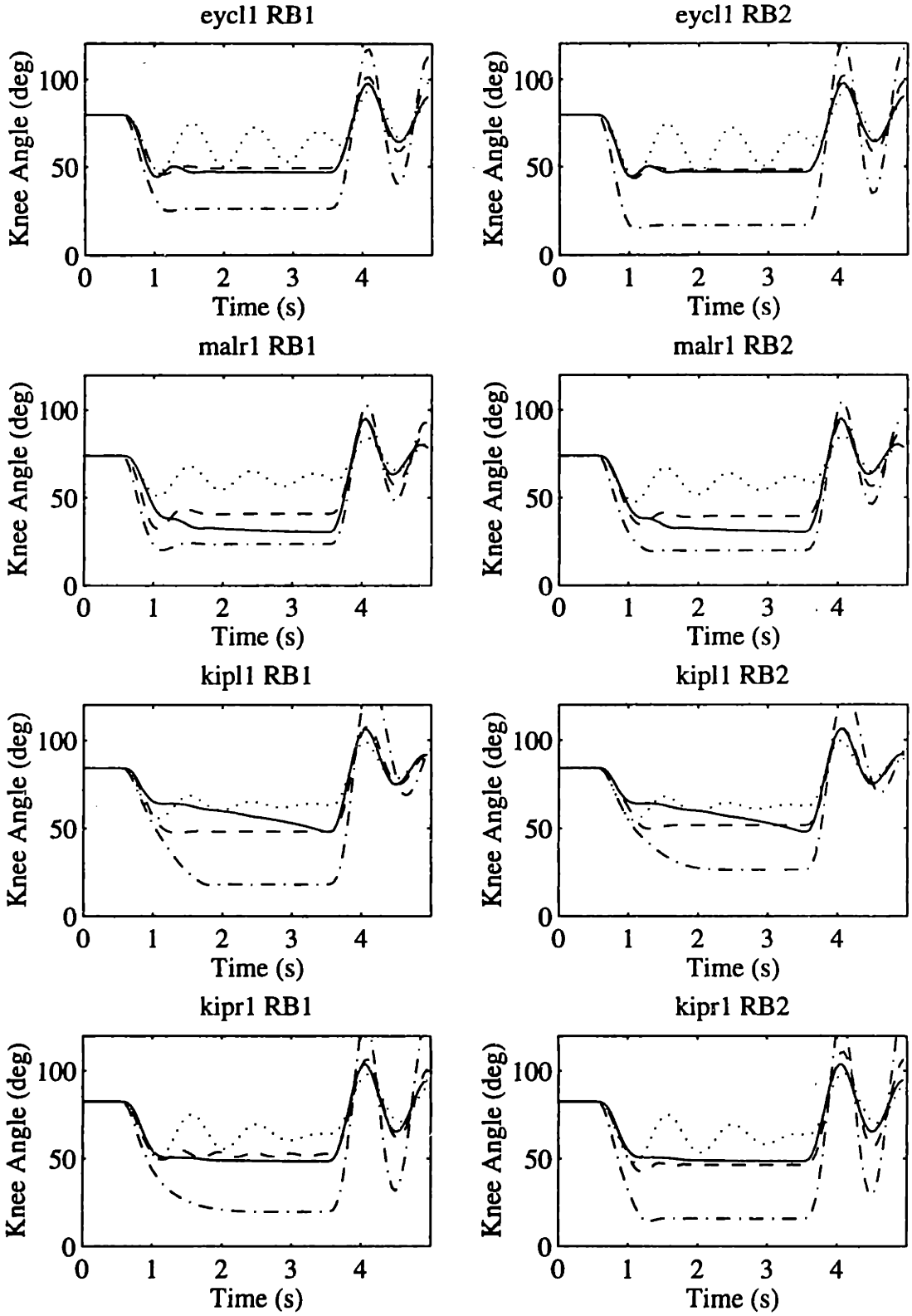

Figure K-1: (continued) Step response: (−) Experimental knee angle and predictions with (− −) full model, (− · −) single-segment model and (· · ·) torque generator model.

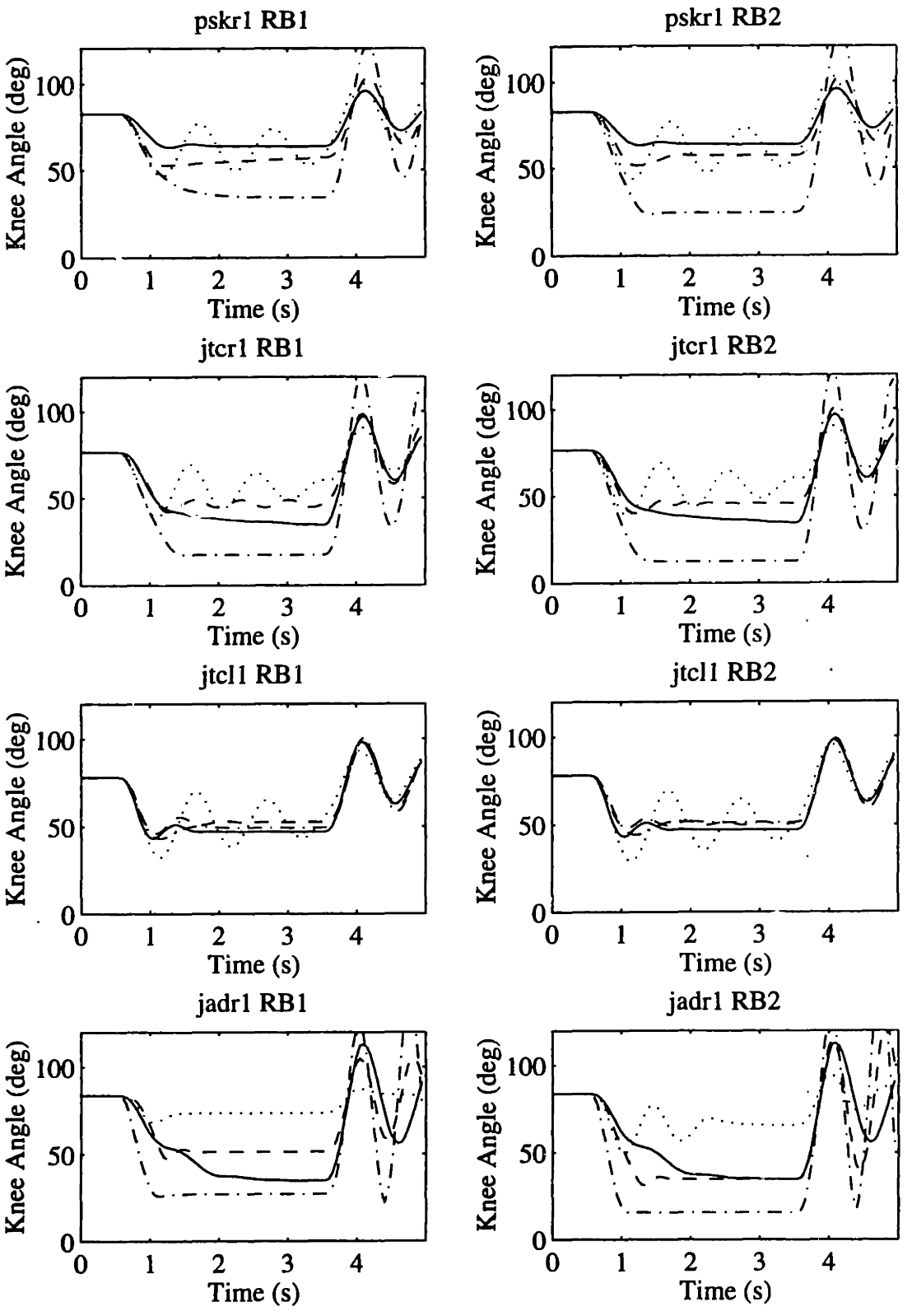

Figure K-1: (continued) Step response: (−) Experimental knee angle and predictions with (− −) full model, (− · −) single-segment model and (· · ·) torque generator model.

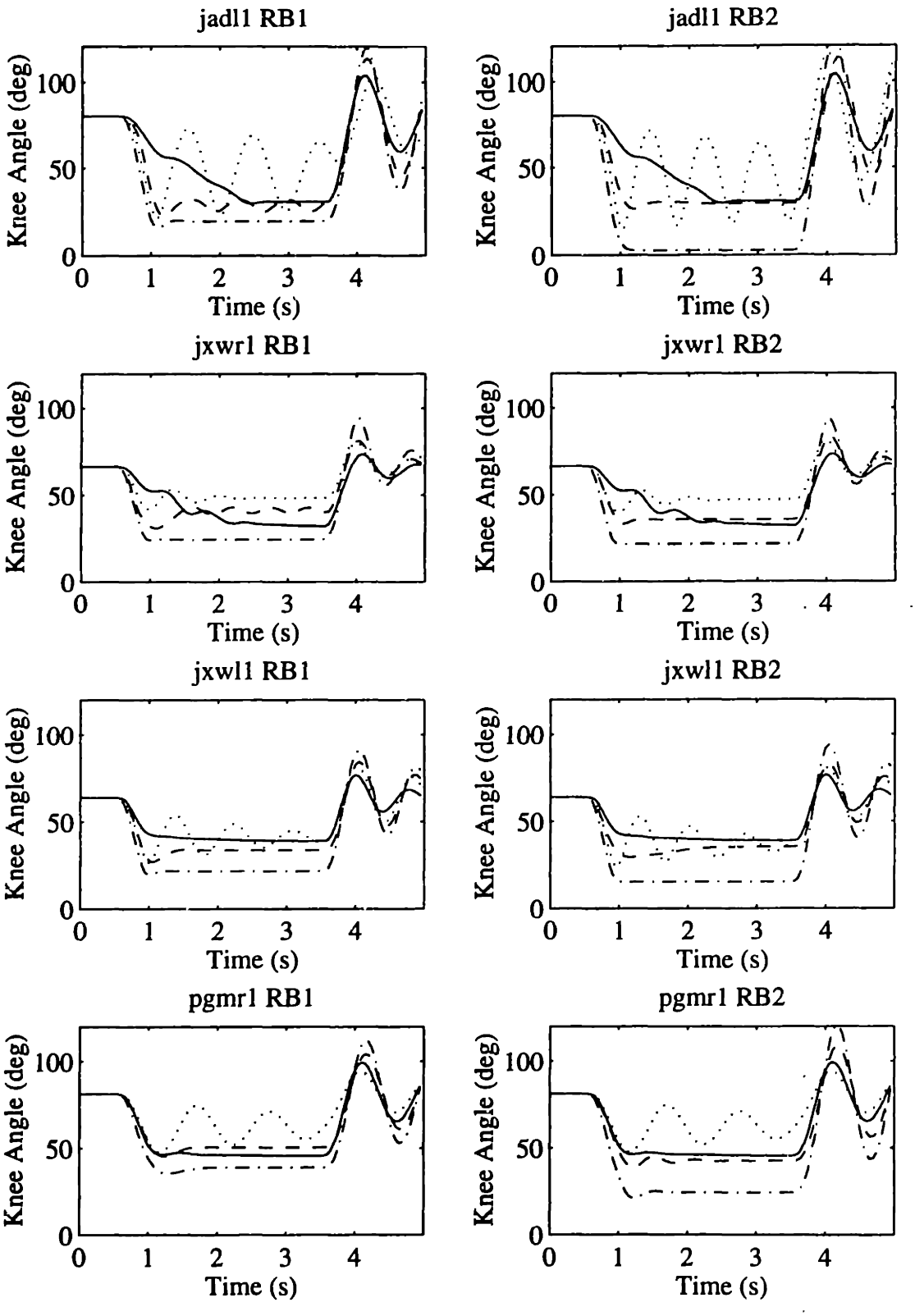

Figure K-1: (continued) Step response: (−) Experimental knee angle and predictions with (−−) full model, (−·−) single-segment model and (···) torque generator model.

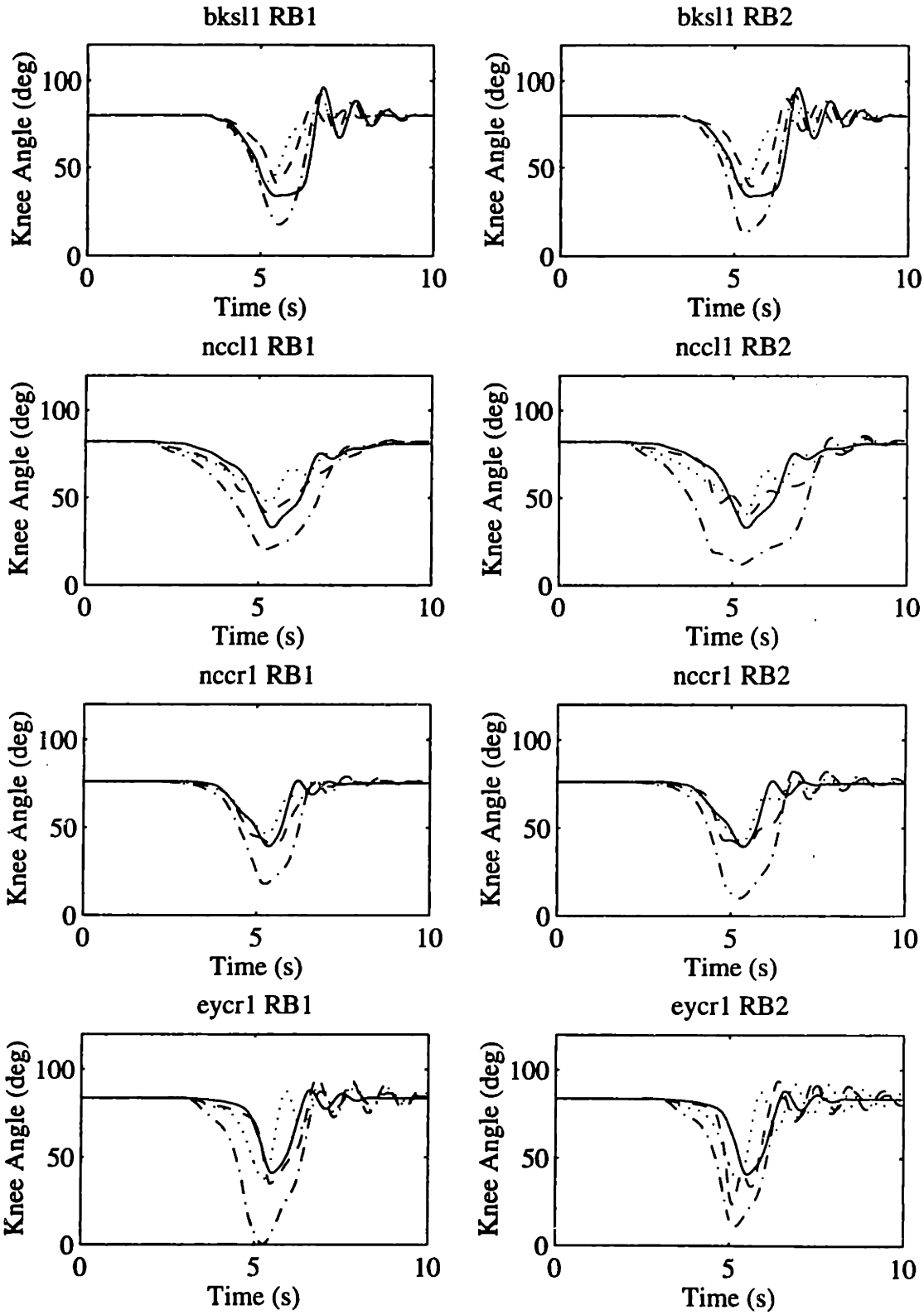

Figure K-2: Ramp response: (−) Experimental knee angle and predictions with (−−) full model, (− · −) single-segment model and (· · ·) torque generator model.

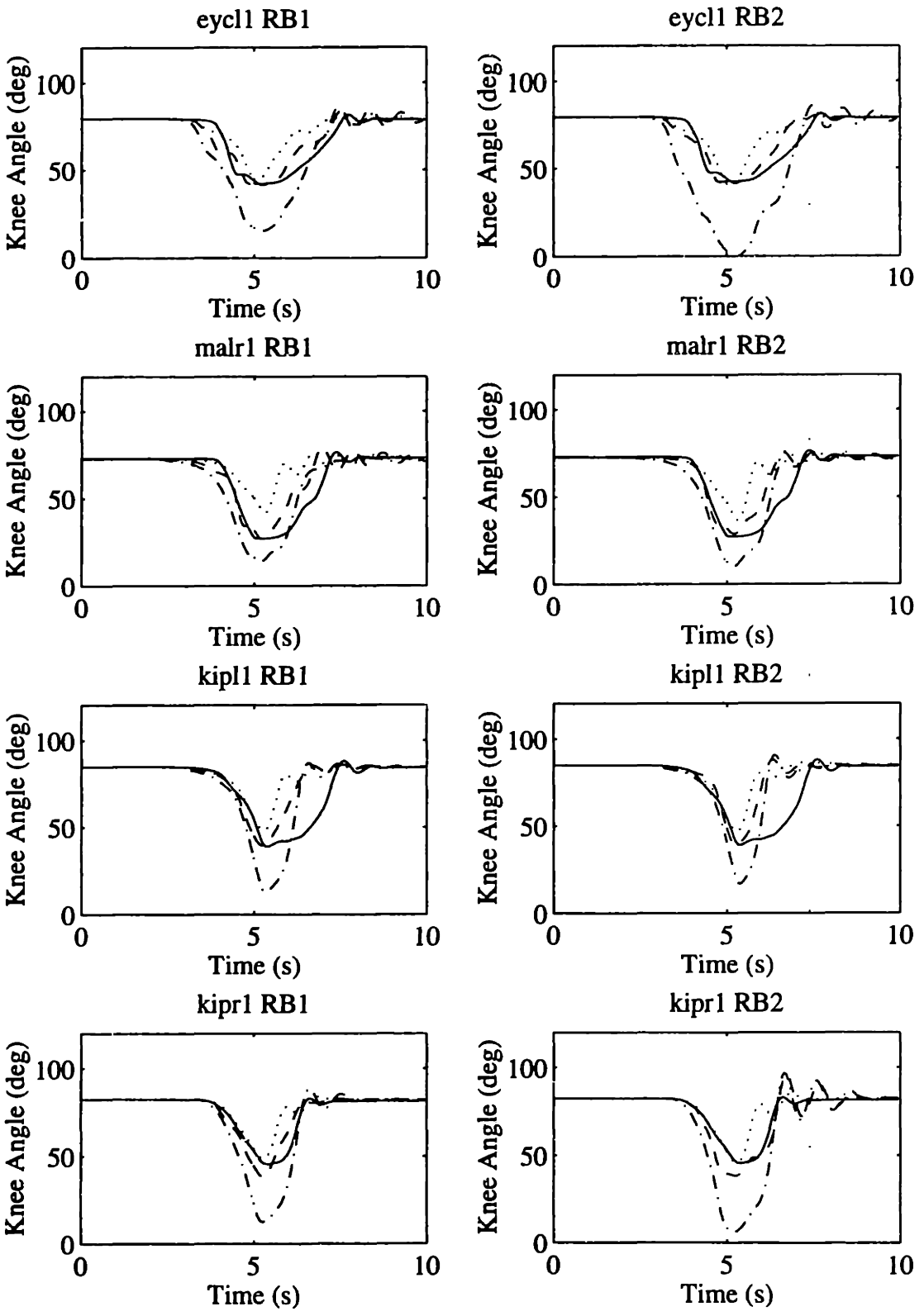

Figure K-2: (continued) Ramp response: (–) Experimental knee angle and predictions with (– –) full model, (– · –) single-segment model and (· · ·) torque generator model.

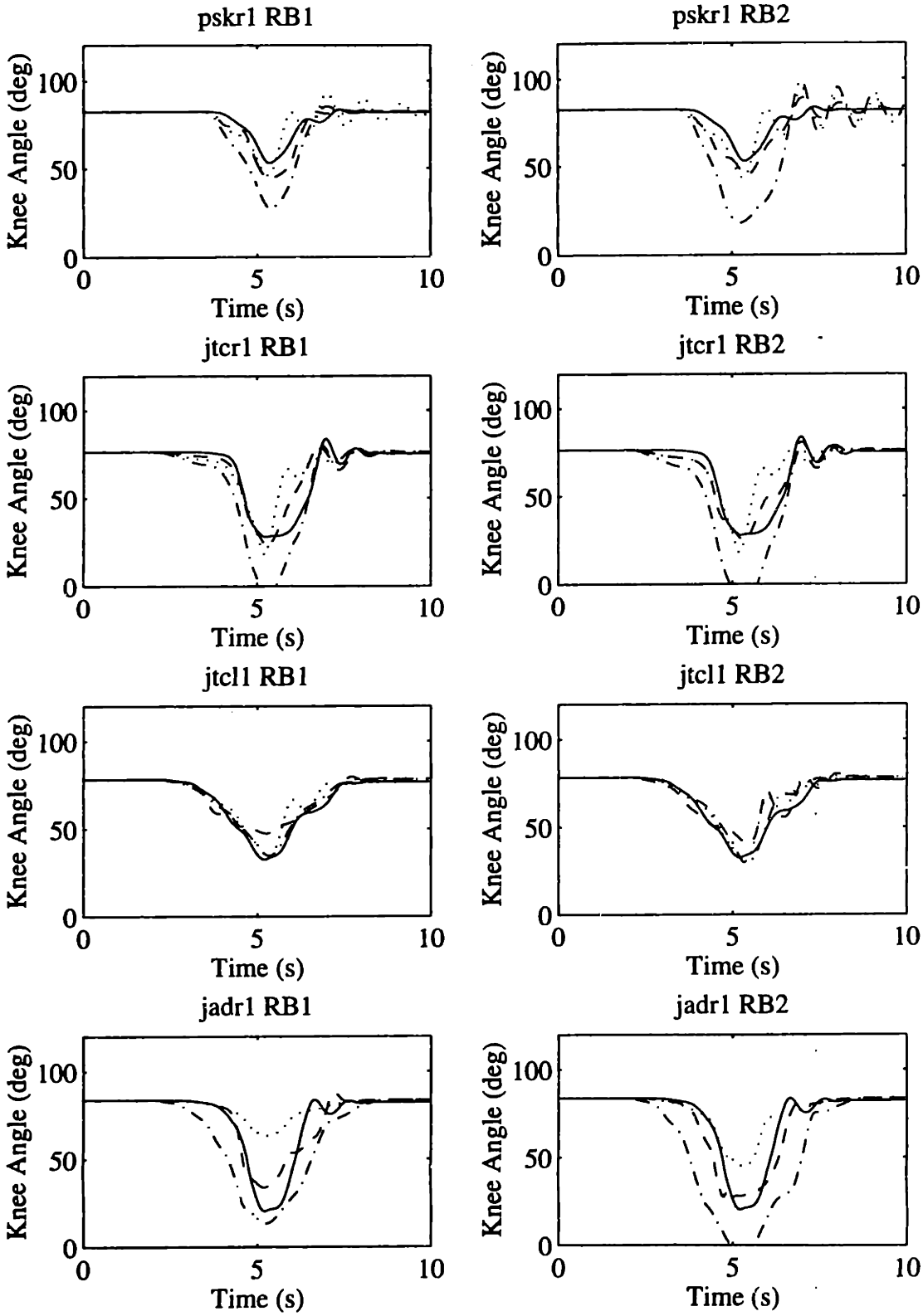

Figure K-2: (continued) Ramp response: (−) Experimental knee angle and predictions with (− −) full model, (− · −) single-segment model and (· · ·) torque generator model.

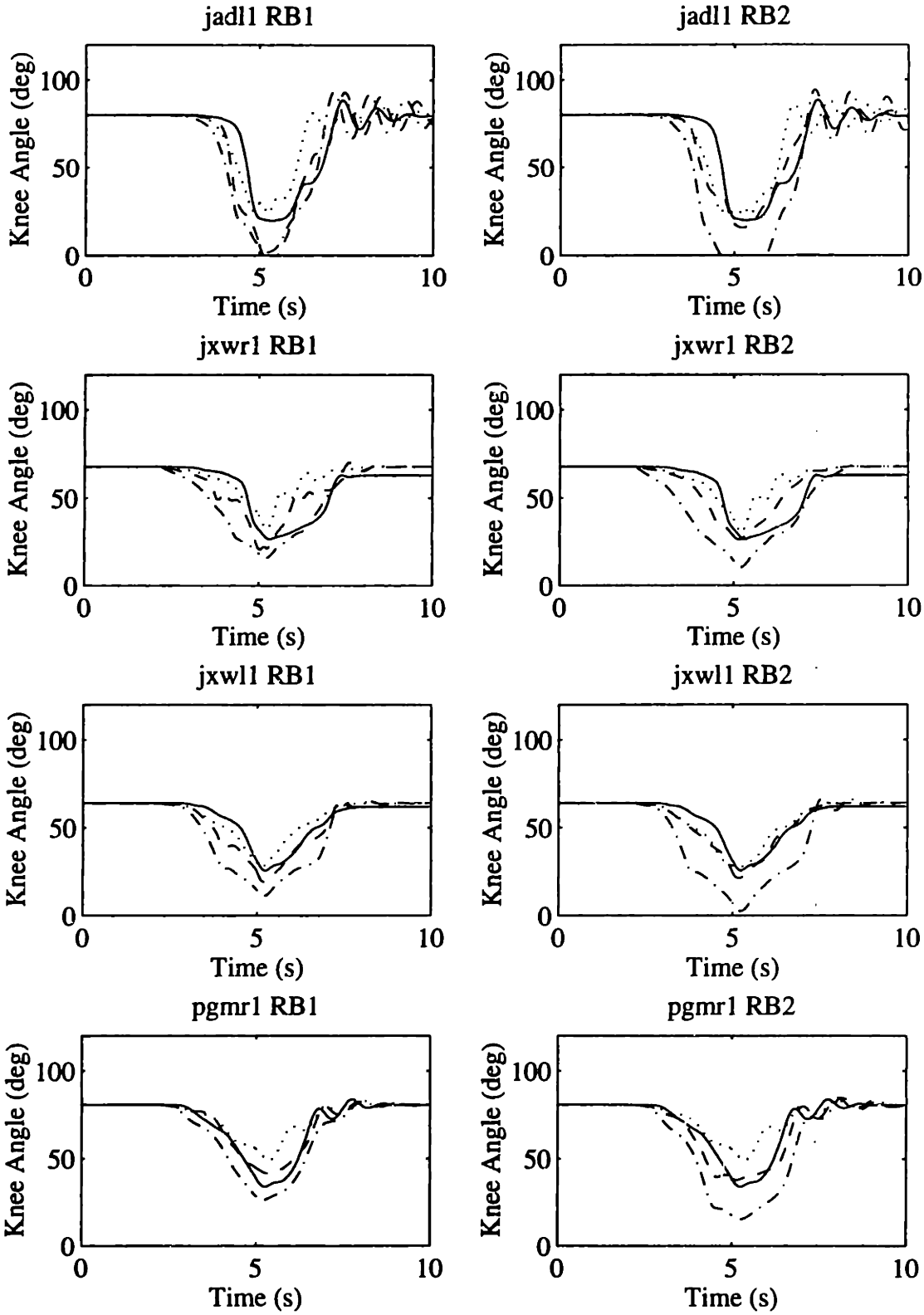

Figure K-2: (continued) Ramp response: (−) Experimental knee angle and predictions with (−−) full model, (− · −) single-segment model and (· · ·) torque generator model.

RMS ERROR for Swept-Sine Response Prediction

	Model Type					
	Full		Single-Segment		Torque Generator	
Subject	RB1	RB2	RB1	RB2	RB1	RB2
bksl1	11.785	12.247	14.043	16.290	13.231	13.178
nccl1	9.066	9.730	15.984	25.114	9.424	8.808
nccr1	6.227	8.792	15.439	20.941	6.647	6.377
eycr1	6.548	11.728	24.435	19.397	17.014	17.024
eycl1	5.248	8.818	15.867	25.298	13.114	12.998
malr1	7.285	7.945	10.164	10.473	16.833	15.843
kipl1	14.255	16.441	17.597	17.880	18.533	18.294
kipr1	6.915	5.707	15.051	19.877	13.697	13.515
pskr1	6.886	8.960	15.181	23.181	11.136	11.708
jtcr1	7.314	6.800	16.353	20.651	16.714	16.697
jtcl1	6.499	6.146	4.669	6.733	7.706	8.556
jadr1	11.096	9.588	15.966	26.232	23.513	27.383
jadl1	12.921	10.079	16.334	28.241	19.410	22.634
jxwr1	7.202	7.101	14.108	17.754	7.916	7.471
jxwl1	6.845	5.707	13.473	18.347	6.302	6.736
pgmr1	5.998	8.230	9.224	16.636	9.542	9.539

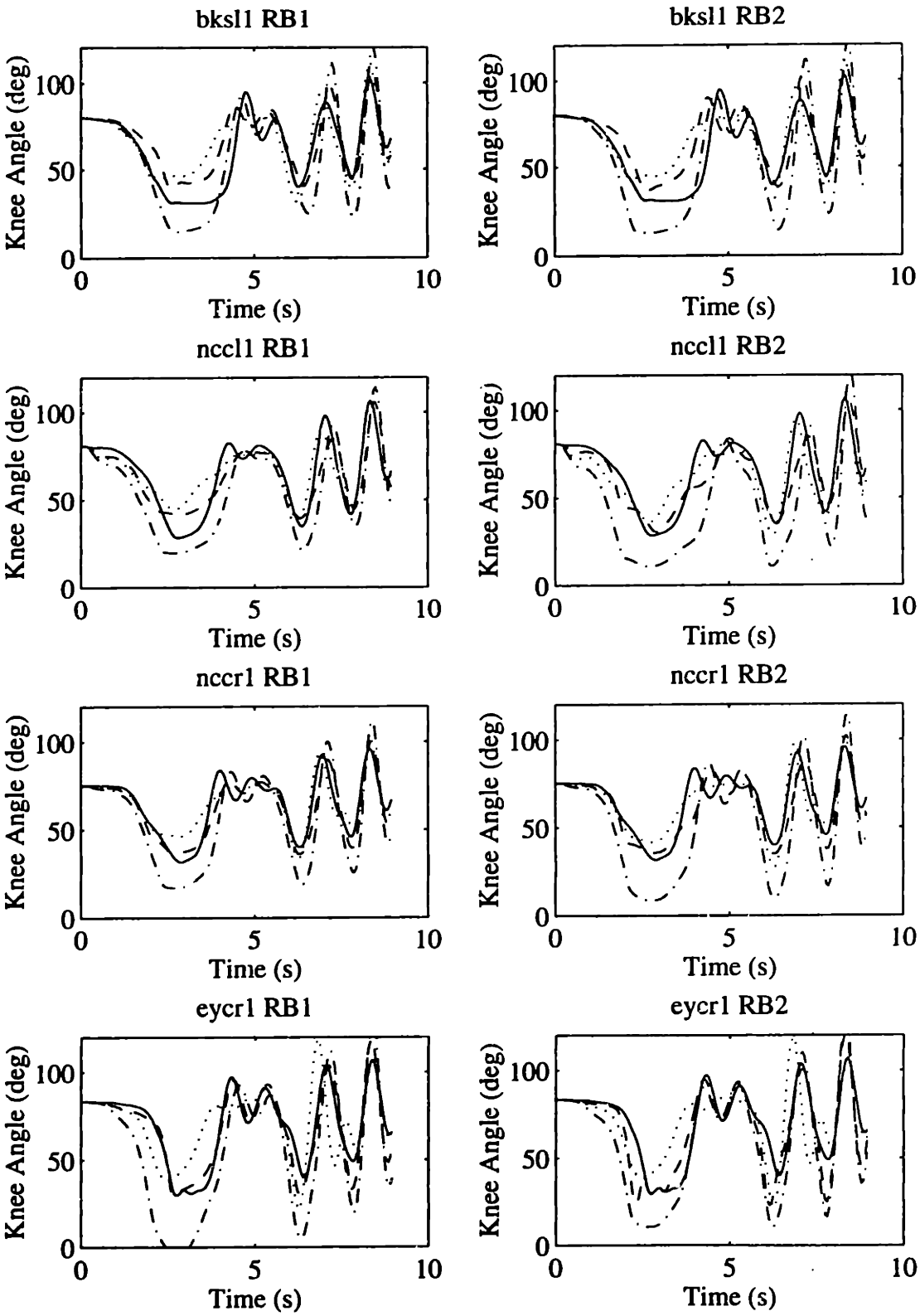

Figure K-3: Swept-Sine Response: (−) Experimental knee angle and predictions with (−−) full model, (− · −) single-segment model and (· · ·) torque generator model.

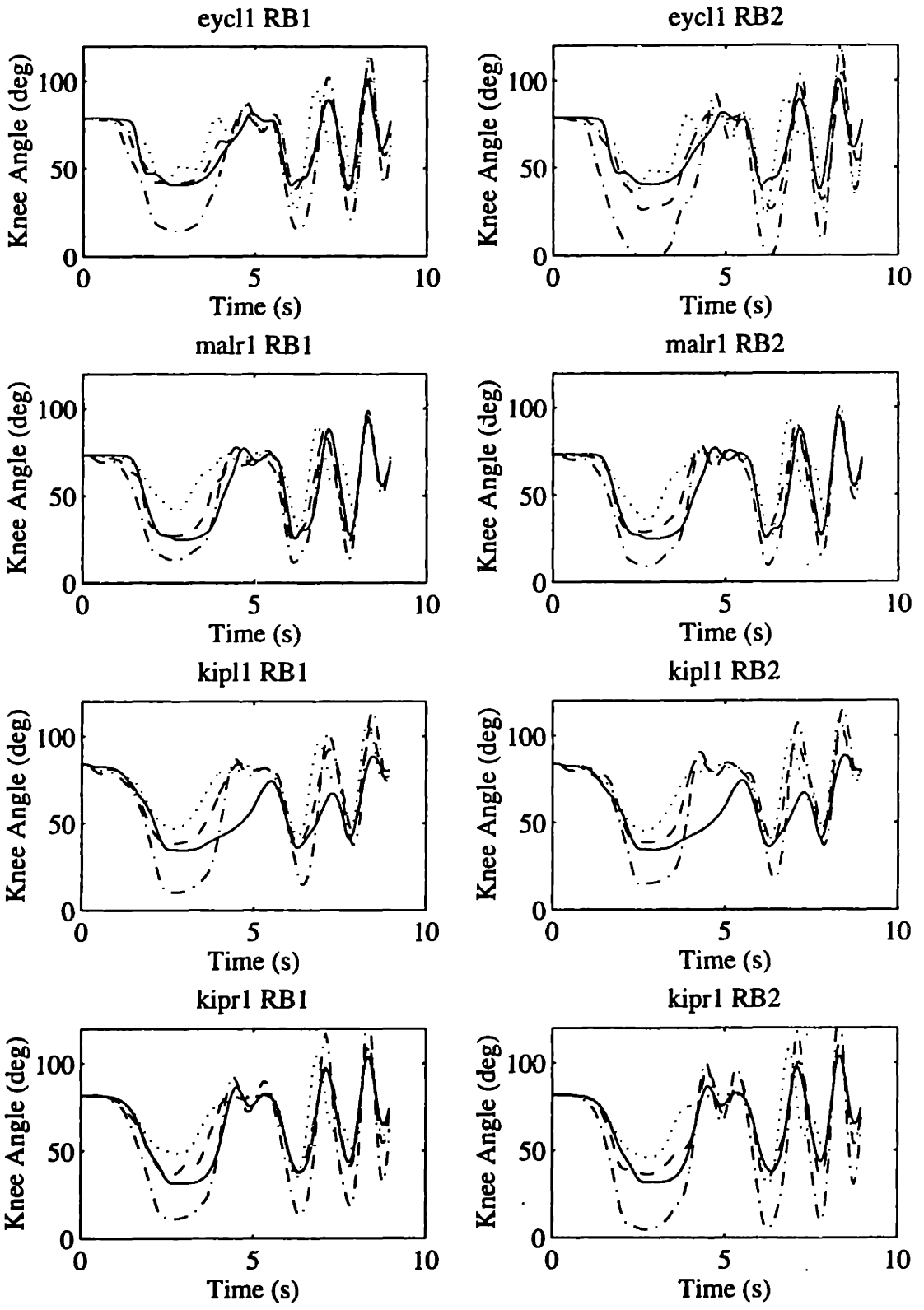

Figure K-3: (continued) Swept-Sine Response: (−) Experimental knee angle and predictions with (−−) full model, (− · −) single-segment model and (···) torque generator model.

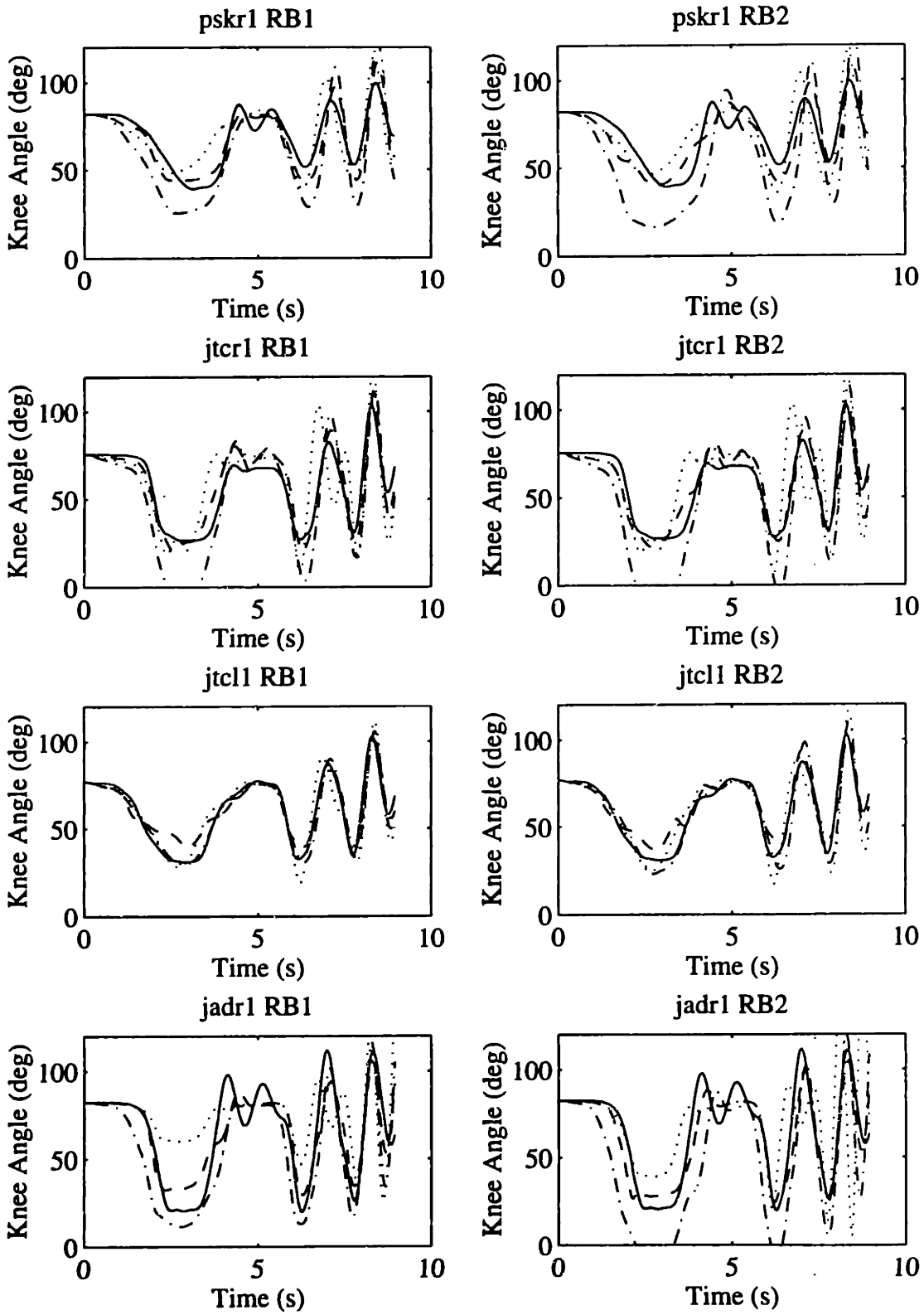

Figure K-3: (continued) Swept-Sine Response: (−) Experimental knee angle and predictions with (−−) full model, (− · −) single-segment model and (· · ·) torque generator model.

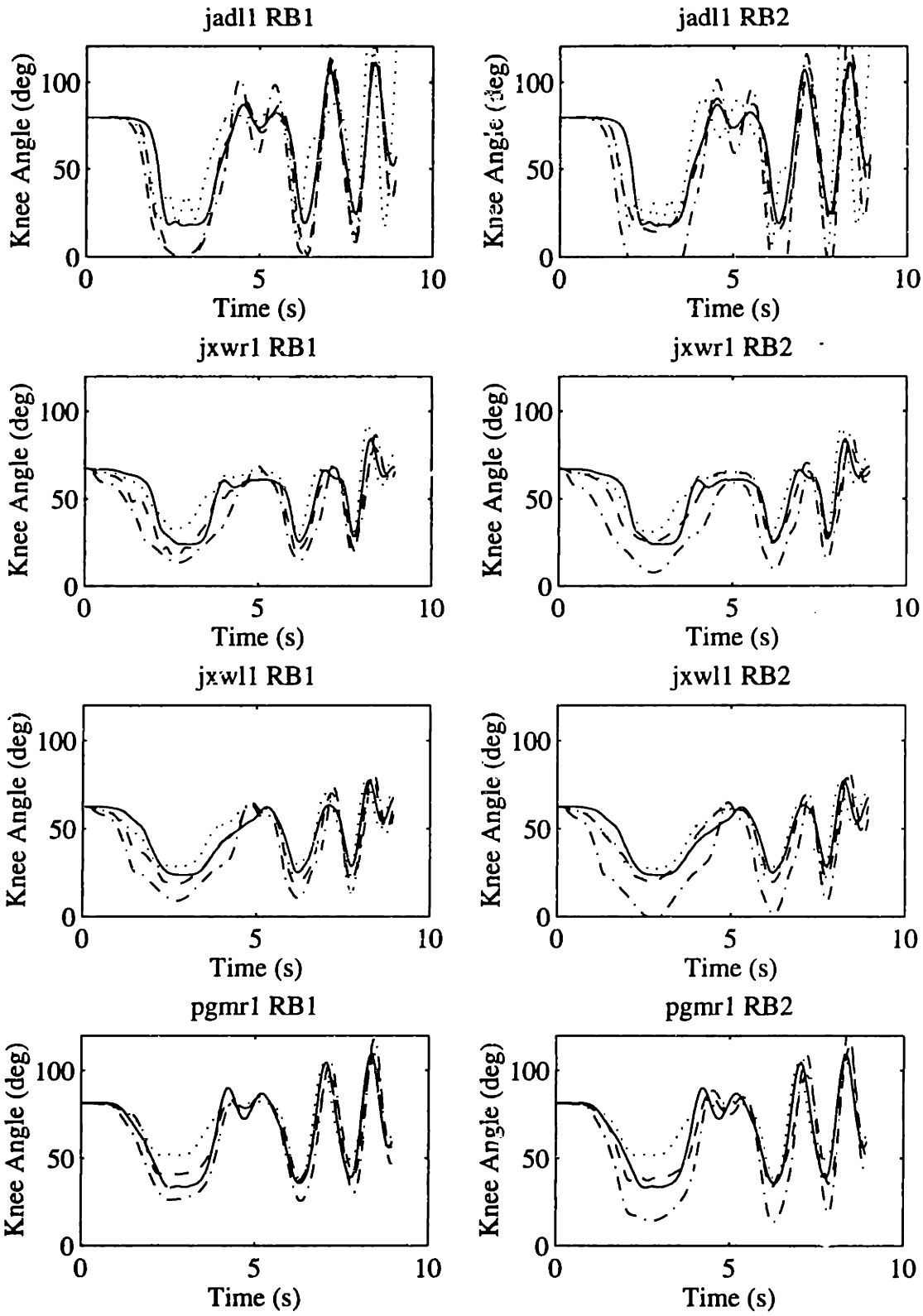

Figure K-3: (continued) Swept-Sine Response: (−) Experimental knee angle and predictions with (− −) full model, (− · −) single-segment model and (···) torque generator model.

RMS ERROR for Random Binary Trajectory #1 Response Prediction

	Model Type					
	Full		Single-Segment		Torque Generator	
Subject	RB1	RB2	RB1	RB2	RB1	RB2
bksl1	7.396	8.090	11.639	15.784	15.980	16.278
nccl1	3.554	6.346	14.065	23.888	14.762	17.455
nccr1	4.221	7.224	14.233	22.062	10.213	11.120
eycr1	7.188	14.293	27.023	20.334	21.027	21.038
eycl1	4.769	5.912	17.603	27.244	14.901	16.190
malr1	8.359	8.645	14.080	14.774	20.825	19.904
kipl1	4.927	4.653	17.604	12.196	11.008	10.771
kipr1	5.019	8.752	18.607	26.286	12.523	12.998
pskr1	3.945	5.531	13.088	22.541	18.185	19.291
jtcr1	4.467	6.223	16.881	21.928	11.469	11.502
jtcl1	7.503	10.323	5.890	9.018	15.542	16.121
jadr1	12.599	13.726	22.373	37.589	766.751	1872.724
jadl1	16.773	11.319	15.735	28.355	28.811	53.731
jxwr1	9.505	7.625	13.639	16.874	15.560	16.520
jxwl1	5.519	5.338	9.133	14.093	20.077	20.880
pgmr1	4.567	7.830	11.983	21.852	20.380	20.385

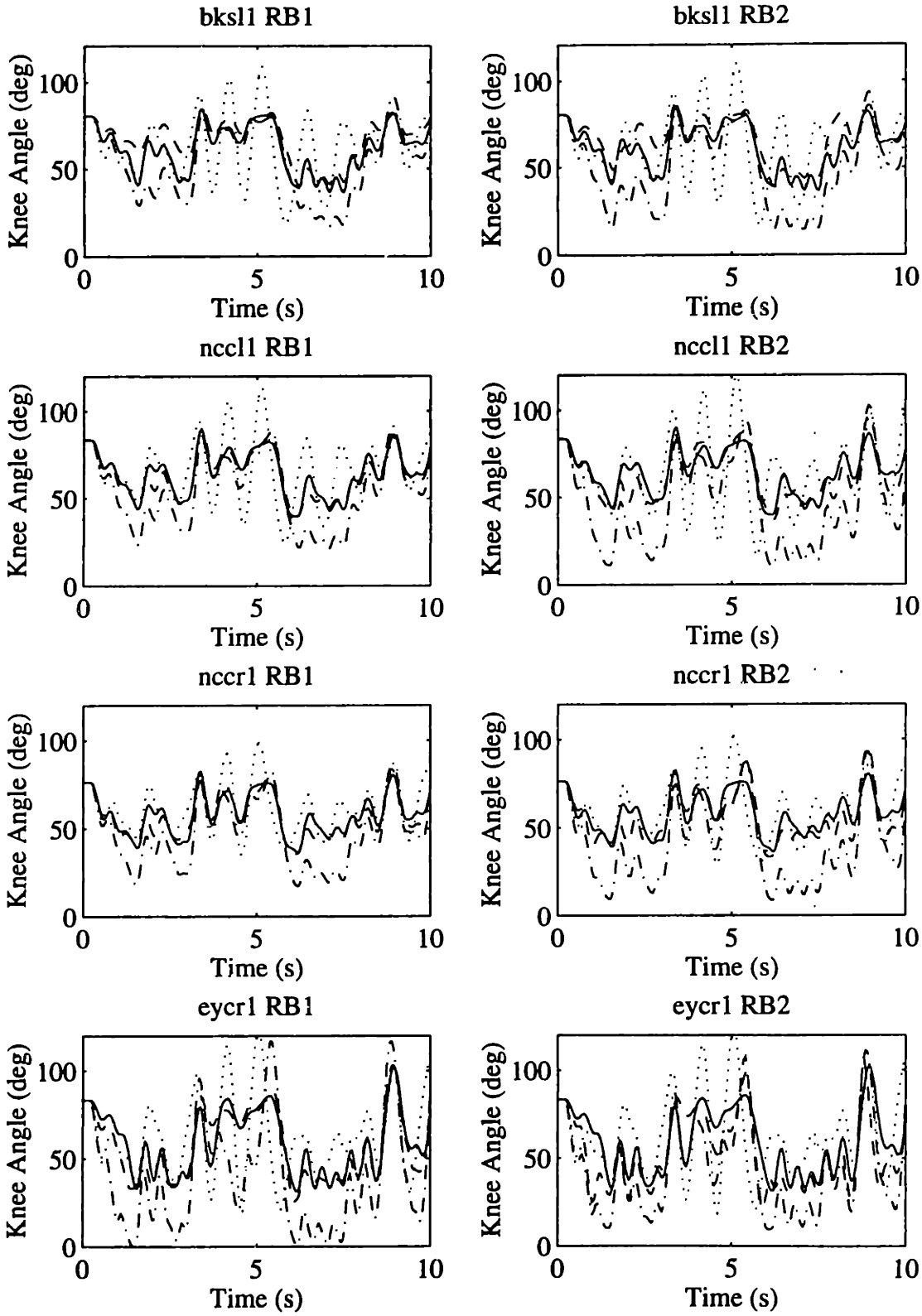

Figure K-4: Random binary 1 response: (−) Experimental knee angle and predictions with (−−) full model, (−·−) single-segment model and (···) torque generator model.

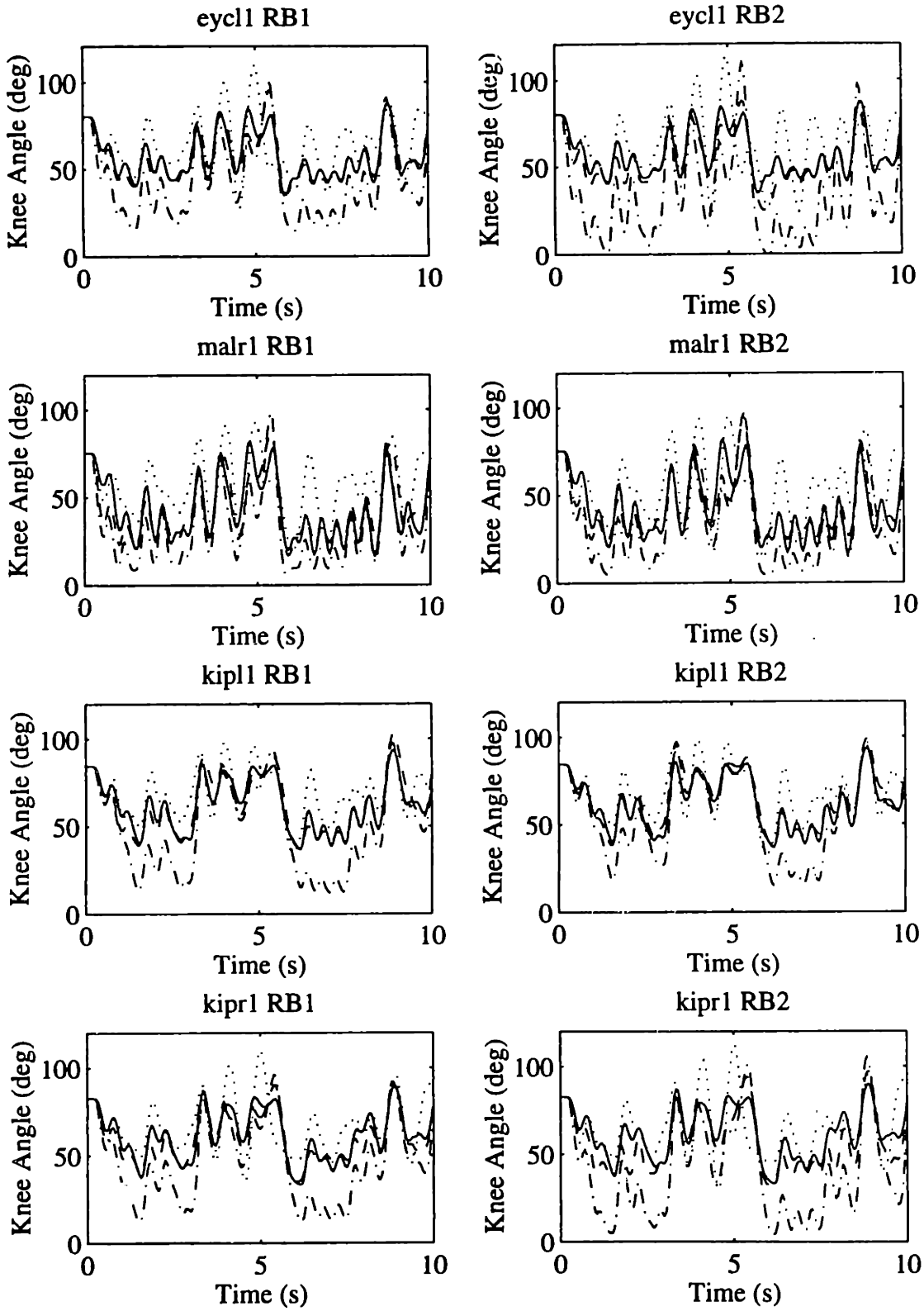

Figure K-4: (continued) Random binary 1 response: (−) Experimental knee angle and predictions with (−−) full model, (− · −) single-segment model and (· · ·) torque generator model.

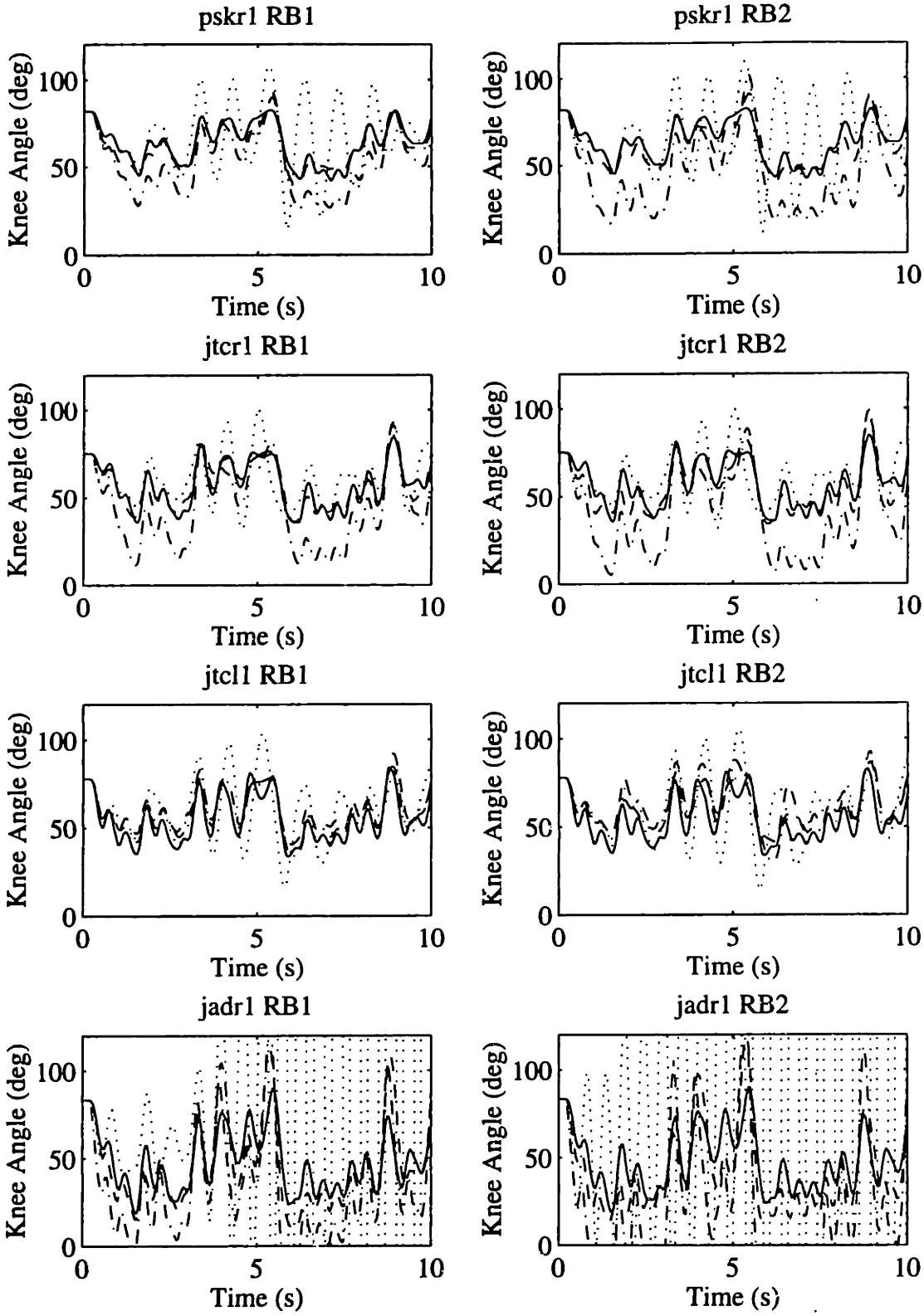

Figure K-4: (continued) Random binary 1 response: (–) Experimental knee angle and predictions with (– –) full model, (– · –) single-segment model and (· · ·) torque generator model.

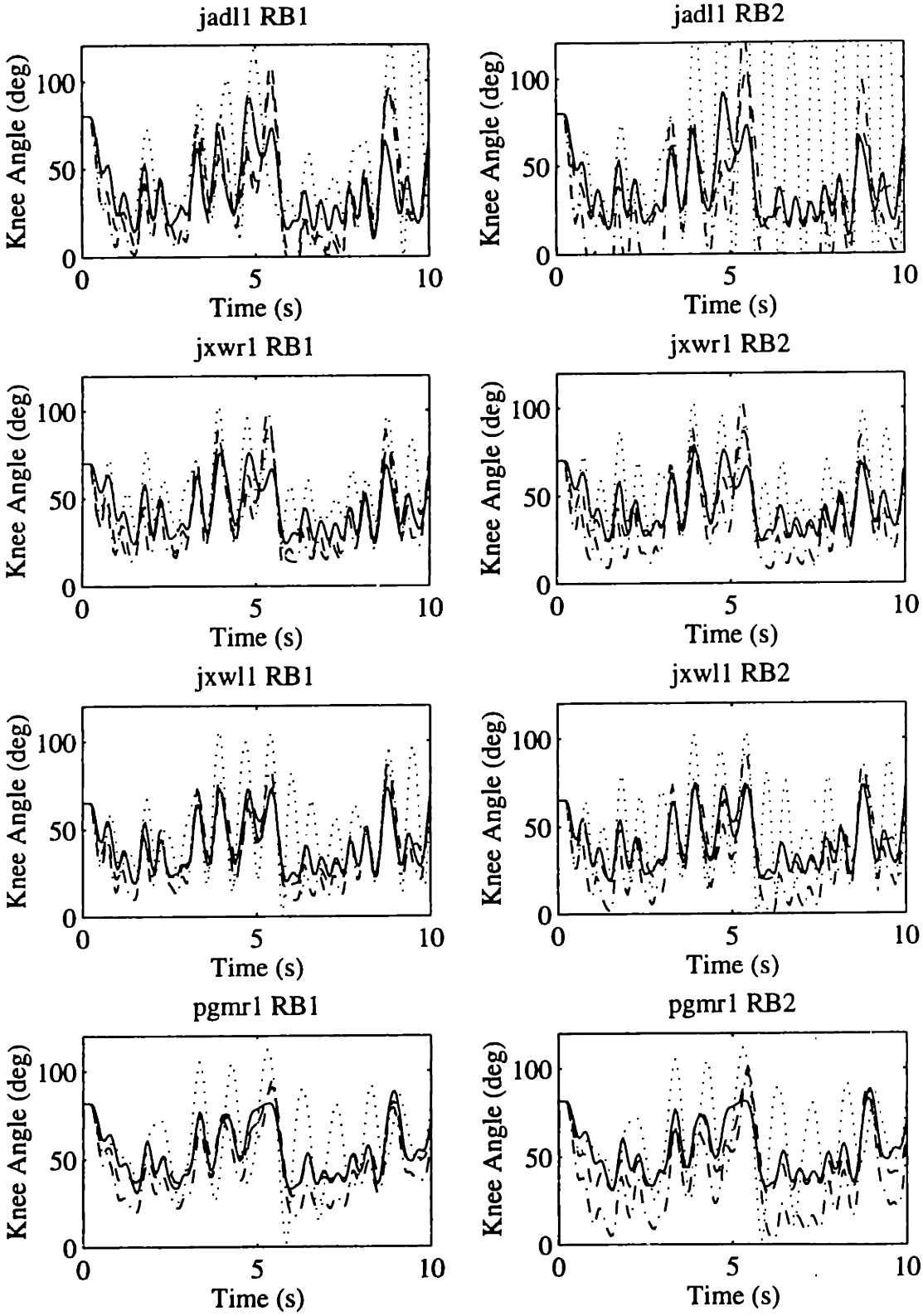

Figure K-4: (continued) Random binary 1 response: (−) Experimental knee angle and predictions with (− −) full model, (− · −) single-segment model and (· · ·) torque generator model.

RMS ERROR for Random Binary Trajectory #1 Response Prediction

	Model Type					
	Full		Single-Segment		Torque Generator	
Subject	RB1	RB2	RB1	RB2	RB1	RB2
bksl1	7.106	7.017	13.465	15.179	14.924	15.422
nccl1	5.915	7.963	12.311	20.786	14.895	17.737
nccr1	5.014	7.146	14.595	20.930	11.316	12.093
eycr1	9.508	12.413	24.444	19.812	26.098	26.194
eycl1	4.912	8.324	17.283	27.059	18.398	16.933
malr1	7.282	7.650	14.940	14.878	17.954	17.014
kipl1	6.744	4.000	17.722	12.544	9.528	9.440
kipr1	9.032	7.991	18.905	24.053	15.663	16.697
pskr1	9.106	7.798	15.025	23.261	15.833	17.194
jtcr1	6.403	5.740	15.927	20.750	13.163	13.194
jtcl1	7.392	9.062	4.014	7.604	11.667	12.319
jadr1	24.605	16.595	30.657	44.301	671.188	3418.587
jadl1	21.090	11.000	22.582	32.129	42.023	62.856
jxwr1	10.730	8.468	13.900	16.883	15.780	16.976
jxwl1	5.770	5.040	10.553	15.117	21.432	24.177
pgmr1	5.518	6.108	12.894	20.102	18.204	18.209

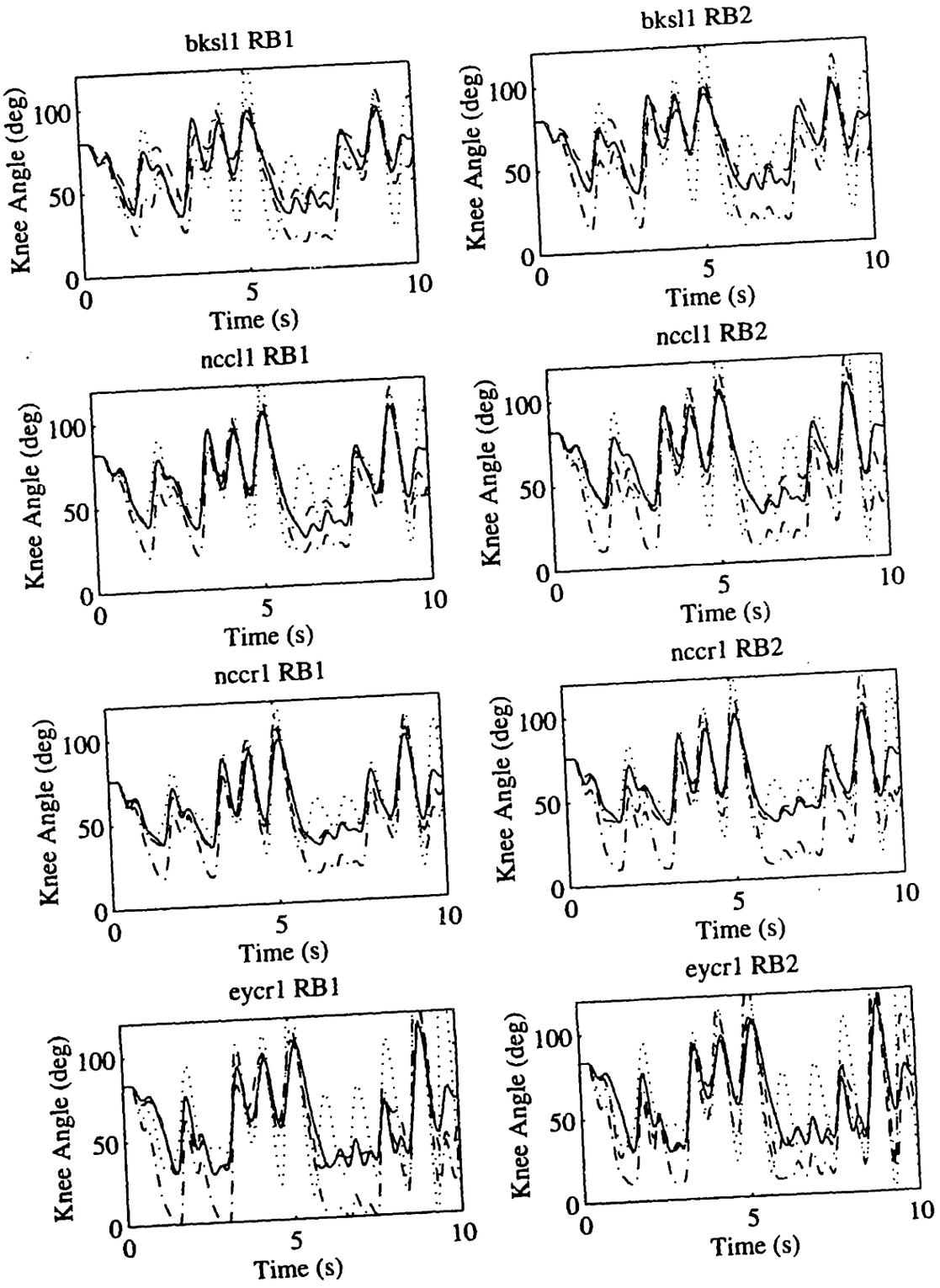

Figure K-5: Random binary 2 response: (−) Experimental knee angle and predictions with (−−) full model, (−·−) single-segment model and (···) torque generator model.

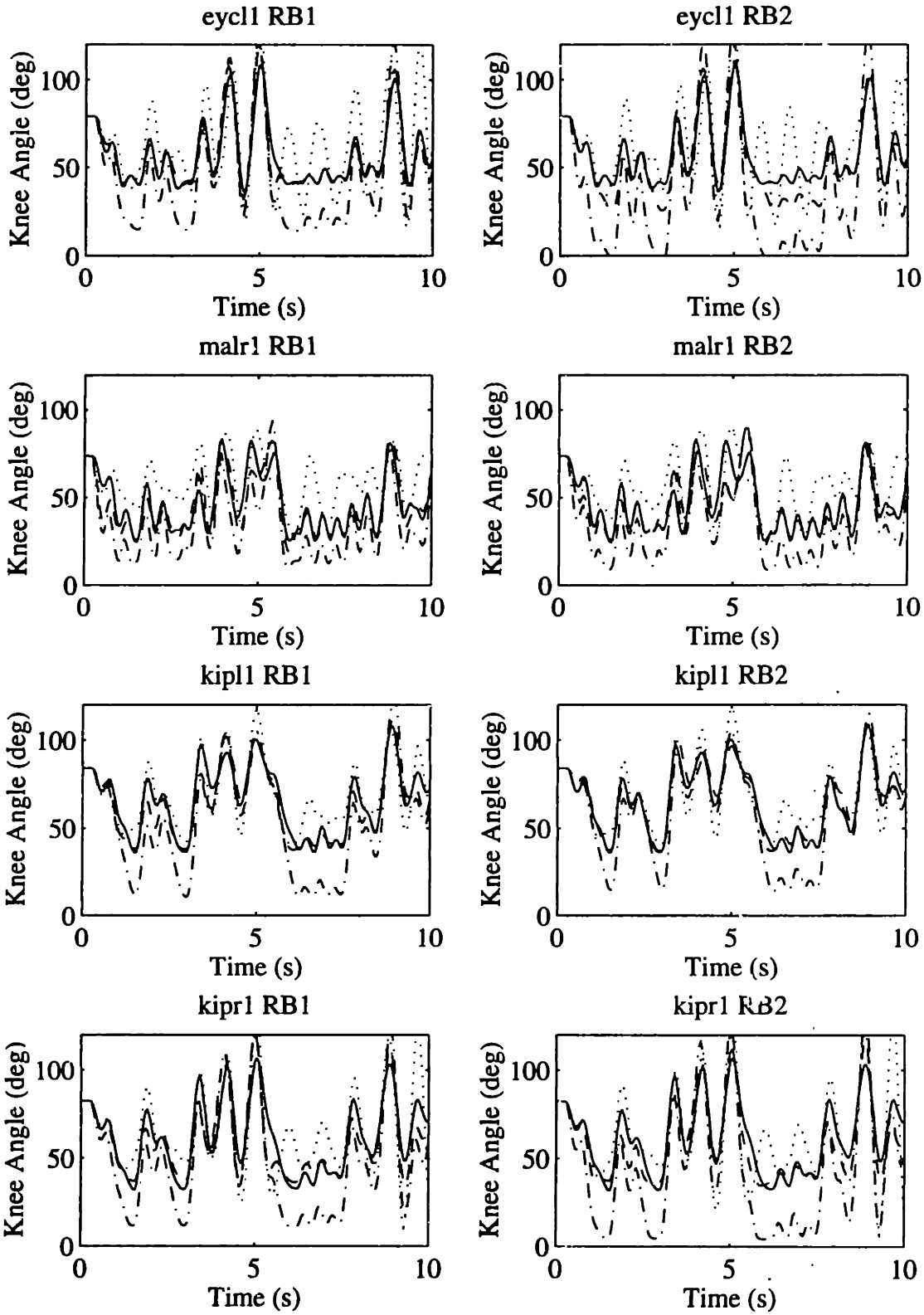

Figure K-5: (continued) Random binary 2 response: (−) Experimental knee angle and predictions with (− −) full model, (− · −) single-segment model and (· · ·) torque generator model.

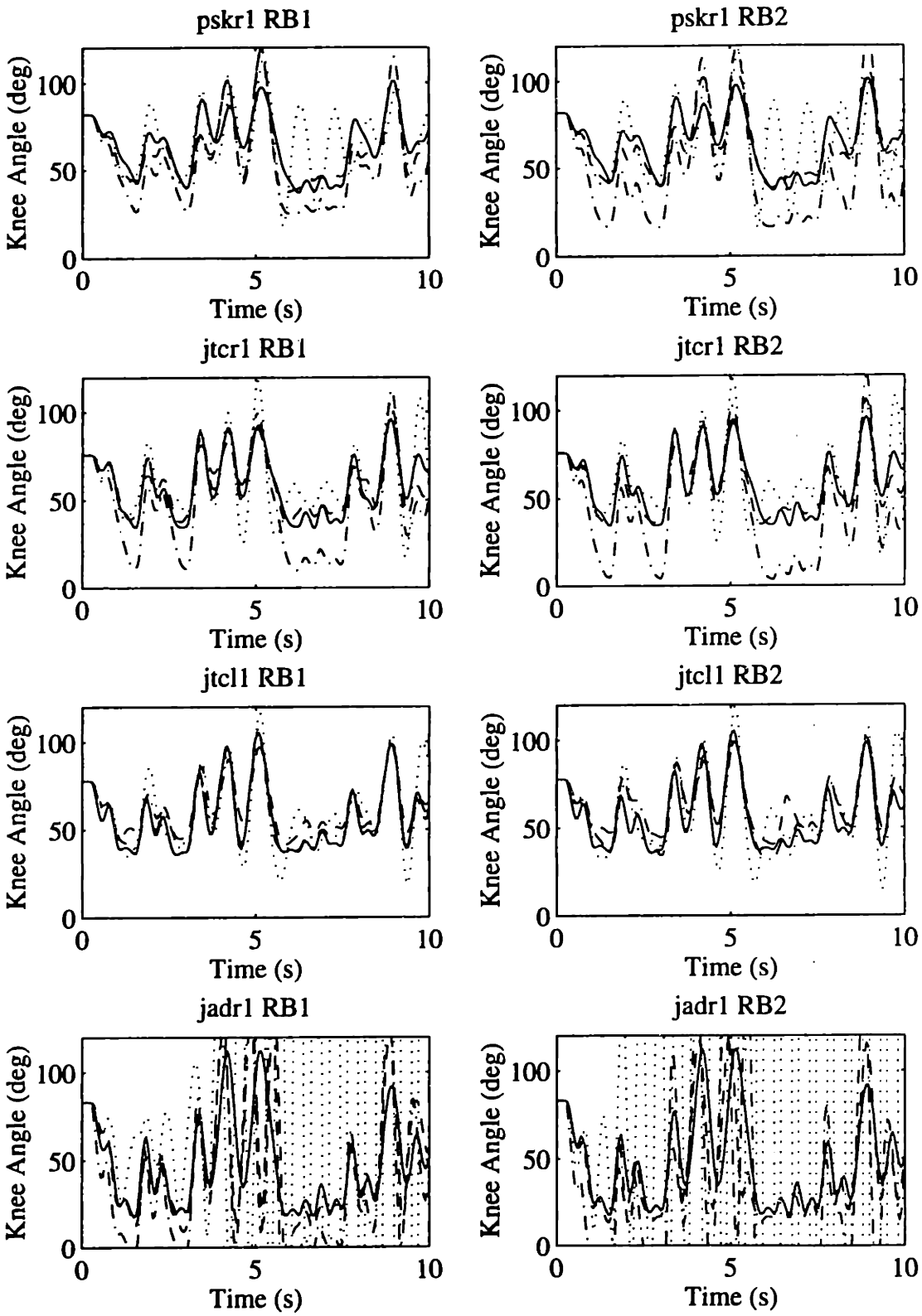

Figure K-5: (continued) Random binary 2 response: (−) Experimental knee angle and predictions with (− −) full model, (− · −) single-segment model and (· · ·) torque generator model.

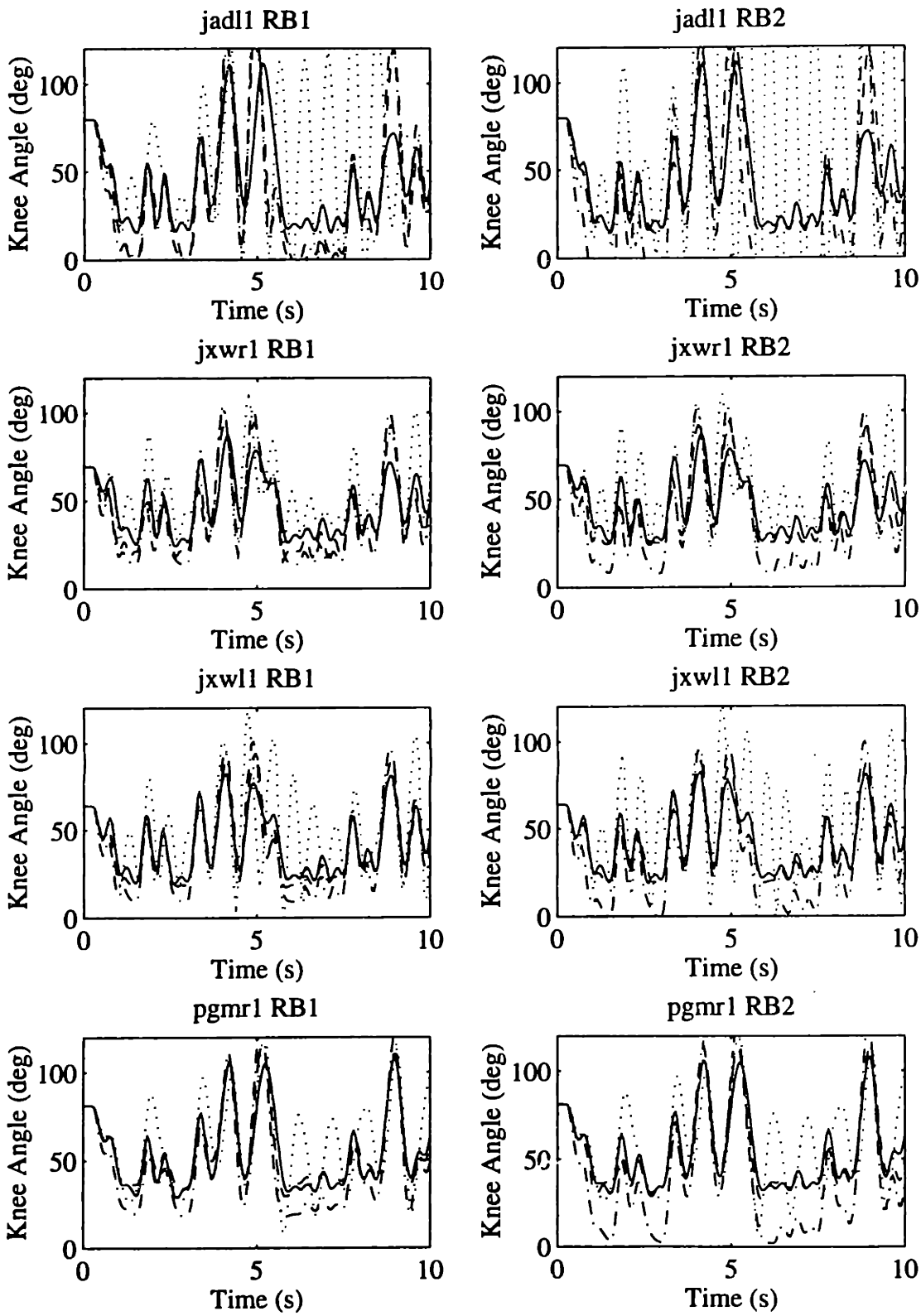

Figure K-5: (continued) Random binary 2 response: (−) Experimental knee angle and predictions with (− −) full model, (− · −) single-segment model and (· · ·) torque generator model.